SMALL-SCALE SOLAR MAGNETIC FIELDS: AN OVERVIEW

SAMI K. SOLANKI
Institut für Astronomie, ETH-Zentrum, CH-8092 Zürich, Switzerland

(Received 8 December, 1992)

Table of Contents

Space Science Reviews **63:** 1–188, 1993.

Abstract. An overview is given of the observational and the theoretical methods used to investigate solar magnetic fields. It includes an introduction to the Stokes parameters, their radiative transfer in the presence of a magnetic field, and empirical techniques used to measure various properties of solar magnetic features, such as the strength and direction of the magnetic field, magnetic flux, temperature, velocity, size and lifetime. The MHD equations are introduced and some of the most common simplifications used to describe solar magnetic features are outlined.

The application of these techniques to small-scale magnetic features is surveyed. The results of empirical and theoretical investigations of small-scale solar magnetic features are reviewed. Current views on their magnetic structure, thermal stratification, velocity field, size, distribution and evolution are presented. Finally, some open questions concerning small-scale solar magnetic fields are listed.

1. Introduction

In 1908 the sun became the first star on which magnetic fields were detected (Hale 1908) and not until 1947 did it cease to be the only star on which magnetic fields were known (Babcock 1947). In the intervening four decades Hale and his co-workers uncovered an astounding variety of facts on sunspot magnetic fields and on the global solar magnetic cycle. Hale also discovered the first signs of magnetic fields outside of sunspots in regions he referred to as 'invisible sunspots' (Hale 1922, not to be confused with the 50 G global solar magnetic field falsely found by Hale 1913, cf. Stenflo 1970). During a large fraction of this period the Mt. Wilson team was practically on its own in the direct measurement of solar magnetic fields. In the meantime the number of investigators and investigations has increased to such an extent that it is almost impossible to review all aspects of solar magnetic fields without being forced to remain at a relatively superficial level. Therefore, I have chosen to restrict the subject matter to small-scale magnetic fields. This allows me to avoid making too large concessions in the depth of the coverage, while not taxing the endurance of the reader beyond bearable limits. Some simplifications and omissions are unavoidable, but for the disappointed reader a list of reviews on this subject is given at the beginning of Section 5.

The present overview is structured as follows. Section 2 gives a brief introduction to the radiative transfer of polarized light in the presence of a magnetic field. It introduces the Stokes parameters and other quantities later required to understand the diagnostics used to investigate magnetic features. The basics of magnetic flux tube modelling are discussed in Section 3. It covers simple 2-component models used to interpret observations, as well as more sophisticated ones based on the solution of the magnetohydrodynamic equations. In Section 4 the diagnostics used to derive information on solar magnetic features from observations are critically reviewed. Section 5 gives an overview of the properties of small-scale solar magnetic fields derived from observations as well as from theory. A brief summary is given at the end of each subsection of Section 5. A list of open questions forms Section 6.

At this point I wish to apologize to all researchers whose work has found no or only inadequate mention in the following pages. This may well have to do with my incomplete grasp of the importance or relevance of individual contributions, but is with equal probability a result of my incomplete knowledge of the literature.

2. Spectral Lines in a Magnetic Field

Magnetic features are best studied in polarized light, since the Zeeman effect gives a very definite and unmistakable spectro-polarimetric signature which allows them to be identified with great ease. The use of polarized light also helps to counter the largest single problem facing the investigator of the physical nature of solar magnetic features, namely the insufficient spatial resolution available to resolve

the small-scale features (due to image degradation by the earth's atmosphere). The present section deals with a description of polarized light, its production and its propagation through the solar atmosphere.

2.1. Zeeman Effect

In the absence of a magnetic field the energy E_J of the atomic levels of all except hydrogenic ions depends on the absolute value of the total angular momentum J [in the following, quantum numbers are often used instead of the operator eigenvalues for simplicity, e.g. J instead of $\hbar J(J+1)$], but not on any of its components, so that each level is $(2J+1)$-fold degenerate. This degeneracy disappears in the presence of a magnetic field and the energy of each level can then be written as

$$E_{J,M} = E_J + \mu_0 g M_J B. \tag{2.1}$$

The energy now also depends on M_J, the component of $\mathbf{J}$ parallel to the magnetic vector $\mathbf{B}$ $(-J \leq M_J \leq J)$. In deriving Equation (2.1) it has been assumed that the coupling of the field to the atom is small compared to the spin-orbit interaction, so that first order perturbation theory can be used to describe it (linear Zeeman effect). This assumption is generally fulfilled by solar magnetic fields. For stronger fields, or for particular spectral lines, the quadratic Zeeman effect and partial or complete Paschen-Back effect have to be considered (cf. Maltby 1971, Chang 1987, Mathys 1990). In Equation (2.1) $\mu_0 = e\hbar/(2mc)$ is the Bohr magneton (e is the electric charge, $\hbar = h/2\pi$ is Planck's constant, m the electron mass and c the speed of light) and g is the Landé factor given by

$$g = 1 + \frac{J(J+1) + S(S+1) - L(L+1)}{2J(J+1)} \tag{2.2}$$

in LS coupling (L and S are the total orbital and spin angular momentum quantum numbers, respectively). Other coupling schemes are described by, e.g., Sobel'man (1972). The main observational consequences of this splitting of the atomic levels is a splitting of the spectral lines formed between two such levels into three groups of lines (Zeeman, 1897) according to $\Delta M_J = 0, \pm 1$. The unshifted ($\Delta M_J = 0$) component is called the π-component, while the $\Delta M_J = \pm 1$ components are referred to as the $\sigma^{\pm}$-components.

For the special case of a transition between a $J = 1$ and a $J = 0$ level or between two levels with equal g-values, the line splits into exactly three components. In this case the line is called a *Zeeman-triplet* and it is straightforward to assign a g-value to the whole line. In the more common case of anomalous Zeeman splitting each π and σ-component is in general itself composed of two or more subcomponents. For such anomalously split lines an "effective Landé factor" can be defined

$$g_{\text{eff}} = \frac{1}{2}(g_l + g_u) + \frac{1}{4}(g_l - g_u)(J_l(J_l+1) - J_u(J_u+1)). \tag{2.3}$$

It corresponds to the Landé factor of a Zeeman triplet whose σ-components have wavelengths corresponding to the centre-of-gravity wavelengths of the σ-components of the anomalously split line.

Although it is in principle sufficient to consider only the intensity profile of a Zeeman-split line in order to derive the field strength responsible for the splitting, in practice the splitting in solar magnetic features is often not larger than the Doppler width of a spectral line, so that it is not possible to cleanly separate the effects of a magnetic field from those of line broadening agents like temperature or velocity. The influence of the magnetic field on the observed profile may also be substantially reduced if the magnetic feature is not spatially resolved. However, by measuring polarization the effects of the magnetic field can be easily identified due to the distinctive polarization signature of the Zeeman effect: For a longitudinal field (i.e. for a magnetic vector parallel to the line of sight, LOS) no π-component is visible and the two σ-components are oppositely circularly polarized. For a transverse field (i.e. a magnetic vector perpendicular to the LOS) the π-component is linearly polarized parallel to **B**, while the σ-components are linearly polarized perpendicular to **B**. For a general angle between **B** and the LOS the light is in general elliptically polarized. More details on the Zeeman effect are to be found in Mathys (1989) and in references therein.

2.2. Polarized Light

In astronomy, polarized light is generally described by the four Stokes parameters I, Q, U and V, where I is the total intensity (i.e. the sum of the polarized and the unpolarized fractions of the light), and

$$\begin{aligned} Q &= I_{\text{lin}}(\chi = 0) - I_{\text{lin}}(\chi = \pi/2), \\ U &= I_{\text{lin}}(\chi = \pi/4) - I_{\text{lin}}(\chi = 3\pi/4), \\ V &= I_{\text{circ}}(\text{right}) - I_{\text{circ}}(\text{left}). \end{aligned} \tag{2.4a}$$

Here $I_{\text{lin}}(\chi)$ refers to linearly polarized radiation whose electric vector makes an angle χ to some reference direction (defined by the measuring apparatus). I_{circ} refers to circularly polarized light. The Stokes parameters are directly measurable quantities. Note that except for resonance lines observed near the solar limb, which may show intrinsic linear polarization due to scattering (e.g. Stenflo *et al.* 1983, 1984b), $Q = U = V = 0$ if $B = 0$. This is an extremely useful property, since by measuring Stokes Q, U, or V one obtains information exclusively on the magnetic features, even if these are spatially unresolved. There is one exception to this rule. If a ray passes through both magnetized and unmagnetized gas, then Stokes Q, U and V formed along this ray may also be affected by the unmagnetized material in a limited manner.

If the light is completely polarized, then the 4 Stokes parameters are no longer independent of each other:

$$I^2 = Q^2 + U^2 + V^2. \tag{2.4b}$$

Consequently, completely polarized light can be adequately described by only 3 Stokes parameters.

2.3. LTE Radiative Transfer in a Magnetic Field

In LTE (local thermodynamic equilibrium) the transfer equation for polarized radiation in the presence of a sufficiently strong magnetic field (no Hanle effect) can be written as

$$\frac{\mathrm{d}\mathbf{I}_\nu}{\mathrm{d}\tau} = (\mathbf{E} + \mathbf{\Omega}_\nu)(\mathbf{I}_\nu - \mathbf{1}B_\nu), \tag{2.5}$$

where $\mathbf{I}_\nu$ is the Stokes vector at frequency ν, $\mathbf{E}$ is the unity matrix, τ is the continuum optical depth along the line of sight, B_ν is the Planck function, $\mathbf{1} = (1,0,0,0)^{\mathrm{T}}$ ($^{\mathrm{T}}$ signifies transposition) and $\mathbf{\Omega}_\nu$ is the absorption matrix

$$\mathbf{\Omega}_\nu = \begin{pmatrix} \eta_I & \eta_Q & \eta_U & \eta_V \\ \eta_Q & \eta_I & \rho_V & -\rho_U \\ \eta_U & -\rho_V & \eta_I & \rho_Q \\ \eta_V & \rho_U & -\rho_Q & \eta_I \end{pmatrix}. \tag{2.6}$$

Here

$$\begin{aligned} \eta_I &= \frac{\eta_0}{2}\sin^2\gamma + \frac{\eta_{+1}+\eta_{-1}}{4}(1+\cos^2\gamma), \\ \eta_Q &= \left(\frac{\eta_0}{2} - \frac{\eta_{+1}+\eta_{-1}}{4}\right)\sin^2\gamma\cos 2\chi, \\ \eta_U &= \left(\frac{\eta_0}{2} - \frac{\eta_{+1}+\eta_{-1}}{4}\right)\sin^2\gamma\sin 2\chi, \\ \eta_V &= \frac{\eta_{-1}-\eta_{+1}}{2}\cos\gamma, \end{aligned} \tag{2.7}$$

$$\begin{aligned} \rho_Q &= \left(\frac{\rho_0}{2} - \frac{\rho_{+1}+\rho_{-1}}{4}\right)\sin^2\gamma\cos 2\chi, \\ \rho_U &= \left(\frac{\rho_0}{2} - \frac{\rho_{+1}+\rho_{-1}}{4}\right)\sin^2\gamma\sin 2\chi, \\ \rho_V &= \frac{\rho_{-1}-\rho_{+1}}{2}\cos\gamma. \end{aligned} \tag{2.8}$$

In Equations (2.7) and (2.8) γ is the angle between $\mathbf{B}$ and the line of sight and χ is the azimuthal angle of $\mathbf{B}$. The angles are illustrated in Figure 2.1. The $\eta_{0,\pm1}$ are the ratios of the line to the continuum absorption coefficients of the π and $\sigma_\pm$-components, respectively, while $\rho_{0,\pm1}$ are the corresponding magnetooptical coefficients (cf. e.g. Landi Degl'Innocenti 1976, Kalkofen 1987 and Jefferies *et al.*

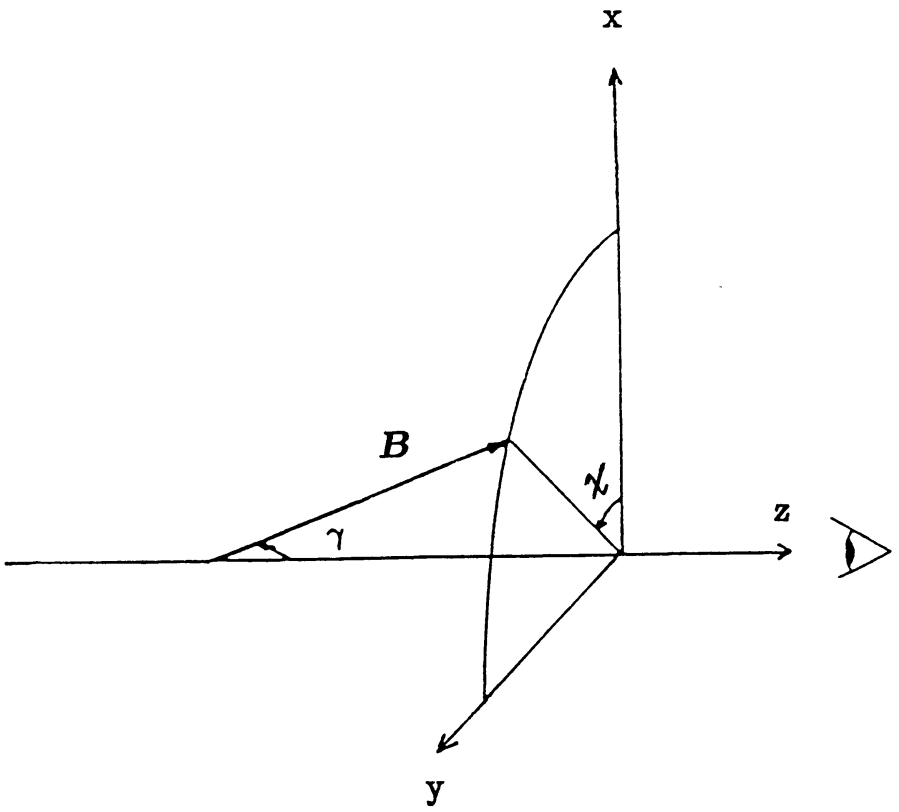

Fig. 2.1. Definition of the angles γ and χ used in the radiative transfer of Zeeman-split spectral lines (Adapted from Muglach 1991).

1990). The Zeeman splitting manifests itself in the strengths and shifts of the $\eta_{\pm1,0}$ and $\rho_{\pm1,0}$ values. For a Zeeman triplet

$$\eta_{\pm1}(\lambda) = \eta_0(\lambda \pm \Delta\lambda_H),$$
$$\rho_{\pm1}(\lambda) = \rho_0(\lambda \pm \Delta\lambda_H).$$

Here $\Delta\lambda_H = (e/4\pi mc^2) g_{\text{eff}} B\lambda^2$ is the Zeeman splitting. Equations (2.5)–(2.8) have been derived classically by Unno (1956), Rachkovsky (1962), Jefferies *et al.* (1989) and Stenflo (1991b). A quantum mechanical derivation has been given by Landi Degl'Innocenti and Landi Degl'Innocenti (1972) and a quantum electrodynamical approach has been taken by Landi Degl'Innocenti and Landi Degl'Innocenti (1983) and Mathys (1983). Reviews of the radiative transfer of polarized light in a magnetic medium have been given by Stenflo (1971), Rees (1987) and Murphy (1990). See also the other papers in the second half of the volume edited by Kalkofen (1987).

For an atmosphere in which Ω_ν is height independent, implying that the field strength is also height independent, and in which the Planck function has the form

$$B_\nu = B_{\nu_0}(1 + \beta_0\tau) \tag{2.9}$$

(Milne-Eddington model), an analytical solution of Equation (2.5) may be obtained (Unno 1956, Rachkovsky 1967, Landi Degl'Innocenti and Landi Degl'Innocenti 1985). In the absence of magnetooptical effects ($\rho_Q = \rho_U = \rho_V = 0$) the solution is particularly simple (Unno 1956)

$$\begin{aligned} I(\mu) &= B_{\nu_0}\left(1+\beta_0\mu\frac{1+\eta_I}{(1+\eta_I)^2-\eta_Q^2-\eta_U^2-\eta_V^2}\right), \\ Q(\mu) &= -B_{\nu_0}\beta_0\mu\frac{\eta_Q}{(1+\eta_I)^2-\eta_Q^2-\eta_U^2-\eta_V^2}, \\ U(\mu) &= -B_{\nu_0}\beta_0\mu\frac{\eta_U}{(1+\eta_I)^2-\eta_Q^2-\eta_U^2-\eta_V^2}, \\ V(\mu) &= -B_{\nu_0}\beta_0\mu\frac{\eta_V}{(1+\eta_I)^2-\eta_Q^2-\eta_U^2-\eta_V^2}, \end{aligned} \tag{2.10}$$

where μ is the cosine of the angle between the LOS and the normal to the solar surface.

The denominator in Equation (2.10) is responsible for line saturation. Obviously, a magnetic field causes the line to desaturate. For example, consider a longitudinal field. Then $\eta_Q = \eta_U = 0$ and η_V^2 varies between 0 for $\Delta\lambda_H = 0$ and $\eta_V^2 = \eta_I^2$ for complete splitting. Thus the denominator decreases from $(1+\eta_I)^2$ to $(1+2\eta_I)$ as B increases.

Numerical solutions of the system of four coupled equations (2.5) may be obtained by direct Runge-Kutta integration (Beckers 1969a, b, Wittmann 1974, Landi Degl'Innocenti 1976), by numerical evaluation of a series expansion (Staude 1969), by a Feautrier technique (Auer *et al.* 1977, Rees *et al.* 1989), by formal integration, which results in the Runge-Kutta integration of an equivalent system of equations (Van Ballegooijen 1985a), or by other fast methods (Rees *et al.* 1989, see also articles in the volume edited by Kalkofen 1987, in particular for NLTE Problems).

In the presence of height-dependent phenomena it is often interesting to know the height of formation of a particular spectral line. Contribution functions for Zeeman split Stokes profiles have been defined and calculated by, e.g., Staude (1972), Van Ballegooijen (1985a), Grossmann-Doerth *et al.* (1988a) and Murphy (1990). Sometimes it may be of greater interest to know the response of a spectral line to perturbations in a given atmospheric variable. Response functions for Zeeman split lines have been introduced by Landi Degl'Innocenti and Landi Degl'Innocenti (1977), cf. Grossmann-Doerth *et al.* (1988a). A general expression for the response functions of the Stokes profiles of a Zeeman-split line has been derived by Sánchez Almeida (1992).

2.4. Further Properties of Zeeman-split Stokes Parameters

In the following I list some additional properties of the Stokes profiles that are of interest for the further discussion. Firstly, Stokes I and V do not depend on

χ and Stokes Q and U are invariant to changes in χ that are multiples of 180°. Also, Stokes V changes sign if the longitudinal component of **B** changes its polarity, while Stokes I, Q and U do not. It is also worth noting that for lines formed in LTE, Stokes I, Q and U are symmetric around the line core wavelength in the absence of velocity gradients, while Stokes V is antisymmetric (Auer and Heasley 1978, Landi Degl'Innocenti and Landi Degl'Innocenti 1981). Not only is the symmetry of the profile shapes lost in the presence of longitudinal velocity gradients, but even the areas of the blue and red lobes of Stokes V may be unequal (Illing *et al.* 1975). The shape and field-strength dependence of Zeeman-split Stokes profiles is illustrated in Figure 2.2 for an often-used spectral line.

For weak fields the Stokes I profile closely resembles the unsplit profile, while Q, U and V are very weak and increase in amplitude, but not in peak separation, with B. At large B the line is completely split, i.e., the peak separation increases linearly with B and the amplitudes of Q, U and V become independent of B (often referred to as Zeeman saturation).

Finally, let us consider a relation between Stokes I and V for not too strong lines formed in a static atmosphere. The Taylor expansion of Stokes V may then be expressed in terms of I_m, the unsplit Stokes I profile formed in the atmosphere of the magnetic feature (Stenflo *et al.* 1984b, Solanki and Stenflo 1984),

$$V(\lambda) = \cos\gamma \sum_{n=0}^{\infty} \frac{1}{(2n+1)!} (\Delta\lambda_H)^{2n+1} \frac{\partial^{2n+1}}{\partial\lambda^{2n+1}} I_m(\lambda). \tag{2.11}$$

For the weak field case ($\Delta\lambda_H \ll \Delta\lambda_D$) this reduces to

$$V(\lambda) \approx \cos\gamma \Delta\lambda_H \frac{\partial I_m(\lambda)}{\partial\lambda}. \tag{2.12}$$

Equation (2.12) is also valid for strong lines (Landi Degl'Innocenti and Landi Degl'Innocenti 1973, Solanki 1987c, Solanki *et al.* 1987, Jefferies *et al.* 1989, Rees *et al.* 1989). By integrating Equation (2.12) it is possible to define the so called I_V profile,

$$\frac{I_c - I_V}{I_c} = -\frac{1}{\cos\gamma\Delta\lambda_H} \int_{\lambda_1}^{\lambda} \frac{V(\lambda')}{I_c} \, \mathrm{d}\lambda'. \tag{2.13}$$

Here I_c is the continuum intensity and λ_1 is a wavelength so far in the blue wing of the line that $V(\lambda_1) \approx 0$. I_V is a good approximation of I_m in the weak-field approximation. Similar relationships between Stokes Q and $d^2I/d\lambda^2$, respectively Stokes U and $d^2I/d\lambda^2$ are only valid for very weak lines (Solanki *et al.* 1987), or only at the central wavelength, λ_0. However, the relations between Q, U and $dI/d\lambda$ derived by Jefferies *et al.* (1990), cf. Equation (4.33) in Section 4.4, is valid for stronger lines as well, at all wavelengths except λ_0 (Landi Degl'Innocenti 1992).

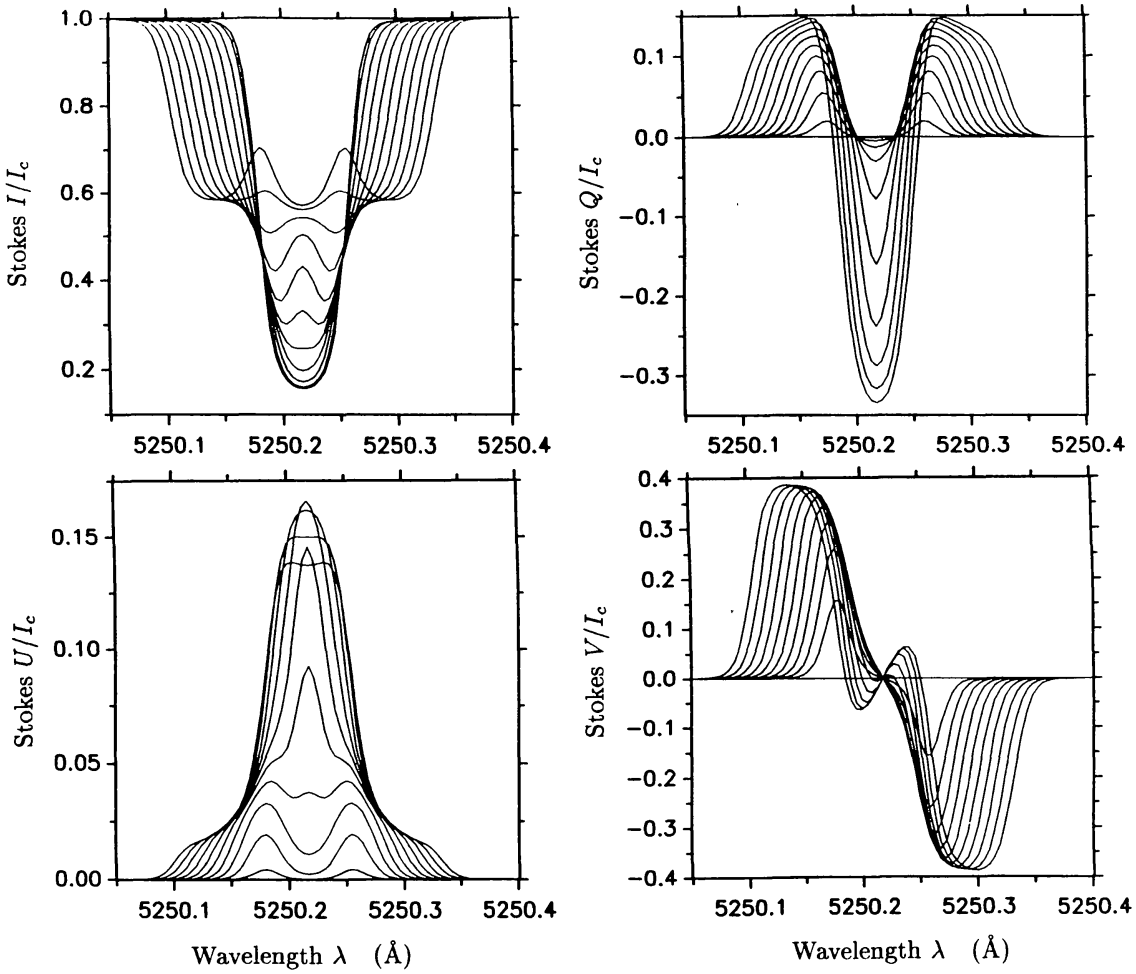

Fig. 2.2. Stokes I, Q, U and V profiles of Fe I 5250.2 Å calculated for a quiet sun model atmosphere at solar disc centre ($\mu = 1$), $\gamma = 45°$, $\chi = 0°$ and field strengths $B = 0$, 200, 400, 600, 800, 1000, 1200, 1400, 1600, 1800 and 2000 G. The lines are broadened by a microturbulence of 0.8 km s^{-1}, but no macroturbulence. Note the different splitting regimes, e.g., in the Stokes V profile: For $B = 200$ and 400 G its amplitude increases almost linearly with field strength, while the peak separation remains almost unchanged (weak field regime with $\Delta\lambda_H/\Delta\lambda_D \ll 1$), for $B = 600$–1200 G $\Delta\lambda_H/\Delta\lambda_D \approx 1$, and for $B \gtrsim 1400$ G the Stokes V profile exhibits the behaviour of a completely split spectral line ($\Delta\lambda_H/\Delta\lambda_D \gg 1$). The I and Q profiles begin to enter the fully split regime at 2000 G.

2.5. Hanle Effect

In the absence of a magnetic field, spectral lines due to transitions into the ground state of an atom can become linearly polarized due to fluorescent or resonant scattering. In the presence of a magnetic field the level of linear polarization is generally reduced. If the field is sufficiently weak then the depolarization is only partial and, in most cases, the plane of polarization is rotated. This is the observational signature of the Hanle effect (Hanle 1924). For some spectral lines an increase in the polarization may also appear at finite field strengths. The physical basis for this finite-field effect is level-crossing interference. Here only the simplest case of optically thin emission lines is briefly and qualitatively outlined. One

prerequisite for the Hanle and level-crossing depolarization effects is the presence of coherent scattering in the spectral line, i.e. only lines with cores whose radiative transfer is dominated by scattering processes can show these effects (lines formed in NLTE). In the absence of a magnetic field, radiatively excited emission lines exhibit resonant or fluorescent polarization if the radiation which excites the atom into its upper level is either polarized or anisotropic.* In the solar atmosphere the exciting radiation is anisotropic (due to limb darkening or brightening), hence the requirement for resonant or fluorescent polarization is fulfilled. However, for a spherically symmetric sun, the different directions of polarization cancel at solar disc centre, so that a net polarization is only seen near the solar limb. Therefore, the Hanle and level-crossing interference effects are not visible at disc centre unless local anisotropies in the radiation field exist and can be spatially resolved.

The quantum mechanical explanation of the Hanle effect is based on the interference (coherence) between almost overlapping energy states of the upper level of the transition. Ensembles of particles without mutual interactions, e.g. atoms or photons, may be described by a density matrix whose diagonal elements are the populations of the the Zeeman sublevels with different M_J and off-diagonal elements represent coherences between the M_J states. The atomic density matrix associated with unpolarized and isotropic light is a scalar (i.e., with off-diagonal elements equal to zero and identical diagonal elements). The atomic density matrix associated with an anisotropic or polarized radiation field shows non-uniform populations of the M_J states and non-zero coherences. The absorption of such a radiation field by atoms leads to non-uniform populations of the Zeeman sub-levels of the upper atomic level and to phase relationships (coherences) among them. Significant coherences only occur if the separation in energy between the levels is smaller than their (radiative and collisional) damping width.* In the absence of magnetic fields and collisions, the re-emitted radiation is linearly polarized according to the density matrix of the atoms (e.g. for a $J = 0$ to $J = 1$ transition) and the atoms decay to the unpolarized ground state.

Coherency is only established as long as B is sufficiently small. As the field strength increases and the splitting between the sublevels becomes of the order of their damping widths, the coherence produced by the anisotropic radiative excitation and therefore the linear polarization begins to decrease. The degree of polarization of the emitted radiation, is controlled by the ratio of $g\omega_L$ to τ, where g is the Landé factor of the upper level of the transition, $\omega_L = eB/2m$ is the Larmor frequency (e = electron charge, m = electron mass) and τ is the natural

* The absorption and re-emission of light by an atom is referred to as resonant scattering if the final (deexcited) state is the same as the initial state (i.e. the atom passes from an initial state into an excited state by the absorption of a photon and then back into the initial state through the emission of another photon) and fluorescence if the final state is different from the initial state (i.e. the atom relaxes from the excited state through emission to a third state).

* However, note that strong lines with highly developed damping wings may show interference effects over larger energy differences. An example is the interference between the Ca II H and K lines, Stenflo 1980).

or radiative lifetime of the upper level. The resulting polarization is lower than in the absence of a magnetic field (the coherences are smaller), and the polarization plane is rotated.

Clearly, lines with different damping widths, which, in an optically thin plasma, implies different lifetimes of their upper levels, are sensitive to fields with different upper limits. Actually, the limiting field strength is determined by the ratio of damping width to Zeeman splitting.

In some cases a coherent state is achieved at a finite field strength. For example, two sublevels (belonging to different J_u) that are well separated for $B = 0$, may overlap for a certain $B \neq 0$, so that polarization is also observed within a range of higher field strengths. This effect is termed level-crossing interference.

Therefore, depending on the exact energy structure of a given atom and the Landé factors of its levels, it exhibits the Hanle or level-crossing interference effects for a given set of field strengths and may be used to diagnose these. More details on the theoretical description of the Hanle effect are given by Moruzzi (1991) and Stenflo (1991b) for the classical treatment and by Moruzzi (1991) for the quantum-mechanical treatment. Its applications to solar physics have been reviewed by, e.g., Leroy (1985), Stenflo (1991a) and Faurobert-Scholl (1992c). Its most widely known applications have been to prominences (cf. reviews by Leroy 1988, Démoulin 1990, Kim 1990, Landi Degl'Innocenti 1990, Bommier *et al.* 1992) and the turbulent magnetic field (Stenflo 1982, Faurobert-Scholl 1992b).

Two formulae derived by Breit (1925) give expressions for the percentage polarization, P, and the angle of rotation, Ω, for optically thin lines formed in pure scattering (no collisions). The linear polarization when measuring along the field is

$$P = \frac{P_0}{1 + (2g\omega_L\tau)^2}, \tag{2.14}$$

where P_0 is the percentage polarization in the field-free case. The angle of rotation is given by

$$\tan 2\Omega = 2g\omega_L\tau. \tag{2.15}$$

It is important to note that, unlike the Zeeman effect, the signal of the Hanle effect is independent of the Doppler width of the line, as long as the Zeeman splitting is much smaller than the Doppler width. The Hanle signal is, however, very sensitive to the collisional de-excitation of the upper level. Also, no Hanle depolarization is seen if the magnetic vector is parallel to the symmetry direction of the illuminating radiation field.

3. Modelling Techniques

The modelling of magnetic features has a number of objectives. Simple, often highly abstracted, physical models serve to understand the nature of individual

physical processes. By neglecting many of the physical interactions present in a magnetic feature, it is possible to isolate processes of particular interest and study them in depth. However, before any theory can be considered completely successful, it must satisfy the constraints imposed by observational data. For such complex structures as solar magnetic features simple models often fail to meet this requirement. More complex, invariably numerical, models are then needed, which take as many physical processes into account as feasible. Such models have generally also led to a substantial increase in our understanding of the basic physics, since the interaction between different physical processes, e.g. energy transport mechanisms, can qualitatively modify the behaviour of magnetic features. Finally, empirical models attempt to derive information from the observational data under some physical constraints. They often bridge the gap between the raw data and theoretical models. Also, as long as theoretical models do not reproduce the observations with sufficient accuracy, empirical models are required in order to interpret observations. For example, it is of great advantage to have a good knowledge of the temperature within a magnetic feature when deriving its magnetic vector from polarized spectra.

3.1. Simple Concepts Used for Empirical Modelling

Magnetic features in the solar photosphere are generally modelled by flux tubes or flux slabs, i.e., solutions of the MHD equations possessing either cylindrical or translational symmetry. However, for the interpretation of observations much simpler concepts are often used.

The first simple group of models consists of the 1-D (i.e. plane-parallel) models. This is the oldest type of empirical model and still popular for some types of investigations. The assumption of a plane-parallel atmosphere is justified if the solar magnetic features can be spatially resolved, i.e. for large magnetic features, like sunspots. Then a single atmospheric component for each observed solar surface element is sufficient. However, even for sunspots, one-component models have a limited applicability due to the presence of unresolved fine structure (e.g., umbral dots, penumbral filaments). Prior to constructing a 1-component model it is important to clarify that no hidden, sub-resolution structure is present, since otherwise the resulting model may not represent any real solar feature. As an example, consider faculae. It is straightforward to construct a 1-component model that reproduces low spatial resolution Stokes I data. However, high spatial resolution and polarimetric data clearly show that faculae are composed of at least two distinct components, none of which corresponds to the 1-component model. In spite of these caveats 1-component models still have their uses.

The vertical stratification of the atmospheric variables within a single-component model can be determined either in a physically self-consistent manner (e.g. assuming hydrostatic equilibrium) or arbitrarily (e.g. assuming a height-independent field strength or, even more restrictively, a Milne-Eddington atmosphere). The latter is mainly useful for test and exploratory calculations, since it allows individual at-

mospheric parameters to be changed in a highly controlled manner.

In recent years 2-component models have been more commonly used for the interpretation of observational data. They are based on the assumption that within a spatial resolution element two atmospheric components are present, one covering a fraction α of the surface, the other covering the remaining fraction $(1-\alpha)$. In faculae (plages), or in the network, magnetic elements constitute the first component and the intervening non-magnetic atmosphere the other. The magnetic component is generally assigned the surface fraction α, called the magnetic filling factor.

If the two components are spatially unresolved then the observed radiation is the weighted mean of the radiation coming from each, so that the observed Stokes parameters may be written as

$$\begin{aligned} \langle I \rangle &= \alpha I_{\mathrm{m}} + (1-\alpha) I_{\mathrm{s}}, \\ \langle Q \rangle &= \alpha Q_{\mathrm{m}}, \\ \langle U \rangle &= \alpha U_{\mathrm{m}}, \\ \langle V \rangle &= \alpha V_{\mathrm{m}}. \end{aligned} \tag{3.1}$$

The brackets $\langle\ \rangle$ denote averaging over the spatial resolution element, the subscript 'm' signifies light from the magnetic component, the subscript 's' light from the non-magnetic surroundings. The great advantage of Stokes $\langle Q \rangle$, $\langle U \rangle$ and $\langle V \rangle$ over Stokes $\langle I \rangle$ is evident from Equation (3.1). In a 2-component model $\langle Q \rangle$, $\langle U \rangle$ and $\langle V \rangle$ only convey information on the magnetic component and are totally independent of the non-magnetic component.

The 2-component model may also be applied to sunspot umbrae and penumbrae. For sunspot umbrae the dark umbral core and the brighter umbral dots may be chosen as the two components, for sunspot penumbrae the components may be the bright and dark filaments. In these cases both components have a magnetic field, so that all 4 Stokes parameters obtain contributions from both components. If we refer to the two components as bright (subscript 'b') and dark (subscript 'd') and assume that they cover fractions α and $1-\alpha$ of the resolution element, respectively, then we must replace Equation (3.1) by the following expressions for the observed (spatially averaged) Stokes parameters

$$\begin{aligned} \langle I \rangle &= \alpha I_{\mathrm{b}} + (1-\alpha) I_{\mathrm{d}}, \\ \langle Q \rangle &= \alpha Q_{\mathrm{b}} + (1-\alpha) Q_{\mathrm{d}}, \\ \langle U \rangle &= \alpha U_{\mathrm{b}} + (1-\alpha) U_{\mathrm{d}}, \\ \langle V \rangle &= \alpha V_{\mathrm{b}} + (1-\alpha) V_{\mathrm{d}}. \end{aligned} \tag{3.2}$$

The extention of such models to a larger number of components is straightforward. Multi-component models are discussed by Stenflo (1968).

It is important to keep the differences between multi-*component* and multi-*dimensional* models clearly in mind. In contrast to multi-dimensional models, multi-component models assume that the individual atmospheric components are

completely independent of each other. Each component is in itself a simple plane-parallel atmosphere. This implies that the horizontal extent of each component is large compared to the height over which the modelled spectra are formed. The 2-component concept breaks down if this assumption is violated. For example, thin tubes viewed near the limb are ill represented by a 2-component model, since almost all the rays along which the spectra are formed pass across the boundary between the magnetic and non-magnetic features (see Figure 3.1). The assumption of the independence of the two components is, therefore, grossly violated in this example.

If the expansion of the field with height, as required by the magnetohydrostatic equations, is taken into account, then even flux tubes observed at disc centre do not fit into the 2-component picture, since the expanding field forms a canopy, i.e., it overlies non-magnetic gas. Therefore, even at disc centre a large fraction of all rays pass through both components of the atmosphere, leading to a breakdown of the 2-component model. However, for many purposes the 2-component approach still works, since Stokes V, Q and U obtain their dominant contribution from the completely magnetized central cylinder of the flux tube (Solanki 1989) and 2-D modelling is only necessary for a few diagnostics, e.g. the Stokes V asymmetry and the profile shapes of strongly Zeeman-split spectral lines.

3.2. MHD Equations

For a realistic and physically consistent description of magnetic features, it is necessary to solve the magnetohydrodynamic (MHD) equations. For an inviscid and (on macroscopic scales) electrically neutral plasma, the MHD equations are composed of a mass, a momentum and an energy conservation equation,

$$\frac{\partial \rho}{\partial t} + \nabla(\rho \mathbf{v}) = 0\,, \tag{3.3}$$

$$\rho\left(\frac{\partial \mathbf{v}}{\partial t} + (\mathbf{v}\cdot\nabla)\mathbf{v}\right) = -\nabla p + \rho\mathbf{g} + \frac{1}{c}\mathbf{j}\times\mathbf{B}\,, \tag{3.4}$$

$$\rho C_V\left(\frac{\partial T}{\partial t} + (\mathbf{v}\cdot\nabla)T\right) = \nabla\cdot(K\nabla T) - \nabla\cdot\mathbf{F}_R - p(\nabla\cdot\mathbf{v}) + \eta\mathbf{j}^2\,. \tag{3.5}$$

Here ρ is the gas density, $\mathbf{v}$ is the gas velocity, p the gas pressure, $\mathbf{g}$ the gravitational acceleration vector, $\mathbf{j}$ the electric current density, $\mathbf{B}$ the magnetic field (or, more precisely, the magnetic induction), C_V the specific heat of the gas at constant volume, T the temperature, K the thermal conductivity, $\mathbf{F}_R$ the radiative energy flux and η the electrical resistivity. Note that when deriving Equation (3.5) the internal energy density was represented by $e = C_V\rho T$. This expression takes into account the internal structure of the constituent particles of the gas: excitation and ionization energy of atoms and the electronic, rotational and vibrational excitation energies and the disassociation energy of molecules. The neglect of the viscosity ν is justified for most purposes by its small value in the solar photosphere, $\nu \approx$

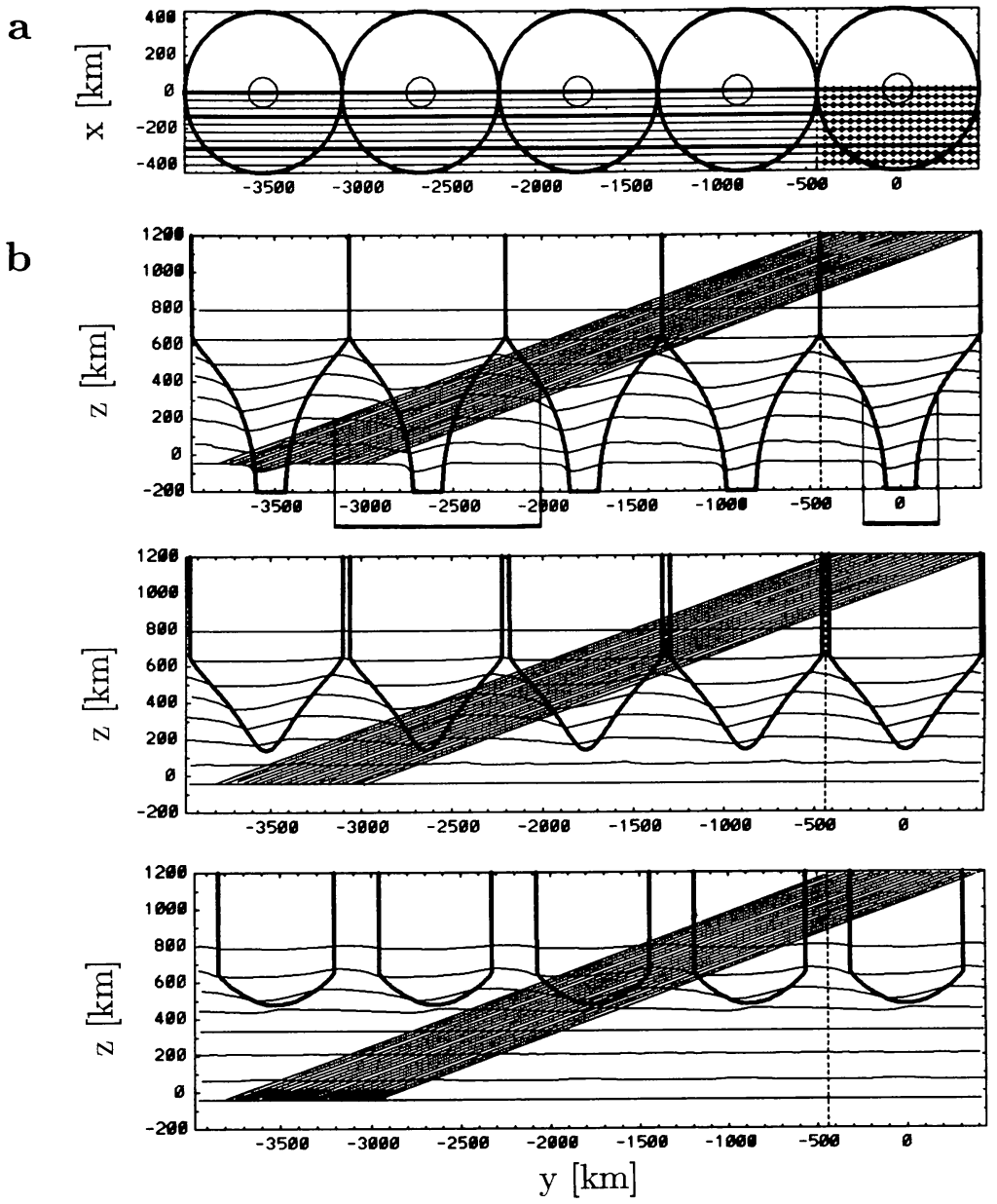

Fig. 3.1. Illustration of the model geometry for Stokes profile calculations near the solar limb in a 2-D model of an array of axially symmetric flux tubes. **a** An array of merged flux tubes as seen from above (thick circles). The thin circles outline the flux tube boundary at $z = -200$ km ($z = 0$ corresponds to $\tau = 1$ at disc centre in the quiet sun). Each horizontal line is the projection of a vertical plane cutting the model (the thick lines represent the planes shown in Figure 3.1b). Each point to the right of the dashed line is the entry point into the top of the model of a ray lying in one of the vertical planes. **b** Illustration of the three vertical cuts indicated in Figure 3.1a. The first frame represents the plane of symmetry (uppermost thick line in Figure 3.1a), while the middle and bottom frames correspond to the middle and lowest thick lines in Figure 3.1a, respectively. The rays entering the model to the right of the dashed line for an "observation" close to the solar limb ($\theta = 70°$, i.e. $\mu = 0.34$) are visible as the group of slanted parallel lines. Due to the periodicity of the flux tubes in the considered model, this set of rays is representative for all observations, except those with spatial resolution better than $\approx 0.5''$. The thick lines are the contours where the flux tubes intersect the vertical planes. The thin, almost horizontal lines represent surfaces of equal optical depth τ, in steps of $\Delta \log \tau = 1$ from $\log \tau = -6$ to $+1$. Note that each ray passes through a flux tube boundary at least once (from Bünte *et al.* 1991).

$10^3 - 10^4$ cm^2 s^{-1} (Kovitya and Cram 1983), but see the arguments presented by Cowley (1990) in favour of the importance of a second viscosity (due to the internal binding energy of electrons and the finite relaxation time characterizing the exchange of the translational energy of electrons). The MHD equations including viscosity may be found in, e.g., Deinzer *et al.* (1984a).

Further equations are required to close the system (3.3)–(3.5). These include the remaining Maxwell equations for quasistationary electromagnetic fields (i.e. neglecting $\frac{1}{c}\,\partial\mathbf{E}/\partial t$ terms),

$$\nabla \times \mathbf{B} = \frac{4\pi}{c}\mathbf{j}\,, \tag{3.6}$$

$$\nabla \times \mathbf{E} = -\frac{1}{c}\frac{\partial \mathbf{B}}{\partial t}\,, \tag{3.7}$$

$$\nabla \cdot \mathbf{B} = 0\,, \tag{3.8}$$

and Ohm's law (also neglecting viscous terms)

$$\mathbf{j} = \frac{1}{\eta}\left(\mathbf{E} + \frac{1}{c}\mathbf{v} \times \mathbf{B}\right)\,. \tag{3.9}$$

Note that in a time dependent problem, $\nabla \cdot \mathbf{B} = 0$ need be specified only as an initial condition. It can be shown by taking the divergence of Equation (3.7) that Equation (3.8) is then satified for all times.

Another equation required to close the set is the equation of state. The ideal gas law is generally adequate in the solar atmosphere.

$$p = \frac{k}{m_p}\rho T, \tag{3.10}$$

where k is Boltzmann's constant and m_p is the mean particle mass.

In Equations (3.3)–(3.10) K, η, C_V and m_p are material properties, and in general depend on gas or electron density, temperature, etc. Their determination often requires the calculation of the complete ionization and excitation equilibria of all the atomic and molecular species in the solar atmosphere. The radiative energy flux $\mathbf{F}_R$ still remains unaccounted for. It is related to the radiative intensity I_ν through

$$\mathbf{F}_R = \iint \mathbf{e}\, I_\nu \, d\Omega \, d\nu\,, \tag{3.11}$$

where $\mathbf{e}$ is a unit vector describing the direction of the net radiative energy flow, $d\Omega$ is a solid-angle element and $d\nu$ is a frequency element. I_ν is in turn determined by solving the radiative transfer equation. Since the presence of magnetic fine structure often causes the geometry to depart from being plane-parallel, multi-dimensional radiative transfer must be carried out to determine $\mathbf{e}I_\nu$. A common simplification is

to assume a form for the radiative flux term similar to that of the thermal conduction term:

$$\mathbf{F}_R = -K_R \nabla T, \tag{3.12}$$

where K_R is the radiative conductivity or diffusivity. This so-called diffusion approximation is valid at large optical depths, i.e. in the solar interiour, but cannot be reliably used in the solar atmosphere for layers with $\log \tau \lesssim -1$, where τ is a mean optical depth (e.g. based on the Rosseland mean opacity).

Before considering simplifications of the MHD equations, it is instructive to rewrite Equation (3.4), i.e. the momentum conservation or force balance equation, after substituting the current density using Equation (3.6),

$$\rho \left(\frac{\partial \mathbf{v}}{\partial t} + (\mathbf{v}\nabla) \cdot \mathbf{v} \right) = -\nabla (p + \frac{B^2}{8\pi}) + \rho \mathbf{g} + \frac{1}{4\pi} (\mathbf{B} \cdot \nabla)\mathbf{B}. \tag{3.13}$$

The action of the magnetic field has been split into two terms, a magnetic pressure term $\nabla B^2/8\pi$ and a magnetic tension term $(\mathbf{B} \cdot \nabla)\mathbf{B}/4\pi$. In small-scale magnetic features the former is generally the dominant term and the curvature force may for many purposes be neglected. For larger features, like pores or sunspots, and in the solar chromosphere both terms are important.

By combining Equations (3.6), (3.7) and (3.9), $\mathbf{E}$ and $\mathbf{j}$ may be eliminated. The resulting equation is called the induction equation,

$$\frac{\partial \mathbf{B}}{\partial t} = \nabla \times (\mathbf{v} \times \mathbf{B}) + \frac{\eta c^2}{4\pi} \nabla^2 \mathbf{B},$$

and is central to dynamo theories describing the generation of the solar magnetic field (cf. Parker 1979a, Priest 1982, Schüssler 1983, Stix 1990).

One way of simplifying the MHD equations is to neglect radiation, thermal conduction and Joule heating in Equation (3.5), so that only flows transport energy. In this ideal MHD case, Equation (3.5) reduces to

$$\frac{\partial}{\partial t}(p\rho^{-\gamma}) + (\mathbf{v} \cdot \nabla)(p\rho^{-\gamma}) = 0. \tag{3.14}$$

This adiabatic approximation provides a poor description of magnetic structures in the solar photosphere, although it describes some of their dynamics to first order.

In some situations the energy transport due to radiation, or, for some plasmas, conduction may be considerably more important than the dynamics of the gas. Such cases, for example the stable phases of flux tubes, may be described by the magnetohydrostatic (MHS) approximation. The MHS equations can be obtained by setting $\mathbf{v} = 0$ and $\partial/\partial t = 0$ in Equations (3.3) – (3.10).

$$-\nabla (p + \frac{\mathbf{B}^2}{8\pi}) + \rho \mathbf{g} + \frac{1}{4\pi} (\mathbf{B} \cdot \nabla)\mathbf{B} = \mathbf{0}\,, \tag{3.15}$$

$$\nabla(K\nabla T) - \nabla \cdot \mathbf{F}_R + \eta \mathbf{j}^2 = 0\,, \tag{3.16}$$

$$\nabla \cdot \mathbf{B} = 0\,, \tag{3.17}$$

$$p = \frac{k}{m_p}\rho T\,. \tag{3.18}$$

In Equation (3.16), $\mathbf{j}^2$ may be expressed in terms of $\mathbf{B}$ using Equation (3.6). In addition to these equations the condition of pressure equilibrium across any magnetic boundary with the coordinates $\mathbf{x}_b$, e.g. between a magnetic m and a non-magnetic n component of the atmosphere, must be fulfilled,

$$\frac{B_m^2}{8\pi}(\mathbf{x}_b) + p_m(\mathbf{x}_b) = p_n(\mathbf{x}_b). \tag{3.19}$$

3.3. Magnetohydrostatic Equilibrium of Flux Tubes

The magnetic field in the solar interiour and in the lower solar atmosphere is concentrated into discrete structures having a strong magnetic field, surrounded by a relatively field-free atmosphere. Although in reality the magnetic flux concentrations are probably devoid of symmetry (like most sunspots), for computational expedience they have generally been modelled as axially symmetric tubes or translationally symmetric slabs (with an additional mirror symmetry).

Even for these idealized geometries the exact solution of the MHS equations can be a complex numerical undertaking and further simplifications have often been introduced. A few of these are described below. The subject has been reviewed with great insight by Schüssler (1986) for small flux tubes and by Pizzo (1987) mainly for sunspots. The equilibrium of flux tubes has also been discussed in the monographs by Parker (1979a) and Priest (1982).

3.3.1. Radial Expansion: The Thin-Tube Approximation

This approach assumes that the width of a flux tube is small compared to the scale of the vertical stratification, e.g. the pressure scale height,

$$H_p = \frac{kTR_\odot^2}{Gm_pM_\odot} = \frac{p}{\rho g}\,, \tag{3.20}$$

where $R_\odot$ and $M_\odot$ are the solar radius and mass and G is the gravitational constant. Then, for an axisymmetric flux tube in cylindrical coordinates, all the dependent variables can be expanded in a Taylor series according to the radial coordinate r (Ferriz Mas and Schüssler 1989):

$$f(r,z) = \sum_{n=0}^{\infty} \frac{r^n}{n!}\left(\frac{\partial^n f}{\partial r^n}\right)\Big|_{r=0}\,. \tag{3.21}$$

Here f represents each dependent variable in turn, i.e. B, p, T, ρ, etc. These expansions are introduced into Equations (3.15)–(3.18). An approximate set of

equations can be found by neglecting all terms higher than a certain order. The simplest set of equations is obtained if only zeroth order terms are included (Defouw 1976). This is referred to as the thin-tube or slender-tube approximation.

$$\frac{B^2(z)}{8\pi} + p_m(z) = p_s(z)\,, \tag{3.22}$$

$$\frac{dp_{m,s}}{dz} = \rho_{m,s} g\,, \tag{3.23}$$

$$\pi R^2(z) B(z) = \Phi = \text{const}\,, \tag{3.24}$$

$$p_{m,s} = \frac{k}{m_p} \rho_{m,s} T_{m,s}\,, \tag{3.25}$$

$$\nabla \cdot (K \nabla T) - \nabla \cdot \mathbf{F}_R = 0. \tag{3.26}$$

Index m describes quantities within the magnetic flux tube, index s describes quantities in the non-magnetic surroundings. R, the radius of the tube, has to be small compared to H_p for Equations (3.22)–(3.36) to be valid. Note that in this approximation magnetic curvature terms are completely neglected (i.e. force balance reduces to pressure balance) and the vertical and horizontal components of the pressure balance decouple from each other. Equation (3.26) looks similar to Equation (3.16), but now all radial derivatives are zero except at $r = R$. The infinitely sharp boundary in the thin-tube approximation implies $\eta = 0$. Strictly in zeroth order $B = B_z$ and $B_r = 0$, where B_z is the vertical and B_r the radial component of the field. In first order, B_z and B_r may be obtained as follows:

$$B_r = -\frac{r}{2} \frac{dB}{dz}\,, \tag{3.27}$$

$$B_z^2 + B_r^2 = B^2\,. \tag{3.28}$$

If terms up to 2nd order are kept, then the lowest order approximation that includes curvature forces is obtained. Equation (3.15) then reduces to an ordinary (but still non-linear) differential equation of the same form as the one describing similarity solutions (Sect. 3.3.3). However, unlike in similarity solutions, the radial dependence of **B** is not self-similar in shape.

3.3.2. Force-Free and Potential Fields

Equation (3.15) can also be rewritten as

$$-\nabla p + \frac{1}{4\pi} (\nabla \times \mathbf{B}) \times \mathbf{B} + \rho \mathbf{g} = \mathbf{0}\,. \tag{3.29}$$

If the magnetic field is sufficiently strong to dominate over the other forces then the force-free approximation

$$(\nabla \times \mathbf{B}) \times \mathbf{B} = \mathbf{0} \tag{3.30}$$

becomes valid. For the interiour of a magnetic flux tube this condition is fulfilled if the plasma β is sufficiently small, i.e.

$$\beta = \frac{8\pi p}{B^2} \ll 1\,. \tag{3.31}$$

Small-scale magnetic fields are expected to fulfill this condition in practically all the observable layers. Note that no assumptions regarding the field geometry need be made in order to derive Equation (3.30), although the presence of a magnetic boundary does impose additional constraints. If, in addition, the current **j** vanishes then it follows from Equation (3.6) that

$$\nabla \times \mathbf{B} = 0 \tag{3.32}$$

and consequently

$$\mathbf{B} = -\nabla\varphi\,, \tag{3.33}$$

where φ is a scalar potential and the resulting **B** is called a potential field. The field in a flux tube can be potential if it is axially symmetric and untwisted. Potential fields fill the whole atmosphere unless bounded by a current sheet. A potential field bounded by a current sheet and in approximate pressure balance with the surroundings provides a relatively good approximation of the magnetic structure of a flux tube. In fact, a thin tube has a potential field in its interiour.

A method of finding the boundary between a potential field and the external field-free atmosphere for arbitrary pressure stratifications (i.e., a solution of the free boundary problem) has been developed by Schmidt and Wegmann (1982). All potential field models are strictly static, since they do not allow a coupling to wave modes except in the boundary current sheet.

3.3.3. Self-Similar Fields

The basic idea of similarity solutions is to reduce Equation (3.29) to an ordinary differential equation by specifying the cross-sectional shape of the magnetic field distribution within an axisymmetric flux tube. The relative shape remains the same at all heights (Schlüter and Temesvary 1958), explaining why such solutions are called self-similar. The B_z and B_r components take the form:

$$B_z = f(r/R(z))B_0(z)\,, \tag{3.34}$$

$$B_r = -\frac{r}{2}f(r/R(z))\frac{dB_0}{dz}(z)\,, \tag{3.35}$$

where B_0 is the field strength at the flux-tube axis and $R(z)$ is the radius of the tube. $R(z)$ is determined by magnetic flux conservation. The shape of the function f may be freely chosen, as long as $f \neq 0$ for $r/R < 1$ and $f = 0$ for $r/R > 1$. The choice $f(r/R) = 1$ for $r/R < 1$ results in the thin tube approximation. For a

non-constant $f(r/R)$ Equation (3.29) reduces to the following ordinary differential equation

$$B_0'' - \frac{1}{2B_0}(B_0')^2 - q(B_0^2 - 8\pi\Delta p) = 0\,, \tag{3.36}$$

where a prime denotes d/dz, B_0 is the field strength at the axis of the flux tube, q is a constant depending on the choice of f, and Δp is the pressure difference between the surroundings and the flux tube. An azimuthal component of the field B_θ may also be introduced (Yun 1971). It simply adds another term to Equation (3.36).

3.3.4. Solution of the Full Magnetohydrostatic Force Balance

There are basically two approaches to solving this problem, a relaxation approach and a direct (iterative) solution of the MHS equations. In the former approach, a solution of the time-dependent MHD equations (3.3)–(3.9) is developed from an initially prescribed state until a static, or stationary (or possibly oscillatory) state is achieved. Details of this approach are given by Deinzer *et al.* (1984a,b).

Most of the direct solutions of Equation (3.14), or of the set (3.14)–(3.17), make use of the formalism described by Low (1975). He expresses magnetostatic equilibrium of an axisymmetric poloidal field in terms of a scalar potential ψ (flux function)

$$\frac{\partial^2\psi}{\partial r^2} - \frac{1}{r}\frac{\partial\psi}{\partial r} + \frac{\partial^2\psi}{\partial z^2} = -4\pi r^2 \left.\frac{\partial p}{\partial\psi}\right|_z . \tag{3.37}$$

The ψ = const curves describe the field lines of the system. The vertical and radial field components may then be expressed in terms of ψ as

$$B_z = \frac{1}{r}\frac{\partial\psi}{\partial r}, \qquad B_r = -\frac{1}{r}\frac{\partial\psi}{\partial z}\,.$$

The case of the twisted flux tube has also been studied (Low 1975, Steiner *et al.* 1986). Methods for the iterative numerical solution of Equation (3.37) have been developed by Pizzo (1986) and Steiner *et al.* (1986). The latter authors have also included a boundary current sheet and twist in their treatment. Pizzo (1990) has applied multigrid methods to the solution of Equation (3.37), cf. Cally (1991), in order to accelarate the computations.

3.4. Flux Tube Waves

Flux tube waves are simplest to describe in the thin tube approximation. In this approximation three wave modes can travel along the tube, a torsional Alfvén wave, a longitudinal magneto-acoustic wave (tube wave or sausage mode) and a transverse wave (kink mode). The three wave modes are illustrated for an unstratified medium in Figure 3.2.

Consider now the more realistic, but still highly idealized situation of linear thin-flux-tube waves in a stratified, but isothermal atmosphere. Then the pressure

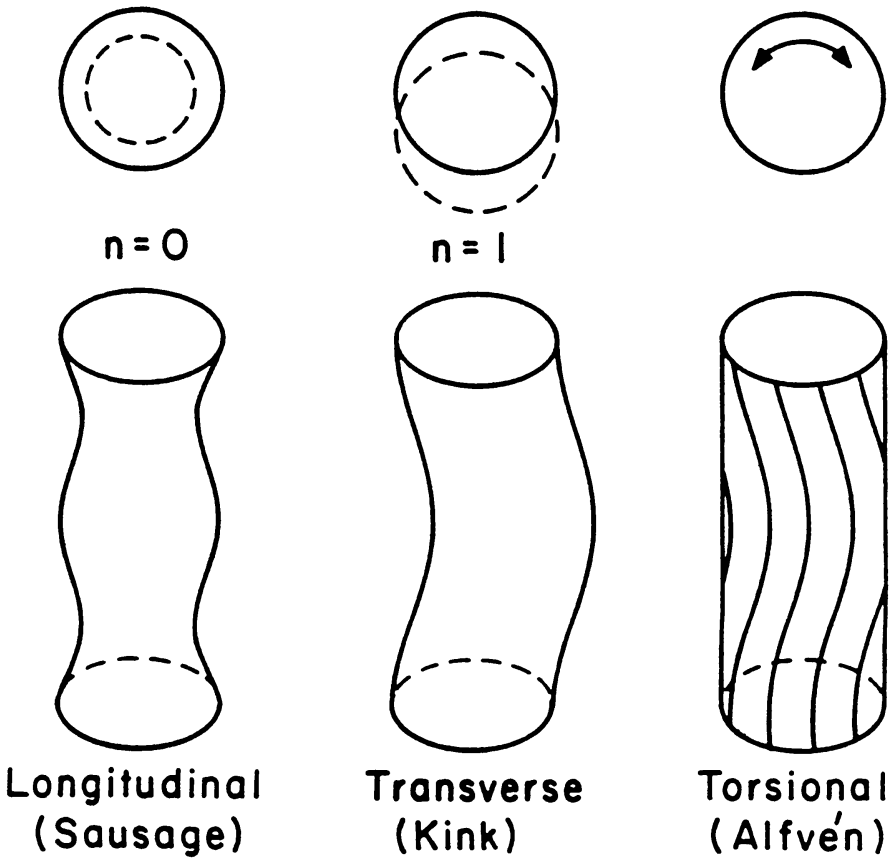

Fig. 3.2. Illustration of the three basic wave modes in a thin, cylindrical and unstratified flux tube (adapted from Thomas 1985)

scale height, H_p, is the same in the magnetic and the non-magnetic parts of the atmosphere and the static, vertical flux tube may be described as

$$p_m(z) = p_{m0} \exp(-\frac{z}{H_p}) = \frac{p_{m0}}{p_{s0}} p_s \,, \tag{3.38}$$

$$B(z) = B_0 \exp(-\frac{z}{2H_p}) = \sqrt{8\pi(p_{s0} - p_{m0})} \exp(-\frac{z}{2H_p}) \,, \tag{3.39}$$

$$R(z) = R_0 \exp(\frac{z}{4H_p}) = \sqrt{\frac{\Phi}{\pi B_0}} \exp(\frac{z}{4H_p}) \,, \tag{3.40}$$

where subscript 0 signifies the value of a quantity at $z = 0$. It may be seen from Equations (3.39) and (3.40) that the field strength decreases exponentially with height, while the flux tube radius increases exponentially. The wave is treated as a small perturbation of the static flux tube. Assuming adiabaticity and small velocity amplitudes compared to the propagation velocity of the waves (i.e. linear waves) we can write the velocity as

$$v(z,t) = v_0 \exp\left(\frac{z}{4H_p}\right) \exp i(\omega t - kz) \,, \tag{3.41}$$

where ω is the frequency and k the wavenumber of the wave. For a damped wave, k is generally complex. The factor $\exp(z/4H_p)$ in Equation (3.41) can be obtained quite simply by imposing energy conservation. Then $\rho_m(z)v^2(z)R(z) = \text{constant}$, where ρ_m is the gas density in the flux tube. Since the stratifications of ρ and R are known, $v(z)/v_0$ can be easily derived. This equation is valid for all three wave modes, but the interpretation of $v(z,t)$ depends on the wave mode. For the Alfvén mode v is the torsional velocity, for tube waves v is the longitudinal velocity (i.e. directed parallel to the field) and for kink mode waves it is a radial velocity.

The Alfvénic torsional mode has a linear dispersion relation,

$$\omega = v_A k\,, \tag{3.42}$$

where ω is the frequency, k is the wave number and v_A is the Alfvén speed,

$$v_A = \frac{B}{\sqrt{4\pi\rho}}\,. \tag{3.43}$$

The two other wave modes have quadratic dispersion relations,

$$\omega^2 = C_T^2 k^2 + \omega_{c,T}^2 \tag{3.44}$$

for longitudinal tube waves and

$$\omega^2 = C_K^2 k^2 + \omega_{c,K}^2 \tag{3.45}$$

for kink waves. Here

$$C_T = \frac{C_S v_A}{\sqrt{C_S^2 + v_A^2}} \tag{3.46}$$

is the tube speed, i.e. the propagation velocity of tube waves with frequencies well above the cutoff frequency $\omega_{c,T}$, $C_S = \gamma p/\rho$ is the sound speed (γ is the ratio of specific heat capacities) and

$$C_K = \sqrt{\frac{\rho_m}{\rho_m + \rho_s}}\, v_A = \frac{B}{\sqrt{4\pi(\rho_m + \rho_s)}} \tag{3.47}$$

is the propagation velocity of kink waves for sufficiently large frequencies compared to the cutoff frequency $\omega_{c,K}$. The frequencies $\omega_{c,T}$ and $\omega_{c,K}$ are expressed in terms of the acoustic cutoff frequency $\omega_{c,S}$ in Equations (5.3) and (5.4). Note that $C_K < v_A$, $C_T < v_A$ and $C_T < C_S$. The interaction between a kink mode travelling along a flux tube and the external atmosphere is obvious, and is taken into account in Equation (3.47) through the presence of ρ_s in the denominator. The tube mode also interacts with the non-magnetic atmosphere through the 'breathing' motions of the flux tube. This interaction has been neglected in the derivation of the above equations.

The longitudinal tube wave was first studied by Defouw (1976) and Roberts and Webb (1978), while the kink mode has been investigated by Spruit (1981b).

4. Diagnostic Techniques

4.1. Introduction

One important aim of observationally oriented solar-physics research is to derive empirical information on physical variables, solar features and processes. However, the observational data are generally influenced by many physical parameters and processes on the sun, by the earth's atmosphere and by the instrument. Therefore, we must choose the data and diagnostics (i.e. the method of information extraction) with care, so as to separate the influence of the parameter or process of interest from the rest.

Examples of quantities on which we require information are the magnetic field strength B, the angle γ between the field and the line of sight (LOS), the azimuthal angle χ of the field (B, γ and χ describe the full magnetic vector **B**), the magnetic flux Φ, the velocity vector **v**, temperature T, gas pressure p and elemental abundances ϵ. On the sun most of the above quantities are a function of space and time. For example, an accurate knowledge of $\mathbf{B}(x, y, z, t)$ (x and y are coordinates parallel to the solar surface, z is the vertical coordinate and t denotes time) would allow a number of the fundamental unanswered questions of solar physics to be resolved. It would show how magnetic fields are distributed on the solar surface and provide an indication of how they are swept around by convection. It would allow sizes and lifetimes of magnetic features to be determined and the processes leading to their creation and destruction to be analysed in detail, e.g. emergence, submergence, reconnection and fragmentation of magnetic flux on time scales ranging from that of a flare to that of the evolution of a whole active region. It could confirm or refute current theoretical ideas on magnetic flux concentration (convective collapse) and confinement (pressure balance). It should allow a determination of the anchoring depth of the magnetic field lines, and much more. Similarly, a knowledge of $T(x, y, z, t)$ would be ideal to put our understanding of the energy budget of the solar atmosphere on a solid foundation.

Unfortunately, it is at present impossible to carry out the ideal observation which would determine, e.g., the magnetic field vector with sufficient spatial and temporal resolution and coverage, as well as a sufficiently large spectral resolution and range (cf. Harvey 1985, 1986, for the specifications of an "ideal" instrument which may realistically be constructed with present technology). It is therefore particularly important to develop and apply techniques aimed at extracting the maximum of information from a given data set within the constraints and trade-offs of the real world. Such techniques are the subject of the current section.

In the following I have ordered the diagnostics according to the physical quantity they provide information on. However, since many of the diagnostics used currently and in the past are indirect (e.g. sizes of magnetic elements have often been identified with the sizes of bright points) I discuss sizes, shapes, morphology and evolution of magnetic features separately.

Previous critical compilations of diagnostic techniques related to solar magnetic

features are relatively rare, examples being overviews by Stenflo (1976, 1978), Landi Degl'Innocenti (1985) and Semel (1986). Most of the numerous reviews related to small-scale solar magnetic fields have concentrated on presenting results.

4.2. Magnetic field strength

The measurement of the magnetic field strength on the sun has attracted considerable interest and a variety of techniques have been developed specifically to this end. Techniques of field strength determination have been reviewed by Stenflo (1976, 1977, 1978), Harvey (1977a), Landi Degl'Innocenti (1985b) and Semel (1986). Here I discuss mainly diagnostics based on Zeeman splitting. Hanle effect diagnostics and their application to solar magnetic fields have been reviewed by Leroy (1985, 1988), Démoulin (1990), Kim (1990), Stenflo (1991a) and Faurobert-Scholl (1992c). The reviews of the Hanle effect, with the exception of those by Stenflo and Faurobert-Scholl, concentrate mainly on applications to prominences.

To bring some kind of order into the list of various methods, while attempting to keep the discussion general, i.e. not restricting it too strongly to a given type of magnetic feature, I shall break it up into a number of cases according to the values of the parameters α, the filling factor, and $\Delta\lambda_H/\Delta\lambda_D$, the Zeeman sensitivity.

The ratio of the Zeeman splitting $\Delta\lambda_H$ to the "Doppler" width $\Delta\lambda_D$ of the line, $\Delta\lambda_H/\Delta\lambda_D$, is a measure of the sensitivity of a particular line to a given field strength. $\Delta\lambda_H$ is given by

$$\Delta\lambda_H = kgB\lambda^2, \tag{4.1}$$

where g is the Landé factor (for lines with anomalous Zeeman splitting, g must be replaced by the effective Landé factor, g_{eff}), B is the field strength, λ is the wavelength of the line and $k = e/4\pi mc^2 = 4.6686 \times 10^{-13}$ for B in Gauss and λ in Å. $\Delta\lambda_D$ is the total half-width of the line in the absence of a field. It includes broadening due to temperature (Doppler broadening), line saturation, turbulent or other non-stationary velocities, velocity gradients, limited instrumental spectral resolution and, for disc integrated spectra of the sun or other stars, solar (stellar) rotation. Thus, $\Delta\lambda_D$ corresponds to the width of a $g = 0$ line which is otherwise identical to the considered line.

For a given atmosphere (i.e. for a given B, turbulence velocity etc.), $\Delta\lambda_H/\Delta\lambda_D$ is proportional to the Landé factor and the wavelength of the line, while being inversely proportional to its width, which, other things being equal, is determined by the amount of line saturation. $\Delta\lambda_H/\Delta\lambda_D$ only increases approximately linearly with λ, since $\Delta\lambda_H \sim \lambda^2$, while $\Delta\lambda_D$ is approximately proportional to λ. Ideally, one would have to observe a weak (unsaturated) line with large g in the far infrared to obtain maximum Zeeman sensitivity. However, this may not always be possible or desirable. For example, detectors are more efficient and easier to employ in the visible and the near infrared. Also, lines in the far infrared are formed higher in the atmosphere, where field strengths often are smaller.

$\Delta\lambda_H/\Delta\lambda_D$, besides being a function of the spectral line and the field strength, is partly also affected by the thermodynamics. The temperature changes the line strength and saturation and thus $\Delta\lambda_D$. Similarly, a velocity can also affect $\Delta\lambda_D$. For the purposes of the following discussion it is sufficient to divide the $\Delta\lambda_H/\Delta\lambda_D$ parameter range into 3 regimes: the weak field case of $\Delta\lambda_H \ll \Delta\lambda_D$, the strong field case of $\Delta\lambda_H \gg \Delta\lambda_D$ and the intermediate case when $\Delta\lambda_H \approx \Delta\lambda_D$,

Figure 2.2 illustrates the 3 regimes. In the weak field case ($B \lesssim$ 400–600 G in this example), Stokes I remains almost unaffected and Stokes Q, U and V also remain almost unchanged except for a growth in amplitude as $\Delta\lambda_H$ increases. In the strong field case ($B \gtrsim$ 1400–2000 G in this example), the amplitude of the the σ components remains independent of $\Delta\lambda_H$, but their separation increases linearly with $\Delta\lambda_H$. The intermediate case exhibits the transition from one type of behaviour to another.

Every diagnostic requires some underlying model assumptions on which the extracted information is crucially dependent. Here three types of models are considered. Model I assumes that the magnetic features are adequately described by a simple 1-D 2-component model. The first component covers a fraction α of the surface and has a height independent field strength B. The other component covers the remaining surface $(1-\alpha)$ and has no field. In Model II a field is present in both components: $B_1 \neq 0$ and $B_2 \neq 0$ cover fractions α and $1-\alpha$, respectively. It is straightforward to extend this model to the more general case of an n-component model (cf. Stenflo 1968, who has discussed n-components in detail). Both B_1 and B_2 are assumed to be independent of height. Finally, Model III introduces a height dependent magnetic field strength. The angles γ and χ are assumed to be uniform in Models I and II.

When discussing Model I, it is not only necessary to separate the different $\Delta\lambda_H/\Delta\lambda_D$ regimes, but also to distinguish between a spatially resolved magnetic feature (i.e. $\alpha = 1$ in the spatial resolution element of the observations) and the spatially unresolved case, i.e. $\alpha < 1$ in the resolution element. The boundary between these two cases is a fuzzy one. The magnetic field in sunspots is generally considered spatially resolved, but often, in particular for umbral measurements involving Stokes I, scattered light can be a major problem not to be underestimated, as dramatically demonstrated by Brants and Zwaan (1982). Therefore, for the measurement of umbral B values either purely umbral lines, i.e. lines which are very weak outside the umbra, or measurements in polarized light should be used. Similarly, scattered light and the magnetic fine structure (e.g. Degenhard and Wiehr 1991) also pose problems for penumbral measurements, so that Stokes Q, U and V again have advantages over Stokes I. The condition $\alpha = 1$ is thus never strictly valid in the solar photosphere, but is often fulfilled to a high degree.

4.2.1. Model I: 2-Component Model, with One Field-Free Component

4.2.1.1. *Case I: $\Delta\lambda_H \gg \Delta\lambda_D$, $\alpha \approx 1$: Spatially Resolved Strong Field.* On the sun the applicability of this case is restricted to sunspots and pores (the latter if

the spatial resolution is sufficiently high). Note that due to the presence of a π component, Stokes I, Q and U are completely split only if $\Delta\lambda_H \gtrsim 2\Delta\lambda_D$. The field strength may be determined directly from the wavelength difference, $2\Delta\lambda_H$, between the minima of the two σ components of Stokes I of a Zeeman triplet or from the σ maxima of its $|V|$, $|Q|$ or $|U|$ profiles. Anomalously Zeeman split lines may also be used, but the wavelength of the centre-of-gravity of the σ components must be used instead. The centre-of-gravity wavelengths of the σ components also give an average value of the field strength if it varies horizontally or vertically within the spatial resolution element. However, note that the measurement of the centre-of-gravity requires that the whole profiles of the π and σ components are unblended. If the splitting is not complete then the measured wavelength shift of the centre-of-gravity of the Stokes I σ components underestimates B, while the corresponding measurements of the Stokes V, Q or U profiles overestimates B. Instead of taking the centre-of-gravity of the σ components it is also possible and generally recommended to fit the observed line profiles with calculated profiles (e.g., obtained from the Milne-Eddington model, or by numerically solving the transfer equation, or, for a Zeeman triplet, by representing each σ-component by a Gaussian). This avoids the problems associated with interpreting minimum or centre-of-gravity wavelengths in terms of B.

Another possible technique involves the difference between the centre-of-gravity wavelengths of $I+V$ and $I-V$ (note the difference to the centre-of-gravity mentioned above). However, this so-called centre-of-gravity technique (Rees and Semel 1979, see Case III below) only gives the longitudinal component, $B\cos\gamma$, of the magnetic field even for completely split lines.

In order to obtain unique results it is necessary to observe the full line profile. When choosing a line for such observations, care should be taken that the continuum on both sides of the line, as observed in the quiet sun, is clean, since the splitting may cause previously unblended neighbouring lines to blend with the σ components of the strongly split line. Even this precaution may not be sufficient, since a piece of clean continuum in the quiet sun may become strongly contaminated by molecular lines in sunspot umbrae. For example, compare the various spectra in Figure 1 of Livingston (1991).

4.2.1.2. *Case II: $\Delta\lambda_H \gg \Delta\lambda_D$, $\alpha < 1$: Spatially Unresolved Strong Field.* Case II is encountered in many different types of features on the sun, but only spectral lines in the infrared (at 1.5 μm and beyond) are sufficiently Zeeman sensitive to be completely split outside of sunspot umbrae and pores. If only Stokes V, Q, or U are used then the field strength may be determined in exactly the same manner as for Case I. For sufficiently large α the wavelength difference between the Stokes I σ-components may also be used. However, in solar plages or network regions α is often so small that the σ components of Stokes I are too weak to be easily distinguished from the wings of the unsplit line, or from the weak blends (see Figure 4.1). Then, if no observations in polarized light are available, alternative

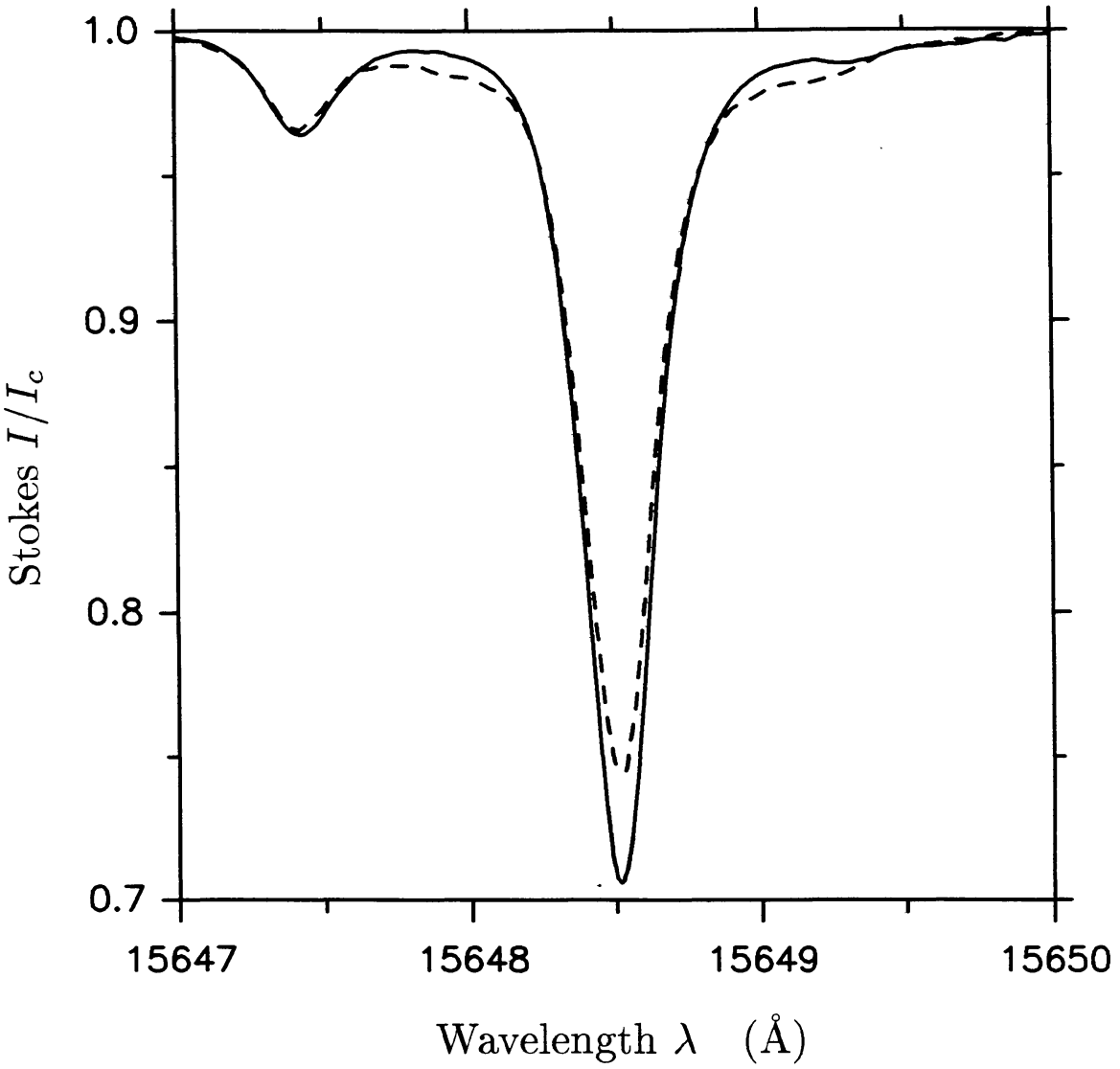

Fig. 4.1. High S/N (> 1000) Stokes I profiles of the $g = 3$ line Fe I 15648.5 Å observed in the quiet sun (solid profile) and in a network region with a magnetic filling factor of approximately 5% (dashed). The influence of the magnetic field and of the weak blends is of the same magnitude in the line wings, which effectively limits the reliability of the magnetic field measurements. The relatively large difference at line centre is partly due to line weakening caused by the different temperature in magnetic features.

Stokes I based techniques such as the one proposed by Robinson (1980, see Case VI) may be applied.

4.2.1.3. *Case III:* $\Delta\lambda_H \ll \Delta\lambda_D$, $\alpha \approx 1$*: Spatially Resolved Weak Field.* Observations of, e.g., upper chromospheric fields, or sunspot fields with low-g lines belong to this case. An estimate of $B\cos\gamma$ can be obtained from the centre-of-gravity technique (Semel 1967, 1971, Rees and Semel 1979, Semel 1986). The

centre-of-gravity wavelengths of the $I \pm V$ profiles are defined as

$$\lambda_{I\pm V} = \frac{\int (I_c - I \pm V)\lambda \, d\lambda}{\int (I_c - I \pm V) \, d\lambda}. \tag{4.2}$$

The difference between these two wavelengths is related to B by

$$|\lambda_{I+V} - \lambda_{I-V}| = 2kg_{\rm eff}\lambda_0^2 B \cos\gamma = 2\Delta\lambda_H \cos\gamma. \tag{4.3}$$

The centre-of-gravity wavelengths, $\lambda_{I\pm V}$, are integral quantities and thus relatively unaffected by noise. However, their difference is small for small αB values, so that the final result may be quite sensitive to noise (Zwaan 1989).

$B\cos\gamma$ can also be obtained from a comparison of V and $dI/d\lambda$ using Equation (2.12),

$$\frac{V(\lambda)}{dI(\lambda)/d\lambda} = kg_{\rm eff}\lambda_0^2 B\cos\gamma = \frac{\int_{\lambda_1}^{\lambda_0} V\,d\lambda}{\int_{\lambda_1}^{\lambda_0} (dI/d\lambda)d\lambda}. \tag{4.4}$$

The second equality of Equation (4.4) makes use of the fact that the first equality holds at every wavelength (except line centre) if $\alpha = 1$ and $\Delta\lambda_H$ is sufficiently small. Due to the derivative in the numerator, relatively noise-free Stokes I data are required in order to apply Equation (4.4).

Both techiques require only a single spectral line and are simple to apply (no radiative transfer or other explicit model calculations are required). Both methods only give a lower limit to the true field strength (e.g. in the extreme case of a transverse field both methods give $B = 0$). Note that both techniques are dangerous when applied to sunspot umbrae due to the problem of spatial stray light. It generally affects Stokes I more than Stokes V, thus violating one of the implicit assumptions underlying Equations (4.3) and (4.4), namely that I and V arise in the same solar region. This may be one of the reasons why Martínez Pillet *et al.* (1990) see no correlation between V and $dI/d\lambda$ of Ca II K in many sunspot umbrae. In order to determine the field inclination γ, which is required if the true field strength is to be obtained, observations of all four Stokes parameters are required. Therefore, a fit to the four Stokes parameters is probably the method of choice for obtaining the true field strength in this case (e.g. Auer *et al.* 1977, cf. Section 4.4). One particularly important application of this case is the upper solar chromosphere, where magnetic fields have expanded sufficiently to be relatively homogeneous. A nearly ideal spectral line for measuring upper chromospheric magnetic fields is He I 10830 Å. In addition to being formed in the weak-field limit in a homogeneous magnetic field, it is formed exclusively in the upper chromosphere and is optically thin (Avrett *et al.* 1992), so that the determination of the magnetic vector from the 4 Stokes parameters becomes particularly simple.

If the field is sufficiently weak, then it may be measured using the Hanle effect (Stenflo 1982, 1991a, Harvey 1986, Faurobert-Scholl 1991, 1992a, 1992b, cf. Section 2.5). In the Hanle weak-field limit, however, the influence of the magnetic field on the linear polarization via the Hanle effect strongly depends on the orientation of the field. If the magnetic vector is parallel to the direction of illumination (e.g. vertical in a plane-parallel atmosphere), then it does not affect the resonance polarization and remains invisible. Also, a field that is distributed symmetrically around the direction of illumination leads, at the most, to a depolarization, but not to a rotation of the plane of polarization (Stenflo 1982, Faurobert-Scholl 1992b).

4.2.1.4. *Case IV:* $\Delta\lambda_H \ll \Delta\lambda_D$, $\alpha < 1$*: Spatially Unresolved Weak Field.* Observations of intranetwork fields (if they are intrinsically weak), or the turbulent component of the photospheric field may correspond to this case. The Zeeman effect can only give upper and lower limits on the field strength in this case. Unfortunately, the limits tend to lie rather far apart. A rough *lower* limit is obtained by applying the methods described in Case III and assuming $\alpha = 1$. Equation (4.4) now gives $\alpha\delta_c\delta_l B\cos\gamma$ instead of simply $B\cos\gamma$. Here δ_c and δ_l are factors describing the respective ratios of continuum and line intensity in the magnetic region to the spatially averaged values. The results of Equation (4.3) are similarly affected, cf. Semel (1981). The best such limit is obtained using all four Stokes parameters and a temperature insensitive line. A generally large *upper* limit is obtained by assuming that $2\Delta\lambda_H = \lambda_r - \lambda_b$ ($\lambda_{b,r}$ are the wavelengths of the blue and red V maxima or centres-of-gravity). The best such limit is obtained by using an intrinsically narrow line with large Zeeman sensitivity (i.e. by maximizing $\Delta\lambda_H/\Delta\lambda_D$). If possible, lines with $\Delta\lambda_H \approx \Delta\lambda_D$ should be searched for, so that the diagnostics listed under Case VI may be applied. Another possibility is to improve the spatial resolution of the observations in the hope of reducing the problem to that of Case III. Again, as in Case III, the Hanle effect may be used to measure sufficiently weak fields.

4.2.1.5. *Case V:* $\Delta\lambda_H \approx \Delta\lambda_D$, $\alpha \approx 1$*: Spatially Resolved Magnetic Field of Intermediate Strength.* This case is encountered when, e.g., observing sunspot penumbrae with high-g lines in the visible. If only Stokes I is measured then there are two possible approaches. The first is based on the Robinson technique, the other on the Stenflo-Lindegren method. The technique developed by Robinson (1980) depends on the comparison of two lines with different Zeeman sensitivities, for one of which $\Delta\lambda_H \ll \Delta\lambda_D$, while for the other $\Delta\lambda_H \approx \Delta\lambda_D$. It is described in detail under Case VI (Method 4). It is relatively reliable for $\alpha \approx 1$, but loses accuracy if $\alpha \ll 1$.

One variant of the Robinson technique requires measurements of the line core only. Two almost identical lines (with almost equal W_λ and χ_e in the quiet sun which belong to the same element), but with different Landé factors, e.g. Fe I 5250.2 Å and Fe I 5247.1 Å, differ in a magnetic feature since the depths of the two

lines are differently affected by the magnetic field (Schüssler and Solanki 1988). The advantage of this technique over the other Stokes I-based methods is that it can be applied to filtergrams. On the other hand, it requires model calculations of the line profiles and is rather susceptible to noise and systematic affects (e.g. the exact continuum level in the spectra or weak blends in one of the lines). The technique has been extended to include the whole Stokes I profile by Sánchez Almeida and García López (1991). In this manner the model calculations can be dispensed with. Recently, Solanki and Brigljević (1992) have questioned the reliability of this technique when applied to Fe I 5250.2 Å and Fe I 5127.1 Å, with a hidden blend being the probable cause (see Livingston and Wallace 1985, Carter *et al.* 1992).

The Stenflo-Lindegren technique is also based on the comparison between lines with different Zeeman sensitivities. However, in this approach a large number of lines is used. To simplify the procedure only certain line parameters are considered instead of the complete line profiles. The most commonly used magnetically sensitive line parameter is the line width at a given intensity level, v_D. The influence of the non-magnetic parameters of the atmosphere and the atom on the line width must be removed before B is determined. The approach taken by Stenflo and Lindegren (1977) consists of empirically modelling the dependence of the line width on other line parameters by a multivariate regression equation. They assume that the influence of the thermodynamics of the atmosphere can be parameterized, for example, in the following manner,

$$v_D = x_0 + x_1 \frac{v_m^2 \lambda^2}{v_0} + x_2 \frac{\lambda^2}{v_0} + x_3 S + x_4 S^2 + x_5 \chi_e v_0. \tag{4.5}$$

Here S is the line strength, χ_e is the excitation potential, $x_0, \ldots, x_5$ are regression coefficients to be determined from a fit to the data,

$$v_0 = y_0 + y_1 S + y_2 S^2 \tag{4.6}$$

is an approximation of the line width, with y_0 and y_1 also being regression coefficients to be derived from the data (v_D itself is not used in order to achieve statistical independence), λ is the wavelength of the line and v_m is a measure of the Zeeman broadening,

$$v_m^2 = (g_{\text{eff}}^2 + X_\sigma) \frac{1 + \cos^2 \gamma}{2} + X_\pi \frac{\sin^2 \gamma}{2}. \tag{4.7}$$

Here X_π and X_σ are measures of the departures from the Zeeman triplet splitting pattern. They are zero for Zeeman triplets. Exact definitions of and formulae for X_π and X_σ have been given by Landi Degl'Innocenti (1985), Mathys and Stenflo (1987) and Mathys (1989).

With the help of Regression Equation (4.5), the influence of line strength (x_3 and x_4 terms), excitation potential (x_5 term) and wavelength (x_2 term) on the line width is empirically quantified and separated from the influence of the magnetic

field (x_1 term). Tests with many different forms of the regression equation have shown that Equation (4.5) reproduces the dependences shown by the data relatively well (Mathys and Solanki 1989). Once x_1 has been determined, a simple model, which assumes that the magnetic field affects the line profile in the same manner as a Gaussian macroturbulence (i.e. a convolution model of the Zeeman splitting), allows a straightforward determination of the field strength from x_1,

$$B = \frac{\sqrt{x_1}}{kc}, \tag{4.8}$$

where c is the speed of light and $k = e/4\pi mc^2$.

A more realistic model could involve calculating synthetic line profiles, determining x_i values from these synthetic spectra and comparing the synthetic x_i with the x_i obtained from the observations. The atmospheric parameters are then varied (in particular B) until the synthetic x_i correspond to the x_i derived from the data. Such a model takes into account such second-order effects as Zeeman desaturation (cf. Section 2.3).

Note that the derivation of Equation (4.7) assumes that $\Delta\lambda_H \lesssim \Delta\lambda_D$, so that this technique should not be applied to Cases I and II. For example, it loses some of its effectiveness for infrared H-band lines in a solar network region due to the relatively large splitting of the lines (Muglach and Solanki 1991, 1992). In this case it is better to use the approximation of complete splitting, although a regression still reduces the scatter. Another disadvantage of the regression technique is that it requires the measurement of many lines, so that it can only be used if Echelle grating or Fourier transform spectrometer (FTS) spectra are available. As can be seen from Equation (4.7), γ must either be known independently or assumed, as in all Stokes I based techniques. On the other hand, Stokes I is the Stokes parameter least affected by γ, so that this point might even be considered an advantage (for example, this technique is less γ dependent than the centre-of-gravity technique). Another advantage is that due to the large number of lines used, the influence on the result of noise and of blends to individual lines is smaller than for techniques based on few lines.

An alternative to the purely Stokes I based approaches is to use the centre-of-gravity technique (cf. Case III) to determine $B\cos\gamma$. This is simple and is not limited to small $\Delta\lambda_H$, but does not make full use of the information in the Stokes I and V profiles. All the Stokes V based techniques presented under Case VI should also work for the present case, in general even better than for the spatially unresolved fields. Finally, the field strength can be determined with great accuracy by the least-squares fitting procedure based on the Milne-Eddington model (Auer *et al.* 1977). A detailed description of the method, in the case when all 4 Stokes parameters are determined, is to be found in Section 4.4, cf. Case VI, Method 6. Even better are fits obtained using synthetic profiles resulting from numerical solutions of the transfer equations in realistic atmospheric models (Solanki *et al.* 1992b, Ruiz Cobo and Del Toro Iniesta 1992). Although this refinement ought not to

change the derived field strengths significantly, it is important to fix magnetic field gradients and take the thermodynamics and field geometry properly into account (Sections 4.3.2 and 4.9). However, these improvements are obtained at the cost of computational efficiency. The reliability of the least-squares fit can be improved if two lines with different Zeeman sensitivities, but otherwise similar properties, are used (see Methods 1 and 6 of Case VI below).

4.2.1.6. *Case VI: $\Delta\lambda_H \approx \Delta\lambda_D$, $\alpha < 1$: Spatially Unresolved Magnetic Field of Intermediate Strength.* Outside of sunspots this is the most common case on the sun and a number of techniques have been developed to deal specifically with it. Most observations of small-scale magnetic fields using high-g spectral lines in the visible are described by this case.

Method 1. Line ratio of two Stokes V profiles (Stenflo 1973, Wiehr 1978, Stenflo and Harvey 1985, Solanki *et al.* 1987, Sánchez Almeida *et al.* 1988a, Zayer *et al.* 1990): The technique is based on comparing the Stokes V profiles of two lines which are almost identical except for their sensitivity to the magnetic field. The magnetic line ratio (MLR) is defined as either the ratio r_V between the Stokes V profiles of the two lines at a given wavelength $\Delta\lambda$ from line centre ($\Delta\lambda = \lambda - \lambda_V$, where λ_V is the Stokes V zero-crossing wavelength),

$$r_V = \frac{g_{\mathrm{eff},2}}{g_{\mathrm{eff},1}} \frac{V_1(\Delta\lambda)}{V_2(\Delta\lambda)}, \tag{4.9}$$

or as the ratio R_V of the Stokes V amplitudes a_V,

$$R_V = \frac{g_{\mathrm{eff},2}}{g_{\mathrm{eff},1}} \frac{a_{V,1}}{a_{V,2}}. \tag{4.10}$$

The behaviour of the latter definition is somewhat simpler to interpret without model calculations. For weak fields ($\Delta\lambda_H \ll \Delta\lambda_D$ for both lines), R_V approaches unity if the two lines are equal in strength. For strong fields ($\Delta\lambda_H \gg \Delta\lambda_D$ for both lines) R_V approaches approximately the inverse ratio of the Landé factors of the lines, $g_{\mathrm{eff},2}/g_{\mathrm{eff},1}$, if both lines are Zeeman triplets and equally strong. For anomalously split lines, due to the splitting between the sub-components of each σ component, the V amplitudes of the lines do not saturate at a fixed value for strong fields but start decreasing again, after reaching a maximum. Therefore, the line ratio between most line pairs continues to change slightly with B, even for very high field strengths. However, the bulk of the variation takes place at intermediate field strengths. Then R_V varies smoothly from one limit to the other as B changes (note that R_V and r_V depend directly on B and to first order not on $\cos\gamma$). The behaviour of r_V is more involved and depends on $\Delta\lambda$. See Stenflo (1973, 1976) and Wiehr (1978) for a discussion.

To interpret the line ratio, a relation between R_V or r_V on the one hand and B on the other is needed, i.e. the MLR must be calibrated in terms of B. With

the exception of the analytical solution outlined below and the approach taken by Stenflo *et al.* (1987b), this calibration implies radiative transfer model calculations, either in the form of a Milne-Eddington, or of a numerical solution. The Milne-Eddington calibration turns out to be relatively accurate, at least for interpreting observations obtained near solar disc centre (compare e.g. the Milne-Eddington results of Stenflo and Harvey 1985 with the numerical results of Solanki *et al.* 1987). The sensitivity of R_V to various atmospheric and instrumental parameters has been investigated in detail by Solanki *et al.* (1987), Solanki (1987a) and Keller *et al.* (1990a). The two Fe I lines at 5250.2 Å ($g = 3$) and at 5247.1 Å ($g_{\text{eff}} = 2$) form an almost ideal line-pair for the MLR (Stenflo 1973).

Together with the profile fitting technique applied to 2 lines (Method 6, which may be considered to be a further development of the line-ratio technique), the MLR technique is the method of choice if the magnetic features are spatially unresolved and no completely split spectral lines can be observed. It has the advantage of accuracy, relative model independence (if both lines are thermodynamically sufficiently similar) and considerable sensitivity, as long as $\Delta\lambda_H$ is not too small or too large. Since its introduction by Stenflo (1973) it has been extended, considerably refined and extensively applied. The MLR can also be applied to the Stokes Q and U profiles (Solanki *et al.* 1987), which may have certain advantages over using Stokes V (cf. Section 4.2.2). Like all few-line techniques it suffers from its sensitivity to blends and noise. Also, it only works if the Zeeman splitting lies within a given range. To be completely accurate, the MLR technique requires γ to be known (Solanki *et al.* 1987, Grigoryev and Selivanov 1990).

One advantage of the MLR technique, and in particular of using r_V, is that it does not require the observation of the full profiles of the two lines, although their observation does increase the accuracy and reliability of the results considerably (particularly important are an accurate knowledge of $\Delta\lambda_D$ and of wavelength shifts between Stokes I and V). The MLR-technique has been successfully applied to Babcock- and filter-magnetograph data by Stenflo (1973), Frazier and Stenflo (1978), Wiehr (1985) and Keller *et al.* (1990b).

Sánchez Almeida *et al.* (1988a) have presented an analytical calibration of the MLR that allows the field strength to be derived without explicit radiative transfer calculations. For sufficiently similar lines, the Stokes V profiles of both lines can be expressed in terms of the unsplit profile in the magnetic atmosphere I_m (common to both lines) by a Taylor expansion according to λ (Equation 2.11),

$$V_{1,2} = \sum_{n=0}^{\infty} \frac{\Delta\lambda_{H_{1,2}}^{2n+1}}{(2n+1)!} \left(\frac{\partial^{2n+1}}{\partial\lambda^{2n+1}} I_m \right) . \tag{4.11}$$

If only the $n = 0$ term is kept then Equation (4.11) reduces to Equation (2.12), valid in the weak field approximation. The higher order terms express the so-called Zeeman saturation, i.e., the non-linear relationship between a_V and $\Delta\lambda_H$ for large Zeeman splittings. As long as $\Delta\lambda_H \approx \Delta\lambda_D$, it is generally sufficient to break off

the expansion after the $n = 1$ term. Although Equation (4.11) cannot be directly used to derive B, since I_m is still an unknown function of λ, it is possible to express V_1 as a function of V_2 by combining and rewriting the Taylor expansions of both lines

$$V_1(\lambda) = \frac{\Delta\lambda_{H,1}}{\Delta\lambda_{H,2}} \left(V_2(\lambda) + \frac{(\Delta\lambda_{H,1}^2 - \Delta\lambda_{H,2}^2)}{6} \frac{\partial^2 V_2}{\partial\lambda^2} + \cdots \right)$$

$$= \frac{g_1}{g_2} \left(V_2 + a \frac{\partial^2 V_2}{\partial\lambda^2} + \cdots \right). \tag{4.12}$$

Except for the coefficient a, all the quantities on the right-hand-side of Equation (4.12) are known or may be derived from the observations. By fitting the right-hand-side of Equation (4.12) to the observed V_1 profile, a may be determined and B can then be obtained from

$$B^2 = \frac{6 a g_2 \lambda_2^2}{k^2 g_1 \lambda_1^2 (\lambda_1^4 g_1^2 - \lambda_2^4 g_2^2)}. \tag{4.13}$$

One advantage of this "analytical" approach compared to the "standard" MLR calibration is that since the line profile shape must neither be synthesized nor assumed, no mistakes can be made regarding the line width etc. The measured V_2 profile serves as a model profile for V_1. Also, this method is quick. Its main disadvantage is that since a second derivative must be calculated, spectra (no magnetograms) with a very high S/N ratio are required. Furthermore, the analytical approach does not include the effects of the Zeeman-splitting-induced desaturation between the σ and π components for $\gamma \neq 0$. Although this point has not yet been adequately tested, the approach chosen by Stenflo *et al.* (1987b), which also neglects saturation induced interaction between σ and π components, gives results for $\gamma \neq 0$ that are not compatible with numerical radiative transfer calculations (Solanki *et al.* 1987). Therefore the analytical technique should only be applied to nearly longitudinal fields.

Method 2. The Fourier transform of the Stokes V profile (Title and Tarbell 1975): The Stokes V profile of a Zeeman triplet in a region with filling factor α and a longitudinal field is given by

$$V(\lambda) = \pm\frac{\alpha}{2}[I_m(\lambda + \Delta\lambda_H) - I_m(\lambda - \Delta\lambda_H)], \tag{4.14}$$

where I_m is the Zeeman-unsplit line profile in the magnetic region. The two signs on the RHS represent the two possible polarities of the field. Equation (4.14) is equivalent to describing the longitudinal Zeeman effect by the convolution of two Dirac δ functions with I_m, which is an accurate description, as long as the inclination angle of the field, $\gamma = 0$. The Fourier transform of Equation (4.14) is

$$\tilde{V}(s) = i\alpha \tilde{I}_m(s) \sin(s\Delta\lambda_H), \tag{4.15}$$

where $i = \sqrt{-1}$, s is the frequency variable in Fourier space and $\tilde{I}_m$ is the Fourier transform of I_m (a tilde marks the Fourier transform of a quantity).

Since I_m is not initially known, it must be assumed. For a weak spectral line, I_m may be approximated by a Voigt profile. Since the Fourier transform of a Gaussian, Lorentzian, or a Voigt function never drops to zero at a finite s, any zero in the Fourier transform is due to the magnetic field (in the absence of noise). B may therefore be obtained from Equation (4.15) by determining the first $s = s_0$ at which $\tilde{V}(s_0) = 0$,

$$B = \frac{\pi}{s_0 k g \lambda^2}. \tag{4.16}$$

As long as the line-saturation-induced interaction between the σ and π components can be neglected, Equation (4.16) gives a relatively accurate value of B, even for inclined fields. The influence of line saturation has been studied by Tarbell and Title (1976). Note that the smaller the $\Delta\lambda_H$ the larger s_0 becomes. Since $\tilde{I}_m$ decreases rapidly with increasing s a smaller field strength requires correspondingly better S/N to be reliably determined.

The advantages of this technique are that it is fast and that under ideal conditions the zero of the transformed profile can be determined to great accuracy (it is claimed by Title and Tarbell 1975 to be less noise-affected than direct profile fitting). Also, there is no upper limit on the field strength to which it may be applied. Its disadvantages are: 1. Magnetooptical effects are neglected and their influence on this technique has not been tested. These effects are particularly important for inclined fields and $\Delta\lambda_H \approx \Delta\lambda_D$. 2. For strong, saturated lines the errors in B increase considerably, particularly for inclined fields and incomplete splitting. 3. The technique assumes Stokes V to be exactly antisymmetric, and even asumes that the two σ components are each symmetric. Therefore it produces errors if applied to anomalously split line profiles and to line profiles formed in the presence of vertical or horizontal magnetic field strength gradients. In particular, the technique assumes that the blue and red wings of the V profiles are equally strong. This is manifestly not the case for most Stokes V profiles observed in solar plages.

Method 3. Stenflo-Lindegren technique for the I_V, i.e. the integrated V, profile (Solanki and Stenflo 1984): Exactly the same procedure is followed as when analysing the Stokes I profiles (described under Case V). However, since the I_V profile, defined in Section 2.4, is formed only within the magnetic features, the intrinsic field strength is obtained. A regression equation that is formally equivalent to Equation (4.5) can also be applied to the width of the I_V profile. Due to differences between the properties of I_V and Stokes I, the equation for deriving B from x_1, assuming a simple convolution type model, now reads (Solanki and Stenflo 1984)

$$B = \frac{\sqrt{3x_1}}{kc}. \tag{4.17}$$

As in the case of the Stokes I regression, more realistic models can also be used to interpret the regression coefficients. The advantages and restrictions of the original Stenflo-Lindegren technique are in general also valid for the I_V regression technique. The comparison of this method to the line-ratio technique suggests that the latter is more accurate, at least as long as the Stenflo-Lindegren technique is interpreted with the simple convolution model.

Method 4. The Fourier transform of Stokes I (Robinson 1980, but see also Giampapa *et al.* 1983): In a 2-component atmosphere, let I_m denote the unsplit line profile in the magnetic feature to be investigated and I_s the profile in the non-magnetic surroundings within the resolution element. For a weak Zeeman triplet we can write the observed profile as

$$\mathrm{I}(\lambda) = \alpha \mathrm{C}[\mathrm{I_m}(\lambda + \Delta\lambda_\mathrm{H}) + \mathrm{I_m}(\lambda - \Delta\lambda_\mathrm{H})] + \alpha \mathrm{D} \mathrm{I_m}(\lambda) + (1 - \alpha)\mathrm{I_s}(\lambda), \quad (4.18)$$

where

$$C = \frac{1}{4}(1 + \cos^2\gamma), \qquad D = \frac{1}{2}\sin^2\gamma. \quad (4.19)$$

To reduce the number of unkowns, additional information on the line profile in the absence of B must be available. This is obtained by either observing a second line for which $\Delta\lambda_H \ll \Delta\lambda_D$, but which is otherwise similar, or else using the profile of the high g line observed in a non-magnetic region as the reference profile. Using a Voigt profile, as in Method 2, is too inexact, since for a small filling factor the effect of B on Stokes I is much more subtle than on Stokes V (cf. Figure 4.1, or Figure 2.2). Here we only follow the two-line approach. The single-line approach using the line profile in a non-magnetic region as a reference can be developed in exactly the same manner. The reference profile may be written as

$$I_2 \approx \alpha I_m + (1 - \alpha) I_s. \quad (4.20)$$

The Fourier transforms of the two line profiles are

$$\tilde{I}_1 = \alpha \tilde{I}_m [D + 2C\cos(s\Delta\lambda_H)] + (1 - \alpha)\tilde{I}_s,$$

$$\tilde{I}_2 = \alpha \tilde{I}_m + (1 - \alpha)\tilde{I}_s. \quad (4.21)$$

Here $\tilde{I}_m$ and $\tilde{I}_s$ are unknown functions of s, while α, γ (which enters through C and D) and $\Delta\lambda_H$ are unknown constants. If $\alpha = 1$ (i.e. the field is resolved), then $\tilde{I}_m = \tilde{I}_2$ is known and the $\tilde{I}_s$ term disappears. Else one assumes $\tilde{I}_m = \tilde{I}_s = \tilde{I}_2$. Some value of γ has to be assumed in both cases. In the former case

$$\frac{\tilde{I}_1}{\tilde{I}_2} = D + 2C\cos(s\Delta\lambda_H), \quad (4.22)$$

while in the latter

$$\frac{\tilde{I}_1}{\tilde{I}_2} = 1 + \alpha[D + 2C\cos(s\Delta\lambda_H) - 1]. \tag{4.23}$$

For a given γ, a simple 2 parameter fit to $\tilde{I}_1/\tilde{I}_2$ using Equation (4.23) then provides B and α. A more detailed description of this technique and of tests involving it is given by Robinson (1980). One advantage of Method 4 is that unlike the MLR it can also be applied to strong fields. However, in its basic form, the technique has all the *dis*advantages of Method 2 and the additional major one of assuming $I_m = I_s$ for unresolved fields. It is also less sensitive to B than any Stokes V based technique. Therefore, this technique should be avoided whenever possible. Its main application has been to late-type stars, where, due to flux cancellation, Stokes V based techniques often cannot be used (cf. the reviews by Marcy 1983, Saar 1987, 1990, 1991a, b, Mathys 1990 and Solanki 1991). The technique has been developed further by Gray (1984) to include more lines and the explicit influence of turbulent, rotational and instrumental broadening of the line profile.

Method 4 can be improved by directly fitting the observed line profiles with synthetic profiles calculated in a 2-component model using either the Unno solution (Equation 2.10) in the Milne-Eddington approximation (Saar 1988, cf. Marcy and Bruning 1984, who take an intermediate step), or a numerical solution of the LTE transfer equations (Basri and Marcy 1988, Marcy and Basri 1989). Two line profiles must still be observed, a Zeeman-split and an unsplit or weakly split one. The latter profile is required to fix free parameters of the transfer calculations like η and $\Delta\lambda_D$ for the Unno solutions, or $\log(g^\star f\epsilon)$, $\xi_{\rm mic}$ and $\xi_{\rm mac}$ for numerical solutions. Note, however, that the profiles I_m and I_s must still be prescribed. Generally $I_m = I_s = I_Q$ is chosen (I_Q is the profile in the quiet sun). The need to assume an I_m and an I_s is a problem inherent to all Stokes I based methods when applied to data from spatially unresolved magnetic features.

Method 5. Extended centre-of-gravity technique (Del Toro Iniesta *et al.* 1990a): They apply the centre-of-gravity technique (cf. Case III) to multiple spectral lines using a 2-component model. Let $\langle B\cos\gamma\rangle_i^{\rm cg}$ denote $|\lambda_{I+V} - \lambda_{I-V}|/2kg_{\rm eff}\lambda_0^2$, a rough measure of the average longitudinal field, in analogy to Equation (4.3), obtained from the centre-of-gravity wavelengths $\lambda_{I\pm V}$ of $I \pm V$ of line No. i. Then, after some algebra, they obtain an expression relating $\langle B\cos\gamma\rangle_i^{\rm cg}$ to the longitudinal component of the true intrinsic field within the magnetic features, $B\cos\gamma$, and the average magnetic field strength, $\alpha B\cos\gamma$, within the spatial resolution element:

$$\frac{\langle I_c\rangle}{I_{cs}}\frac{\langle W\rangle_i}{W_{si}}\langle B\cos\gamma\rangle_i^{\rm cg} = \left(\frac{\langle I_c\rangle}{I_{cs}}\frac{\langle W\rangle_i}{W_{si}} - 1\right) B\cos\gamma + \alpha B\cos\gamma, \tag{4.24}$$

where $\langle I_c\rangle$ is the average measured continuum intensity, I_{cs} the continuum intensity of the non-magnetic surroundings, $\langle W\rangle_i$ the average observed equivalent width of

line i and W_{si} its equivalent width in the non-magnetic part of the resolution element. They determine B and α by carrying out a linear regression through the

$$\left(\frac{\langle I_c \rangle}{I_{cs}} \frac{\langle W \rangle_i}{W_{si}} \langle B \cos\gamma \rangle_i^{\rm cg} \ , \ \frac{\langle I_c \rangle}{I_{cs}} \frac{\langle W \rangle_i}{W_{si}} - 1 \right)$$

point pairs. However, except for differences caused by the thermodynamic structure of the unresolved magnetic features, the $\langle B \cos\gamma \rangle_i^{\rm cg}$ ought to be equal for different i (Semel 1981). Since this technique uses the (unknown) *thermal* structure of magnetic features to determine their *magnetic* properties, Equation (4.24) does not guarantee a reliable determination of B. The technique of Del Toro Iniesta *et al.* (1990a) also inherits the disadvantages present in the centre-of-gravity technique and has the additional disadvantage that some value for I_{cs} and W_{si} must be assumed. So far the extended centre-of-gravity technique has given rather fluctuating results, which partly contradict those of other techniques. In addition, it has not yet been tested against model calculations.

Method 6. Least-squares fitting of Stokes profiles (Harvey *et al.* 1972, Auer *et al.* 1977): In its original form this is a single-line technique. Profiles calculated using the Milne-Eddington model are fitted to the observed Stokes I, V and, when available, Q and U profiles. The technique derives not only the field strength, but often also γ, χ and thermodynamic parameters. It is described in greater detail in Section 4.4. Here only the aspects related to the field strength are briefly discussed.

The technique, as formulated by Auer *et al.* (1977), works best if profiles of all 4 Stokes parameters are available, which is all too rarely the case (however see Harvey *et al.* 1972, Lites *et al.* 1990, 1991). On the other hand, the use of all 4 Stokes parameters means that this method does not suffer from any uncertainty in γ. Being a single-line technique it can run into problems if the Zeeman splitting is not complete. Only Harvey *et al.* (1972) have used it to determine the intrinsic field strength in small-scale magnetic features by fitting the whole line profile (cf. Skumanich *et al.* 1992). The advantages of using more realistic numerical solutions, mentioned under Case V, also apply here. Keller *et al.* (1990a) and Zayer *et al.* (1990) have recently determined B by applying a least-squares fitting technique to individual line parameters.

The main disadvantages of the original, single-line fitting technique are shared with other single-line techniques. They include a low sensitivity to field strengths at which the line is not completely split and possible falsification of results due to the influence of temperature and velocity broadening. These disadvantages can be overcome by including a second line in the analysis (the lines should, if possible, be chosen according to the same criteria as for the MLR). Then the technique may also be restricted to Stokes V alone, at the cost of a slightly larger uncertainty in B due to the unknown γ. Since, unlike the line-ratio technique, it fits the whole line profile and not just a single parameter, two-line Stokes profile fitting can also determine (large) field strengths at which the MLR becomes insensitive. It is also

less affected by noise than the MLR. On the other hand, the MLR is more sensitive to small B than simply fitting the full V profiles of the two lines, without explicitely fitting their ratio (Emonet 1992).

4.2.1.7. *General Remarks.* Before discussing Model II, let me make some general remarks on the techniques described so far.

1. When $\Delta\lambda_H \approx \Delta\lambda_D$ (Cases V and VI) the determined B value is often critically dependent on the ratio $\Delta\lambda_H/\Delta\lambda_D$ and it is often implicitly this ratio and not B itself which is determined by the different techniques. Thus the derived apparent field strength may be underestimated if $\Delta\lambda_D$ is underestimated. It is therefore necessary to obtain $\Delta\lambda_D$ accurately from the observations and to model it properly when calibrating the results. This implies that, in general, radiative transfer calculations are to be preferred over simpler models, since only the former take line broadening due to line saturation properly into account. Broadening due to velocity and to spectrograph and slit profiles must also be accounted for. The Fourier techniques are not as directly affected as the others, but a change in $\Delta\lambda_D$ can significantly affect their sensitivity to a particular field strength.
2. To first order, many, but not all, of the techniques presented here derive B independently of the true inclination of the field, However, second order effects still remain, except when the splitting is complete (Cases I and II). Such second order effects, e.g. differential saturation of the σ vs. the π components, affect the results since, for $\gamma \neq 0$, both σ and π components contribute to the V profile (as can be seen from the transfer equations, Section 2.3). In general, as γ increases π gets stronger relative to σ and the derived field strength appears to decrease (Solanki *et al.* 1987). Models which do not take this effect into account (e.g. the extended centre-of-gravity method of Del Toro Iniesta *et al.*, or the simple interpretations of the line ratio of Stenflo *et al.*, 1987b, and Sánchez Almeida *et al.* 1988a) therefore give artificially low field strengths near the limb. These effects are particularly important when $\Delta\lambda_H \approx \Delta\lambda_D$.
3. The discussion so far has always assumed LTE. How strongly could NLTE effects falsify the derived B values? Only a single study has attempted to answer this question. Stenholm and Stenflo (1978) showed that the line ratio (Stenflo 1973, Method 1, Case VI) is practically unaffected by departures from LTE, although the two individual lines may both be considerably changed by it. The insensitivity to NLTE is due to the fact that the line ratio is generally formed between lines with similar strengths belonging to the same multiplet. The influence of NLTE effects will have to be tested for techniques based on a single line (e.g. the Title and Tarbell 1975 and the Auer *et al.* 1977 techniques), or based on a comparison between lines with relatively different properties (e.g. the del Toro Iniesta *et al.*, 1990a, technique or the Stenflo and Lindegren, 1977, method).

4.2.2. Model II: Model with Two Magnetic Components

Consider a 2-component model with a field strength B_1 covering a fraction α of the surface and field strength B_2 covering the rest of the resolution element, $(1-\alpha)$. If $\mathbf{B_1} \cdot \mathbf{B_2} > 0$ (for example if $\mathbf{B_1} \uparrow\uparrow \mathbf{B_2}$) and $|\Delta\lambda_H(B_1) - \Delta\lambda_H(B_2)| \lesssim \Delta\lambda_D$, then most techniques described in Section 4.2.1 give a "weighted mean B" value which may be qualitatively expressed as

$$B \approx \frac{B_1\alpha(I_{c1}-I_1) + B_2(1-\alpha)(I_{c2}-I_2)}{\alpha(I_{c1}-I_1) + (1-\alpha)(I_{c2}-I_2)}, \tag{4.25}$$

or

$$B \approx \frac{B_1\alpha V_1 + B_2(1-\alpha)V_2}{\alpha V_1 + (1-\alpha)V_2}, \tag{4.26}$$

depending on whether the technique is based on the I or the V profile. I_i and V_i are the intensity and net circular polarization arising in the i-th component of the model (I_i corresponds to line centre, V_i to the Stokes V peaks). I_{ci} is the continuum intensity of the i-th component. Similar expressions can also be written for Stokes Q and U. The extension of the above formulae to more field strength components (or even a continuum of field strengths) is straightforward. Of course, it is necessary to check whether B_1 and B_2 can both be determined with the same technique, since many techniques are limited to a certain range of $\Delta\lambda_H/\Delta\lambda_D$ into which both B_1 and B_2 would have to fall. If not, then Equations (4.25) and (4.26) may not be valid. In particular, Equation (4.25) is not valid for $B_1 = 0$ or $B_2 = 0$. Note also, that if $|\Delta\lambda_H(B_1) - \Delta\lambda_H(B_2)| \gtrsim \Delta\lambda_D$, then the two components can be separated in the line profile(s) and B_1 and B_2 may be measured individually (see below).

The case of $\mathbf{B_1} \cdot \mathbf{B_2} < 0$ (for example $\mathbf{B_1} \uparrow\downarrow \mathbf{B_2}$) is more complex. Although Stokes I is insensitive to polarity, techniques based on Stokes V may give wrong results in this case if $0.2\Delta\lambda_D \lesssim |\Delta\lambda_H(|B_1|) - \Delta\lambda_H(|B_2|)| \lesssim \Delta\lambda_D$. The reason is the dependence of the sign of Stokes V on the magnetic polarity, which leads to cancellation and changes in the shape of the final Stokes V profile.

As an example consider the case of $B_1 = -400$ G, $B_2 = 1200$ G, $\alpha_1 = 0.5$, $\alpha_2 = 0.5$. Figure 4.2 shows $-V(B_1)$ and $V(B_2)$ of 5250.2 Å, as well as the composite profile, $V(B_1) + V(B_2)$, which exhibits a larger splitting than the V profiles of either of the individual components. All profiles have been normalized to the same $V_{\max}$ to emphasize differences in shape. In addition, if Fe I 5247.1 Å is also calculated for the same atmospheric parameters, then the ratio between the composite V profiles of the two lines is smaller than the ratio between the two lines in each component. Thus, if the Zeeman splitting is not complete, a mixture of opposite polarity features mimics a larger field strength than actually present, as first pointed out by Semel (1986).

There are various ways of obtaining a more reliable average value of B in the presence of mixed polarities. For example, one may apply the line-ratio technique

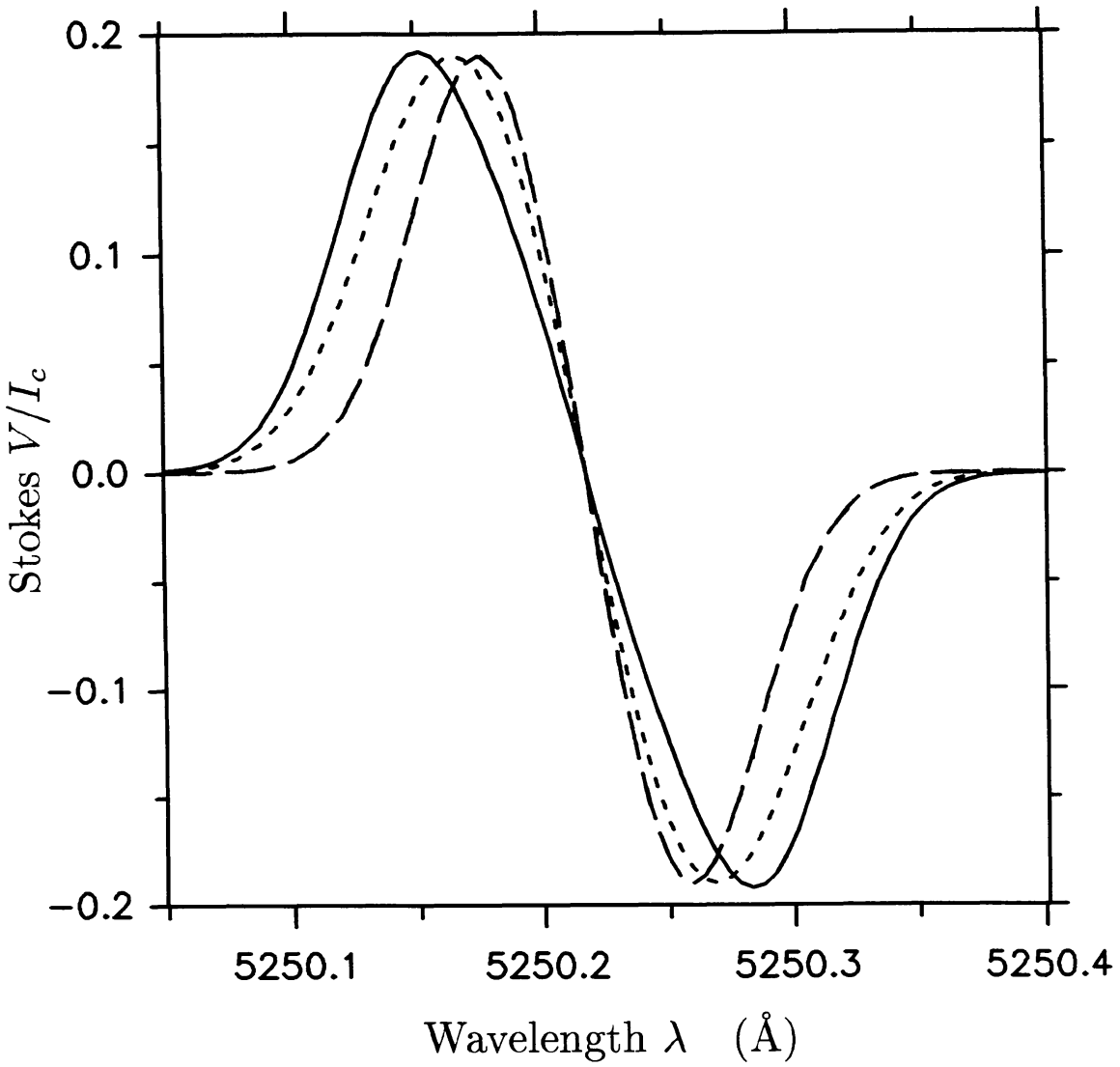

Fig. 4.2. Stokes V profiles of Fe I 5250.2 Å calculated using the average quiet-sun temperature stratification. Profile 1: single magnetic component with $B_1 = 400$ G (dashed curve), profile 2: single magnetic component with $B_2 = 1200$ G (dotted curve), and profile 3: composite of two magnetic components having field strengths $B_1 = -400$ G and $B_2 = 1200$ G, each with filling factor $\alpha_1 = \alpha_2 = 0.5$ (solid curve). Thus the third profile is a combination of the first two profiles, whereby the weak field has been assumed to have the opposite polarity to the strong field. All the profiles have been convolved with a macroturbulence of 2 km s^{-1} and have, for clarity, been normalized such that all three of them have the same amplitude. Since weakly split V profiles scale with αB, the true ratio of amplitudes $V(B_1)/V(B_2) \approx 1/3$. Note that the composite profile exhibits the largest splitting.

to Stokes Q or U (Solanki *et al.* 1987). Since η_Q and η_U are proportional to $\sin^2\gamma$, they do not distinguish between unipolar and mixed polarity regions. However, they do require a non-isotropic transverse B component in order to be observed. Also, reliable measurements of Stokes Q and U profiles are comparatively rare due to the prevalent instrumental cross-talk in heliostat and ceolostat systems commonly employed in solar telescopes. Techniques based on Stokes I (e.g. Robinson 1980) may also be used, since η_I only contains $\cos^2\gamma$ and $\sin^2\gamma$ terms. However,

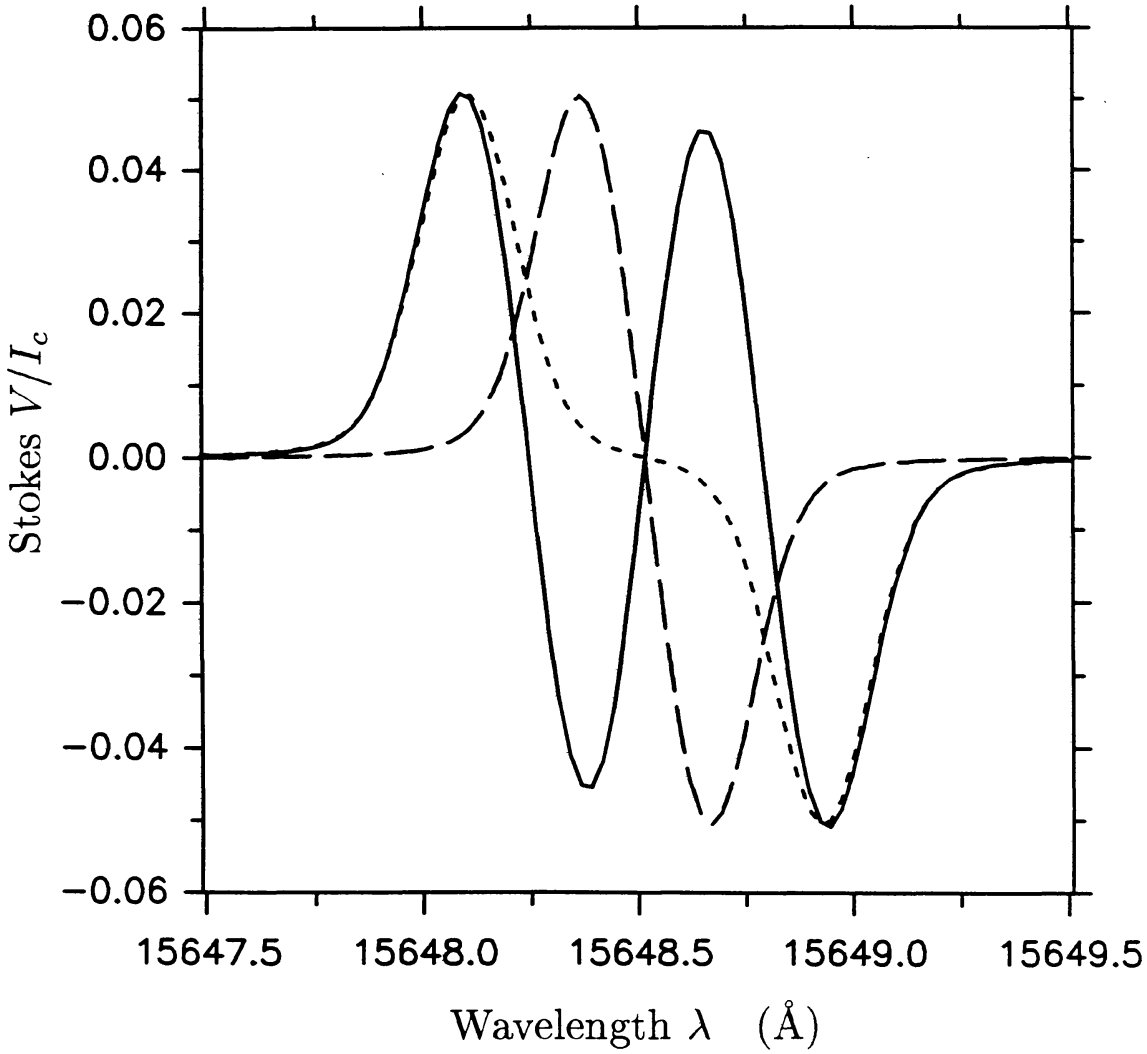

Fig. 4.3. Stokes V profile of Fe I 15648.5 Å calculated for the same atmosphere and magnetic parameters as the Fe I 5250.2 Å line shown in Figure 4.2.

there are other major disadvantages inherent in Stokes I-based techniques (cf. Section 4.2.1). Another possibility is to attempt to improve the spatial resolution of Stokes V observations and resolve the individual features of opposite polarity. However, under some circumstances it may be better to improve the resolution in the Zeeman domain. For example, if a sufficiently Zeeman sensitive line is used, then $|\Delta\lambda_H(|B_1|) - \Delta\lambda_H(|B_2|)|$ may be larger than $\Delta\lambda_D$ and the two components may become individually visible in the Stokes V profile. Figure 4.3 shows the V profiles of the $g = 3$, 15648.5 Å line calculated for the same parameters as the 5250.2 Å in Figure 4.2. Obviously, it is easy to deduce the presence of two magnetic components from the composite profile (solid) and to determine their field strengths individually.

4.2.3. Model III: Model with a Vertical Field-Strength Gradient

In Section 4.2.2 the qualitative influence of a spatially unresolved *horizontal* distribution of field strengths on the derived average field strength was discussed. Consider now models with a *vertical* gradient of the field strength: $B = B(z)$. For the moment we neglect that $dB/dz \neq 0$ also implies that the size of a magnetic feature changes with height due to magnetic flux conservation.

Investigators studying the effect of a non-vanishing dB/dz on the derived B values find that the measured field strength corresponds to the B at a z value close to the mean formation heights of the lines used (e.g. Landolfi 1987, Solanki *et al.* 1987, Grossmann-Doerth and Solanki 1990). This implies that the heights of formation of the lines determine to a certain extent the value of the field strength measured (Grossmann-Doerth and Solanki 1990). Therefore, the heights of formation must be known in order to determine the height associated with the measured field strength, which is required in order to compare measured B values with MHD model calculations. Unfortunately, the heights of formation of most lines used to determine B are relatively sensitive to the temperature stratification, so that, although B at some unknown height of line formation may be determined easily in a "model independent" manner using techniques described in Section 4.2.1 and 4.2.2, it becomes impossible to translate this into the B value at a given geometrical or optical depth without making some assumption regarding the thermodynamical properties of the magnetic features.

In order to associate a measured B value with a z-value two distinct steps are required, although they are often combined. First the τ_c of formation of the line must be calculated and then, in the second step, the z corresponding to this τ_c must be determined. The first step involves the Stokes contribution functions, while the second depends upon the continuum opacity, κ_c, which, due to its temperature sensitivity, can by itself lead to considerable differences in the height at which B is measured. Due to the strong dependence of κ_c on T, $\tau_c = 1$ is reached at a greater height in a hot atmosphere than in a cool one. For purely this reason one would expect to see the field at greater depth within sunspot umbrae than within small magnetic elements (e.g. Schüssler 1987). This effect is also partly responsible for the result, found by Zayer *et al.* (1990), that B varies by 1000 G at $\tau_c = 1$ between regions with different filling factors, but by less than 200 G at a fixed geometrical heigth ($z = 0$, i.e. $\tau_c = 1$ in the quiet sun). Since B generally decreases with height on the sun, lines formed deeper see a stronger field than those formed higher.

Finally, let me briefly discuss the effects of including magnetic flux conservation into the model. Since flux conservation causes the size of the magnetic features to change with height, the radiative transfer must be carried out along multiple rays (1.5-D radiative transfer), or, for NLTE calculations, in 2-D (see Section 3.1). At present, only numerical radiative transfer calculations are sufficiently adaptable to be applied.

A number of interesting new effects are observed in such a model, due partly to the fact that a single ray may pass through both magnetic and non-magnetic features,

so that Stokes V, Q and U may actually obtain a part of their contribution from the non-magnetic atmosphere (for such rays only). Figure 4.4 shows the Stokes V contribution function of a line formed along a ray in two complementary 2-layered models. In the first $B = 0$ above $\log\tau = -1.5$ and $B = 1000$ G below it, while in the second $B = 0$ up to $\log\tau = -1.5$ and $B = 1000$ G above it. In the first case Stokes V obtains its contribution only inside the magnetic feature, in the other case both inside and outside. This behaviour is consistent with the following definition of the contribution function: The intensity contribution function is a measure of the amount of radition at a wavelength λ that is emitted at a given depth τ and escapes to the upper boundary of the atmosphere. According to this definition the contribution function at τ depends on the properties of the atmosphere above τ, but not below that height. The contribution functions in Figure 4.4 confirm this behaviour. Note that the contribution function to Stokes V can become negative, since it represents the difference between two contributions (just as Stokes V itself is a difference between two intensities and can become negative). Consequently, Stokes Q, U and V are to some extent affected by the atmosphere outside the magnetic features and also by the atmosphere at the boundary of the magnetic feature. For the measurement of B this boundary may be important, since its thickness may decide how much weak field the line sees. In particular, it is important to take care that in 2-D models the width of the boundary reflects the physical situation and is not determined by some artificial quantity like the numerical grid size. A too wide boundary enhances the influence of the weak field component on the synthetic profile, to compensate for which the average field strength of the feature as a whole must be raised. Thus a wrong field strength may be determined (in particular if $\Delta\lambda_H \gg \Delta\lambda_D$, since then Stokes V amplitudes are independent of field strength). The effect of the boundary is enhanced if a thin magnetic structure (flux tube) is observed at an angle to its axis, since then every ray passes through the boundary at least once (cf. Figure 3.1).

4.3. Magnetic Field-Strength Gradients and Distribution

The present section deals with the *measurement of gradients* of the field strength, which should not be confused with the measurement of the field strength in the presence of a field-strength gradient (the subject of Sections 4.2.2 and 4.2.3). Many of the techniques listed below under the headings "horizontal gradients" and "vertical gradients" are in reality techniques for determining transverse and longitudinal gradients, respectively, so that I implicitely consider solar disc centre when discussing them.

4.3.1. Horizontal Gradients

In spatially resolved magnetic features, e.g. sunspots, horizontal gradients of the field may be derived by measuring the field strength at an array of points on the solar surface using one of the techniques described in Section 4.2. High spatial resolution and an imaging capability are obviously of advantage.

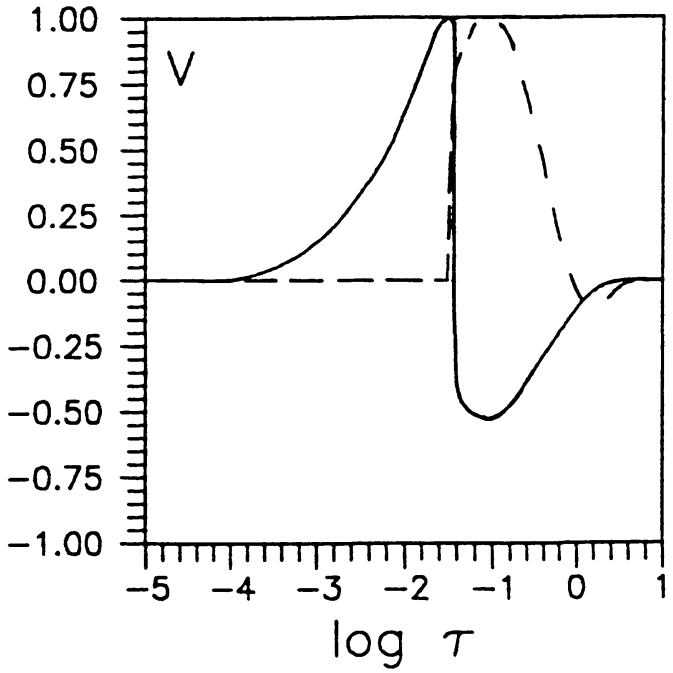

Fig. 4.4. The Stokes V contribution function of a high-excitation Fe I line formed in a two-layered atmosphere. The dashed curve is the contribution function in an atmosphere which is field-free above $\log\tau = -1.5$ and has $B = 1000$ G below that level. The solid curve is the contribution function for the opposite case, i.e. an atmosphere that is field-free below $\log\tau = -1.5$. Note how in the latter case the Stokes V contribution function is non-zero in the non-magnetic part of the atmosphere as well (from Larsson *et al.* 1991).

Even if the magnetic field varies on a smaller scale than the spatial resolution, information on the total range of field strengths, $\Delta B = B_{\max} - B_{\min}$, in the resolution element can be obtained if a line with $\langle \Delta\lambda_H \rangle \gg \Delta\lambda_D$ is used (the brackets $\langle\ \rangle$ signify an average over all values in the resolution element), particularly if either the field free region covers only a small fraction of the resolution element or if the longitudinal component of B always has the same polarity. A horizontal distribution of field strengths broadens the σ components of a strongly split line, but leaves the σ components of a weakly split line relatively unaffected. By comparing the widths of the individual σ components of lines with large $\Delta\lambda_H$ to those of lines with small $\Delta\lambda_H$ it should be possible to separate the broadening due to ΔB from that due to non-stationary velocity or the instrumental profile (Zayer *et al.* 1989). A similar method, based on comparing the widths of the σ to that of the π component of a single Stokes I profile of a completely split Zeeman triplet, has been proposed by Deming *et al.* (1988). The use of a Zeeman triplet has the advantage that although the σ components are broadened by a field-strength distribution, the π component remains unaffected. The Deming *et al.* (1988) technique only works if little non-magnetic material is present in the resolution element, since otherwise the π component does not arise from the same region in the atmosphere as the σ components. It is not possible to derive a unique distribution of B from Stokes V, since, e.g., $\mathbf{B_1} \uparrow\downarrow \mathbf{B_2}$ makes the σ components *narrower* rather than broadening

them. Therefore, under certain conditions it may be worthwhile to consider the shapes of Stokes I, Q or U profiles in addition to Stokes V. One condition is that $\Delta\lambda_H$ must be sufficiently large, since, due to the presence of the π component, Stokes I, Q and U are completely split only for $\Delta\lambda_H \gtrsim 2\Delta\lambda_D$. To make use of Stokes I, the magnetic feature must, in addition, be almost spatially resolved (i.e. $\sum \alpha_i$, where the index i runs over all the magnetic components, must be relatively close to unity). Note that even when using all Stokes parameters, this method of determining the horizontal field strength distribution is not model independent, since the shape and width of the σ components also depends on the temperature in each field-strength component. This temperature distribution can be determined only if two lines with large $\Delta\lambda_H$ and very different temperature sensitivities are used.

Finally, there is the problem that, by itself, a strongly split line cannot distinguish vertical gradients of the field strength from horizontal gradients, since the former also broaden σ components, while leaving the π component unchanged. Therefore, the determination of vertical and spatially unresolved horizontal magnetic field gradients is strongly coupled. The two parameters may be separated by additionally comparing lines formed at different heights.

4.3.2. Vertical Gradients

The following are brief descriptions of techniques that have in the past been used to diagnose vertical field-strength gradients.

1. The vertical gradient of B may be obtained by comparing the field strength derived from lines formed at different heights. The comparison may be between lines formed, e.g., in the transition region and the photosphere (Hagyard *et al.* 1983, Henze *et al.* 1982), or between purely photospheric lines (Wittmann 1974, Stenflo *et al.* 1987b, Zayer *et al.* 1989). For sunspot umbrae a relatively large set of possible spectral lines is available (due to the large field strength and $\alpha = 1$), but for small-scale magnetic features only relatively few lines can be reliably used. The field strength must be determined with considerable accuracy ($\pm 25\%$ is generally not sufficient, if only photospheric lines are used). Therefore, the spectral lines have to be chosen with great care.
2. The line ratio technique of Stenflo (1973, Method 1 of Case VI, Section 4.2.1) only requires the ratios at a single wavelength point in the two lines to derive the field strength. Since for $\Delta\lambda_H \lesssim \Delta\lambda_D$ the line core is formed higher in the atmosphere than the line wings, it is possible to obtain the field strength at different heights by forming the magnetic line ratio at different wavelengths in V profiles of two well-chosen lines (e.g. Fe I 5250.2 Å and Fe I 5247.1 Å, Stenflo 1984a). If the field strength decreases with height then the difference in formation height between core and wings is enhanced, since the higher layers give rise to weakly split profiles for which the Stokes V signal is concentrated near line centre. The line ratio between the Q or U profiles of the two lines may also be used. This has the advantages that since Q and U are non-zero at the

line core, a greater range of heights can be covered than with Stokes V. This technique requires the measurement of full line profiles with a very high S/N ratio. The sensitivity and reliability of this technique has recently been tested using realistic models and an inversion code (see Section 4.9). It recovers the original magnetic gradient only if the signal-to-noise ratio in the simulated data is sufficiently high (Emonet 1992).

3. Lines are generally formed higher in the atmosphere closer to the solar limb. Therefore, it is in principle possible to obtain $B(\tau)$ by measuring $B(\mu)$. However, it is not advisable to use this procedure, except possibly for completely Zeeman-split lines. It mixes information due to the vertical gradient in B, the different viewing angles of the magnetic features (which also changes the line profile shape) and intrinsic differences between different solar regions. The following example illustrates the care that must be taken when applying this method. For solar magnetic elements a simple analysis, by Stenflo *et al.* (1987a,b), of the CLV of the line ratio suggested that B decreases rapidly with height. However, Solanki *et al.* (1987) later showed that the line profiles change so strongly from disc centre to the limb (due purely to line-transfer and velocity-broadening effects, which were neglected by Stenflo *et al.* 1987a,b) that no information on the vertical gradient of the field can be obtained from the CLV of the line ratio. For a completely Zeeman-split line profile, shape changes pose less of a problem, but the comparison between different regions, with potentially different field strengths, is unavoidable.
4. The widths of the σ components of strongly split spectral lines are increased by a vertical field-strength gradient. Therefore, this line parameter may serve as a diagnostic of vertical gradients, in particular if the σ width of a high and a low $\Delta\lambda_H$ line are compared, or if the σ width is compared to the π width of the Stokes Q and U profiles of the high $\Delta\lambda_H$ line (see also Section 4.3.1). The σ width has the disadvantage that it cannot readily differentiate between vertical and horizontal field strength gradients and is most effective when used in conjuction with one of the other diagnostics listed in this section. However, it is possible to distinguish between vertical and horizontal field-strength gradients simply by comparing the σ components of the two lines. If the two lines are sufficiently similar and sufficiently strong to be relatively saturated, then the presence of a longitudinal gradient changes the ratio of the strengths (i.e. areas) of the σ components of the two lines, while a transverse gradient leaves this ratio unaffected (Solanki *et al.* 1992a).
5. An asymmetry between the blue and red lobe areas of Stokes V often, but not always implies the presence of a vertical (i.e. longitudinal) magnetic field gradient (cf. Section 4.7.2), in addition to the necessary presence of a (longitudinal) velocity gradient. Unfortunately, it is not always straightforward to distinguish between gradients in B, the magnetic inclination, γ, or azimuth, χ, just from the V asymmetry (although this may be possible if additional information is available, e.g., Sánchez Almeida and Lites 1992). If the velocity stratification,

$v(z)$, is known, and γ and χ are constant (and, ideally, also known), then an estimate of the field-strength gradient may be obtained. In view of the uncertainties generally present in measured $v(z)$ and γ values, this technique generally only provides the sign of dB/dz and possibly very rough estimates of its amplitude.

6. Landolfi (1987) extended the Auer *et al.* (1977) inversion technique to include the retrieval of gradients in velocity and magnetic field under the assumptions that they are i) small and ii) linear in τ. He uses analytical solutions and response functions to describe the gradient of the Stokes vector with respect to inversion parameters. He has tested the technique on simulated data and finds it to generally give reasonable results (gradients of the inclination angle γ and azimuthal angle χ can also be recovered, but usually decrease the accuracy of the results).

In general, it is not possible to derive vertical gradients of B in a model-independent manner, since both the median height of line formation and the width of the contribution function of a spectral line depend strongly on the atmospheric model (Larsson *et al.* 1991, Bruls *et al.* 1991).

4.4. Magnetic Field Vector

The measurement of the magnetic vector has been reviewed by Stenflo (1985) and Landi Degl'Innocenti (1985). An accurate measurement of the full magnetic vector generally requires the measurement of all four Stokes parameters in, preferrably, multiple spectral lines. Techniques for deriving $B = |\mathbf{B}|$ have been described in Sections 4.2.1–4.2.3. The main problem is then to determine γ, the angle between the field and the line of sight, and χ, the azimuthal angle of the field measured relative to a direction fixed by the polarimeter. For the interpretation of solar observations, this direction is best chosen to be parallel or perpendicular to the limb. Once γ and χ are known, it is straightforward to derive the angles ϕ and ψ relating the direction of $\mathbf{B}$ to the solar surface using a linear transform. If the x' axis from which χ is measured lies perpendicular to the solar limb, then the transforms read

$$\cos\phi = \cos\gamma\cos\theta - \sin\gamma\cos\chi\sin\theta, \tag{4.27}$$

$$\sin\psi = \frac{\sin\gamma\sin\chi}{\sin\phi}, \tag{4.28}$$

where ϕ is the angle between the surface normal and the magnetic vector, θ is the angle between the surface normal and the line of sight ($\theta = \arccos\mu$) and ψ is the azimuthal angle of the field measured from the intersection of the solar surface with the plane spanned by the surface normal and the line-of-sight (LOS). The various angles are illustrated in Figure 4.5. The transformation of whole vector magnetograms has been discussed by, e.g., Hagyard (1987), Venkatakrishnan *et al.* (1988) and Gary and Hagyard (1990). For magnetic images covering a significant fraction of the solar surface, z' cannot be chosen to lie in the (x, z)-plane for every

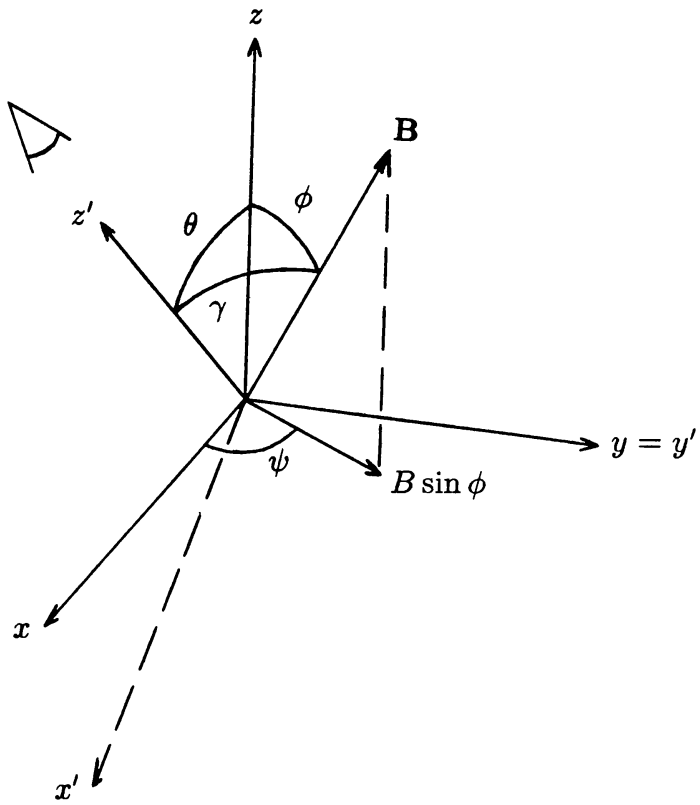

Fig. 4.5. Illustration of the angles required for the transformation from the coordinates of the observer (x', y', z') into local coordinates on the solar surface (x, y, z). The line of sight, z', lies in the (x, z)-plane, i.e the solar limb is parallel to the $y = y'$ axis. The angle χ is measured from x', which also lies in the (x, z)-plane. x' is plotted dashed, since it lies below the (x, y)-plane.

point in the magnetogram and the transformation is more complex than the simple Equations (4.27) and (4.28).

If the observed spectral line or lines are weak and γ and χ do not vary along the LOS, then one can assume that

$$V \sim \eta_V \sim \cos\gamma,$$

$$Q \sim \eta_Q \sim \sin^2\gamma\cos 2\chi,$$

$$U \sim \eta_U \sim \sin^2\gamma\sin 2\chi. \tag{4.29}$$

Now, γ may be obtained from

$$\frac{V}{\sqrt{Q^2+U^2}} \sim \frac{\cos\gamma}{\sin^2\gamma} \tag{4.30}$$

and χ from

$$\frac{U}{Q} \sim \tan 2\chi, \tag{4.31}$$

where V, Q and U refer to the Stokes profiles at a fixed wavelength.

The approximations (4.29) are better in the wings where saturation is smaller. Note that the above relations are only proportionalities and that $V/\sqrt{Q^2+U^2}$ and U/Q also depend on other atmospheric and line dependent parameters besides γ and χ. The main additional parameters affecting Equation (4.31) are magnetooptical effects, as pointed out by Landolfi and Landi Degl'Innocenti (1982) and implemented into their analyses by Landolfi *et al.* (1984). Neglecting magnetooptical effects can cause the derived χ to be wrong by up to 20–30°, in particular for a combination of relatively strong lines, small γ and $\Delta\lambda_H/\Delta\lambda_D \approx 1$–2 (Landolfi and Landi Degl'Innocenti, 1982). Thus, Landi Degl'Innocenti (1979) was able to show that the spiral structure of sunspot fields seen by Hagyard *et al.* (1977) is mainly due to the neglect of magnetooptical effects in their analysis. The expression $V/\sqrt{Q^2+U^2}$ is affected not only by magnetooptical effects (which, at least for $\Delta\lambda_H \lesssim \Delta\lambda_D$, are larger in Q and U than in V, e.g. Landi Degl'Innocenti and Landi Degl'Innocenti 1973), but also by the position in the line profile (V has a totally different profile shape than Q or U), the field strength and velocity broadening. Note also that any technique using Stokes V is going to suffer a loss of accuracy in the presence of opposite polarities in the resolution element. Such a constellation reduces the Stokes V signal, but leaves Q and U unaffected, so that Equation (4.30) leads to an overestimate of γ. This problem may be resolved by considering also the MLR, since for mixed polarity fields it produces different results for V than for Q and U (if the field strength is different in the two polarities). As shown in Section 4.2.2, even better is to consider a spectral line that is completely Zeeman split. Stokes Q and U, on the other hand, suffer complete cancellation if the field is isotropic in the plane perpendicular to the LOS. Such a situation may be present when observing along the axis of symmetry of a small flux tube.

For a weak field ($\Delta\lambda_H \ll \Delta\lambda_D$), the σ amplitudes of V are proportional to B, while those of Q and U are proportional to B^2. For a strong field ($\Delta\lambda_H \gg \Delta\lambda_D$), on the other hand, the amplitudes of V, Q and U become equally independent of B. Stenflo (1985) has estimated the error in γ induced by neglecting the spatially unresolved nature of the small-scale magnetic structures, i.e. by assuming that the spatially averaged field strength is the true field strength of the magnetic features. He found that for typical lines in the visible, γ may be wrong by up to 5–10° for $\alpha = 0.1$ and by up to 45° for $\alpha = 0.01$. This problem is defused by using a completely split line, e.g. an infrared line, for the γ measurement. For such a line $V/\sqrt{Q^2+U^2}$ remains independent of B for even relatively small values of B (cf. Solanki *et al.* 1992a). The influence of velocity broadening, which changes the Q and U amplitudes by a different amount than the Stokes V amplitude, has been studied by Solanki *et al.* (1987). It has a smaller, but still non-negligible effect. For stronger lines the temperature influences the line widths and amplitudes of Q, U and V by changing line saturation and also affects the π to σ ratio of Stokes Q and U (Solanki *et al.* 1987). In general, π components of Q and U should be

avoided unless line saturation and magnetooptical effects can be properly taken into account in the analysis. In summary, in order to calibrate relations (4.30) and (4.31), radiative transfer calculations are required and some additional information on B, T, the microturbulence $\xi_{\rm mic}$ and the macroturbulence $\xi_{\rm mac}$ must be included to obtain accurate values of γ and χ.

Finally, instrumental depolarization and cross-talk may easily falsify the resulting **B** vector unless an axially symmetric optical system or compensators for oblique reflections, such as those described by Harvey (1985) and Martínez Pillet and Sánchez Almeida (1991) are used. Unfortunately, most major solar telescopes possess one or more oblique reflectors, which unavoidably lead to some cross-talk, except under exceptional circumstances (e.g. Makita and Nishi 1970, Wiehr and Rossbach 1974, Harvey 1985, Balasubramaniam *et al.* 1985, Sánchez Almeida *et al.* 1991, various papers in the volumes edited by Hagyard 1985 and November 1991). Unfortunately, compensators for oblique reflections can lead to a considerable loss of light.

Equations (4.29) and (4.30) are applicable to magnetograph data, which allow a determination of **B** at many positions on the solar surface simultaneously. Without spectral information, however, the calibration of relations (4.30) and (4.31) becomes extremely difficult, but see the techniques of Ronan *et al.* (1987) and Jefferies and Mickey (1991) described below. Often, due to the difficulty in calibrating relation (4.30), only χ is determined from magnetograph observations. Although rather restricted, this still provides interesting information on horizontal shear in the magnetic field.

For unresolved magnetic features, gradients in B and γ (and possibly in χ) can lead to errors in γ and χ, in particular since such gradients imply a particular geometry of the finite sized magnetic feature (flux tubes). Test calculations have shown that if 1-D models are used to interpret the line profiles in a flux tube with a field expanding with height, then γ is consistently underestimated, although by only a small amount.

Ronan *et al.* (1987) present a simple method of calibrating the relations for γ and χ, i.e. of determining the constants of proportionality of Equations (4.30) and (4.31). They make use of integral properties of the Stokes parameters, assume the weak field approximation [i.e. Equation (2.12) and similar relations for Q and U] and neglect magnetooptical effects. Although they never explicitly say so, they assume the case of weak lines [i.e. no saturation, compare, e.g., their Equation (12) with the discussion in Section 2.1 of Solanki *et al.* 1987]. Furthermore, their calibrations are only valid for spatially resolved fields. The accuracy of the derived magnetic parameters is acceptable for some applications (errors in B range up to 500 G and χ is very poorly determined).

Jefferies and Mickey (1991) also discuss the measurement of the magnetic vector in the weak field approximation, with the help of relations derived by

Jefferies *et al.* (1990):

$$\left|\frac{\Delta\lambda_H}{\Delta\lambda_D}\right| \cos\gamma = V \Big/ \frac{dI}{d\Lambda}, \tag{4.32}$$

$$\left(\frac{\Delta\lambda_H}{\Delta\lambda_D}\frac{\sin\gamma}{2}\right)^2 = \left|\frac{H'(a,\Lambda)}{H''(a,\Lambda)}\sqrt{Q^2+U^2}\Big/\frac{dI}{d\Lambda}\right|, \tag{4.33}$$

$$\tan 2\chi = \frac{U}{Q}. \tag{4.34}$$

Here H' and H'' are the first and second derivatives of the Voigt function with respect to $\Lambda = \Delta\lambda/\Delta\lambda_D$. From tests based on Milne-Eddington solutions of the transfer equations they conclude that sufficiently far in the line wings the weak-field approximation is acceptable (for errors in the field strength of approximately 20%) up to 4000 G for a line at 6000 Å with $g_{\rm eff} = 1$. The technique of Jefferies and Mickey differs from that of Ronan *et al.* (1987) mainly in that it is based on a single wavelength, as compared to an integral over wavelength. However, it is not a truly single-wavelength technique, since the derivative of Stokes I, $dI/d\lambda$, requires at least two additional measurements of Stokes I. The Jefferies and Mickey method should be applicabile to stronger lines as well (cf. Landi Degl'Innocenti 1992), but only works for spatially resolved fields. Qu *et al.* (1992) have recently extended the work of Jefferies *et al.* (1990) to include terms up to $(\Delta\lambda_H/\Delta\lambda_D)^3$. This has the advantage that their expressions are valid for larger field strengths than Equations (4.32)–(4.34). Since it uses the Stokes I profile, the method of Qu *et al.* (1992) is also restricted to spatially resolved fields.

The angles γ and χ may also be determined from the Fourier transforms of the Stokes Q, U and V parameters. More details are given by Title and Tarbell (1975) and Tarbell and Title (1976). Fourier transform techniques require the measurement of the full line profile.

Auer *et al.* (1977) proposed a method of determining **B** by fitting measured I, Q, U and V profiles with the Milne-Eddington solutions of the transfer equations given in Equation (2.10). Their technique, generally referred to as an inversion technique, has been extended to include magnetooptical effects by Landolfi *et al.* (1984) and non-linear dependences of the source function by Lites *et al.* (1988). For a *spatially resolved* magnetic feature ($\alpha = 1$) there are eight free parameters. B, γ, χ, $\Delta\lambda_0$ (wavelength shift due to stationary flows), $\delta\lambda_D$ (Doppler width of absorption coefficient),* a (ratio of damping constant to $\delta\lambda_D$), η_0 (line centre absorption coefficient normalized to the continuum absorption coefficient) and β (gradient of the Planck function).

The technique has been extensively tested for different sets of free parameters, as well as for reliability in the presence of noise, gradients of B and velocity v, limited

* The Doppler width $\delta\lambda_D$ is not to be mistaken with the e-folding width of the line profile, $\Delta\lambda_D$, which, in addition to the Doppler width of the absorption coefficient, takes into account many other contributions to the line-profile width.

spectral resolution, etc. by Auer *et al.* (1977), Landolfi *et al.* (1984), Skumanich *et al.* (1985), Lites and Skumanich (1985), Skumanich and Lites (1987) and Murphy (1990), and has been applied to sunspot data in a number of investigations by the HAO and Florence groups (e.g. Lites *et al.* 1987, 1988, Lites and Skumanich 1990, Murphy 1991, Sánchez Almeida and Lites 1992, Arena *et al.* 1990). If $\alpha = 1$, then B, γ, χ are determined relatively accurately for $\Delta\lambda_H \gtrsim \Delta\lambda_D$, even in the presence of gradients of B, γ, χ, v etc. On the other hand, η_0, $\Delta\lambda_D$ and a are not well reproduced (e.g. Murphy 1990), implying that the Auer *et al.* technique often cannot be used to derive thermodynamic properties.

The technique has been briefly tested for spatially unresolved fields, with α as the 9th unknown, by Auer *et al.* (1977) and by Lites and Skumanich (1990) and more extensively by Skumanich *et al.* (1992). Lites and Skumanich (1990), introduce a stray-light parameter instead of a filling factor, but its influence on the profiles is the same. The accuracy of the inversion for unresolved magnetic features is smaller than for resolved features if only a single incompletely split spectral line is used. For unresolved features the reliability of the technique can be improved by including a second line in the analysis (e.g. Lites *et al.* 1988). For example, for the line pair introduced by Stenflo (1973), i.e. Fe I 5250.2 Å and Fe I 5247.1 Å, the total number of unknowns remains the same, but effects due to the magnetic field vector can be much better distinguished from those of α, $\Delta\lambda_D$ and a. In the presence of gradients in B, γ and v, the Milne-Eddington inversion technique returns B, γ and v values corresponding to those at some average height of line formation. Landolfi (1987) has extended the Auer *et al.* technique to determine the gradients themselves (see point 6 in Section 4.3.2). The magnetic vector components derived, on the one hand, from spectrograph data using the Unno-based and Ronan *et al.* (1987) inversion techniques and, on the other hand, from filtermagnetograph data are compared by Wang *et al.* (1992). They find significant differences in the results, some of which appear to be systematic.

For spatially resolved magnetic features without stray light etc., any three Stokes parameters are in principle sufficient to derive the full magnetic vector, due to Equation (2.4b). For spatially unresolved fields (small-scale fields) **B** often has to be derived using only the polarized Stokes parameters V, Q and U [Equations (4.30) and (4.31) are valid for $\alpha < 1$ as well]. Stokes I often cannot be reliably used due to the generally unknown filling factor, α (Section 4.5), and continuum contrast, δ_c (Section 4.6.2). Nevertheless, under some circumstances Stokes I may still be quite useful. For example, in sunspots Stokes I may help, in conjunction with the other 3 parameters, to determine the amount of straylight. Also, $\delta_c\alpha$ may be determined from the line ratio between the Stokes I profiles of two lines that are identical except for their $\Delta\lambda_H$ values (more details are given in Section 4.5). Once $\delta_c\alpha$ is known the problem of determining **B** reduces to that of the resolved field. The main restrictions to this technique are that, in order to be reliable, the Stokes I line ratio requires very high S/N data (10^4 in Stokes I continuum), a sizable α and complete freedom of the used lines from any, even slight, blends. Unfortunately,

these restrictions may be crippling for practical applications.

Finally, Stokes I may have to be applied if too few other Stokes parameters have been or can be measured. Information on γ may be inferred from Stokes I and V only, particularly for spatially resolved magnetic fields (e.g. Beckers and Schröter 1969), but partly also for spatially unresolved fields. The simplest such approach, which requires completely split spectral lines, is to derive γ from the ratio betweem the σ components of Stokes V and Stokes I, or alternatively, from the ratio of Stokes I σ to its π component. In the presence of stray light both ratios can be combined to give an estimate of both γ and α, which parameterizes the amount of stray light $\sim 1-\alpha$ (Solanki *et al.* 1992b). This combined technique only works well for $|\gamma| \gtrsim 35°$. Other approaches are to compare the spatial positions of distinct Stokes V peaks in magnetograms obtained in lines formed at different heights (e.g. Wiehr 1978), or to compare the width of the Stokes I profile to the amplitude of Stokes V (Brants 1985). However, there are considerable problems associated with the two last-named techniques and they should only be used as a last resort. Achieving exact alignment between two magnetograms is, in general, no simple task. The comparison of Stokes I width to Stokes V amplitude also gives large γ values when there is a partial cancellation of magnetic flux (but this also happens if V, Q and U are used) or if there is a large velocity broadening or line strengthening (line broadening due to saturation), or decrease in the temperature gradient.

4.5. Magnetic Filling Factor and Flux

The magnetic flux through a portion of the solar surface is defined as

$$\Phi = \int_{y_a}^{y_b} \int_{x_a}^{x_b} B_z(x,y)dx\,dy, \tag{4.35}$$

where x and y describe the position on the solar surface. The boundaries x_a, x_b of the inner integral may depend on y. The magnetic flux, Φ, being an integral quantity, has the advantage that its definition is independent of the type of model picture made for the magnetic features, so that it may also be applied to, e.g., the return flux model of sunspots (Osherovich 1982). However, since the sign of B_z enters into Equation (4.35), Φ is only a measure of the net flux through the solar surface.

The magnetic filling factor, α, is generally defined in a 1-dimensional, 2-component model, in which α is the fraction of the surface covered by a constant magnetic field of strength B, with the remaining fraction, $(1-\alpha)$, being field-free. In 2-D or 3-D models, a filling factor may have a useful meaning if the magnetic features are described by flux-tube models with current sheets and the field does not exhibit significant horizontal variation within a tube. An example is a model based on the thin tube approximation. However, when using α in 2-D models, it must be explicitly stated to which height α refers, since the flux tube cross-section and, consequently, α generally changes with height. In models in which B varies

smoothly over the solar surface, α has no meaning. An example of a model for which the concept of α cannot be used is the return flux model.

If all (spatially unresolved) magnetic features are assumed to have the same field strength and polarity, then the product of filling factor and field strength is a measure of the spatially averaged field strength. In such a simple 2-component model with a purely longitudinal field

$$\Phi = \alpha B A, \tag{4.36}$$

where A is the observed solar surface area. This equation is true for both cases discussed below. I assume here that α is the filling factor of the total flux, so that Equation (4.36) is not valid in a mixed polarity region.

Both Φ and α have a low information content in the sense that they give no information on the sizes and the shapes and only little on the distribution of unresolved magnetic features. The extent to which the measured values of magnetic flux and filling factor depend on the spatial resolution of the measurements is a function of the distribution of the magnetic features on the solar surface. Consider two extreme cases: 1) All the field is concentrated into a single unresolved magnetic flux tube and 2) it is distributed over a periodic array of spatially unresolved flux tubes. In the first case, the magnetic flux remains constant as the size of the resolution element is increased, while the magnetic filling factor changes in inverse proportion to the solar surface area in the resolution element. In the second case, α is independent of spatial resolution, while the magnetic flux increases proportionally to the size of the spatial resolution element. Situations akin to both these cases are found on the sun.

After these preliminaries let me turn to the diagnostics of Φ and α. For a longitudinal field the amplitude of the Stokes V profile of a weakly split line is proportional to αB, or, equivalently, Φ/A. The Stokes V amplitude of a strongly split lines ($\Delta\lambda_H \gg \Delta\lambda_D$) is proportional to α and independent of field strength. Unfortunately, the Stokes V amplitude also depends on the temperature at the level of line and continuum formation, on the velocity broadening, instrumental spectral resolution, depolarization and cross-talk, on the inclination of the field and the possible presence of opposite polarity flux in the resolution element. Neglecting these dependences and uncertainties can lead to α or Φ values easily wrong by a factor of between 2 and 10 (Grossmann-Doerth *et al.* 1987, Solanki and Stenflo 1986). When comparing filling factor values derived from different lines, it is also important to keep in mind that they can be formed at different heights in the atmosphere and thus sample different filling factors (cf. Grossmann-Doerth and Solanki 1990).

How can the accuracy of α or Φ be improved? Using slightly different line parameters, like the difference between the centre-of-gravity wavelengths [Equations (4.2) and (4.3)], may improve the situation to a certain extent, but not sufficiently (Grossmann-Doerth *et al.* 1987). Improved values are also obtained if a temperature insensitive line is used, or if $T(\tau)$ is taken from a model determined with a

method described in Section 4.6.2. In this manner the influence of the temperature at the level of line formation can be eliminated. A further improvement results from measuring and analysing Stokes Q and U in addition to V. The unknown γ may then be determined. Velocity broadening and spectrograph instrumental smearing may be determined by comparing the width of a calculated Stokes V profile with the observed one. Again, it is worth using a temperature insensitive, or else a weak line to optimize the diagnostics of this parameter. Telescopic depolarization and cross-talk between the Stokes parameters may be compensated for by "anti-telescope" devices (Harvey 1985), or by numerically transforming the observed profiles through the inverted Müller matrix of the telescope. But the other uncertainties remain, particularly the danger of flux cancellation and the uncertainty due to the unknown continuum intensity. The question of flux cancellation may be addressed by increasing either the spatial resolution or the Zeeman resolution (i.e. $\Delta\lambda_H/\Delta\lambda_D$). The influence of the former step is obvious, while the latter helps if the opposing fields are unequal in strength (Rüedi *et al.* 1992a, cf. Section 4.2.2). The problems raised by flux cancellation and, in some cases, instrumental depolarization may be circumvented by using the Stokes I profile to derive α or Φ, or, preferably, complementing the analysis based on Stokes V, Q and U with Stokes I. There are four purely Stokes I-based techniques, which are outlined below.

1. The statistical analysis of Stokes I line widths (Stenflo and Lindegren 1977, Section 4.2.1, Case V), including the extension to unresolved fields in a two-component model by Solanki and Mathys (1988) and Mathys and Solanki (1989), gives

$$x_1 = \sqrt{\delta_l \delta_c \alpha} B \tag{4.37}$$

when applied to data from unresolved magnetic features (as do all techniques based on Stokes I profiles with $\Delta\lambda_H \lesssim \Delta\lambda_D$, see also Gray 1984). Here δ_l and δ_c are factors describing the line weakening and continuum enhancement in the magnetic feature. However, by carrying out the regression at different intensity levels in the line profile, it is possible to separate the effects due to the field strength and the filling factor from each other. The results of the technique must be calibrated with model calculations. It gives the product $\delta_l \delta_c \alpha$. If δ_l is known, then $\delta_c \alpha$ may be determined.

2. The Robinson technique (1980), including further developments by, e.g., Saar (1988) and Basri and Marcy (1988), also gives $\delta_l \delta_c \alpha$ (cf. Section 4.2.1).

3. The depth of the σ components relative to the π component of a fully Zeeman-split Stokes I profile is a measure of $\delta_c \alpha$ (Saar and Linsky 1985), if the field inclination and the line weakening in the magnetic feature are known [see Equations (4.18) and (4.19), for $\Delta\lambda_H \gg \Delta\lambda_D$].

4. The ratio of the Stokes I profiles of two lines that are identical but for their Landé factors also gives $\alpha\delta_c$ (Schüssler and Solanki 1988). The technique depends on the fact that the Stokes I profiles of both lines are identical outside the magnetic feature, irrespective of the non-magnetic atmospheric structure.

If we write $\langle I \rangle$ for the observed Stokes I profile normalized to the observed continuum intensity, I_m for the similarly normalized Stokes I profile from the magnetic feature and I_s for the normalized Stokes I profile from the non-magnetic surroundings of the magnetic feature, then

$$\alpha\delta_c = \frac{\langle I \rangle - I_s}{I_m - I_s}. \tag{4.38}$$

I_m may be obtained from an empirical model of the magnetic feature (Section 4.6), while I_s, which cannot be otherwise determined without a prior knowledge of the filling factor, may be obtained from the ratio of the Stokes I profiles of the two lines (denoted by subscripts 1 and 2) using the fact that

$$\frac{I_{s,1}}{I_{s,2}} = \frac{I_{q,1}}{I_{q,2}}, \quad \text{if} \quad \frac{I_{q,1}}{I_{q,2}} \approx 1. \tag{4.39}$$

If the thermodynamical properties of the two lines are the same, then I_s of line 1 may be written as

$$I_{s,1} = \frac{\langle I_1 \rangle I_{m,1} - \langle I_2 \rangle I_{m,1}}{(I_{m,2} - I_{m,1}) - (\langle I_2 \rangle - \langle I_1 \rangle)}. \tag{4.40}$$

$I_{s,2}$ may be similarly expressed. The advantage of the method is that, unlike the Robinson and the Stenflo-Lindegren techniques, it assumes no model for the non-magnetic surroundings. However, it does require data having an extremely high S/N ratio, so that in practice it does not work very well for small α values, but this problem is shared with all methods based on Stokes I. Also in common with the other Stokes I based diagnostics it is very susceptible to weak blends in either line, probably even more so than the others.

As first pointed out by Schüssler and Solanki (1988), all the techniques published until now only give $\alpha\delta_c$ instead of α, with $\delta_c = I_{cm}/I_{cq}$. The reason is that, in addition to not knowing the I_c of the magnetic fraction of the atmosphere in the resolution element, I_{cm}, we generally also do not know the continuum intensity of the non-magnetic fraction, I_{cs}. Assuming I_{cs} to be the same as the quiet sun value, I_{cq}, is often too gross a simplification. All the improvements discussed so far have not resolved this problem.

In principle, α may be obtained independently of δ_c by resolving the magnetic features. However, in practice it may often not be possible to achieve complete resolution. One way of at least reducing the dependence of α on δ_c is to observe in the infrared, where the Planck function is less dependent on temperature and consequently the continuum contrast is lower. As an example assume that $\delta_c = 2.0$ at 0.5 μm. At 1.5 μm the corresponding δ_c is 1.4, while at 12 μm the δ_c is only 1.2 if I_{cq} and I_{cm} have the spectral dependence of black bodies.

Let me now describe a method which may be able to determine the magnetic flux and the continuum contrast of magnetic features separately. The proposed

technique is based on two main premises: 1. B decreases with height and magnetic elements expand rapidly until they merge with neighbouring elements at or slightly above the temperature minimum, particularly within active regions (e.g. Jones 1985, Solanki and Steiner 1990). 2. Stokes V profiles are, to first order, formed only inside magnetic features.

From points 1 and 2 it follows that the V profile of a chromospheric line is formed over a larger area and sees a different continuum than the V profile of a photospheric line. In particular, if $\alpha(z = 0) \gtrsim 5$–10% (e.g. in an active region plage), then the magnetic filling factor at the formation height of the inner flanks of the chromospheric line, $\alpha_{\rm ch}$, is close to unity (Solanki and Steiner 1990). By comparing the Stokes V profiles of a chromospheric and a photospheric line, it should be possible to separate the influence of δ_c and α on the lines and to determine these quantities individually.

Using one of the techniques described earlier in this section $\alpha_{\rm ph}\delta_c\Delta$ can be determined, where $\alpha_{\rm ph}$ is the filling factor at the level of line formation of the photospheric line, $\delta_c = I_{cm}/I_{cq}$ and Δ is a factor which takes into account the expansion of the field between the continuum-formation and line-formation heights. Δ can be determined with sufficient accuracy from model calculations.

For a chromospheric line whose core (i.e. Stokes V amplitude wavelength) is formed in almost pure scattering and is very insensitive to the local electron temperature (e.g. Mg Ib 5172 Å, Lemke 1986), the Stokes V amplitude normalized to the average continuum intensity may be written approximately as

$$V_{\rm ch}^{\rm max} \sim Z_{\rm ch} t_{\rm ch} \alpha_{\rm ch} B_{\rm ch} \cos\gamma \frac{(\alpha_{\rm ph} I_{cm} + (1-\alpha_{\rm ph}) I_{cs})}{\langle I_c \rangle} = Z_{\rm ch} t_{\rm ch} \alpha_{\rm ch} B_{\rm ch} \cos\gamma, \qquad (4.41)$$

where $Z_{\rm ch}$ is a factor containing the atomic physics (oscillator strength, Landé factor, etc.), $t_{\rm ch}$ takes into account the thermodynamics of the magnetic feature in the line forming layers (mainly level populations), $\alpha_{\rm ch}$ is the value of α in the chromosphere, $B_{\rm ch}$ is the field strength in the chromosphere, $\cos\gamma$ is the approximate influence of magnetic field inclination and $\langle I_c \rangle$ is the continuum intensity averaged over the resolution element.

$Z_{\rm ch}$ is generally obtainable from published sources. The problem of an unknown $t_{\rm ch}$ is alleviated by the choice of a line whose source function has almost completely decoupled from the local temperature, so that $t_{\rm ch}$ for a magnetic feature with unknown temperature should not differ significantly from the $t_{\rm ch}$ determined from a model of the average chromosphere. Finally, $\cos\gamma$ can be determined by measuring all four Stokes profiles (Section 4.4).

The continuum intensity seen by a chromospheric line is very close to $\langle I_c \rangle$ if $\alpha_{\rm ch} \approx 1$, as already incorporated in Equation (4.41). It is therefore possible to determine $\langle B \rangle = \alpha_{\rm ch} B_{\rm ch}$ directly by scaling a calculated profile of the chromospheric line to match its observed profile. However, note that in Equation (4.41) the assumption has been made that the continuum intensity affects the Stokes V amplitude linearly. This condition is fulfilled to high accuracy in LTE, as shown by

model calculations in which only $T(\tau_c \gtrsim 1)$ is changed, while leaving $T(\tau_l \approx 1)$ unchanged (τ_l is the optical depth in the spectral line). However, due to the importance of the continuum radiation field for the ionization and excitation balance in NLTE, this still has to be tested for any chromospheric line used.

By combining simultaneous observations of both lines, it is possible to derive even more information. If the observations are averaged over a sufficiently large spatial region then the magnetic flux therein is conserved with height, i.e.,

$$\langle B \rangle = \alpha_{\rm ch} B_{\rm ch} = \alpha_{\rm ph} B_{\rm ph}. \tag{4.42}$$

Since $\langle B \rangle$ and $B_{\rm ph}$ are now known, it is possible to derive $\alpha_{\rm ph}$. Finally, since the product $\delta_c \alpha_{\rm ph}$ is also known, δ_c can be determined as well.

This technique does have shortcomings. It requires the accurate NLTE calculation of the Stokes V profile of the chromospheric line. On the other hand, the possible Zeeman saturation of these lines should be no problem. It must also be tested how strongly the Stokes V amplitude of the chromospheric line is affected by the fact that many individual rays pass through both magnetic and non-magnetic atmospheres. One problem may be finding a suitable chromospheric line, namely a line whose core is formed sufficiently high and is practically unaffected by the local temperature.

Finally, in the long run it may be best to determine δ_c directly, either from very high spatial resolution observations, or by applying spectral techniques (e.g. by fitting Stokes V profiles of C I lines, Section 4.6.2). Once δ_c is known it is relatively straightforward to derive α by applying one of the techniques giving $\alpha\delta_c$.

Van Ballegooijen (1985c) pointed out that α is underestimated near the solar limb if the magnetic field is concentrated into very thin flux tubes. However, his results are valid only for single flux tubes. Recent calculations using a model similar to the one illustrated in Figure 3.1 show no strong dependence of the calculated V amplitudes on flux tube size, *as long as α is kept constant* in the model.

4.6. Temperature and Abundances

Temperature and abundance diagnostics are intertwined. To determine the temperature from the spectral lines of a given element we must know or assume its abundance. Conversely the derivation of abundances relies on an accurate knowledge of the temperature stratification (e.g., Holweger 1979). Therefore, I discuss the diagnostics for temperature first and then briefly outline how, once $T(\tau)$ has been obtained from the continuum or the spectral lines of a single element, the relative abundances of the elements may be determined. I do not discuss the determination of abundances in detail, since at present there is no compelling reason to suppose that the abundances in solar magnetic features are different from the mean solar photospheric abundances.

4.6.1. Temperature of Spatially Resolved Magnetic Features

If the magnetic feature is spatially resolved, then the stratification of its temperature $T(z)$ may be determined either from the Stokes I profiles of a set of spectral lines, the wings of a very strong line, or from the continuum intensity I_c at different wavelengths. In principle, it is also possible to derive $T(\tau)$ from the centre-to-limb variation (CLV) of I_c or of line profiles. However, this last technique is at present not to be recommended, since the finite size of magnetic features, their complex geometry and the presence of internal structure make the reliable combination of observations obtained near disc centre and near the limb very difficult. For example, the temperature of the flux tube walls may not be the same as the temperature in the body of a flux tube. Furthermore, a CLV study must either combine the temperature derived from different objects together into a single model, or follow a single feature (e.g. a sunspot) from disc centre to the limb. In contrast to the quiet sun, there is no a priori reason why two observed magnetic features should have the same temperature. Therefore, in the first case (i.e. when different regions are compared) the resulting $T(\tau)$ may not represent any existing magnetic feature at all. See Deming *et al.* (1984) for the fluctuating results of such an analysis in the quiet sun, based on molecular lines, or the large scatter in the data points of Walton (1987), who uses the CLV of spectral lines to derive facular models. In the second case (i.e. following a single feature across the disk), due to temporal evolution, the resulting $T(\tau)$ may again not represent the true $T(\tau)$ at any given time. The only reasonably reliable way of obtaining the temperature stratification from a CLV analysis is to apply a statistical approach by observing many features. The main advantage of a CLV analysis is that it allows some connection to be made between geometry and temperature (e.g. are the walls of magnetic elements hot?).

The continuum intensity, $I_c(\lambda)$, may be used to derive $T(\tau)$, since the continuum absorption coefficient is a function of wavelength, so that I_c is formed at different heights for different wavelengths [see e.g. Figure 1 of Vernazza *et al.* 1976, which shows $z(\tau = 1)$ vs. λ for the quiet sun]. This technique has been widely used to derive models of the quiet solar atmosphere (e.g. Gingerich *et al.* 1971, Vernazza *et al.* 1976, 1981, Maltby *et al.* 1986), of sunspot umbrae (e.g. Maltby *et al.* 1986) and penumbrae (e.g. Maltby 1972, Kjeldseth Moe and Maltby 1974). A wide range of wavelengths must be observed in order to obtain even a reasonable height coverage. For example, in order to make a model of the photospheric layers alone, λ must vary either between 1600 Å and 4000 Å, or between 1.6 μm and 300 μm. The latter wavelength range is to be preferred, since it offers far more continuum windows. On the other hand, the spatial resolution achievable at the longest wavelengths is currently substantially lower than in the visible. Unfortunately, it is impossible to achieve complete height coverage of even the photosphere without observing from satellites (in the UV) or from balloons (in the infrared).

Deriving the temperature of resolved magnetic features from spectral lines is similar to deriving the temperature in the quiet sun (e.g. Holweger 1967). With known $g^\star f\epsilon$ ($g^\star f$ is the statistically weighted oscillator strength of the line, ϵ is the

relative abundance) it is possible to derive T at one τ value from a comparison of the calculated to the observed profile of a single temperature-sensitive photospheric line.* Two lines formed at different heights give the vertical temperature gradient, while a more detailed form of the $T(\tau)$ stratification may be obtained by using many photospheric lines. A classic example of this approach is the quiet sun model of Holweger (1967), who combined the determination of T and ϵ (cf. Holweger and Müller 1974). Alternatively, the wings or the shape of a strong line like Ca II H or K, or Mg II h or k may also be used since they map the source function, $S_\nu(\tau)$, onto $I(\lambda)$ (e.g. Shine and Linsky 1974, Ayres and Linsky 1976, Morrison and Linsky 1978). These diagnostics are limited to heights at which $S_\nu(\tau)$ follows $B_\nu(\tau)$ closely. They often break down in the cores of strong lines. The shape of a line of even intermediate strength should allow the temperature stratification to be determined with reasonable accuracy according to Ruiz Cobo and Del Toro Iniesta (1992).

When modelling sunspot umbrae, the contamination of spectra by spectral and spatial straylight must be taken into account. Since Stokes V is not significantly affected by spectral straylight (Zayer 1990), the Stokes V lobe areas of weakly split lines or Stokes V amplitudes of completely split lines may be used instead of Stokes I line depths. However, when using V of weakly split lines to derive the temperature, $B\cos\gamma$ must be determined first, since the strength of the Stokes V signal depends on this parameter. For lines with $\Delta\lambda_H \gtrsim \Delta\lambda_D$ it is necessary to know $\cos\gamma$, irrespective of which Stokes parameter is used. A knowledge of B and $\cos\gamma$ is not necessary if ratios between well-chosen lines are considered. For more on diagnostics involving Stokes V, Q and U and line ratios see Section 4.6.2.

Finally, and this is true for unresolved fields as well, althought the observations give $T(\tau)$, often $T(z)$ is required for a comparison with theory. The conversion from the τ to the z scale itself depends on B (via the evacuation of flux tubes) and on $T(\tau)$, via the continuum opacity, and generally involves the use of a hydromagnetic model.

4.6.2. Temperature of Spatially Unresolved Magnetic Features

To determine the temperature in unresolved magnetic features, Stokes I is generally not suitable, since its use requires not only a prior knowledge of $\alpha\delta_c$, but also some idea of the line or continuum intensity, I_{cs}, of the non-magnetic surroundings (Schüssler and Solanki 1988, cf. Section 4.5). In other words, the determination of the temperature within unresolved magnetic regions presumes a good knowlege of the filling factor and of the temperature structure of the non-magnetic atmosphere. Unless the magnetic filling factor is minute the latter generally does *not* correspond to the quiet sun temperature stratification. If α and I_{cs} are not well known, and they generally are not, then a considerable uncertainty in the derived

* Note that the temperature sensitivity of a line is itself temperature dependent. In general, lines from minority ionization species are the most suitable for temperature determinations, but less suitable for abundance determinations.

temperature structure of the magnetic features is unavoidable (as demonstrated by Walton 1987). The only way of obtaining the temperature in unresolved magnetic features using Stokes I without having to assume I_s explicitely is by comparing $\sqrt{\alpha\delta_c}B$ derived from temperature sensitive lines with $\sqrt{\alpha\delta_c}B$ obtained from temperature insensitive lines (e.g. using the technique of Stenflo and Lindegren 1977, of Robinson 1980, or of Schüssler and Solanki 1988). If the two values differ, then the temperature in the magnetic feature is different from that in the assumed model (Solanki and Mathys 1987, Mathys and Solanki 1989).

Temperature determinations using Stokes Q, U, or V are, in general, to be preferred to the diagnostics relying on Stokes I. However, since Stokes Q, U and V profiles scale with α, single-line methods must rely on exploiting the changes in line shape induced by the temperature. Such changes are best visible in Stokes Q and U, for which the ratio between the π and σ components depends strongly on temperature if the line strength lies in the correct range and $\Delta\lambda_H \lesssim \Delta\lambda_D$ (Solanki *et al.* 1987). For a weakly split line, the π component corresponds to the line core and is thus more strongly saturated than the σ components which correspond to the line flanks. A change in temperature affects the saturation of a temperature sensitive line and thus the σ to π ratio. The ratio also depends on the field strength, but not on α, which is much harder to determine. Therefore, the σ to π ratio, if used in conjunction with a field strength diagnostic, is a measure of the temperature. More details are given by Solanki *et al.* (1987).

If two lines, identified here by subscripts 1 and 2, one of which is more temperature sensitive than the other, are measured, then the ratios Q_1/Q_2, U_1/U_2, or V_1/V_2 serve as temperature diagnostics (often referred to as a thermal line ratio). The lines should either have a similar Landé factor, wavelength and strength, but a different excitation potential (Landi Degl'Innocenti and Landolfi 1982, Stenflo *et al.* 1987a), or they may be similar in all respects, except for their line strengths. It is important that at least one of the used lines lies on the linear part of the curve of growth, i.e. that its line depth (which corresponds to the Stokes V lobe areas or amplitudes, depending on $\Delta\lambda_H/\Delta\lambda_D$) reacts directly to temperature. Figure 4.6 illustrates the different temperature sensitivity of the Stokes V profiles of a weak low-excitation (panel a), a weak high-excitation (panel b) and a strong low-excitation (panel c) hypothetical Fe I line. The solid profiles were calculated in a quiet-sun atmosphere, the dashed ones in a hotter empirical flux-tube model. The V profile of the weak low-excitation line is most strongly weakened in the flux tube, followed by that of the weak high-excitation line. The V profile of the strong low-excitation line is even strengthened slightly, since the I profile loses its wings and thus becomes narrower, with steeper flanks. Thermal line ratios (constructed indirectly) were first introduced and interpreted by Harvey and Livingston (1969).

There are two main points regarding this technique that must be borne in mind.

1) The calibration of the technique requires model calculations (like practically all temperature diagnostics of small magnetic features) and it is important to test the response of a thermal line ratio to the temperature before applying

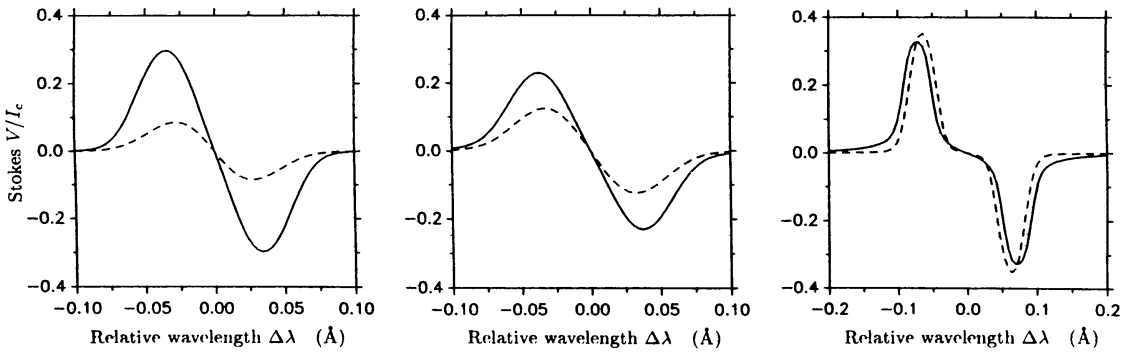

Fig. 4.6. An illustration of the different temperature sensitivity of different lines. **a** A relatively weak, low-excitation line (excitation potential of 0) for two different temperatures, a quiet sun model (solid profile) and a hotter flux-tube model (dashed profile). $W_\lambda = 50$ mÅ in the quiet sun. $B = 1000$ G in both models. **b** A relatively weak, high-excitation line for the same two models (excitation potential of 4 eV). $W_\lambda = 50$ mÅ in the quiet sun. Since this line is slightly broader and shallower than the line in panel a, its Stokes V profile in the quiet sun is slightly weaker. Note the change in ratio of high-excitation to low-excitation Stokes V profile from one model to another. **c** A relatively strong low-excitation line (excitation potential of 0) for the same two models. $W_\lambda = 150$ mÅ in the quiet sun.

it to data (e.g. Solanki and Stenflo 1984, 1985, Keller 1989, Keller *et al.* 1990a). If self-consistent models are used for the calibration, then the coupling between the field strength and the temperature stratification of such models may lead to unexpected changes in the "thermal" line ratio, if, say, the field strength is changed (Steiner and Pizzo 1990). This problem can be defused by considering not only a thermal diagnostic, but simultaneously also a diagnostic of the magnetic field in the analysis.

2) Since two lines with different temperature sensitivities are generally not formed at the same height, the thermal line ratios give a mixture of information on the temperature and on its gradient. In particular, the difference in heights of formation of the two lines is itself $T(\tau)$ dependent, i.e. it depends on the models used (Larsson *et al.* 1991).

The two-line technique may be easily extended to many lines, which, given a judicious choice of lines, allows T to be determined over a range of τ values. Best results are achieved if a large number of lines with a mixture of line strengths, S_I, and excitation potentials, χ_e, are used. Although the temperature sensitivity decreases with both S_I and χ_e, the heights of formation increase with S_I, but decrease with χ_e. Therefore, if a sufficient number of lines with a sufficiently broad and dense coverage of the (χ_e, S_I)-plane are used, then $T(\tau)$ may be determined over a range of heights and the influence of T on the diagnostics may be decoupled from that of $dT/d\tau$. Since, for $\Delta\lambda_H \lesssim \Delta\lambda_D$, Stokes V has its peak in the line flanks, its height of formation usually varies somewhat less than that of the Stokes I line core (Larsson *et al.* 1991). Consequently the higher photospheric layers are not easily accessible with Stokes V. Thermal ratios between the π components of Q profiles reach higher in the atmosphere, but are expected to become very noisy

for strong lines due to the strongly saturated line cores, which result in very weak π components.

An additional advantage of using a large number of lines is that it reduces the importance of blends and uncertainties in the atomic parameters (e.g. Landé factors) of some lines. The major disadvantage is the need to observe many line profiles simultaneously, which, with current instrumentation, means the loss of temporal and spatial resolution. In addition, the analysis is lengthy and computationally intensive. On the other hand, for many purposes only individual line parameters (e.g. Stokes V lobe area) need to be considered. The temperature determination using a many-line approach may also be automated with the help of a least-squares fitting technique, as pioneered by Stenflo (1975) and Keller *et al.* (1990a). More details are given in Section 4.9.

The many-line approach may be applied either directly to Stokes V or to the integrated V profile (I_V). The latter has the advantage that it can be parameterized in exactly the same fashion as Stokes I and the sensitivity to temperature may be increased by comparing directly with Stokes I profiles taken from the quiet sun, e.g., by using $\ln(d_V/d_I)$ vs. W_λ diagrams, where d_V and d_I are the depths of the I_V and Stokes I profiles, respectively (Solanki and Stenflo 1984, 1985). The disadvantage is that I_V is a valid approximation of I_m only for $\Delta\lambda_H \lesssim \Delta\lambda_D$ (Solanki 1987c).

Semel (1981) used the comparison between the field strength derived from $|\lambda_{I+V} - \lambda_{I-V}|$ (i.e. using the centre-of-gravity technique, Section 4.2.1, Case III) of different lines as a temperature diagnostic. However, this parameter is not quite independent of the local Stokes I profile. Assuming Stokes I to be symmetric and Stokes V to be antisymmetric one can write using Equation (4.2),

$$\lambda_{I+V} - \lambda_{I-V} = \frac{2}{W_\lambda(I)} \int \frac{V(\lambda)\lambda}{I_c} d\lambda, \tag{4.43}$$

where $W_\lambda(I)$ is the equivalent width of the local observed Stokes I profile and $\lambda = 0$ at line centre. In general, the error in the above equation, due to the assumption of particular symmetries of I and V, is expected to be less than 1%. The $W_\lambda(I)$ in the denominator is the main detractant from this parameter as a diagnostic, since it must be reproduced by the model calculations as well. This means that I_s and α have to be prescribed, so that much of the advantage of using Stokes V is lost. The value of the diagnostic can be enhanced if instead of W_λ of the locally measured Stokes I profile, the W_λ of the quiet-sun I profile is used, or if W_λ is left aside completely, i.e. if $\int V\lambda\, d\lambda/I_c$ is used. This parameter is not too different from the Stokes V lobe areas ($\sim \int V\, d\lambda$). For weakly split lines, $\int V\lambda d\lambda/I_c$ gives larger weight to the line wings which are formed deeper in the atmosphere, thus lowering this parameter's potential for diagnosing the temperature of the higher layers.

Some questions, such as the one regarding the lowest temperature in magnetic features may require the application of special techniques, or a special choice

of spectral lines. For example, it may be possible to answer the above question by analysing and modelling Stokes V profiles of electronic transitions within molecules (cf. Banwell 1972), or atomic lines arising from levels that are populated only at low temperatures (e.g. low-excitation Ti I lines).

4.6.3. Remarks to Temperature Diagnostics

In this section I briefly list some points which should be borne in mind when deriving $T(\tau)$ or related quantities.

1. Velocity broadening and, if necessary, instrumental broadening of observed line profiles must be properly taken into account if the temperature is to be reliably deduced (Solanki 1986). For example, velocity broadening decreases the line depth or Stokes V lobe area. Furthermore, it affects weak or low-excitation lines more strongly than strong or high-excitation lines (since the latter are intrinsically broader). Therefore, unless taken into account, velocity or instrumental broadening makes the temperature derived empirically from a thermal line ratio appear higher than the true value.
2. NLTE effects are important. Consider the case of iron, the element with so far the best studied non-LTE equilibrium in small-scale magnetic features. For Fe I, departures from LTE are mainly due to overionization of Fe I into the dominant species Fe II by the UV radiation field. The overionization causes Fe I lines to weaken relative to Fe II lines. The fact that low-excitation Fe I lines are formed higher in the atmosphere than Fe II and high-excitation Fe I lines, at a height where level populations depart more strongly from their LTE values, enhances this relative weakening. The end result is that NLTE effects in many ways mimic the effect of a higher temperature in the magnetic feature (Rutten and Kostik 1982, Solanki and Steenbock 1988). Unfortunately, one of the main solar parameters determining the magnitude of departure from LTE, the continuum intensity, is itself not the easiest of quantities to determine reliably (see point 4 below).

   As demonstrated by Stenholm and Stenflo (1978), the influence of NLTE is considerably enhanced if the small horizontal size of most magnetic features is taken into account, since the hot or warm walls of small magnetic features greatly increase the amount of UV radiation seen by a particular atom and thus the overionization of minority species. The influence of hot walls is particularly important for atoms situated below the $\tau = 1$ level of the non-magnetic atmosphere. Note, however, that Stenholm and Stenflo (1978) considered an extreme case, with an unrealistically large temperature jump at the magnetic boundary. Actual non-LTE effects, coupled to the flux tube geometry, may be less pronounced than their findings (Stenflo, private communication 1992). All the same, neglecting NLTE effects in the modelling of observational data leads to an overestimate of the temperature.

   For some investigations NLTE calculations are a must, in particular for the determination of the temperature in the higher atmospheric layers. For example,

LTE models cannot contain a chromospheric temperature rise without producing emission cores in lines whose observed profiles show purely absorption cores. NLTE calculations can easily reconcile low-lying chromospheres and the absence of emission cores (Bruls and Solanki 1992b).

3. If not taken into account, the geometry and internal structure of the magnetic feature may also give rise to the determination of a wrong $T(\tau)$ structure, even in LTE. Consider a spatially unresolved, horizontally inhomogeneous temperature profile within a single magnetic feature, or two magnetic features with different temperatures lying within a single spatial resolution element. Examples of hot and cool magnetic features which cannot be spatially distinguished by most, if not all, current observations are the smallest bright and dark filaments in sunspot penumbrae, umbral dots and the dark umbral background in umbrae, and neighbouring magnetic elements with different temperatures in plages. If a horizontally homogeneous model is used to interpret the observations of such unresolved structures, then some "intermediate" temperature stratification results which may not correspond to the temperature stratification at any point in the feature and is very likely not a simple average of the different temperatures, since a horizontal temperature variation on the sun is converted into a vertical temperature stratification in a horizontally homogeneous model. This is particularly true if the lines forming the temperature diagnostics are separated into two distinct groups with different temperature sensitivities and different formation-height ranges, e.g. Fe I and II lines (Holweger, private communication 1985). Fe I lines obtain larger contributions in the cooler parts of the atmosphere, while Fe II lines obtain a larger contribution in the hotter portions. In addition, low-excitation Fe I lines are formed higher in the atmosphere than Fe II lines, so that a model derived using such lines should correspond more closely to the cooler magnetic features in the higher layers and should resemble the hotter ones in the lower layers.

   Then there are effects due to the finite size of smaller magnetic features. Most rays passing through a small magnetic feature pass through both the magnetic and non-magnetic parts of the atmosphere. Although Stokes V, Q and U are not directly affected by the temperature in the non-magnetic atmosphere (i.e. the level populations in the non-magnetic layers do not influence V, Q, or U), they are coupled to the Stokes I profile formed in the external atmosphere by the transfer equations. At disc centre the finite size of magnetic elements and their expansion with height have only a negligible effect on the temperature diagnostics (Solanki 1989, Keller *et al.* 1990a). Away from disc centre the temperature of the non-magnetic atmosphere may significantly influence the polarized line profiles (De Martino 1986, Ringenbach 1987, Bünte *et al.* 1991, 1992b), but more tests are required. Audic (1991) pointed out that the Stokes V, Q and U profiles formed along a ray passing from a magnetic into a non-magnetic medium get attenuated exponentially. Polarized profiles formed along rays passing from the non-magnetic into the magnetic atmosphere are affected

in a somewhat more complex manner, although the general tendency is again for the polarization to be reduced by the unmagnetized material.

4. The continuum brightness, I_{cm}, of unresolved magnetic features remains difficult to measure. It is a delicate task to estimate the reliability of the directly measured I_c, due to the often unknown admixture of light from the non-magnetic surroundings. The main problem is that the determination of both, the continuum brightness of the surroundings, I_{cs}, and the magnetic filling factor depend on I_{cm} (Section 2.3.4), so that it is not known by how much the observed I_c must be corrected in order to obtain I_{cm}. Only simultaneous magnetograms and I_c measurements at extremely high resolution (such as those of Keller 1992a) have any hope of giving a reliable I_{cm}. The other possibility is to use spectral lines observed in polarized light. One as yet untested method of obtaining I_{cm}, namely by comparing the Stokes V profiles of a photospheric and a chromospheric line, has been described in Section 4.5. A more straightforward way of determining I_{cm} is to use Stokes V profiles formed at low heights in order to determine $T(\tau)$ close to the $\tau = 1$ level in the magnetic feature. Unfortunately, almost all temperature-sensitive lines are formed well above $\tau_{5000} = 1$. Even weak high-excitation Fe I lines around 1.6 μm (the wavelength of the opacity minimum) do not obtain a sizeable contribution below $\log \tau = -0.5$. Additionally, these lines are not sufficiently temperature sensitive to set interesting limits on the temperature or temperature gradient in magnetic features (Muglach and Solanki 1991, 1992). More promising are high-excitation lines of C I or O I, which are also formed very deep in the atmosphere (contribution function maxima of V peaks around $-0.5 \lesssim \log \tau_{5000} \lesssim 0.0$). One candidate is C I 5380.3 Å, whose Stokes I profile has been used to derive the temperature in deep atmospheric layers (Livingston *et al.* 1977, Elste 1985). It is both, temperature sensitive (Livingston *et al.* 1977) and formed in LTE (Stürenburg and Holweger 1990). A technique for determining I_{cm} using the ratios of C I to Fe II Stokes V profiles has been developed by Solanki and Brigljević (1992). These ratios are sensitive temperature diagnostics, which work also for spatially unresolved features, particularly when combined with diagnostics of the temperature in higher layers.
5. The pressure within magnetic features cannot be obtained in a straightforward manner from the usual pressure diagnostics like the strong wings of Balmer lines, since the line wings usually disappear in the noise in the Stokes V, Q and U profiles (recall that $V \sim dI/d\lambda$ and $Q, U \sim d^2I/d\lambda^2$ in the line wings). Furthermore, the pressure in magnetic features is greatly reduced compared to the surroundings only at a given geometrical height and not necessarily at a given optical depth (the gravitational acceleration is the same at all points on the solar surface).* Therefore, pressure is best determined from the momentum equation under the assumption of hydrostatic equilibrium. The density then

* For example, at $\tau = 1$ in sunspot umbrae it is almost a factor of 2 larger than at equal τ in the quiet sun (e.g. Maltby *et al.* 1986, Walther 1992).

follows from the equation of state.

6. The major atomic parameters required for a determination of T are the statistically weighted oscillator strength, $\log g^\star f$, the elemental abundance, ϵ, and the Zeeman splitting pattern, i.e. g_u, g_l, J_u, J_l (u = upper, l = lower, g = Landé factor, J = total angular momentum quantum number). In LS coupling the Zeeman pattern may be calculated for a known transition (e.g. Beckers 1969c). In the presence of departures from LS coupling, laboratory measurements or detailed computations of g_u and g_l must be used (as listed by, e.g., Corliss and Sugar 1985, Johannson and Learner 1990, Kurucz 1991, cf. Mathys 1990). Lists of empirical $g_{\rm eff}$ values for lines of solar interest have been given by Solanki and Stenflo (1985) and Solanki *et al.* (1990). The list of Kurucz contains reliable values for many thousand spectral lines.
   Oscillator strength values may be taken either from precise laboratory measurements (e.g. Blackwell *et al.* 1979a, b, 1980, 1982a, b, c, d, e, 1983, 1986a, b, c, see Huber and Sandeman 1986 for a review), or, now with almost equal reliability, but for many more lines, from fits to quiet sun equivalent widths or line profiles (Gurtovenko and Kostik 1981, 1982, 1989, Thévènin 1989, 1990). An even larger selection of $\log(g^\star f)$ values, although of lower quality, has been calculated by Kurucz (1991).

4.6.4. Abundances

In the past it has generally been assumed that elemental abundances in solar magnetic features are the same as in the quiet sun. In the photosphere and the chromosphere this assumption is very reasonable, but it has to my knowledge never been tested with high accuracy. In resolved magnetic features the abundances may be determined either by first deriving the temperature structure from the continuum and then determining ϵ from the equivalent widths of weak lines, or by applying the approach pioneered by Holweger (1967) of determining the abundance from the W_λ of the lines and $T(\tau)$ from their depths.

For unresolved magnetic features there is no reliable method of deriving absolute abundances, due to the dependence of Q, U and V on α or $\langle B \rangle$. However, it is possible to make consistency tests of abundances relative to a given element (e.g. to iron) if the model atmosphere used to describe the magnetic feature was derived using lines of this element only.

4.7. Velocity

4.7.1. Spatially Resolved Magnetic Features

The various (Stokes I based) techniques developed to study velocity fields in the quiet sun may also be applied to spatially resolved magnetic features. The main velocity sensitive parameters of Stokes I are the line width, line shift and line-bisector shape or line asymmetry. The shift of, e.g., the line core gives a measure of the spatially and temporally averaged velocity in the resolution element (but see below). Vertical velocity gradients are also averaged and weighted by the velocity

response function, R_F (Beckers and Milkey 1975, Caccin *et al.* 1977):

$$\Delta\lambda_I \approx \frac{\lambda_I}{c} \frac{\sum_{i=1}^{N} \int v_i(\tau) R_{Fi}(\tau)\, d\tau}{\sum_{i=1}^{N} \int R_{Fi}(\tau)\, d\tau}, \tag{4.44}$$

where i runs over different spatial components. If the measurement integrates over time, then Equation (4.44) should also include an integral over time. Note that R_{Fi} scales with the continuum intensity and the line strength in each spatial component. The relation is only approximate, since R_{Fi} is strictly valid only for small velocity perturbations and its use assumes that the changes of other atmospheric parameters produced by the velocity perturbation (e.g. changes in pressure and temperature) do not affect the line profile.

An absolute wavelength shift can only be determined if the wavelength of the measured spectrum can be calibrated using either a laboratory light source or telluric lines (i.e. lines formed in the earth's atmosphere). Additionally, the solar-terrestrial relative velocity and the solar and terrestrial rotational velocities must be compensated for. However, useful information may be obtained by comparing the wavelength on one part of the solar surface with that on another part where it is known, e.g. in the quiet sun, or at the solar limb. Of course, the accuracy of such, solar, calibrations is limited, e.g. by fluctuations in the longitudinal velocity field near the limb due to the supergranulation.

More information on the velocity field can be derived if the wavelength shift (given, e.g., by $(\lambda_r + \lambda_b)/2$, where $\lambda_{b,r}$ are the wavelengths at the same intensity value in the blue and red line flanks, respectively) is determined at many depths in the line profile, i.e., if the line bisector, a measure of the (Stokes I) line shift and asymmetry, is calculated. It is straightforward to see from Equation (4.44) that in the absence of any vertical or horizontal velocity *gradients* [i.e. $v_i(\tau) = v =$ const.], the line bisector is simply a vertical straight line. Therefore, the shape of the line bisector is a diagnostic of velocity gradients. The bisector of a single line cannot readily distinguish between vertical and horizontal gradients, particularly when the latter are coupled to gradients in the temperature, or continuum intensity.

The literature on the measurement of solar line shifts and bisectors is large and for further details the interested reader is referred to the following text books, proceedings and reviews (Beckers 1981, Dravins 1982, Keil 1984, Gray 1988, Rutten and Severino 1989).

The measurement of the time dependence of the velocity is quite similar to the measurement of a stationary velocity, except that now time series of the line shift, or the line bisector, are measured. Amplitudes and periods of oscillations or waves may in some cases be obtained directly from the measured $v(t)$ signal, or else from its power spectrum. Generally, two methods are used to distinguish between propagating and standing waves (e.g. Evans and Michard 1962, Frazier 1968, Deubner 1974, Schmieder 1976, Lites and Chipman 1979, Deubner and Fleck 1989).

I. Comparison between the velocity signal obtained from two lines formed at different heights, using a phase-sensitive technique, e.g. a cross-correlation: This allows the propagation velocity to be determined, although the solution is not unique unless some help is taken from theory.

II. Comparison between wavelength shift and intensity of the Stokes I line core of a single spectral line: Standing waves and upwards and downwards propagating compressible waves produce a distinguishable phase difference between $\Delta\lambda$ and intensity, although radiative damping complicates the picture. This approach also requires theoretical input.

Unsurprisingly, a combination of both approaches, i.e. a measurement of line core wavelength and intensity fluctuations in a number of lines is the most powerful tool. Such a combination may also allow the radiative damping to be estimated.

Finally, in some cases the only, or at least the main, influence of the velocity field is to change the line width. Examples are a turbulent velocity, an incompressible wave with a wavelength much smaller than the width of the line's velocity response function, or horizontal velocity gradients within the spatial resolution element which are uncorrelated with temperature fluctuations. It requires a velocity gradient to increase the line width, but, like the line bisector, line broadening cannot differentiate between vertical, horizontal or temporal gradients in the velocity and, in addition, cannot give any information on the sign of the gradient. Line broadening of Stokes I due to turbulent and granular velocities has been discussed by, among others, Evans *et al.* (1975), Holweger *et al.* (1978), Nordlund (1984) and Carlsson and Scharmer (1985). Line broadening of Stokes V due to turbulent velocities has been considered by, e.g., Solanki (1986) and Solanki *et al.* (1987) and due to longitudinal tube waves by Solanki and Roberts (1992).

Unfortunately, the sensitivity and response of all these line parameters (line shift, line asymmetry and line width) to the velocity is influenced by other atmospheric parameters, foremost of all the temperature. The temperature enters into Equation (4.44) through the response function, whose temperature sensitivity stems from its dependence on continuum intensity, line strength (i.e. $g^\star f\epsilon$ and level populations) and height of line formation. The Zeeman splitting can also affect the velocity diagnosis; a large $\Delta\lambda_H/\Delta\lambda_D$ mainly decreases the sensitivity of the line to velocity. Measured line shifts and bisectors are particularly susceptible to misinterpretation if the velocity is inhomogeneous within the resolution element. A classical example is the solar granulation. Spectra that do not spatially resolve the granules show blueshifts of typically a few 100 m s^{-1} and curved (C-shaped) bisectors. However, a net shift of the lines can be produced without any net flows; a correlation between intensity and velocity is sufficient (e.g. bright upflows and dark downflows, as in the granulation, Schröter 1957, Dravins *et al.* 1981). Propagating compressible waves may, again due to their temperature-velocity correlation, also lead to a net line shift, even when averaged over a full wave period (e.g. Solanki and Roberts 1992).

Consequently, no velocity diagnostic is model independent. This implies that

velocity diagnostics should, whenever possible, be used in conjunction with diagnostics of the temperature and the magnetic field strength. It is also important to note that each velocity diagnostic is sensitive to only a certain type of velocity field and to obtain a maximum of information all velocity diagnostics should be used in combination.

At or close to disc centre all three diagnostics discussed above only measure the vertical component of the velocity. To obtain an idea of the horizontal velocity field, one can either observe the above line parameters near the limb or follow the movement of a well defined magnetic feature (e.g. in a Videomagnetogram sequence, Martin 1990) or brightness feature thought to be associated with magnetic fields (e.g. in a filtergram, Title *et al.* 1989) on the solar surface. Needless to say, the last-named diagnostic should only be used if the physical connection between the tracked brightness features and the magnetic field is well established.

4.7.2. Spatially Unresolved Magnetic Features

If the magnetic features cannot be resolved, then Stokes I is sensitive to a combination of the velocity in the magnetic and the non-magnetic regions (weighted by the filling factor, continuum intensity, etc.). Stokes V, Q and U, on the other hand, react mainly to the velocity within the magnetic features, with the important exception of the line profile asymmetries, which are also sensitive to flows in the immediate surroundings of magnetic features (see below).

The main diagnostic of stationary flows within the magnetic features is the Stokes V zero-crossing wavelength, λ_V. The minimum wavelength, λ_π, of the π component of Stokes Q and U may in principle also be used, but has so far never been. In a 2-component (but not a 2-D) model, λ_V behaves in a manner similar to the minimum wavelength of I_m, as long as the Zeeman splitting is not too large. Consequently, the caveats noted in Section 4.7.1 apply to Stokes V as well. In 2-D models of magnetic features, a particular ray may pass through both non-magnetic and magnetic atmospheres. Although the Stokes I wavelength formed along such a ray is influenced by the velocity in both parts of the atmosphere, λ_V reacts only to the velocity in the magnetic feature (Grossmann-Doerth *et al.* 1988b, 1989a). In particular near the limb, where each ray that passes through small-scale magnetic features also samples the non-magnetic atmosphere, no amount of increase in spatial resolution can make Stokes I and V give the same result, since the Stokes I wavelength along all rays also reacts to the flows in the non-magnetic atmosphere.

Since λ_V is easily affected by noise if $dV/d\lambda$ is small in the line core, lines with large $dV/d\lambda$ should be used when measuring λ_V. For relatively weak lines $dV/d\lambda$ increases with increasing W_λ, but for strong, saturated lines with broad cores, $dV/d\lambda$ at λ_V is again quite small (as can be easily seen from the proportionality between V and $dI/d\lambda$, Equation 2.12). Similarly, $dV/d\lambda$ initially increases with increasing $\Delta\lambda_H$ (for $\Delta\lambda_H \ll \Delta\lambda_D$), but decreases again as $\Delta\lambda_H$ becomes of the order of $\Delta\lambda_D$ or larger. Therefore, strongly split or strongly saturated lines are not suited to determine λ_V. Adding together the wavelengths of, e.g., the two Stokes

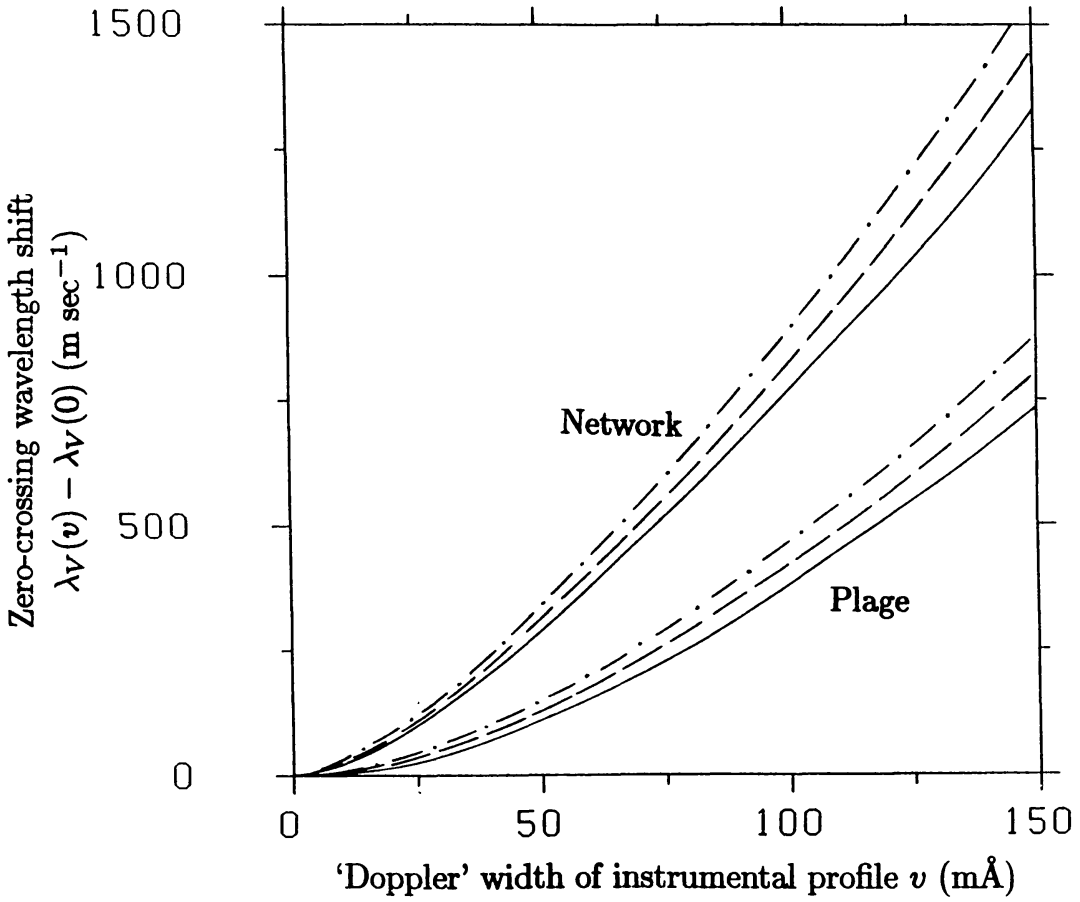

Fig. 4.7. Zero-crossing wavelength shift $\lambda_V(v) - \lambda_V(v = 0)$ induced by instrumental smearing (in velocity units) vs. v, the "Doppler width" of the instrumental profile. The solid curves are produced by a Gaussian instrumental profile, the dashed curves by an apparatus function with a Voigt profile shape and "damping constant" $a = 0.1$, the dot-dashed curves by a Voigt apparatus function with $a = 0.2$. The upper set of curves represents the zero-crossing shift of network data induced by spectral smearing. The lower set of curves represents plage data. The relevant parameter that distinguishes between the two datasets is the blue-red asymmetry of the Stokes V profiles, which is larger in the network data (from Solanki and Stenflo 1986).

V peaks to obtain an estimate of λ_V of such lines is only a limited substitute to a proper λ_V measurement, since for lines with $\Delta\lambda_H \lesssim \Delta\lambda_D$ this parameter reacts quite differently to a given velocity field, being intimately connected to the Stokes V asymmetry.

As with the measurement of the Stokes I line bisector, high *spectral* resolution is required, or spurious flows may be deduced from λ_V, since spectral smearing combined with any asymmetry between the blue and red lobes of Stokes V induces a shift in λ_V (Solanki and Stenflo 1986). This effect is illustrated in Figure 4.7, where the spurious shift in λ_V is plotted as a function of spectral smearing. The two unsmeared profiles were observed in a solar plage and a network region, respectively. Their blue peaks are stronger than their red peaks by approximately 10% and 20%, respectively (relative amplitude asymmetry, see below).

Waves or oscillations in magnetic features may be studied by obtaining time series of λ_V. However, for very small magnetic features with locally excited wave modes, the oscillations or waves may not be in phase across the spatial resolution element, so that the velocity signal seen in $\lambda_V(t)$ can be washed out by the finite spatial resolution of the observations.

The "width" of Stokes V, Q, or U is, like the half-width of Stokes I, a measure of the amplitudes of spatially or temporally averaged "non-stationary" velocities (turbulence, waves, oscillations, or a distribution of stationary velocities, Solanki 1986, Degenhardt and Kneer 1992). The "width" of the Q, U and V profiles may be parameterized in different ways, e.g., by the wavelength difference between the V, Q, U σ peaks, or by the half-width of the individual σ peaks, or by the half-width of the I_V profile. The interpretation of the Stokes V, Q and U widths in terms of velocity amplitudes presumes a knowledge of the temperature. For $\Delta\lambda_H \gtrsim \Delta\lambda_D$ the field strength must also be known. It is important to note that any velocity outside the magnetic features (even if present along a ray which also passes through the magnetic feature) does *not* influence the width of Stokes V (Solanki 1989) or of Q and U.

The final Stokes V based diagnostic of the velocity is the blue-red asymmetry. Although Stokes Q and U should also become blue-red asymmetric in the presence of a suitable velocity field, these Stokes parameters have so far not been studied in sufficient detail and are not discussed further here (but see Sánchez Almeida and Lites 1992). An asymmetry between the *shapes* of the blue and red Stokes V wings can be produced by vertical, horizontal, or temporal velocity gradients (dv/dz, dv/dr, or dv/dt). Such an asymmetry has generally been parameterized by the asymmetry between the blue and red Stokes V *amplitudes*,

$$\delta a = (a_b - a_r)/(a_b + a_r), \tag{4.45}$$

where a_b and a_r are the amplitudes of the blue and red Stokes V lobes, respectively. On the other hand, an asymmetry between the unsigned *areas* of the blue and red Stokes V lobes can only be produced by a longitudinal velocity gradient. It is defined as

$$\delta A = (A_b - A_r)/(A_b + A_r), \tag{4.46}$$

where A_b and A_r are the areas of the blue and red Stokes V lobes, respectively. An additional requirement for the production of a non-zero δA is that either the field is *not* longitudinal (Auer and Heasley 1978, Landi Degl'Innocenti and Landolfi 1983), or that it has a longitudinal gradient in strength (Illing *et al.* 1975), azimuth (Makita 1986), or inclination (Sánchez Almeida and Lites 1992). A gradient in the field strength, inclination or azimuth is, in general, considerably more efficient in producing δA than the presence of an inclined field by itself. Fig. 4.8 illustrates the mechanism involving velocity and field-strength gradients for a simple, but relevant, case. The atmosphere is assumed to be composed of two layers, a lower,

field-free ($B_l = 0$) layer with a downwards directed velocity v_l and a static ($v_u = 0$) upper layer with a magnetic field of strength B_u. The mechanism based on gradients of the magnetic inclination works due to changes in the relative strength of the σ- and π-components of the line and differential saturation effects. The azimuthal angle of the field affects Stokes V through magnetooptical effects.

Another mechanism, proposed by Kemp *et al.* (1984) and by Landi Degl'Innocenti (1985), is based on differentially populating Zeeman sublevels (i.e. orienting the atoms in the magnetic field) by highly anisotropic optical pumping. However, although it works in the laboratory (Kemp *et al.* 1984), it appears unlikely that this exotic mechanism is required to explain any existing observations on the sun.

The following is a brief list of some of the properties of the Stokes V asymmetry, as produced by velocity gradients.

1. In general, a velocity field producing a non-vanishing δA also produces a non-zero δa.
2. If the velocity and the magnetic field overlap spatially, then in general a shift in λ_V is also produced. The magnitude of this shift depends on the velocity near the formation height of the line core, whereas the asymmetry depends on the velocity gradient at the height of formation of the line wings (Sánchez Almeida *et al.* 1988b). However, if $v(\tau)$ and $B(\tau)$ do not overlap anywhere (as is the case illustrated in Figure 4.8), then it can be shown rigorously that the λ_V of the resulting line profile is equal to the rest wavelength of the line, although an asymmetry is still produced (Grossmann-Doerth *et al.* 1988b, 1989a).
3. The sign of the δA produced by a field-strength gradient is given by the following expression (Solanki and Pahlke 1988, Sánchez Almeida *et al.* 1989),

$$\mathrm{sign}(\delta A) = \mathrm{sign}\left(-\frac{d|B|}{d\tau}\frac{dv}{d\tau}\right), \tag{4.47}$$

while the sign of δA produced by a change in field inclination, γ, is given by (Solanki and Montavon 1993)

$$\mathrm{sign}(\delta A) = \mathrm{sign}\left(-\frac{d|\cos\gamma|}{d\tau}\frac{dv}{d\tau}\right). \tag{4.48}$$

Note that Equations (4.47) and (4.48) only apply if B and $\cos\gamma$ do not change sign along the LOS. Otherwise, the resulting V profiles can have complex shapes, such as some V profiles observed in sunspot penumbrae or on Ap stars (so-called crossover effect, e.g. Babcock 1951, Kjeldseth Moe 1967, Grigorjev and Katz 1972, Golovko 1974, Sánchez Almeida and Lites 1992) and the definition of δA, Equation (4.46), loses its meaning.

4. The asymmetry is produced by the different saturation in the two polarizations (cf. Figure 4.8), so that, for not too strong lines, δA increases with line strength for a given $v(\tau)$, $B(\tau)$ and $\gamma(\tau)$ (Solanki and Pahlke 1988).
5. On the other hand, for a given line saturation δA is largest when the change in line shift due to the velocity gradient $\Delta\lambda_v \approx \max(\Delta\lambda_H, \Delta\lambda_D)$. Therefore, for

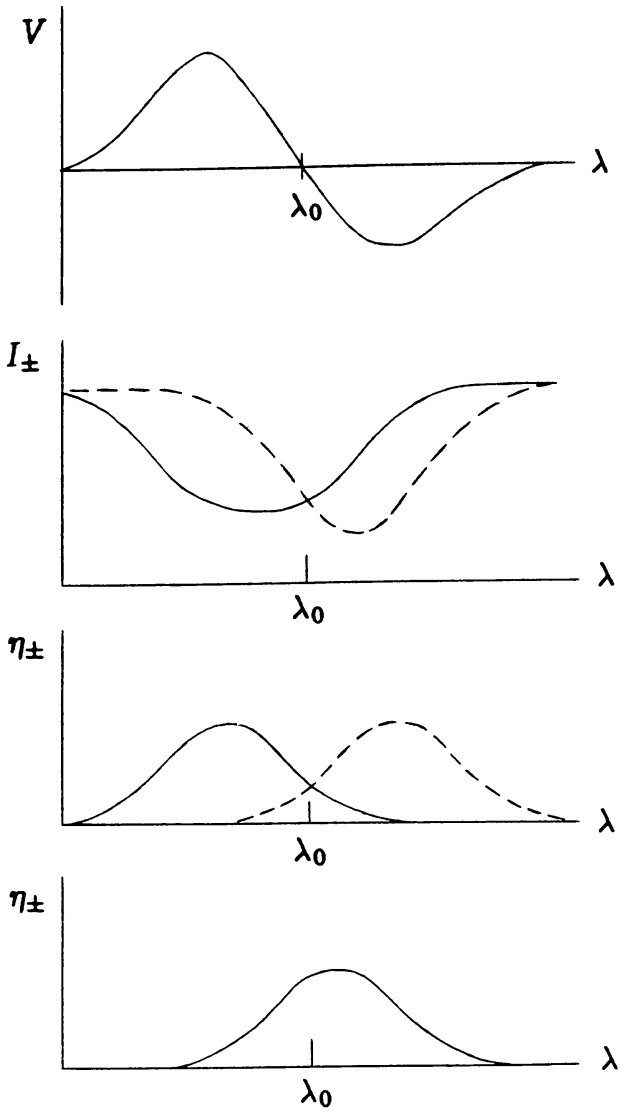

Fig. 4.8. Schematic illustration of the production of an asymmetric Stokes V profile with an unshifted zero-crossing wavelength $\lambda_V = \lambda_0$ in a two-layered atmosphere (λ_0 is the rest wavelength). Only the simplest case of a longitudinal magnetic field is considered. Bottom frame: profiles of $\eta_\pm$ (absorption coefficients for right and left circularly polarized light, respectively) in the lower atmospheric layer, which has no field, but a downflow. Therefore, the two profiles are identical and redshifted. Second lowest frame: $\eta_\pm$ in the upper layer, where there is a magnetic field, but no velocity. The two η profiles are shifted relative to each other due to the Zeeman effect, but the absorption is symmetric around λ_0. Third lowest frame: $I_\pm = I \pm V$, the emergent intensity profiles for the two polarizations. I_+ has a larger equivalent width than I_-. This is due to the fact that η_- is largest at almost the same wavelength in both atmosperic layers, while η_+ is spread over a broad wavelength range. Therefore, the core of I_- is much more strongly saturated than the core of I_+. Topmost frame: An asymmetric $V = I_+ - I_-$ profile, with a larger blue lobe than red lobe. Line saturation plays an important role in producing the asymmetry. Note that, since in both layers $\eta_+ = \eta_-$ at the rest wavelength, λ_0, $V(\lambda_0) = 0$ as well. I.e., the Stokes V profile produced in such an atmosphere is asymmetric, but unshifted (from Solanki 1990).

the strongest lines δA may decrease again for a given velocity and magnetic stratification, since for these lines $\Delta\lambda_D \gg \Delta\lambda_v$ (Sánchez Almeida *et al.* 1989, Grossmann-Doerth *et al.* 1989a). Also, very strongly Zeeman-split lines, such as the $g = 3$, Fe I line at 15648.5 Å, are not expected to show a sizable δA, since $\Delta\lambda_H \gg \Delta\lambda_v$.

4.8. Size, Distribution, Lifetime and Evolution of Magnetic Features

4.8.1. Sizes of Magnetic Features

The size of a spatially resolved magnetic feature may be determined quite simply by measuring it out on a magnetogram, or determining the size of a corresponding feature in a white-light, spectro-heliogram, or filtergram image (e.g. the outer penumbral boundary of a sunspot).

For magnetic features with sizes just at or below the spatial resolution more care must be taken and a greater effort is required. The first approach is to enhance the spatial resolution of images of the magnetic features. For a given telescope this may be achieved with the help of frame selection (i.e. selecting the sharpest image within a given period of time, e.g. Muller and Keil 1983, Scharmer 1989), deconvolution of the telescope modulation transfer function (MTF, Koutchmy 1977), or, at the highest level of sophistication currently possible, speckle interferometry (Von der Lühe 1989). Another method of achieving very high spatial resolution is to follow the lunar limb across the solar disc during an eclipse and to time the disappearance of magnetic features (Harvey 1986). On the instrumental side, selection of a site with laminar airflow (Brandt *et al.* 1989), reduction of dome and telescope seeing (Dunn *et al.* 1985), tracking with the help of an active mirror (correlation tracking, Tarbell and Smithson 1981, Von der Lühe 1988, Von der Lühe *et al.* 1989) and adaptive optics (e.g., Gordon and Wilkerson 1981, Shao *et al.* 1981, Smithson and Tarbell 1981, Merkle *et al.* 1987, Acton 1989, 1990) are possible approaches, as is going into space with a large telescope (e.g. the Orbiting Solar Laboratory, OSL).

Not all these approaches are equally advantageous. For example, although frame selection is often quite powerful to enhance resolution in, say, white-light images, the still poorly known white-light signature of small-scale magnetic features and possibly similar signatures produced by non-magnetic events in the granulation (produced, e.g., by shocks, Cattaneo *et al.* 1990, Steffen 1991), make it necessary to apply the above techniques to Stokes V and ideally to Stokes Q and U as well.* However, the signal-to-noise ratio is often considerably smaller for the polarized Stokes parameters than for the intensity. Firstly, they must be studied in narrow bands with widths corresponding to less than half the width of a spectral line (although this may be overcome by an instrument with a spectral mask at the position of many spectral lines, like the CORAMAG, Borra *et al.* 1984). Secondly, even for a resolved magnetic feature, the maximum Stokes V in a spectral line

* It may be partly possible to separate magnetic from non-magnetic continuum bright points by cross-checking with Ca II K bright features. Unfortunately, the very large scatter in the relationship between Ca II K brightness and spatially averaged field strength leaves a considerable uncertainty.

rarely exceeds 30% of the continuum intensity, with typical values in unresolved features being below 10%.

One way of improving the S/N ratio, while keeping the seeing-induced smearing low, is to superpose various images through destretching, i.e. assuming one selected image to be the true one and transforming the other images so that the cross-correlation is maximized (Topka and Tarbell 1984, November 1986, Keller 1989). If I and V have been obtained simultaneously (i.e. if $I + V$ and $I - V$ have been observed simultaneously) then the destretching parameters obtained from Stokes I may also be applied to Stokes V (see Keil *et al.* 1989). Similarly, for speckle interferometry, the problem of low S/N in the individual frames in Stokes V (which is particularly acute due to the extremely short exposure times required for this technique, cf. Harvey 1986) may be circumvented by carrying out the reconstruction first for a broad-band intensity channel and then with the same parameters also for the simultaneously obtained Stokes V (Keller and Von der Lühe 1992). Since many frames are combined after a successful speckle reconstruction, the final S/N ratio is better than that of individual frames with possibly similar resolution.

It is important to note that for any of these approaches to be successful, both polarization components must be measured strictly simultaneously, since differential seeing effects between the two polarization images can completely distort the Stokes V, Q or U images. More details concerning the image processing of magnetograms are given by Keller *et al.* (1992).

There are basically two indirect techniques for deriving sizes of unresolved magnetic features: a) measuring magnetic flux and field strength of small features with very high flux sensitivity (Wiehr 1978), and b) making use of the fact that the size of a magnetic feature may affect line profiles when observed at an angle to its axis (Walton 1987, Zayer *et al.* 1989). Consider the first of these approaches. If the smallest measured flux, $\Phi_{\min}$, equals the instrumental sensitivity, then an upper limit on the size of the magnetic feature in the spatial resolution element can be set by assuming that the whole flux is concentrated in a single feature. If the intrinsic field strength of the unresolved magnetic feature is known, then a limit on the area $A_{\min}$ covered by the smallest magnetic feature may be obtained,

$$A_{\min} \leq \Phi_{\min}/B. \tag{4.49}$$

On the other hand, if the smallest measured flux is always larger than the instrumental limit, then a lower limit may be set on the size of the magnetic features, since the lower flux limit is now solar in origin and must correspond to the flux within a single unresolved magnetic feature. The inequality (4.49) then becomes

$$A \geq A_{\min} = \Phi_{\min}/B. \tag{4.50}$$

One major problem with this technique is obtaining reliable values of $\Phi_{\min}$, since

its measurement depends sensitively on the assumed thermodynamic structure of the smallest magnetic features (see Section 4.5).

The second indirect approach relies on the fact that when a small magnetic feature is observed from the side, its size enters into the line formation process. By carrying out model calculations, varying the size of the model and comparing the resulting profiles with observations it is, under certain assumptions, possible to set limits on the size of the magnetic features, independently of the spatial resolution. More details are given by Zayer *et al.* (1989). However, under other, equally reasonable, assumptions the particular spectral diagnostic used by Zayer *et al.* (namely the splitting of the $g = 3$, Fe I 15648.5 Å line) is not sensitive to flux tube size. The difference between the two calculations is the choice of the thickness of the boundary layer between the magnetic and non-magnetic atmospheres. Therefore, this technique has to be developed further (by testing other possible diagnostic parameters) before it can be applied reliably.

4.8.2. Distribution and Morphology

To study the distribution and the morphology of magnetic features, the observations must ideally combine a good spatial resolution with a large 2-dimensional field of view. Magnetographs and filtergraphs are the instruments most often employed for this purpose, although a very fast spectroheliograph deployed at a site of stable seeing has been demonstrated to be highly successful as well (Johannesson *et al.* 1992, Johannesson 1992). The latter has the advantage that reliable line profiles are obtained at every spatial position. Broad-band polarimeters (Leroy 1962, 1989, 1990, 1991, Illing *et al.* 1974a,b 1975, Makita 1981, Stenflo 1984b, Kemp *et al.* 1987), coupled to a 2-D detector, are yet another possibility. To enhance the S/N ratio, broad-band polarimeters are used with advantage in the blue, where the density of lines is largest (but see Leroy 1990). Both broad-band and narrow-band magnetograms pose interpretational problems due to the very limited spectral information they contain. In addition to the magnetic flux, the magnetograph signal is affected by line weakening, velocity-induced line shifts and broadenings, as well as by changes in Zeeman splitting, field inclination and continuum contrast. These effects cannot be separated from each other without additional spectral information (cf. Grossmann-Doerth *et al.* 1987, although a Doppler compensator can remove part of the line shifts). For a qualitative knowledge of the magnetic morphology, however, magnetograms are adequate.

The spatial-resolution and S/N enhancement techniques mentioned in Section 4.8.1 may all be applied to data gathered for the purpose of determining the morphology of magnetic features, but some of these, in particular speckle interferometry, may be limited in their use due to practical problems, such as the high computational load when applied to a large number of pixels. For very large scale images the influence of the sun's curvature (projection effects) must also be taken into account.

The morphology of magnetic features is often determined by proxy, i.e. the

presence of a magnetic field is deduced from its thermodynamic influence on the structure of the atmosphere. Examples of proxy indicators are Ca II H or K line core flux, Mg Ib line wings, CN band-head (3883 Å) bright points, abnormal granulation and Hα images. Before using any such proxy indicator it is important to calibrate it with the help of simultaneous observations of the magnetic field. Such calibrations often show a large scatter (Frazier 1971, Schrijver *et al.* 1989), so that proxy indicators are mainly useful to qualitatively delineate the field, but cannot replace actual magnetograms for more quantitative studies. Simultaneous observations at various wavelengths help to extrapolate the field to greater heights in the atmosphere (e.g. by correlating the azimuth of the field with the direction of Hα fibrils), clarify the relation of the photospheric field to the heating of the upper atmosphere (e.g. by correlating the magnetic flux with Ca II K, Mg II k, C IV, X-ray brightness), understand the nature of structures visible in other images (e.g. filaments in Hα), etc.

Unfortunately, much of the morphological work, by its very nature, cannot be described quantitatively and thus allows subjective and often non-unique interpretations. However, there are some objective and quantitative analysis techniques. For example, spatial Fourier transforms can give information on dominant spatial frequencies in the magnetic distribution, such as "magnetic" cell sizes. 2-D autocorrelation analyses or explicit cell finding algorithms (e.g. Muller and Keil 1983, Title *et al.* 1987) should also allow the objective determination of cell sizes.

Finally, it may be possible to learn something about the subsurface structure of magnetic features from the study of p-modes in and around them (e.g. Braun *et al.* 1987, 1988, 1992, Lou 1990, Spruit and Bogdan 1992, Rosenthal 1991, 1992).

4.8.3. Lifetimes and Evolution

Lifetimes of relatively large, easily resolved magnetic features are best determined by tracking them across the solar disc from their birth to their death. For features living longer than half a rotation period (2 weeks) solar rotation poses a problem and their lifetimes can only be studied in a statistical sense. To measure the lifetimes and the evolution of individual long-lived features one or more satellites are required, each in circular orbit around the sun at 1 AU, but out of phase to earth. Such a set of satellites was proposed by Hudson and Hildner (1990). An important step towards refining lifetime measurements of less long-lived magnetic features has been the employment of multiple observing stations distributed on the globe (e.g. Wang *et al.* 1989), following the lead of the helioseismology community.

For small, spatially unresolved magnetic features, the main problem is observationally identifying the processes giving rise to their birth and death. As long as these features cannot be resolved individually, it is very difficult to derive their true lifetimes, or to study their detailed evolution. It is only possible to study groups of such small magnetic elements within active regions and along supergranular cell boundaries and to determine the lifetime of a whole group, or magnetic cluster. It is important to bear in mind, however, that the lifespans of the individual

magnetic elements forming a magnetic cluster may be either shorter or longer than the lifetime of the cluster itself. It may be shorter, since the individual flux tubes may dissolve and re-form without changing the overall structure of the cluster. It may also be longer, since a magnetic cluster may dissolve by diffusion of intact flux tubes, which can later become part of other magnetic clusters. Such scenarios may be tested by observations of the time evolution of magnetic features (e.g., do magnetic clusters dissolve exclusively by spreading and fading away, or only through cancellation with clusters of opposite polarity?). Since 2-D images of the field distribution are required to study the time evolution, magnetograms (either obtained classically with the Babcock technique, or in the form of filtergrams) are the data of choice.

Like the morphology, it is difficult to quantify many of the results of evolutionary studies, or to speak of diagnostics for the evolution. The evolution of any given physical quantity with time is best followed by obtaining a time-series of a diagnostic for this physical quantity. However, some additional techniques may be of interest to follow the horizontal motions of magnetic features, i.e., to follow the evolution of the field morphology. One such approach is local correlation tracking (first developed to follow horizontal motions of granules, November 1986, November and Simon 1988). It allows horizontal flows to be traced even if it is difficult to identify and follow individual features in the data with the unaided eye. A related approach is to put "test particles" or "corks" into the 2-D data on a regular grid and track them. Such "cork movies" have been used to study the solar granulation (e.g. Simon and Weiss, 1989). They have the advantage that the corks, having infinite lifetimes, can trace long-term horizontal flows visible only on time-scales longer than the lifetimes of individual magnetic features.

Note that the quality of granulation movies has been greatly improved after the 5 minute oscillations have been filtered out (Title *et al.* 1989). Since such oscillations are also present in magnetic features (e.g. Beckers and Schultz 1972, Giovanelli *et al.* 1978), it may be worthwhile to filter them out there as well in order to obtain good temporal and spatial fidelity.

The global aspects of the evolution of magnetic features, their rotation rates etc. may be studied with Fourier techniques and other standard analysis procedures for time series and are not dealt with here.

4.9. Combined Diagnostics: Inversion Techniques

Often the diagnosis of a given physical parameter requires prior knowledge of another parameter, i.e., there are insufficient clean diagnostics that are sensitive to a single solar atmospheric parameter to the exclusion of all others. For example, the determination of γ and χ requires the prior accurate knowledge of the field strength, the temperature, turbulent line broadening (or total Doppler width), etc. (cf. Section 4.4). But the accurate measurement of the field strength often itself depends on γ, T, etc. It is therefore necessary to combine various diagnostics in order to simultaneously constrain as many physical parameters as possible.

One approach is to invert data to derive the physical conditions giving rise to the observations. A true inversion, however, is generally only possible when the relationship between the physical conditions on the sun and the observational data is linear (Craig and Brown 1986). Even then, a model dependence must be assumed between the observations and the solar physical parameters.

Unfortunately, linearity generally does not count among the properties of models of magnetic features. In particular, there is no straightforward linear relationship between a set of observed parameters (e.g. spectral line parameters) and model parameters (e.g. field strength, temperature, velocity, etc.). Therefore, instead of a direct inversion we must apply what may be termed an "indirect inversion". This is really nothing but the classical least squares fitting approach, although other indicators of maximum agreement between the model (synthetic data) and observations than a minimal χ^2 may also be used. This technique allows the diagnostic process to be largely automated, and also largely eliminates the measure of subjectivity present in the "chi-by-eye" approach. It is stressed, however, that an inversion approach cannot overcome any inadequacies in the model underlying the analysis.

The uniqueness and significance of the parameters of an inverted model basically depends on two factors.

1. Observational data: Is the S/N ratio sufficient? Are there sufficient diagnostic parameters available? Are these sufficiently sensitive and independent?
2. Model: Are there sufficiently few free parameters (fewer than the independent diagnostics)? Are there enough free parameters (otherwise the model may never be able to reproduce the data)? Have the free parameters been properly chosen to correspond to the observed diagnostics? For example, if only Stokes V is measured, then either α or γ, but not both, may be chosen as free parameter, since they would otherwise compensate each other. Has enough physics been employed to narrow down the search for "good" solutions?

The indirect inversion of polarized spectra was pioneered by Harvey *et al.* (1972), cf. Beckers and Schröter (1969). An inversion was used to obtain the flux tube temperature structure from a numerical solution of the transfer equations by Stenflo (1975). An inversion approach was also taken by Frazier and Stenflo (1978), with Milne-Eddington model and horizontal profiles of B and flow velocity to determine the model parameters from a set of observables (magnetograph-type data). It has also been extended and applied by Auer *et al.* (1977), Landi Degl'Innocenti *et al.* (1984), Skumanich and Lites (1987) and Lites *et al.* (1988) using Milne-Eddington (Equation 2.10) or similar analytical solutions of the Unno-Rachkovsky Equations (2.5). The magnetic field vector, wavelength shift, Voigt profile parameters and line absorption coefficient can be determined from a measurement of the Stokes parameters (cf. Section 4.4). Skumanich *et al.* (1992) have presented test calculations which show that this technique can also be applied to spatially unresolved small-scale magnetic features. Using the response functions for Stokes profiles (Landi Degl'Innocenti and Landi Degl'Innocenti 1977) and the diagnostic content of the

residuals between observed Stokes profiles and best fit Unno profiles, Landolfi (1987) has extended the Auer *et al.* technique to determine magnetic field and velocity gradients (the gradients are treated as perturbations to the Milne-Eddington solution). This extended technique has been applied to sunspot spectra by Sánchez Almeida and Lites (1992). By replacing the numerical derivatives of the profiles to the free parameters by response functions, Landolfi (1987) provides a means of speeding up the inversion procedure, which becomes particularly valuable when using numerical profiles for the fitting. Saar and Linsky (1985), Saar *et al.* (1986), Saar (1988) etc. have applied a similar inversion to unpolarized stellar spectra. Finally, Balasubramaniam and West (1991) also describe an inversion code similar to that of Skumanich and Lites (1987). Unfortunately, the Milne-Eddington approach is rather unreliable for diagnosing the thermodynamics (e.g. Murphy 1990, but cf. Lites *et al.* 1992).

An inversion approach making even fewer assumptions is due to Makita (1979, cf. Kawakami 1983). By basing his analysis on carefully chosen linear combinations of the Stokes parameters, he can determine some atmospheric parameters without making any assumptions about η_0 (ratio of the line-centre to continuum absorption coefficients) and B_ν (the Planck function). The restriction that $\Delta\lambda_D$, B, γ, etc. are depth independent still remains, since his approach relies on analytical solutions due to Katz (1971) and Šidlichovský (1976). He also neglects magnetooptical effects. The quantities that can be derived from this approach are an average B, γ, $\Delta\lambda_D$ and a (the damping constant). No direct information on the thermodynamics is obtained, i.e. η_0 and B_ν are not determined. Some information on velocity gradients may be obtained by treating their influence on the line profiles as small perturbations of the normalized absorption matrix.

A considerably more sophisticated approach based on numerical solutions of the transfer equations in realistic atmospheres incorporated into 2-D flux-tube models has been developed and successfully applied to solar Stokes V data by Keller *et al.* (1990a). The field strength, turbulent velocity and, in particular, the temperature stratification can be determined in this manner from a judicious choice of spectral lines. Also, gradients in atmospheric quantities, e.g. in the field strength or the velocity, can be treated quite naturally, without restrictions (recall that gradients can be incorporated into the analytical approach only if they are small). Keller *et al.* fit carefully selected line parameters, while in the analytical Auer *et al.* approach the complete line profiles are fit. The two other recent Stokes inversion codes, based on numerical LTE solutions of the Stokes transfer equations, also fit line profiles (Solanki *et al.* 1992b, Ruiz Cobo and Del Toro Iniesta 1992). While the code described by Solanki *et al.* (1992b) concentrates more on incorporating physical constraints on the atmospheric structure, Ruiz Cobo and Del Toro Iniesta (1992) enhance the speed of their fitting procedure, particularly when detailed temperature or velocity profiles are to be determined, by following Landolfi (1987) and using response functions to determine the derivatives with respect to the free parameters.

Although an inversion based on the full numerical solution of the Stokes transfer

equations is far more realistic and for many purposes unavoidable (e.g. to obtain the thermodynamical structure of magnetic features), any analytical approach is computationally much less intensive. Inversions based on analytical solutions are more convenient when a large body of data is to be fit quickly and in particular when the vertical variation of quantities like the field strength is negligible (e.g. in sunspots).

5. Properties of Small-Scale Magnetic Features

The small-scale magnetic features that constitute solar faculae have been given a variety of names, e.g. 'invisible sunspots' (Hale 1922a,b, Zirin and Wang 1992), 'microspots' (Alfvén 1967), 'filigree' composed of 'crinkles' (Dunn and Zirker 1973), 'magnetic elements' (Harvey and Livingston 1969), 'magnetic knots' and 'micropores' (Beckers and Schröter 1968a), 'gaps' and 'line gap regions' (Sheeley 1967), 'moustaches' or 'Ellerman bombs' (Severny 1968, Rust 1968, cf. Stellmacher and Wiehr 1991, Rust and Keil 1992), 'magnetic filaments' (Stenflo 1971), 'facular points' (Mehltretter 1974), 'facular granules' (Muller 1977, Hirayama 1978), 'fluxules' (Harvey 1977b), 'facular elements' (Muller and Keil 1983), 'facular knots' (Spruit and Zwaan 1981), 'flux fibers' and 'network bright points' (Zwaan 1987), 'magnetic footpoints' (M. Hayes, private communication 1987), 'protopores' and 'holes' (Title *et al.* 1987), 'magnetic flux concentrations' (Knölker and Schüssler 1988, Schüssler and Solanki 1988) and 'magnetic points' (Knölker and Schüssler 1988).

The names often refer to the appearance of the magnetic features in different diagnostics and may sometimes describe only very transient phenomena. They also distinguish between different types of features, e.g. knots and micropores are thought to be larger (composite?) structures than, say, flux fibers or facular points. In the current paper I have tried to consistently use the terms magnetic elements or (small-scale) magnetic features for the observed structures. Of course, the common denominator of all these features is their theoretical description by flux tubes (flux slabs) having kG fields. There are small-scale fields, however, that do not fit into this scheme, for example the turbulent fields first looked for by Unno (1959) and possibly the intranetwork fields (Livingston and Harvey 1975). Reviews of the empirical aspects of small-scale solar magnetic fields have been given by Beckers (1976), Harvey (1971, 1977a, 1986), Lemaire (1987), Martin (1990), Muller (1987, 1990), Rabin (1992c,d), Semel (1985, 1986), Solanki (1987a,b, 1990, 1992b), Stenflo (1976, 1977, 1978, 1984a, 1985a, 1986, 1989), Title *et al.* (1987b, 1990b), and Zwaan (1978, 1985, 1987). Overviews of the theory have been given by Meyer (1976), Nordlund (1984b, 1985b, 1986), Parker (1979a, 1985, 1986), Priest (1982, 1987, 1990), Roberts (1984, 1986, 1990), Ryutova (1990), Schüssler (1986, 1987, 1990, 1992), Solanki (1992c), Spruit (1981a, 1983), Spruit and Roberts (1983), Spruit *et al.* (1991), Steiner (1992), Stix (1990), Thomas (1985, 1990), Ulmschneider and Muchmore (1986), Weiss (1977), and Zwaan and Cram (1989).

5.1. Magnetic Field Strength

5.1.1. Early Measurements

The first evidence for distinct magnetic features outside sunspots came from the discovery of fields with an average strength of approximately 200–300 G by Hale (1922a,b) in what he termed 'invisible sunspots'. With improvements in instrumentation, the lower limit on the measurable non-sunspot fields decreased, in particular with the introduction of the photoelectric magnetograph (Babcock and Babcock 1952, Thiessen 1952, Kiepenheuer 1953). It allowed maps of the distribution of the (spatially averaged) longitudinal field component to be made with the unprecedented accuracy of a few G (Babcock and Babcock 1952, 1955, see also the review by Babcock 1963). Field strengths, or rather averaged flux densities, in bright regions (i.e. faculae, network) were generally found to lie between 1 G and 200 G at the spatial resolution of around $5''$–$20''$ of the early magnetograms. Higher field strengths were measured in pores and sunspots.

During the 1960s the spatial resolution increased and indications accumulated that the true field strengths outside sunspots are considerably higher than the average strengths measured with low spatial resolution. Thus, Kiepenheuer (1953), Stenflo (1966) and Severny (1967) made multiple scans of a given region with varying aperture sizes and found that the magnetic field strength increased with decreasing aperture. The smallest aperture used by these authors was, however, of the order of $3'' \times 2''$ (excluding seeing). Sheeley (1966) detected field strengths of between 200 and 700 G in small non-sunspot features from magnetograms of quiet and active regions. Sheeley (1967) used the spectral shift of the σ-components of Fe I 5250.2 Å to measure a field strength of approximately 350 G. In active regions Beckers and Schröter (1968a) measured fields of between 400 and 1400 G in magnetic knots after a rough correction for stray light (i.e. for the effects of seeing). Grigorjev (1969) and Abdussamatov and Krat (1969) also observed magnetic knots and measured field strengths ranging from 100 to 650 G. Harvey *et al.* (1972) determined the parameters of a simple model of magnetic elements from least squares fits to observed Stokes V profiles. Their best fits gave an average field strength of 500 G with a scatter of $\pm$ 500 G. They also found a fit of somewhat lesser quality with a higher field strength. Later, Stenflo (1973) reproduced their observations quite well with kG fields. Simon and Zirker (1974) found field strengths of up to 1500 G averaged over their spatial resolution element of approximately $1''$.

These observations provided a clear indication that the true magnetic structures were spatially unresolved, but could not decide which fraction of the field is in "strong-field" form. Howard and Stenflo (1972) and Frazier and Stenflo (1972) addressed this question when they considered the Stokes V ratio of Fe I 5250.2 Å to Fe I 5233 Å. They found that a major fraction (more than 90%) of the magnetic flux visible in Stokes V is in "strong-field" form, but could not specify the true field strength (due to the imperfect choice of lines). In addition, since the two lines differ

not only in their sensitivity to the field strength, but also to the thermodynamics, a hot weak-field feature can conceivably give the same signature as a cooler strong-field feature and consequently be misclassified. Conversely, it is also possible that strong-field features get misclassified as weak field features if they have anomalous thermodynamic properties. The restriction to fields visible in Stokes V also means that their analysis was insensitive to any small-scale 'turbulent' field (e.g. in the form of dipoles with separations smaller than the spatial resolution of 2.4″).

Thus, at the beginning of the 70s, the situation was tantalising. There were various indications of strong fields, but the data were in many respects contradictory and inconclusive.

5.1.2. Kilo-Gauss Fields

The first spatial-resolution- and model-independent field strength values were determined by Stenflo (1973), who used the ratio between the Stokes V profiles of Fe I 5250.2 Å ($g = 3$) and Fe I 5247.1 Å ($g_{\rm eff} = 2$), both belonging to multiplet 1. The peak field strength derived from this magnetic line ratio depends on the assumed horizontal distribution of the field within the individual magnetic features. He found peak field strengths between 2300 G for a Gaussian distribution and 1100 G for a rectangular cross-section. All the magnetic features within the resolution element were assumed to have the same field strength. As in all other determinations prior to 1987 the field strength was assumed to be height independent.

The results of Stenflo (1973) have received numerous confirmations. Harvey and Hall (1975, see also Harvey 1977a) observed the Fe I 15648.5 Å line, which is completely split for $B \gtrsim 0.5$ kG (see Section 5.1.3 and Solanki *et al.* 1992a). The inferred field strengths lie between 1200 and 1700 G for a rectangular horizontal magnetic profile. Unless explicitly stated to the contrary a rectangular magnetic profile is always implied from now on. Chapman (1974) presented various arguments, based on the requirement of internal consistency of facular models (but no new observations), in favour of a unique magnetic field strength of the order of 1500–2000 G. Further confirmation came when Tarbell and Title (1977) used the Fourier technique developed by Title and Tarbell (1975) and Tarbell and Title (1976) to derive the field strength in regions with spatially averaged longitudinal field strengths $\langle B \rangle > 125$ G. For the intrinsic field strength, B, they found values ranging from 1000 to 1800 G, with B being almost independent of $\langle B \rangle$ in their data. Wiehr (1977, 1978) extended the line ratio method of Stenflo (1973) to include three lines. He chose Fe I 6302.5 Å ($g = 2.5$), 6336.8 Å ($g_{\rm eff} = 2$) and 6408.0 Å ($g_{\rm eff} = 1$). He also used the Stokes radiative transfer code of Wittmann (1974), instead of the previously used Unno-Rachkovsky solution, to calibrate the line ratios. He deduced field strengths in the range 1200–1700 G from these measurements. He also measured the field by placing three different exit slits in the wings of Fe I 6173 Å and obtained field values between 1500 and 2200 G with this method. Higher field strengths than found by Stenflo (1973) are expected, since the lines used by the other authors are formed deeper in the atmosphere (higher excitation potentials

and smaller equivalent widths), where field strengths are larger (Section 5.1.3). Furthermore, the 3-slit method, being a single-line technique using incompletely split lines, like that of Tarbell and Title (1977), is more model dependent than the line ratio technique. Koutchmy and Stellmacher (1978) found field strengths of 1000–1500 G from fits of model profiles to $I \pm V$ profiles of Fe I 6301.5 Å and 6302.5 Å observed with 0.75–1″ resolution. Solanki and Stenflo (1984) applied the statistical Stenflo and Lindegren (1977) technique to the I_V profiles (cf. Section 4.2.1) in five Fourier transform spectrometer (FTS) spectra and obtained field strengths between 1400 and 1700 G. Lozitskaja and Lozitskij (1982, 1988) found field strengths ranging up to 3200 G in the photospheric layers of flares simply by applying the centre-of-gravity technique (i.e. using a 1-component model). The presence of such large field strengths is difficult to understand, unless the observations refer to flaring sunspots, and confirmation of these observations using another technique would be of considerable interest. Lozitskij and Tsap (1990) also find kG fields ($B = 2.2$ kG at the axis of a cylindrical tube if a rapid radial decline of B is assumed) by fitting the observed profiles of six lines with calculated profiles.

There have also been a number of further applications of the line-ratio technique, based on the 5250/5247 line pair, to magnetograph and spectrograph data at different levels of sophistication. Frazier and Stenflo (1978) obtained a field strength of 960 G from an application to magnetograms obtained at different positions in the lines. Stenflo and Harvey (1985) studied the dependence of the line ratio on filling factor α. They found only a weak dependence (in agreement with the results of Tarbell and Title 1977), with the field strength increasing from 800 G to 1140 G when α increases by a factor of 6. Rachkovsky and Tsap (1985) redid the classical analysis of Stenflo and also obtained field strengths around 1–1.5 kG. Solanki *et al.* (1987) showed that the centre-to-limb variation (CLV) of the line-ratio measurements is relatively insensitive to the field gradient. If the field is assumed to obey the thin tube approximation, then $B(\tau = 1) \approx 2000$ G for the solar regions considered by them. Sánchez Almeida *et al.* (1988a) found $B \approx 1.2$ kG using a calibration of the line ratio technique that does not rely on radiative transfer calculations (cf. Section 4.2.1, Case VI, Method 1). Bachmann (1991) obtained an average of almost 2000 G from the line-ratio technique applied to magnetograph data. Finally, Keller *et al.* (1990a, b) and Zayer *et al.* (1989, 1990) have also applied the line-ratio technique to solar data. Their results are discussed in greater detail below. All the above investigations confirm the predominance of kG fields in the solar photosphere.

The results of these investigations have been contradicted by Del Toro Iniesta *et al.* (1990a). They applied their extension of the centre-of-gravity technique (Rees and Semel 1979, Section 4.2.1, Case III) to polarized spectra obtained with approximately 1″ resolution. They obtain field strengths between 550 and 1700 G, with a preponderance of lower field strengths, and propose that any difference to older results has to do with the difference in spatial resolution. The weaknesses of the technique used by Del Toro *et al.* (1990a) have been discussed in Section

4.2.1. Keller *et al.* (1990b) also analysed data (magnetograms in Fe I 5247.1 Å and Fe I 5250.2 Å obtained with a universal birefringent filter, UBF) exhibiting a spatial resolution of 0.5″– 1″. They applied the line ratio technique and found that despite a large scatter, a kG field strength is compatible with the observations of all features. The scatter in the line ratio is consistent with the noise in the data. Of course, it is impossible to rule out that a part of the scatter may be of solar origin. Thus, the Keller *et al.* data are too noisy to confirm or refute the dependence of B on α found by Stenflo and Harvey (1985), but are sufficiently sensitive to cast doubt on the results of Del Toro Iniesta *et al.* (1990a).

Finally, let me discuss the two investigations with the so far most sophisticated analysis of visible spectra, namely those of Keller *et al.* (1990a) and Zayer *et al.* (1990). By simultaneously analysing diagnostics of the temperature and the magnetic field using an inversion approach, these authors took the temperature dependence of the line ratio in the presence of magnetic field gradients into account. By using self-consistent models with a height dependent field strength, they were able to derive the field strength at a given geometrical height, and not just at some unknown line-formation level like previous investigators. The surprising result is that the field strengths of all the analysed regions (twenty-three in all) are very similar at a given *geometrical* height. The scatter of 15% corresponds approximately to the uncertainty in the measurements. Therefore, the dependence of B on α found by Stenflo and Harvey (1985) is mainly a thermal effect, since the temperature also depends on the filling factor (cf. Section 5.4) and determines the height of line formation and thus the measured field strength.

A certainly subjective and possibly biased summary of the measurements in the visible is that the field strength in the middle photosphere at the height of formation of the flanks of Fe I 5250.2 Å lies between 1000 G and 1200 G in most of the small-scale magnetic features. When converted into geometrical height using some additional, well founded model assumptions, this translates into a field strength of approximately 1500–1700 G at $z = 0$ (i.e. at $\tau = 1$ in the average quiet photosphere).

5.1.3. Infrared Observations

Many of the major advances in magnetic field measurements have in recent years come from infrared observations. These have concentrated mainly on two wavelength ranges: 1.5–1.8 μm and 12 μm. At 12 μm a host of weak emission lines is present (Murcray *et al.* 1981). The two strongest of these, highly excited (Rydberg) transitions of Mg I, are Zeeman triplets with a Landé factor of 1 (811.57 cm^{-1} and 818.06 cm^{-1}, Chang and Noyes 1983, Lemoine *et al.* 1988), so that in Stokes V they are completely split for field strengths $\gtrsim$ 200 G. (Due to the presence of a π-component it commonly requires a larger field strength of 300–400 G to split Stokes I completely.) Additional emission lines have been observed and identified by Chang (1984, 1987) and Lemoine *et al.* (1988), while Glenar *et al.* (1988) have found Mg I lines in absorption near 9 and 12 μm. The atomic physics of such

lines is reviewed by Chang (1992). All the lines are to be found in the spectral atlas covering the wavelength range 2.3–16 μm, taken from space by Farmer and Norton (1989), cf. Jefferies (1991). The Stokes I profiles of these lines have been observed in active regions by Brault and Noyes (1983), who first pointed out their great Zeeman sensitivity, Deming *et al.* (1988) and Zirin and Popp (1989). The lines have also been observed in sunspots (Brault and Noyes 1983, Deming *et al.* 1988, 1990, Hewagama *et al.* 1993). Excellent reviews on this topic have been given by Deming *et al.* (1991, 1992a), who have also presented measurements of the full Stokes vector (cf. Hewagama *et al.* 1993).

The intrinsic field strengths in active regions, but outside of sunspots, are found to lie in the range 200–500 G, with considerable variation from one point on the solar disc to another (Brault and Noyes 1983, Deming *et al.* 1988). Also, the filling factor, as derived from the relation of the π- to the σ-components, is found to be relatively large in the observed regions at a spatial resolution of a couple of arc s. The variations in the field strength may have to do with the fact that the lines may be formed above the merging height of the field in some parts of active regions. At such heights the field strength is proportional to the filling factor at $\tau = 1$. Other possible explanations, however, such as a sensitivity of the formation height to the temperature are equally probable. A caveat to be borne in mind is that sunspot fields extend well beyond their boundaries in the form of canopies with a base close to or below the formation height of the 12 μm emission lines (Giovanelli and Jones 1982). Furthermore, the field strength in the canopy (Solanki *et al.* 1992b, Hewagama *et al.* 1993) is of the same order as the values expected in small flux tubes at the height of formation of the 12 μm lines. In order to distinguish clearly between the superpenumbral canopy of sunspots and the magnetic field of plage flux tubes using the 12 μm lines, all four Stokes parameters must be measured. The field of sunspot canopies, being almost horizontal, can be distinguished from the more vertical field of plage flux tubes by measuring the magnetic inclination angle.

A subject of considerable speculation and investigation has been the formation height of the 12 μm lines. Zirin and Popp (1989), being firm believers in LTE, put it into the chromosphere, where the outward temperature rise would lead to the formation of an emission line. Deming *et al.* (1988), from oscillation frequencies measured in the 12 μm lines, and Lemke and Holweger (1987), based on the NLTE analysis with artificially imposed small departures, place it near the height of the temperature minimum. A comparison with the field strengths in empirically derived flux tube models extrapolated to the temperature minimum using the thin tube approximation suggests that the 12 μm lines are formed in the upper photosphere near the temperature minimum. Fully self-consistent NLTE calculations by Chang *et al.* (1992) and Carlsson *et al.* (1992), see Avrett (1992) and Rutten and Carlsson (1992) for reviews, give a contribution function that peaks in the upper photosphere (at disc centre). Finally, off-limb observations during the june 1991 eclipse by Deming *et al.* (1992b) and Jennings *et al.* (1992) showed that although the emission

peaks in the upper photosphere, it has a long, only slowly decaying tail that reaches well into the chromosphere. Carlsson *et al.* (1990), Zirker (private communication 1990) and Hoang-Binh (1991) rule out the LTE mechanism proposed by Zirin and Popp (1989). The small departures of the upper level of this line, artificially introduced by Lemke and Holweger (1987) in order to reproduce the quiet sun line profiles, have been shown to be produced without any artificial tuning if the model atom of Lemke and Holweger (1987) is extended somewhat (Hoang-Binh 1991) and Carlsson *et al.* (1992) produce perfect fits to the CLV of quiet-sun profiles with their self-consistent models. Therefore, the best current estimate of the formation height close to disc centre is the upper photosphere or the temperature minimum. The observations of Jennings *et al.* (1992) and Deming *et al.* (1992b) suggest the presence of additional emission from greater heights at the limb; some emission is found up to 2000 km above the visible limb. Far infrared continua also exhibit emission from higher layers above the visible limb than expected from standard 1-D atmospheric models (e.g. Lindsey *et al.* 1986, Hermans and Lindsey 1986). Thus, this property has probably more to do with the breakdown of hydrostatic equilibrium or of 1-D models than with peculiarities specific to the 12 μm lines.

What is required now are further observations of all four Stokes parameters of one of these lines in regions with different magnetic filling factors, as well as calculations of their line profiles in different flux-tube models.

The other wavelength range that has provided new information on the intrinsic strength of small-scale magnetic fields is the infrared H-band ($1.5 - 1.8$ μm), in particular the $g = 3$ Zeeman triplet (Litzén 1976) of Fe I at 15648.5 Å. The Stokes V profile of this line is completely split for $B \gtrsim 500$ G. It takes a somewhat stronger field to completely split Stokes I, in particular if the filling factor is not very large. Another problem with using the I profile of this line is the presence of weak blends at the position of the σ-components for a 2 kG field.

Harvey and Hall (1975) first pointed out the great Zeeman sensitivity of the $g = 3$ line, whose large splitting is clearly visible in the sunspot spectrum of Hall (1974), and obtained field strengths of 1200–1700 G outside of sunspots directly from its splitting (cf. Harvey 1977a). Surprisingly, no further results based on this line were published until a decade later. Sun *et al.* (1986) used it, together with other lines, to measure field strengths in spots and plages. Their main aim was to develop diagnostics for cool-star magnetic fields. Stenflo *et al.* (1987b) obtained H-band FTS spectra at various limb distances and determined B as a function of μ, finding $B(\mu = 1) \approx 1550$ G and smaller B values closer to the limb. This decrease of B with decreasing μ was interpreted as a height variation of the field strength, although no explicit height scale could be given (no radiative transfer calculations were carried out). Zayer *et al.* (1989) did a more detailed analysis, involving two H-band lines (15648.5 Å and 15822.8 Å, $g_{\rm eff}$= 0.75) and the 5250.2/5247.1 line pair in the visible. They were able to derive information on the vertical and horizontal distribution of the field strength in the observed network region.

Zayer *et al.* (1989) found that the magnetic field resulting from the thin tube ap-

proximation (Section 3.3.1) can simultaneously reproduce the two infrared Stokes V line profiles, as well as the Stokes V profile shapes and the ratio of the two visible lines. They concluded that the thin tube approximation is a good representation of the vertical and horizontal distribution of the field in magnetic elements, i.e. pressure balance is the main agent confining the field. It must be borne in mind, however, that measurements of field strength gradients and distributions are model dependent (Section 4.3). Zayer (1990) found that using another temperature model (that of Keller *et al.* 1990a, instead of Solanki 1986), a small horizontal distribution of the field strength cannot be ruled out by the V profile of 15648.5 Å. The results of the analysis of Zayer *et al.* (1989) have been confirmed by Muglach and Solanki (1991, 1992) using sixteen spectral lines. They also applied a statistical, many-lines procedure to H-band data and obtained a field strength of $\approx$ 1500 G. Their analysis also showed that the weak field approximation inherent in the Stenflo-Lindegren technique breaks down for H-band lines with $g_{\rm eff} \gtrsim 1.5$, so that reliable field strengths are only obtained if the approximation of complete splitting is made.

The information provided by the 15648.5 Å line has recently been greatly enhanced by the analysis of data from many solar regions obtained with the vertical spectrograph on the McMath telescope using either a single InSb diode as detector (Livingston 1991) or an InSb array detector (Rabin *et al.* 1991, Rabin 1992a,b). The field strengths measured by Livingston (1991) lie between approximately 400 G and over 2000 G, while Rabin *et al.* (1991) and Rabin (1992a,b) find field strengths ranging from 800 G to 1600 G, with a concentration of values near 1600 G. The larger range in field strengths seen by Livingston (1991) is probably due to his superiour spectral resolution. Rabin sees additional magnetic broadening of the σ-components corresponding roughly to a field strength distribution of width 600 G. The field-strength values have been derived either from simple profile fits, or from the wavelength difference between the σ-peaks of the V profiles of 15648.5 Å. For approximately twenty profiles the directly derived field strengths have been confirmed by model calculations (including a realistic radiative transfer) assuming height independent field strengths (Rüedi 1991). For approximately thirty profiles models incorporating the thin tube approximation have been used to fit the data and $B(z = 0)$ has been determined (Rüedi *et al.* 1992a). Before discussing the results of these fits it is interesting to point out that the shapes of the Stokes V profiles of Fe I 15648.5 Å show considerable variation from one solar region to another. A few examples of such observed profiles are shown in Figure 5.1 (solid curves).

Approximately half of the 27 profiles analysed in detail could be reproduced with a single thin-tube-like field. For some a second magnetic component, also assumed to be described by a thin-tube-like field, is required as well. Two components have been sufficient to reproduce all the analysed profiles and no further magnetic broadening has been required (Rüedi *et al.* 1992a). The dashed curves in Figure 5.1 represent synthetic profiles. The $B(z)$ derived in this manner is plotted vs. the spatially averaged field strength, $\langle B \rangle$, in Figure 5.2. The weak fields [$B(z = 0) \lesssim 1250$ G] seen in that figure are discussed in the next section. The $B(z = 0)$ of

the strong fields are very similar to the values found by Zayer *et al.* (1990) from the ratio of Fe I 5250.2 Å to Fe I 5247.1 Å. Thus, measurements in the visible and at 1.5 μm give the same field strength at a fixed geometrical height. The strong fields are close to the limit of field strengths supportable by the pressure of the surrounding gas (Equation 5.1), i.e., magnetic elements are highly evacuated. There is a slight tendency for $B(z = 0)$ to increase with increasing filling factor.

Techniques and results of magnetic measurements using 1.5 μm lines have been reviewed by Rabin (1992c,d) and Solanki (1992b).

In summary, infrared lines have allowed the field strength to be tightly constrained: It lies between 1500 G and 1700 G at $z = 0$ and drops rapidly to a value of 200–400 G in the upper photosphere. Most of the magnetic flux has $B(z = 0)$ values lying within this narrow range. The vertical stratification of B is compatible with the thin-tube approximation.

5.1.4. Weak Fields

Although line ratios in the visible suggest that at least 90% of the *net* magnetic flux is in strong field form (Howard and Stenflo 1972, Frazier and Stenflo 1972), less is known about the strength of a possible component of the field in a 'tangled' state, i.e. with both polarities intermingled on a spatial scale below the resolution of the observations. Large amounts of magnetic flux may remain 'hidden' in this form (e.g. Stenflo 1984a, 1989). Attempts have been made to detect such tangled fields using high spatial resolution magnetograms (Tarbell *et al.* 1979), methods based on Stokes I (Unno 1959, Howard and Bhatnagar 1969, Stenflo and Lindegren 1977, Stenflo 1984a), or Stokes Q and U (Stenflo 1982, 1987, Faurobert 1992a). These measurements have constrained the amount of flux in 'tangled' form, as well as some of its properties. The *spatially averaged* field strength of the 'tangled' field is now thought to lie between 30 and 60 G in the lower photosphere and to drop to 10–30 G in the upper photosphere. This result, obtained using detailed model calculations by Faurobert-Scholl (1992b), demonstrates the power of the Hanle effect. Furthermore, the magnetic polarities must be mixed on a scale smaller than 0.5″ (Tarbell *et al.* 1979) and the field must be nearly isotropically oriented (Stenflo 1987). The term "spatially averaged field strength" is used here to represent roughly the more intricate quantities actually derived by the various techniques. For example, the Stokes I-based line-broadening methods give an average field equal to $\sqrt{\int B\, dA}/\sqrt{A}$, where A is the area of the spatial resolution element. The result of the Hanle effect is yet more complex.*

Possible relatives of the tangled field are the 'inner network fields' or 'intranetwork fields' observed by Livingston and Harvey (1971, 1975, cf. Harvey 1977a), Sivaraman and Livingston (1982), Martin *et al.* (1985a), Livi *et al.* (1985), Zirin (1985), and Martin (1988) under conditions of good seeing in high sensitivity

* The "interfilamentary field" observed by Frazier and Stenflo (1972) is an artifact of an error in reduction software (Stenflo, private communication 1991).

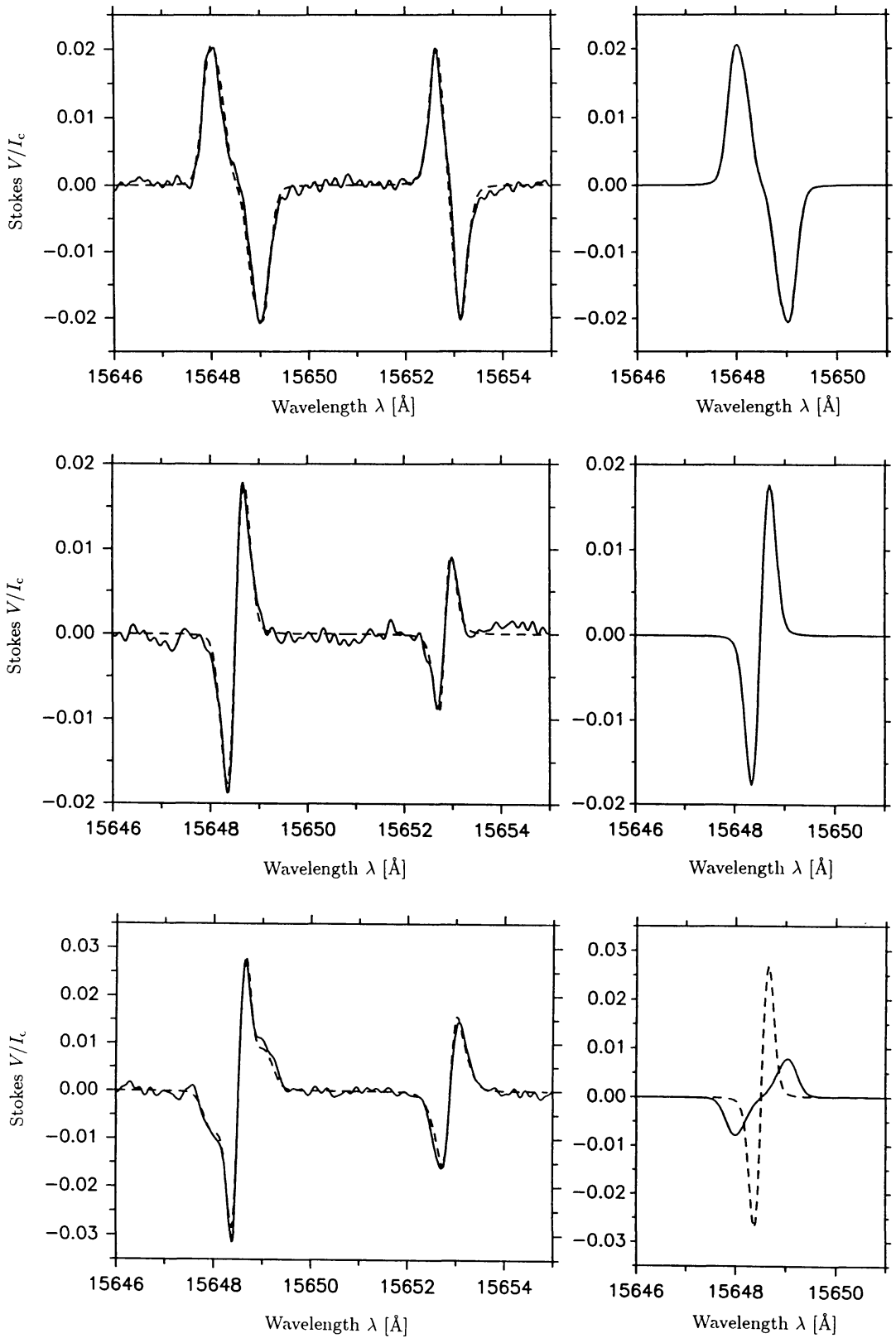

Fig. 5.1(a)–(c).

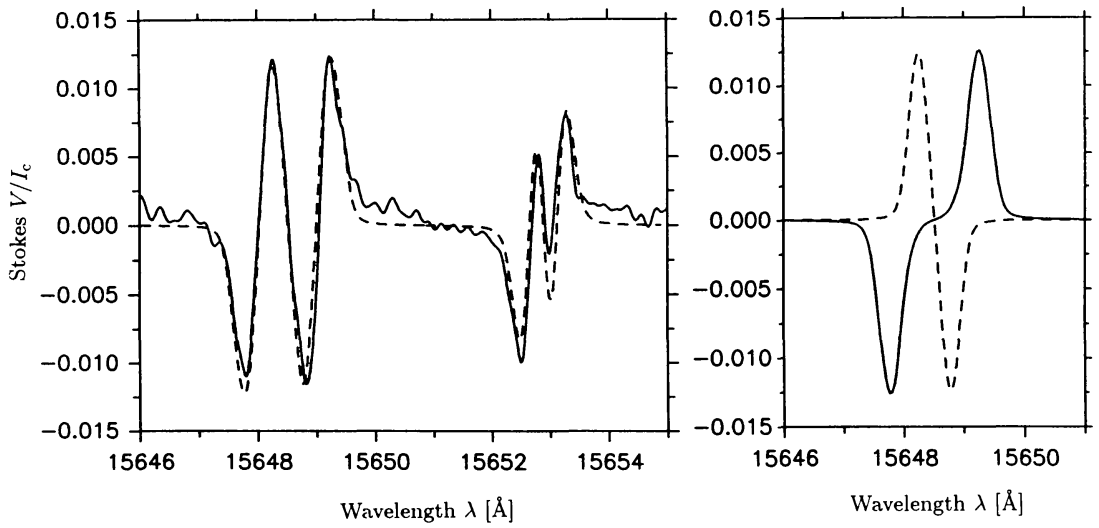

Fig. 5.1(d).

Fig. 5.1. Stokes V profiles of 15648.5 Å ($g = 3$) and 15652.9 Å ($g_{\text{eff}} = 1.53$). The solid curves are profiles observed in active region plages, the dashed ones are best-fit synthetic profiles with one or two magnetic components. The synthetic profiles of the individual magnetic components are shown in the frames on the right. **(a)** Single flux-tube fit with $B(z = 0) = 1520$ G. **(b)** Single flux-tube fit with $B(z = 0) = 750$ G. **(c)** Fit involving two flux-tube components having the same polarity, with $B_1(z = 0) = 1500$ G and $B_2(z = 0) = 500$ G, respectively. **(d)** Fit involving two opposite polarity flux-tube components with $B_1(z = 0) = 1700$ G and $B_2(z = 0) = -1050$ G, respectively. There is no velocity shift between the two components (from Rüedi *et al.* 1992a).

('deep') magnetograms. The importance of high sensitivity is demonstrated by the many unsuccessful attempts to observe intranetwork fields (e.g. Steshenko 1960, Semel 1962, Leighton 1965, Livingston 1968, Beckers and Schröter 1968b, Tarbell *et al.* 1979). As their name suggests, intranetwork fields are found between the network elements in the interiours of supergranular cells. Livingston and Harvey (1971) obtained field strengths of 2–3 G spatially averaged over 5″. There is some indirect evidence that the intranetwork field strengths are intrinsically low. Martin (1988) notes that, in contrast to network fields, the intranetwork elements are just as evident close to the solar limb as near disc centre, suggesting that the field lines are more or less randomly inclined to the solar surface. This observation is not only consistent with the result of Stenflo (1987) for the distribution of orientations in a tangled field, but it also suggests that the intranetwork fields are weak, so that they only experience small buoyancy forces (Spruit *et al.* 1991). They may, all the same, be composed of very thin flux tubes with relatively weak fields that are easily tilted by granular motions (Schüssler 1990). Furthermore, since Tarbell *et al.* (1979) do not observe any field in between the network with high spatial resolution, but with relatively low sensitivity, they argue that the intranetwork field cannot be concentrated into flux tubes above a certain size, since the presence of one such tube would show up as a localized strong field, but a diffuse field or a multitude of very small flux tubes would escape detection.

Recently, direct confirmation of the presence of fields with strengths well below

the kG level in the lower photosphere has come from observations of the 15648.5 Å ($g = 3$) line. From the Zeeman splitting exhibited by this line Livingston (1991) deduced field strengths between 400 and 1000 G in a minority of the observed regions. 400–500 G correspond to the lowest field strength derivable directly from the V peak separation of this line (Section 5.1.3). By carrying out radiative transfer calculations and comparing with the 15652.9 Å line ($g_{\rm eff} = 1.53$, Solanki *et al.* 1990), it is possible to measure field strengths down to 200 G, i.e. to achieve a sensitivity to the field strength rivaling that of the 12 μm lines (Solanki *et al.* 1992a). Detailed fits to the profiles of these lines have indicated the presence of a weak field component also in regions with predominantly strong fields (Rüedi *et al.* 1992a). The strength of this weak field component varies between 400 G and 1200 G. There is no sign of any concentration of the field strength at very small values ($B \lesssim 200$ G), as suggested by Tarbell *et al.* (1979) for tangled fields, based on indirect arguments. The fraction of flux in weak field form has been estimated to be approximately 10% from the infrared data. The intrinsic field strength, B, as a function of the spatially averaged field strength, $\langle B \rangle$ (a measure of the magnetic filling factor), is plotted in Figure 5.2.

At present it is not justified, although very tempting, to identify the weak fields detected in infrared spectra with the intranetwork fields seen in visible light magnetograms. Since the weak fields do not show a preference for the opposite polarity to the strong fields detected in the same spectra, they cannot be identified with the opposite polarity weak fields claimed to be seen by Koutchmy (1991) and Koutchmy *et al.* (1991) in the immediate vicinity of strong fields. The absence of such a signature in the infrared spectra casts serious doubt on the existence of 'return-flux' type configurations in which strong field of a dominant polarity is surrounded by a weak opposite polarity field.

Two questions regarding the nature of the weak fields seen in the infrared can be tentatively answered by the infrared observations, although further observations are required before a final verdict can be given. Firstly, do the observed weak fields belong to freshly emerged flux patches that are undergoing a collapse into strong field form, or are they more stable structures? Secondly, are siphon flows between strong and weak field elements, as predicted by theory, present? Although it cannot be ruled out that a few (3 out of 13) of the observed weak field features are transient and undergoing convective collapse, the lack of systematic downflows suggests that at least some of them are in a more or less convectively stable state. Although the profiles analysed by Rüedi *et al.* (1992a) do not provide any evidence for siphon flows, Rüedi *et al.* (1992b) observe the distinctive signature of a siphon flow across the neutral line of an active region, i.e. a weak field containing upflowing matter and a strong field of opposite polarity with downflowing matter. The rarity of both up- and downflows in weak-field patches suggests that they are relatively long-lived. This appears to support the existence of U-shaped loops (Spruit *et al.* 1987, cf. Section 5.1.5), although it cannot be ruled out as yet that the detected weak fields are all part of sunspot canopies, which give a very similar signature (Solanki

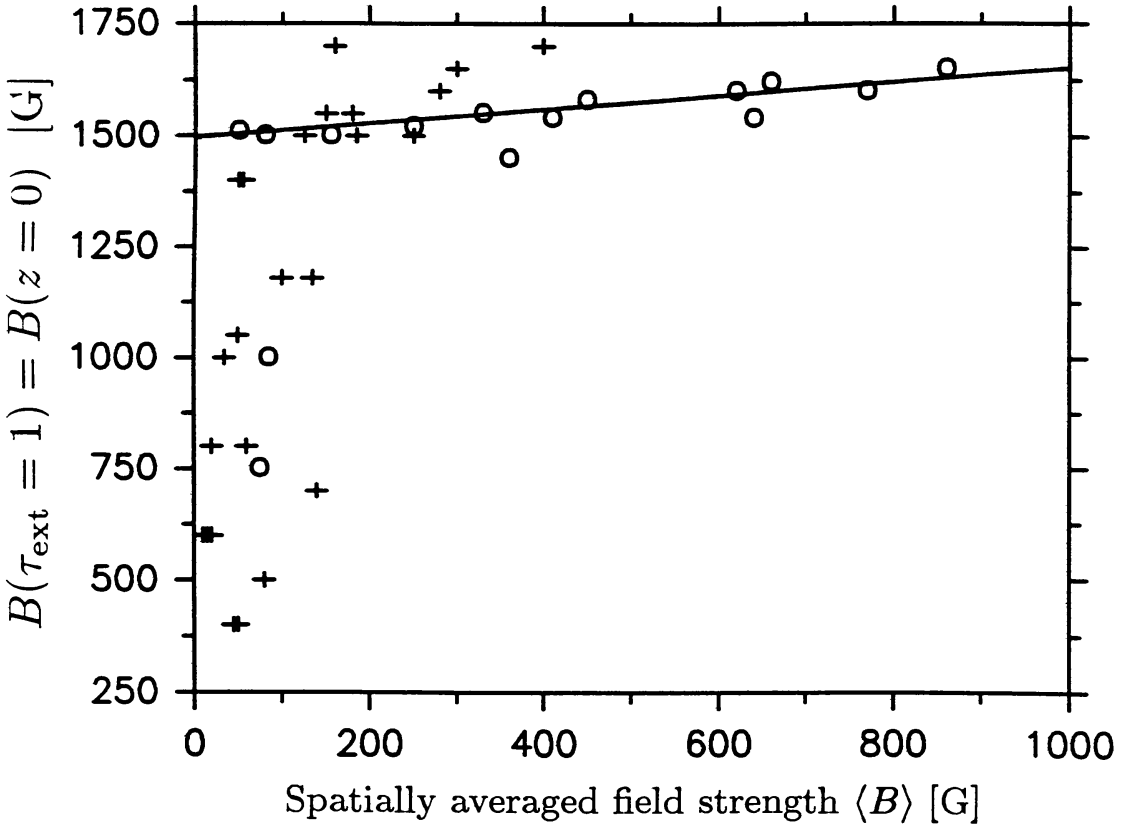

Fig. 5.2. The field strength B at $z = 0$ (corresponding to $\tau = 1$ in the quiet sun) is plotted vs. the spatially averaged field strength, $\langle B \rangle$. The field strength derived from spectra which could be reproduced by a single flux tube are marked by circles, those which result from spectra requiring 2 components are marked by crosses. If two magnetic components were needed to fit the observed profile then the field strength of the synthetic profile of each component is plotted separately vs. the $\langle B \rangle$ of that component. The solid curve is a least-squares fit to the data points with $B(z = 0) \geq 1400$ G (from Rüedi *et al.* 1992a).

et al. 1992b).

Finally, there is evidence for weak fields of 200–400 G in the upper photosphere (from the 12 μm emission lines, Brault and Noyes 1983, Deming *et al.* 1988) and of 20–100 G in the lower chromosphere at $z \approx$ 900–1100 km (from the Hanle effect in Ca I 4227 Å, Faurobert-Scholl 1992a). These field strengths are consistent with the standard flux tube models described in Section 5.1.5.

In summary, there is increasing evidence of a tangled field of 10–50 G filling the space between the kG flux tubes. Fields of intrinsic strengths between 400 and 1000 G have also been detected. Their nature is as yet unknown.

5.1.5. Theory

The magnetic field of small-scale features is confined mainly by the internal gas-pressure deficit; curvature forces play only a small role in the photosphere (Section 3.3). This is now well established (e.g. Spruit 1976, Deinzer *et al.* 1984a,b, Pneuman *et al.* 1986, Knölker *et al.* 1988, Steiner *et al.* 1986, Steiner and Pizzo, 1989). Older

proposals, such as the concentration of flux ropes by an increased twist of the field lines can safely be ruled out (Parker 1976, Steiner *et al.* 1986).

The field strength at a given height depends on the evacuation (i.e. on the reduction of the gas pressure within the flux tube) at that height. At a given geometrical height, z, the maximum field strength supported in this manner is obtained by completely evacuating the flux tube,

$$B_{\max}(z) = \sqrt{8\pi\, p_{\rm ext}(z)}\,, \tag{5.1}$$

where $p_{\rm ext}$ is the pressure in the non-magnetic surroundings of the magnetic feature. However, an increased evacuation also implies a downwards shift of the continuum optical depth scale. This in turn signifies that the lines used to measure the field are formed deeper in the atmosphere, where $p_{\rm ext}$ and consequently the field strength is higher. Figure 5.3 shows $B(\tau = 1)$ vs. $B(z = 0)$ for the simple case of a temperature structure that is independent of evacuation (see Solanki *et al.* 1992a for a detailed discussion of the figure). Therefore, pressure balance by itself sets no limits on the observable field strength. In theoretical models of flux tubes the field strength at a given height (e.g. Steiner *et al.* 1986, Pneuman *et al.* 1986, Steiner and Pizzo 1989), or an evacuation parameter (e.g. Deinzer *et al.* 1984a,b) can indeed be freely prescribed.

The question how flux tubes may become evacuated to the high degree suggested by the observations [most have plasma β values, defined in Equation (3.31), smaller than 0.5, Zayer *et al.* 1990, Rüedi *et al.* 1992a] can only be answered by considering the dynamical evolution of the field from its emergence until the formation of flux tubes, i.e. the dynamics of magnetic flux expulsion and convective collapse. These mechanisms are discussed in Section 5.7.3 in detail. They are quite efficient and should concentrate a patch of weak field into a kG flux tube within a few minutes (Venkatakrishnan 1986a, Schüssler 1990).

There are two configurations in which the field can avoid becoming concentrated. 1) Very small flux patches cannot undergo convective collapse, since they are horizontally optically thin and thus cannot cool down relative to the surroundings, a prerequisite for a successful enhancement of the field above the equipartition value (Schüssler 1990). 2) U-shaped loops, investigated by Spruit *et al.* (1987), effectively suppress the convective instability. A U-loop is expected to be formed when two opposite polarity flux tubes reconnect below the surface (cf. Section 5.7.5). Magnetic buoyancy causes the loop to float upwards. The strong density stratification and mass conservation cause the tube to expand considerably as it rises. Thus, increasingly weaker fields are seen at the solar surface as a function of time (cf. Spruit *et al.* 1991). It is presently unclear, however, whether U-loops actually lead to long-lived weak fields. The two "ends" of the U-loop form the footpoints of Ω-loops. If an Ω-loop is not too large, then a siphon flow should set in once the difference in field strengths between its two foot points, one of which is an endpoint of the U-loop, becomes sufficiently large. Such a siphon flow,

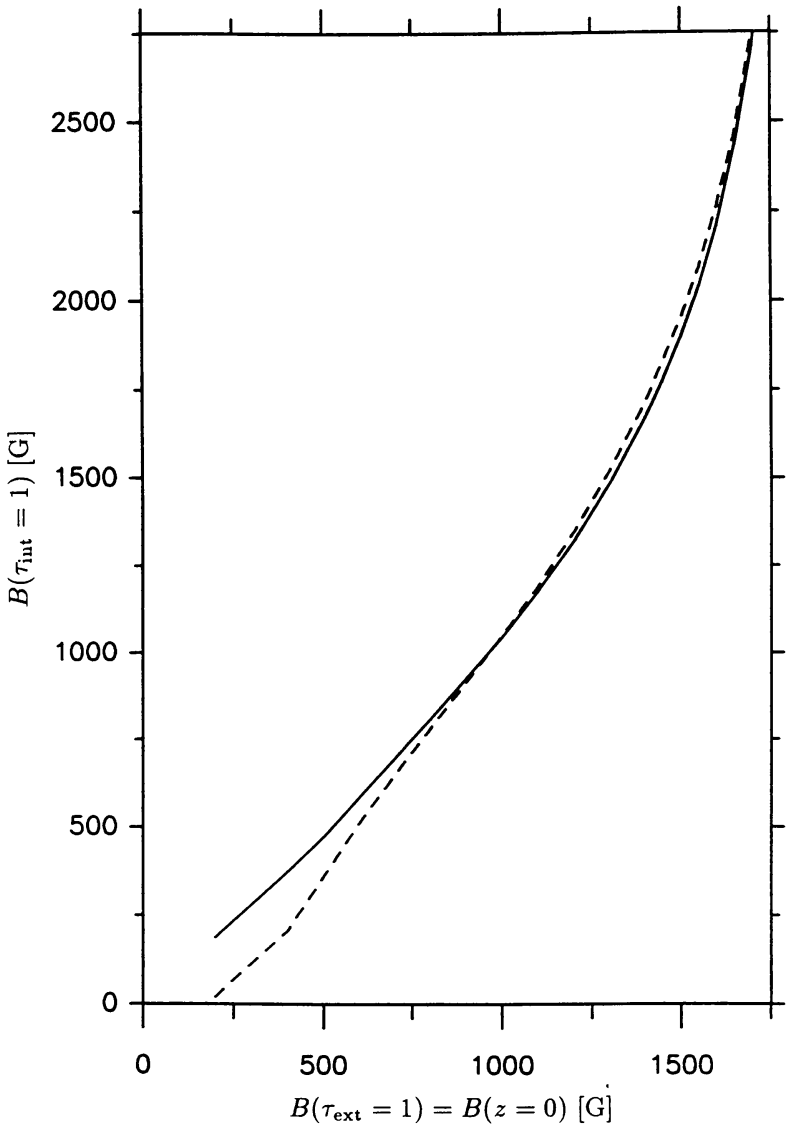

Fig. 5.3. Field strength at unit optical depth within the flux tube, $B(\tau = 1)$, vs. field strength at unit optical depth of the quiet sun, $B(z = 0)$. The field strength is calculated in the thin-tube approximation for a plage flux-tube model (dashed curve) and for a quiet sun model (solid curve) (from Solanki *et al.* 1992a).

carrying matter from the weaker to the stronger field, should evacuate the U-loop and strengthen its surface field.

The structure of the magnetic field within small magnetic flux tubes during their stable phase has been calculated under a wide variety of assumptions. A detailed review of the various approximations used has been given by Schüssler (1986). Although the various models give results that may differ substantially from each other, they share one common property, the field strength decreases nearly exponentially with height.

The simplest approach is to assume cylindrical symmetry and expand all the dependent variables in the MHD equations according to the radial coordinate

(Section 3.3.1). If all terms of order r are neglected (i.e. in the zero-th order or thin tube approximation) then the structure of the field is determined only by pressure balance, and no quantity is allowed to vary across the radius of the tube, except at the boundary current sheet. Often, first order quantities, allowing a linear variation of, e.g., B_r, across the tube, are also included. A vast number of calculations based on the thin tube approximation exist. Examples are those of Parker (1955, 1979a, 1982a, b), Defouw (1976), Roberts and Webb (1978, 1979), Webb and Roberts (1978, 1980a,b), Chapman (1979), Unno and Ando (1979), Unno and Ribes (1979), Spruit and Zweibel (1979), Wilson (1979, 1980), Spruit (1981a, b, 1982), Spruit and Van Ballegooijen (1982), Roberts (1983), Venkatakrishnan (1983, 1985), Roberts (1983, 1985), Hasan (1984, 1985, 1988, 1991), Hasan and Schüssler (1985), Ferrari *et al.* (1985), Kalkofen *et al.* (1986), Solanki (1986, 1989), Solanki *et al.* (1987), Ferriz Mas and Moreno Insertis (1987), Walton (1987), Ferriz Mas (1988), Thomas (1988), Van Ballegooijen and Choudhuri (1988), Montesinos and Thomas (1989), Zayer *et al.* (1989), Degenhardt (1989, 1991), Ferriz Mas and Schüssler (1989), Schüssler (1991), Ulmschneider *et al.* (1991) and Solanki and Roberts (1992).

Spruit (1981b) generalized the thin-tube approximation to tubes with a non-straight axis (cf. Choudhuri 1990, Cheng 1992). Parker (1975a) introduced external flows into the thin tube approximation, Hasan and Schüssler (1985) included viscosity and Van Ballegooijen (1983) and Ferriz Mas and Schüssler (1992) incorporated rotation. Most of the models cited above are dynamic. Due to its simplicity the thin tube approximation is particularly popular for studying dynamic phenomena (waves, overstable oscillations, flows, convective collapse, buoyant rise of flux tubes) and the radiative exchange of energy, as well as for the interpretation of observational data. The thin tube approximation has not only turned out to be sufficiently precise to reproduce all the currently available data, in the photosphere it is also a reasonable approximation to exact solutions of the MHD equations (Steiner *et al.* 1986, Knölker *et al.* 1988), except for some extreme and possibly unrealistic temperature structures (Steiner and Pizzo 1989).

The next higher order approximation is obtained if terms up to order r^2 are retained (Ferriz Mas and Schüssler 1989). Models of this type have been constructed by Wilson (1977a,b), Browning and Priest (1982, 1983), Pneuman *et al.* (1986), Anton (1989) and Ferriz Mas *et al.* (1989). This approach allows a limited radial variation of the variables and of magnetic tension forces. It may thus be applied to somewhat larger tubes than the thin tube approximation. The computational complexity is approximately the same as for self-similar models (Section 3.3.3). However, the expansion approach allows the temperature structure to be prescribed first (e.g. through a solution of the energy equation or from observations) and then determines the corresponding magnetic structure. In the self-similar solutions the fixed radial variation of the field means that only very particular and, in general, unphysical radial temperature distributions are allowed. The work of Anton (1989) and of Ferriz Mas *et al.* (1989) includes dynamical effects (flux tube waves) up to

second order.

Self-similar magnetic fields (Section 3.3.3), first introduced by Schlüter and Temesvary (1958), and used to model sunspots by e.g. Deinzer (1965), Yun (1970), Low (1980) and Osherovich (1982), have been used to describe small flux tubes by Solanki (1982), Osherovich *et al.* (1983) and Solov'ev (1984). Although self-similar fields are exact solutions of the MHS equations, their basic assumption that the horizontal shapes of B_z and B_r are independent of height is somewhat artificial. The models cited above have assumed, e.g., $f(r/R) = \exp(-(r/R)^2)$ or $f(r/R) = (1-(r/R)^2)^{\alpha}$, where α is a free parameter. Observations of the magnetic field strength, on the other hand, are well-reproduced by $f(r/R) = 1$, i.e. the thin tube approximation (Zayer *et al.* 1989), suggesting that these radial dependences are unnecessarily complex. Also, the CLV of the continuum contrast derived from such models is in conflict with observations (Chapman and Gingell 1984).

Potential field models (Section 3.3.2) have been constructed by Simon and Weiss (1970), Spruit (1976, 1977), Gabriel (1976), Meyer *et al.* (1977), Simon *et al.* (1983), Anzer and Galloway (1983) and Van Ballegooijen (1985a). The potential field approximation may be satisfied for sunspots (large field strengths) and in the upper layers of small flux tubes if a current sheet boundary is included in the model.

Models based on the complete solution of the MHS equations in 2-D cylindrical geometry have been published by Steiner *et al.* (1986), Steiner and Pizzo (1989), Fiedler and Cally (1990), Steiner (1990, cf. Steiner and Stenflo 1990), Solanki and Steiner (1990), Cally (1991), Pizzo (1991), and Pizzo *et al.* (1993). Almost all these models possess a boundary current sheet. Exceptions are to be found in the papers by Steiner *et al.* (1986), Steiner and Pizzo (1989), and Pizzo *et al.* (1993). The latter authors have studied the magnetic stucture of a comprehensive grid of models. Steiner *et al.* (1986) have also investigated the influence of a twisted field on the equilibrium of a flux tube. They find that magnetostatic equilibrium cannot be achieved for azimuthal components larger than a critical value, corresponding to approximately a third of the axial field at the bottom of the photosphere. Fiedler and Cally (1990), Steiner (1990, cf. Steiner and Stenflo 1990), and Pizzo *et al.* (1993) have included an energy equation in their models. The Fiedler and Cally (1990) models are restricted to the chromosphere and corona. Similarly, the main emphasis of the Solanki and Steiner (1990) models lies on the chromosphere. The models in this group generally include the merging of the fields of neighbouring tubes with the same polarity. The structure of the field in these models clearly demonstrates that self-similar solutions, with the exception of the $f(r/R) = 1$ thin tube approximation, are incompatible with the merging of neighbouring tubes. Steiner and Pizzo (1989) and Solanki and Steiner (1990) have demonstrated the great sensitivity of the magnetic structure, in particular of the merging height, to the thermal structure of the flux tube relative to its surroundings (cf. Pneuman *et al.* 1986, Steiner *et al.* 1986). Hot flux tubes expand more rapidly than cool tubes.

This effect is particularly noticeable when the internal temperature is larger than the external temperature (and the plasma β, Equation 3.31, increases with height). In this case there is a critical height above which the internal gas pressure becomes larger than the external pressure. Since the field cannot be confined above this level, it expands almost horizontally until it merges with the field of neighbouring flux tubes. During such a phase of rapid expansion the structure of the field deviates strongly from that of a thin tube. The resulting structure, an almost horizontal magnetic field overlying field-free gas, is generally termed a magnetic canopy (Giovanelli 1980).

The full MHD equations have been solved in 2-D slab geometry by Deinzer *et al.* (1984a,b), Knölker *et al.* (1988, 1991), Knölker and Schüssler (1988) and Grossmann-Doerth *et al.* (1989b), cf. Schüssler (1992). In all except the calculations of Knölker *et al.* (1991), the solution relaxes from an initially prescribed situation to a stationary end state. Knölker *et al.* (1991) find an oscillatory end state if the initial state is far from thermal equilibrium. Note that in these models the energy equation is always solved in parallel with the momentum (force balance) equation. With the exception of Knölker *et al.* (1988), who also consider some models with relatively broad boundary current layers, all the models have narrow boundary current sheets. Knölker and Schüssler (1988) have calculated models of larger tubes (diameters of 500 km), the rest of the calculations refer to tubes with diameters of 200 km near the $\tau = 1$ level. These models are valid in the upper convection zone and the photosphere. In these atmospheric layers the field is found to be confined almost exclusively by pressure balance.

Finally, 3-D solutions of the MHD equations, including a comprehensive energy equation, have been published by Nordlund (1983, 1985b, 1986) and Nordlund and Stein (1989) for the solar photosphere. Although these models show the interaction of the magnetic field with convection and reveal the distribution of the field on scales between 200 km and 2000 km, they cannot spatially resolve the internal structure of the magnetic field in individual magnetic structures. One interesting feature of these models is that the field is constantly changing due to the everchanging convective pattern. Individual field lines, which lie close together near the solar surface, need not be neighbours in the subsurface layers and Nordlund has even questioned the validity of the concept of the flux tube.

The properties of the current sheets bounding magnetic elements have been studied by Schüssler (1986) and Hirayama (1992). Schüssler (1986) finds that the thermal, resistive and viscous boundary layers all have similar widths of 3–10 km, while Hirayama (1992) obtains a 2 km thick resisitive boundary.

In conclusion, relatively general solutions, i.e. solutions requiring few assumptions, of the MHD equations are now possible. The resulting magnetohydrostatic and dynamic flux tube models accurately reproduce the measured vertical stratification of the magnetic field. The absolute value of the field strength can also be predicted by theory (see Section 5.7.3 for details).

5.2. Magnetic Field Orientation

5.2.1. Observations

Measurements of the full magnetic vector outside of sunspots are rare. Most of the observational evidence of field line inclinations is indirect, i.e. not based on Stokes vector measurements, and generally extremely dependent on model assumptions. Examples of such indirect and therefore inconclusive studies are those of Stoyanova (1970), Krat (1973), Mehltretter (1974), Schoolman and Ramsey (1976), Tarbell and Title (1977) and Brants (1985a,b). Mehltretter (1974) compares positions of elongated bright points in filtergrams corresponding to different heights and finds that the bright structures at different heights are often aligned along the direction of elongation. Schoolman and Ramsey (1976) and Tarbell and Title (1977) postulate almost horizontal fields in what they call the 'dark component of the network'. Wiehr (1978) compared simultaneously obtained magnetograms with Ca II 8498 images and found the Ca core brightenings to be displaced by $\lesssim 2''$ eastwards of the photospheric magnetic peaks in 11 out of 32 observed monopolar features (the remaining 21 features showed no displacements larger than $1''$). It should be noted, however, that his entrance aperture was itself $2''$, so that all the measured displacements are below his effective spatial resolution. Brants (1985a,b) assumed emerging fields to be inclined when Stokes I of a relatively Zeeman sensitive line is broad and its Stokes V amplitude is small. The results of this and similar techniques must, however, be considered with care, since other explanations of the observations are also probable (cf. Section 4.4). Note that due to the limited spatial resolution only the average inclinations of whole groups of magnetic elements have so far been obtained from the observations irrespective of the technique used.

An often used proxy of the magnetic field orientation in the chromosphere is the orientation of Hα fibrils. The relationship between photospheric magnetograms and Hα filtergrams has been studied by Veeder and Zirin (1970), Schoolman (1971), Zirin (1972), Frazier (1972), and Nakagawa *et al.* (1973). The correlation between the azimuth of the transverse component of the magnetic field (determined from Stokes Q and U) and the direction of the Hα fibrils has been studied by Tsap (1965) for superpenumbrae and by Makita *et al.* (1985) and Kawakami *et al.* (1989) for whole active regions. In active regions the coincidence is approximately 50–60% near $\mu = 1$ and decreases to approximately 20% near the limb. Kawakami *et al.* (1989) explain this CLV by a model taking into account the different heights sampled by Hα and the magnetogram and making use of projection effects.

Direct, i.e. Stokes-profile based, measurements are considerably rarer. Deubner (1975) finds evidence of an almost random distribution of field-line inclinations from vector magnetograms. Solanki *et al.* (1987) derived limits on the inclination with respect to the vertical from the Stokes I, Q and V line profiles of two lines. They found that the magnetic elements in four out of the eight studied regions have an average inclination larger than 10° to the vertical. Lites and Skumanich (1990) also find large inclinations from spectra in all four Stokes parameters in non-spot

regions, but give no numbers. Recently, Bernasconi (1992) has inverted I, Q, U and V spectra of a number of plage regions near the limb. He finds that the flux tubes in the observed regions are inclined by, on the average, 5–15°. All these observations appear to suggest that on some portions of the solar surface the majority of the magnetic features are inclined in a preferred direction. As mentioned in Section 4.4 (cf. Stenflo 1985b) the inclination angle of the field derived from observations may be grossly wrong if the unresolved nature of the field is not taken into account. Only Solanki *et al.* (1987) and Bernasconi (1992) have explicitely included reliable diagnostics of the field strength in unresolved magnetic features in their analysis. However, so far no investigation of the field orientation has taken all the effects due to the finite size of magnetic features into account, i.e. no 2-D models have been used. Since most inclination measurements are made relatively close to the limb (in order to obtain sufficiently large Stokes Q and U signals), 2-D models are particularly important.

The rest of the investigations of field orientation are limited to determining the azimuthal angle of the field from Stokes Q and U, i.e. determining the orientation along the solar surface. The main aim of such investigations is to complement standard magnetograms as a means of deriving the structure of the field within an active region. From maps of line-of-sight average field strength, polarity and the horizontal direction of the field it is possible to obtain an idea of the horizontal shear in the magnetic field. A build up of magnetic shear is thought to be an important precursor, possibly even a necessary precondition, for solar flares. Various groups have published such measurements. Those at Big Bear, Crimea, Hawaii, Huntsville, Potsdam and Tokyo have presented vector magnetograms of regions outside sunspots. More details are to be found in various papers in the proceedings edited by Hagyard (1985) and November (1991). Vector magnetograms (e.g. Krall *et al.* 1982, Hagyard *et al.* 1984, cf. Hagyard 1984) have firmly established the earlier weaker observational link between the shear of the field and the rate of flaring at that position (e.g. Rust *et al.* 1975, Harvey and Harvey 1975, 1979, cf. Harvey 1983).

5.2.2. Theory

In the absence of an external flow and tension forces due to connection with a nearby opposite-polarity flux tube, buoyancy forces ensure that the highly evacuated flux tubes remain strictly vertical. External flows, e.g. due to the granulation, may cause a flux tube to become inclined. For a steady flow the inclination angle results from a balance between the force due to the flow and buoyancy. Schüssler (1986) has estimated that for a flow velocity of 1 km s^{-1}, typical for granular flows, a totally negligible inclination of approximately 1° to the vertical results for flux tubes with a field strength of 1500 G at $z = 0$. On short time scales granular velocities may reach considerably larger values (the newest fully compressible models of convection show the presence of shocks in the solar photosphere with maximum velocities over 10 km s^{-1}, Cattaneo *et al.* 1990, Steffen 1991, Steffen and Freytag

1991), so that flux tubes may well have larger inclinations for short periods.

Following Schüssler (1986) we write for the inclination of **B** to the vertical, ϕ, induced by an external velocity $u_\perp$,

$$\sin\phi = \frac{8\rho u_\perp^2}{B^2}.$$

Taking his values of $B = 1500$ G, $\rho = 3 \times 10^{-7}$ g cm^{-3} and $u_\perp = 1$ km s^{-1}gives $\phi = 0.6°$. However, increasing $u_\perp$ to 5–6 km s^{-1} gives $\Phi = 15$–$22°$, a sizable inclination. For still larger values of $u_\perp$ the assumptions underlying the above equation break down. The most likely consequence of a shock wave hitting a flux tube is a kink-mode wave travelling up the flux tube (Spruit 1982, Zähringer and Ulmschneider 1987, Ulmschneider *et al.* 1991). This may lead to even larger inclinations in the chromosphere, as the wave travels through increasingly more tenuous gas, but can hardly explain the large observed inclinations in the photosphere.

As pointed out by Schüssler (1990), thinner flux tubes follow the dictates of the surrounding granular flow more readily, due mainly to the inefficient concentration of the field and the resulting smaller field strengths (note that for a given velocity, the inclination is proportional to $1/B^2$). Thus, tubes with diameters of the order of 10 km can be substantially inclined, but it appears too premature to deduce the presence of small flux tubes from the large measured inclinations, particularly since the observed field strength in the regions showing a sizable inclination is not exceptionally small.

Regions of flux emergence (or submergence) are expected to contain nearly horizontal fields corresponding to the tops of loops. The emerging horizontal field, however, is again expected to be relatively weak. Stronger fields are more strongly evacuated, so that the field at the footpoints of an emerging loop should become vertical as soon as the convective collapse (Section 5.7.3) is fairly underway.

Finally, in active regions the superpenumbral canopies of sunspots may produce large field inclinations even below their lower boundaries by forcing individual field lines belonging to small flux tubes to bend over and follow the boundary of the superpenumbra. Recently, Stokes V spectra of Fe I 1.5648 μm have shown the signature of a superpenumbral canopy with underlying flux tubes. Magnetic tension (curvature forces) may cause an inclination well below the superpenumbral boundary.

So far, the data have been unable to distinguish between any of the proposed mechanisms. More theoretical work and, in particular, more and better observations and empirical analyses are required to improve the present rather unsatisfactory state of affairs.

The highly inclined, almost horizontal fields in the lower chromosphere deduced from Hanle-effect measurements and magnetograms near the limb are best described in terms of magnetic canopies. Such a canopy is produced at the "critical height" at which the internal and external gas pressure are equal. A critical height

is only present if the internal temperature is larger than that of the non-magnetic atmosphere.

Finally, consider the question of the existence of twisted flux tubes. The limited spatial resolution does not allow any observational investigations with the exception of large structures, such as sunspots.* For these there is evidence of, at the most, slight twists (e.g. Lites and Skumanich 1990). Theoretically, an upper limit can be set on the maximum amount of twist compatible with a magnetohydrostatic solution of a flux tube (Steiner *et al.* 1986). Larger twists must be compensated by dynamical effects. Twisted flux tubes probably exist only if they constitute the footpoints of small loops. Else any twist accumulating in the photosphere travels upwards in the form of an Alfvén wave, unwinding the field as it goes.

In summary, theory predicts that magnetic features having kG fields should be nearly vertical, in contrast to the observations. However, there are still some unexplored mechanisms for producing inclined fields, e.g. the merging of flux tubes with low-lying superpenumbral canopies.

5.3. Magnetic Filling Factor and Flux

The magnetic flux or average flux density (spatially averaged field strength) is one of the most often measured quantities, generally from the magnetogram signal via some, usually simple, calibration formula for a particular spectral line and instrument. However, the filling factor or flux is rarely studied in its own right. It is often used to quantify some intangible like 'magnetic activity' and serves as the independent variable against which other parameters or observables of magnetic features (e.g. Ca II K core emission, temperature, field strength) are expressed. Here I briefly consider some of the measurements aimed at determining the magnetic filling factor or flux.

One type of measurement has aimed at determining the magnetic flux of single magnetic elements. This type includes attempts at finding a lower limit of the magnetic flux of isolated magnetic features by various authors. Wiehr (1979) finds a lower limit of 2.4×10^{18} Mx. Earlier, Stenflo (1973) had estimated the typical flux per magnetic feature to be 2.8×10^{17}–10^{18} Mx. Zirin (1987) quotes 2.4×10^{18} Mx as a typical flux value. Finally, Wang *et al.* (1985) find minimum fluxes of a few times 10^{16} Mx in cancelling magnetic features. This last value may hardly be termed a flux per feature, however, since only the difference in flux between two features is measured. More details on these measurements are given in Section 5.6.1. I only wish to point out here that no specific attempts were made by these authors to counter the uncertainties inherent to flux measurements, which were pointed out in Section 4.5. They assume the flux to be proportional to the V signal (and the size of the spatial resolution element) with a fixed constant

* But see Audic (1991), who presents the possible signature of a twisted small-scale flux tube when observed at very high spatial resolution. However, the diagnostic presented by him, the Q/V ratio as a function of position on the solar surface, may well allow for more than one interpretation, in particular in regions of densely packed flux tubes.

of proportionality. Livingston and Harvey (1969) attempted to determine the flux per magnetic element by searching for evidence of quantization of magnetic flux. Some weak evidence emerged, but has never subsequently been confirmed. Stenflo (1976) presents arguments against the concept of flux quantization and Wiehr (1978) finds no evidence for it in his data sample. Mehltretter (1974) proposed that if Ca II bright points are identified with magnetic elements, the average flux per magnetic element can be determined by counting the number of bright points within a resolution element of a relatively low spatial resolution magnetogram. In this manner he derived a flux per magnetic element of 4.5×10^{17} Mx. Unfortunately, the identification of magnetic elements with bright points does not appear to be unconditionally justified (see Section 5.4.2) and this result, like the others mentioned here, must be treated with caution. For intranetwork elements Harvey (1977a) quotes typical flux values of 5×10^{16} G.

Another topic of research has been the relative amount of flux in the form of concentrated magnetic flux tubes (i.e. magnetic elements) and of diffuse or tangled fields. Tarbell *et al.* (1979) argue for the presence of considerably more flux in weak field form than in strong field form. Stenflo (1984a) pointed out that the *upper limit* on the flux in the turbulent field, set by line profile measurements, is of the order of 100 times the flux in magnetic elements. The recent results of Faurobert (1992) suggest that the true flux ratio of weak (tangled) to strong fields lies between 10 and 50. According to Howard and Stenflo (1972) and Frazier and Stenflo (1972) the amount of *net* flux in weak-field form (as seen in Stokes V) is only 10% of the strong-field flux. This value has recently been confirmed by Rabin (1992a,b), Rüedi *et al.* (1992a) using spectra at 1.5 μm.

In summary, magnetic filling factors and fluxes are hard to measure. Estimates of the flux per magnetic element must be judged inconclusive. The evidence suggests that 90% of the *net* flux visible in Stokes V is in strong field form. Weak tangled fields appear, however, to have 10–50 times the (unsigned) flux of strong fields.

5.4. Temperature

5.4.1. Historical Overview and Correlation of Magnetic Fields with Temperature Indicators

The first spectral evidence for a higher temperature in facular regions is close to seven decades old. St John (1922) observed that Ti II lines are strengthened in faculae relative to Ti I lines. At that time it was not even known that faculae are a mainly magnetic phenomenon. We know now that almost all spectral lines are weakened in faculae. Local line weakenings or 'line gaps' in the unpolarized profiles of Fe I lines were first observed in faculae by McMath *et al.* (1956), who ascribed them to local temperature increases. Sheeley (1967) found that these line weakenings (in the unpolarized profile) are correlated with magnetic fields. Chapman and Sheeley (1968) showed that magnetic splitting is insufficient to explain the weakening in the network and that a temperature enhancement of 100–200 K is required as well. An improved version of their analysis by Grossmann-

Doerth (1970) basically confirmed their result.

The main problem besetting these early investigations was that it was unknown whether the region in which the line is weakened was spatially resolved. If not, then the temperature enhancement found from the observations would depend on their spatial resolution. This is similar to the problems faced by investigators of the field strength at the end of the sixties. An elegant solution was found by Harvey and Livingston (1969). They used the ratios between the Stokes V profiles of, among other lines, Fe I 5250.2 Å and Fe I 5233.0 Å, two lines with very different temperature sensitivities, to determine the true weakening of the Stokes I profile of Fe I 5250.2 Å inside the spatially unresolved magnetic elements (this may be considered to be the first thermal line ratio). They found that a temperature increase of approximately 250 K can explain the deduced true line weakening of Fe I 5250.2 Å. Note that although their technique gives approximately the correct weakening, their estimate of the temperature enhancement suffers from its sensitivity to the, at that time unknown, field strength. They also observed that Fe II 5234.6 Å does not change appreciably in magnetic regions and that the amount of weakening of the unpolarized profiles of Fe I lines is roughly proportional to the spatially averaged field strength $\langle B \rangle$. Similarly, Simon and Zirker (1974) found a good correlation between Fe I 6302.5 Å core weakening and $\langle B \rangle$. Sheeley and Engvold (1970), Frazier (1971) and Frazier and Stenflo (1978) have, amongst others, studied the weakening of Fe I lines as a function of $\langle B \rangle$ in detail. Like most of the correlations discussed in this section, the relation between Fe I core weakening and $\langle B \rangle$ is excellent at a resolution of a few arc s. Unlike many of the others, however, it still appears good even at higher resolution. For example, Koutchmy and Stellmacher (1978) find that the maximum line weakening and Zeeman splitting lie $0.4''$ appart. Considering their claimed spatial resolution of $0.75''$, this corresponds to a good overlap.

There are also a number of investigations that correlate the magnetic flux density with indicators of a higher temperature in different layers of the atmosphere. The correlations between $\langle B \rangle$ and the Ca II H and K core flux (Frazier 1971, Mehltretter 1974, Skumanich *et al.* 1975, Schrijver *et al.* 1989), the 1600 Å continuum intensity (Cook and Ewing 1990, cf. Cook *et al.* 1983, Foing and Bonnet 1984, Foing *et al.* 1986) and the inner wing intensity of the Mg I b lines (Beckers 1976, Dara-Papamargaritis and Koutchmy 1983, cf. Spruit and Zwaan 1981) are well established. Note, however, that all these correlations are on a spatial scale of approximately 2000 km (determined by the pixels of Kitt Peak magnetograms), while magnetic fine structure is known to exist well below this scale. On this, or on even coarser scales the correlation of Ca II intensity and $\langle B \rangle$ is often used as a proxy of the magnetic field, both on the sun (e.g. Immerschitt and Schröter 1989, Kneer and Von Uexküll 1991) and on other cool stars (e.g. O.C. Wilson 1978). The Mg II h and k line core intensities are well correlated to Ca II H and K (correlation coefficient ≈ 0.92, Fredga 1969, 1971) and thus indirectly to $\langle B \rangle$.

It is also generally accepted that magnetic fields are closely associated with

the filigree seen in the wings of Hα (Dunn and Zirker 1973, Simon and Zirker 1974) and with brightenings in the CN band-head near 3883 Å (Sheeley 1969, 1971a, b). Fang *et al.* (1984) and November and Ayres (private communication 1990) have found a correlation between Ca II K_{2v}, K_3 and CN intensity. There is also a correlation (indirectly via Ca II K) of $\langle B \rangle$ to submillimeter (850 μm) brightness emanating from the lower and middle chromosphere (Lindsey *et al.* 1990, Lindsey and Jefferies 1991). Wilson (1981b) and Kitai and Muller (1984) have confirmed that the bright features in various brightness or 'activity' indicators in the upper photosphere and the lower chromosphere (Ca II K, Mg I b_1, Hα red wing and continuum) are cospatial. Note, however, that such correlations between two brightness indicators give no guarantee that the correlation with the magnetic field is equally good, since there is probably also a non-magnetic component to chromospheric heating (e.g. Schrijver 1987). For example, it has been argued that short lived, periodic brightenings seen only in K_{2v} (but not in K_{2r}) are non-magnetic in origin (see the review by Rutten and Uitenbroek 1991 and the very detailed NLTE radiation-hydrodynamic simulations of Carlsson and Stein 1992). In addition, even the best indirect indicators of chromospheric heating, e.g. Ca II K_2 flux, show a considerable scatter in their correlation with the magnetic field at a scale smaller than a few arc s (e.g. Frazier 1971, Schrijver *et al.* 1989).

Emission from the outer solar atmosphere also appears to be related to the photospheric magnetic field, although not so directly. Schrijver (1990) shows that the spatially averaged intensity of the C IV doublet (1548 Å and 1551 Å) is correlated with the spatially averaged magnetic flux, if the spatial averaging is on an active region scale. A point-by-point correlation is fruitless, since C IV is formed in loops between regions of opposite polarity. A relation between photospheric magnetic fields and coronal radio emission has been derived by Xanthakis (1969). Finally, even the first X-ray observations of the solar corona (Vaiana, Krieger and Timothy 1973) revealed the close connection between magnetic fields and coronal heating. Later, Golub *et al.* (1980, 1982) correlated physical parameters derived from X-rays (e.g. coronal pressure and thermal energy content) with photospheric spatially averaged field strength. Again, as for C IV, a direct correlation between X-ray emission and $\langle B \rangle$ is not possible due to changes in the structure of the magnetic field with height. Coronal structures visible in X-rays (Skylab data) have been compared with magnetograms by Sheeley *et al.* (1975). The x-ray emission appears to outline coronal loops connecting regions of opposite polarity in the photosphere.

Correlations between $\langle B \rangle$ and various chromospheric and coronal activity indicators have been reviewed by Beckers (1981) and Schrijver (1989, 1991). All the correlations suggest that the upper photosphere, the chromosphere and the transition zone above magnetic elements are heated considerably more efficiently than the average non-magnetic atmosphere.

5.4.2. Continuum Brightness at Disc Centre

An important class of correlations is that between the magnetic field and the continuum brightness. Again, at a resolution of a couple of arc s such a correlation is well established (Frazier 1970, 1971, Foukal and Fowler 1984, Hirayama *et al.* 1985), although complex. Regions with small magnetic filling factors are associated with a small continuum brightening, while larger filling factors correlate with darkenings of the continuum, right down to sunspots (e.g. Frazier 1971). At such a resolution the continuum brightenings are small, less than 1% of the quiet sun brightness, i.e. faculae are not readily visible at disc centre. The exact value of the measured continuum contrast $\langle \delta_c \rangle = I_c^{\text{faculae}} / I_c^{\text{quiet}}$ at these low resolutions is not particularly interesting for the diagnosis of the internal structure of magnetic elements, since it is difficult to untangle the contributions from the magnetic and the non-magnetic components, but is of considerable interest for the understanding of global solar luminosity variations (Willson and Hudson 1988, cf. Foukal and Lean 1988).

As the spatial resolution increases, so does in general the measured value of the facular "continuum" intensity. Thus, Muller and Keil (1983) found $\langle \delta_c \rangle$ values (after some corrections for seeing and telescope MTF) of $1.3 - 1.5$ in a 60 Å bandpass centred on 5750 Å (facular points), Mehltretter (1974) obtained $\langle \delta_c \rangle$ values of $1.4 - 1.8$ in a 60 Å bandpass at 3934 Å (the bandpass contained Ca II K), and Koutchmy (1977) even ended up with $\langle \delta_c \rangle \approx 2$ at H$\alpha + 2$ Å after some image processing. There are, however, no concurrent high resolution magnetograms to these observations, although Muller and Keil did use Ca II images to identify the bright points. The same authors also point out that a few, unrepresentative points in their total sample of 77 points reach the $\langle \delta_c \rangle$ value inferred by Koutchmy (1977). Von der Lühe (1987, 1989), using speckle interferometry also obtains high "white light" contrasts of $\langle \delta_c \rangle \approx 1.5$ for regions associated with Ca II brightenings. De Boer and Kneer (1992) find active regions to be full of tiny bright points, which become clearly visible only at very high spatial resolution (their claimed resolution, again achieved with the help of speckle interferometry, is $0.2''$). Finally, Keller (1992a) uses the speckle technique developed by Keller and Von der Lühe (1992) to determine the brightness of *magnetic* features (i.e. he reconstructs both a "white light" image and a simultaneously observed magnetogram). He finds that δ_c ($\delta_c = I_{cm}/I_{cq}$, where $I_{cm} = I_c$ of the magnetic feature and $I_{cq} = I_c$ of the quiet sun) is a strong function of the size of the magnetic feature: Features smaller than 300 km in diameter are bright, larger features are dark. The brightest magnetic feature seen in his images has $\delta_c \approx 1.3$.

Del Toro Iniesta *et al.* (1990), on the other hand, find no correlation between continuum brightness and magnetic flux in observations with a claimed resolution better than $1''$. They conclude that magnetic features can be bright only if they are smaller than $0.2''$. Although their lack of correlation contradicts the results of Mehltretter (1974), Skumanich *et al.* (1975) and Frazier and Stenflo (1978), amongst others, it is not surprising given the low sensitivity of their magnetic flux

diagnostic, based on the Stokes I comparison method of Schüssler and Solanki (1988, cf. Section 4.5). Therefore, they probably do not identify the regions with small spatially averaged field strength, which are also the brightest (Frazier 1971, Title *et al.* 1990a, see below).

Title *et al.* (1992) and Topka *et al.* (1992) also do not see any brightening associated with the magnetic field; image positions associated with a significant magnetogram signal are, on average, darker than the quiet sun. For larger values of the magnetogram signal, $\langle B \rangle \gtrsim 500$ G, the low continuum intensity is not surprising, since at their resolution of 0.5–1″ this corresponds to magnetic knots or micro-pores. However, the absence of brightenings at lower magnetogram signals is remarkable. Although this may partially be due to the fact that they observe the true continuum (see next paragraph), it may at least partly also be a consequence of the technique used by Title *et al.* (1992) and Topka *et al.* (1992). Their automated procedure bins together the continuum brightness of all pixels with similar magnetogram signal. The average intensity of each such bin is then plotted against the magnetogram signal. Unfortunately, the interpretation of the results of this procedure is less than straightforward for the bins with low magnetogram signal ($\lesssim 300$ G). It is incorrect to interpret the average continuum intensity in these bins to be due only (and possibly even mainly) to small, spatially unresolved flux tubes located in that pixel. There are two possible sources of error. Firstly, the seeing-smeared signal from larger and darker magnetic features also contributes. Seeing smears both the magnetogram and the intensity signal from large magnetic features into neighbouring pixels, which, in the absence of seeing, would be devoid of field. Due to the smearing the brightness of these pixels is diminished and their $\langle B \rangle$ becomes non-zero. The presence of such a $\langle B \rangle$ (in general $\lesssim 500$ G) causes the dark pixels to be binned together with the pixels containing small magnetic features. This lowers the average continuum intensity of the bins with small $\langle B \rangle$ by an amount that is hard to judge.

Secondly, seeing degrades the magnetic and brightness signals of magnetic elements in such a way that an artificial correlation between low brightness and small magnetogram signals is produced. The important point to note is that seeing leaves the width of the brightness peak of a small, bright magnetic element surrounded by dark intergranular lanes relatively unchanged, although the maximum brightness is lowered. This point can be easily confirmed by convolving a peak sandwiched between two troughs (representing flux tubes and intergranular lanes) with a broad Gaussian (representing the seeing). The troughs are significantly broadened, but the central peak is not. The magnetic field of an individual magnetic element, on the other hand, is spread considerably by spatial smearing (the situation here is analogous to convolving an isolated peak with a Gaussian). Consequently, after spatial smearing each small-scale magnetic feature is surrounded by dark (intergranular) pixels which now also show a magnetic signal. Therefore, bins with small magnetogram signal get falsely associated with a low continuum brightness.

The above, to my mind, casts some doubt on the continuum intensity for small

magnetogram signals found by Title *et al.* (1992) and Topka *et al.* (1992). The contribution of the large magnetic features to the intensity in bins with $\langle B \rangle \lesssim 300$ G is enhanced by the fact that the pixel size ($0.166''$) is significantly smaller than the seeing disc ($0.5''$, or larger). When the pixel size is larger than the seeing disc, this problem should diminish. It should be possible to test the importance of the above effect by increasing the pixel size, i.e. by averaging the signal in 9 neighbouring pixels and redoing the analysis.

Title *et al.* (1992) are well aware of these problems and point out that their results do not contradict continuum-bright flux tubes if these are surrounded by a dark moat. They have modelled the second source of error in considerable detail and Title (private communication 1992) suggests that with the help of their modelling the influence of the spatial smearing may be judged with considerable accuracy and removed.

The earlier high resolution observations were criticized by Foukal *et al.* (1981), who pointed out that none of those published until then referred to the true continuum, but rather reflected the weakening of the lines present in the often quite broad (and heavily line-blanketed) filter windows. From differential measurements of the intensity at two wavelengths (both true continua) they concluded that magnetic features are actually darker than the quiet sun in the true continuum. However, Foukal and Duvall (1985) could explain these and additional observations (in a third wavelength band) by introducing a lower temperature *gradient* in active regions, while the original explanation of Foukal *et al.* (1981) could not reproduce the observations in all three bands. The presence of a lower, spatially averaged temperature gradient in active regions also follows from the CLV of $\langle \delta_c \rangle$ (see Sect 5.4.3) and from the comparison of the Stokes I profile of C I 5380.3 Å to others formed higher in the atmosphere (Elste 1985). Finally, Keller and Koutchmy (1991) have carried out similar $\langle \delta_c \rangle$ observations at higher resolution and have discussed the possibility of explaining the Foukal and Duvall (1985) observations with 2-component models. The latter observations have a relatively low spatial resolution of a few arc s and are interpreted by Foukal and Duvall in terms of single component atmospheres.

The importance of observing at the highest possible spatial resolution when determining the continuum intensity is demonstrated by the calculations of Knölker (private communication, 1992). He took the I_c of theoretical models of narrow flux slabs and applied a spatial smearing approximating an atmospheric and telescopic MTF (modulation transfer function). He finds that the true δ_c at solar disc centre of a flux tube with a diameter of 100 km can be a factor of 7–8 larger than the measured value, even at a spatial resolution of approximately $0.3''$(see Solanki 1992c for more details).

Solanki and Brigljević (1992) have applied a technique, based on comparing Stokes V profiles of C I lines with those of Fe II lines, to FTS Stokes V spectra of an active and a network region. They obtain a δ_c of 1.1–1.4 in the network (i.e. a region with a low α) and 0.7–0.9 in the active region (i.e. a high α region).

This result is in qualitative agreement with that of Frazier (1971, 1978) and Foukal and Fowler (1984): The brightness reaches a maximum at a relatively small filling factor and decreases steadily for larger α. It also agrees well with the results of Keller (1992a) if we make the reasonable assumption that magnetic features are, on average, larger in regions of larger α. However, the results of Keller (1992a) and Solanki and Brigljević (1992) appear to contradict the high $\langle \delta_c \rangle$ values found from high spatial resolution investigations of bright points. One reason may be the admixture of line weakening in the high spatial resolution results (Foukal *et al.* 1981). Another may have to do with selection effects: Only the brightest features are recognized in 'white light' images. Finally, note that a particular feature may change its brightness with time. Mehltretter (1974) and Muller (1983) find that facular points appear and disappear, i.e. change their brightness by factors of 1.3–1.8, on a time-scale of a few minutes (cf. De Boer and Kneer 1992). Since the magnetic flux is unlikely to disappear (and reappear again) on such short time scales, this supports the suspicion that selection effects are present.

The C I lines also contradict the results of Schüssler and Solanki (1988), who found from a comparison of Stokes I profiles of Fe I 5250.2 Å and Fe I 5247.1 Å that $\delta_c \gtrsim 1.4$. Their technique, however, is very sensitive to the presence of blends, even quite weak ones, in the two lines they use. There is evidence of a weak blend of water vapour in 5250.2 Å (Livingston and Wallace 1985, Carter *et al.* 1992).

The continuum intensity in the infrared H-band, near the continuum opacity minimum at 1.65 μm is lower in active regions than in the quiet sun when averaged spatially over at least 3″ (Worden 1975, Foukal *et al.* 1989, 1990, Moran *et al.* 1992), i.e., plage regions emit less energy than the quiet sun in the lowest observable layers, and only in these layers. Thus, basically, magnetic fields appear to take energy from the deeper layers, transport it to higher layers and deposit it there. The excess energy is then seen as an increase in the radiation coming from the higher layers. In agreement with this picture the contrast becomes positive again further in the infrared. Lindsey and Heasley (1981) find faculae to be approximately 1% brighter at 10–25 μm, while Degiacomi *et al.* (1985) find a brightness enhancement in plages corresponding to 250 K at 200 μm. These observations support the idea that in a spatially averaged sense, the temperature gradient is smaller in active regions than in the quiet sun. At higher spatial resolution (0.5–1″) there appears to be a slight positive correlation between 1.6 μm continuum brightness and chromospheric activity (Darvann and Koutchmy 1992), so that the magnetic features themselves appear to be bright at all wavelengths. The importance for the 1.5 μm data of the magnetic filling factor, which unfortunately is unknown for the high-resolution data of Darvann and Koutchmy, has been demonstrated by Moran *et al.* (1992). They find that at small magnetic filling factors no continuum contrast is seen at 1.6 μm and only at large filling factor do dark features appear. At 1.2 μm these dark features are not visible, i.e. show no obvious contrast to the surroundings at the low spatial resolution of the Moran *et al.* (1992) measurements. A combination of these observations suggests that for small filling factors it is

mainly the surroundings of the magnetic features that become dark in the deepest layers, while at larger filling factors the magnetic features themselves probably become dark (magnetic knots, etc.).

In summary, the measured continuum contrast of small-scale magnetic features depends critically on the spatial resolution of the observations. The most recent high resolution observations and indirect techniques give results that are in good agreement. Small magnetic features (or magnetic features in regions with low filling factor) are bright, larger (more closely packed) magnetic features are darker, even when well below the size of normal pores.

5.4.3. Centre-to-Limb Variation of the Continuum Contrast

Early observations, with what was then termed high spatial resolution, of the CLV of $\langle\delta_c\rangle$ were carried out by Ten Bruggencate (1940) and Waldmeier (1949). These observations already showed the main characteristic of the CLV of $\langle\delta_c\rangle$ at medium and low resolution, its steady increase towards the limb up to μ values of 0.3–0.4. Beyond that $\langle\delta_c\rangle$ was observed to decrease again. Other early observations of $\langle\delta_c\rangle$ (μ) were carried out by Rogerson (1961), Kuzminykh (1963), Schmahl (1967), Livshits (1968), Badalyan (1968), Chapman (1970) and Frazier (1971). Maximum contrast values of such observations vary between 1.17 (Livshits 1968) and 1.4 (Rogerson 1961). The latter corresponds to a value of 1.64 after correction for the estimated spatial smearing.

More recently, Muller (1975) has carried out very high resolution observations (0.3″) and finds a maximum corrected $\langle\delta_c\rangle$ value of 1.41 (near $\mu = 0.2$), while Minasyants and Minasyants (1977) find a maximum $\langle\delta_c\rangle$ of 1.73 from lower resolution data, a value also seen by Akimov *et al.* (1982). Hirayama (1978) measures values similar to Muller (1975), but with 1″ resolution. The rather heterogeneous nature of the results of the various investigations and their lack of correlation with the spatial resolution and the wavelength of the observations suggests the presence of faculae with different CLVs of $\langle\delta_c\rangle$ to Akimov *et al.* (1987), who also give a review of the previous measurements. Auffret and Muller (1991) also divide the individual facular points (smaller structures, seen mainly near disc centre) and facular granules (larger structures, seen mainly near the limb) into different categories showing different CLVs. Topka *et al.* (1992) determine the contrast of the true continuum near the centre of the solar disc ($1 \gtrsim \mu \gtrsim 0.7$). They find small contrast values increasing towards the limb. For a magnetogram signal of, e.g., 300 G, they find $\langle\delta_c\rangle \approx 0.98$ at $\mu = 1$ and 1.02 at $\mu = 0.7$. Their $\langle\delta_c\rangle$ are probably systematically depressed for the reasons discussed in Section 5.4.2, but this should not affect the dependence on μ.

These and other measurements (e.g. Badalyan and Prudhovskii 1973, Ingersoll and Chapman 1975, Hirayama 1978, Hirayama and Moriyama 1979) all suggest a steady increase of $\langle\delta_c\rangle$ out to $\mu = 0.2$. Closer to the limb the facular contrast, which becomes rather difficult to measure due to the proximity of the limb and foreshortening effects, is more controversial. The earlier photographic measurements

gave widely different behaviours near the limb, with some suggesting $\langle\delta_c\rangle$ maxima at $\mu = 0.2$ and others finding that $\langle\delta_c\rangle$ increases right out to the limb. More recently, Chapman and Klabunde (1982) have used a photoelectric detector to measure a contrast increasing out to $\mu = 0.065$. Later, Libbrecht and Kuhn (1984, 1985), cf. Kuhn *et al.* (1988), detected a decrease in $\langle\delta_c\rangle$ between $0.2 \gtrsim \mu \gtrsim 0.08$. Lawrence and Chapman (1988), however, confirmed the findings of Chapman and Klabunde. Akimov *et al.* (1982, 1987) studied the brightness evolution of individual faculae near the limb. Although they find large variations from facula to facula, the $\langle\delta_c\rangle$ averaged over all their measured faculae increases up to $\mu = 0.1$. Finally, Wang and Zirin (1987) find a variation which lies between the two extremes. At shorter wavelengths it continues to increase gently out to $\mu \approx 0.09$, while at longer wavelength ($\gtrsim$ 5000 Å) it begins to dip downwards again at $\mu < 0.1$–0.15. At present this point must be considered undecided.

A combination of all the observations suggests that the continuum contrast increases towards the limb until $\mu \approx 0.2$. For smaller μ values the run of $\langle\delta_c\rangle$ (μ) is controversial. Absolute values of $\langle\delta_c\rangle$ (μ) depend strongly on spatial resolution and probably on the type of solar feature.

5.4.4. One-Component Models

One of the main aims of the empirical study of solar magnetic features is to determine their temperature stratification. A comparison with theoretical models then allows heating and cooling mechanisms in magnetic features to be identified. These, in turn, will hopefully lead to a better understanding of the energy balance of the solar atmosphere. A number of such empirical models have been constructed. They include 1-component, 2-component and 2-D models. In the present section I review the 1-component models. If in the following the height-range of validity of a model is not mentioned, then it is restricted to photospheric layers.

Examples of 1-component models are those of Reichel (1953), Livshits (1964), Kuzminykh (1965), Schmahl (1967), all based on the centre-to-limb variation of the continuum contrast, Stellmacher and Wiehr (1971), based on Stokes I line weakenings, Stellmacher and Wiehr (1973), based on previous models derived from Stokes I line weakenings or from continuum contrast at different μ values, Shine and Linsky (1974a), derived from the damping wings of Ca II K and Ca II 8542 Å, Shine and Linsky (1974b), from the cores of Ca II H and K and the Ca II IR triplet (this is a purely chromospheric model and satisfies many other constraints as well, see e.g Lindsey and Jefferies 1991), Caccin *et al.* (1974), an adaptation of Schmahl's (1967) model to newer results on the quiet sun atmospheric structure, Morrison and Linsky (1978), from the wings of Mg II h (2802.7 Å) and k (2795.5 Å), Hersé (1979), a simple 'step' model based on continuum contrast observations near 2000 Å, Basri *et al.* (1979), based on 0.8″ spatial resolution HRTS Ly α measurements (this is an upper chromosphere and lower transition-region model), Lemaire *et al.* (1981), based on OSO8 profiles of Ca II H and K, Mg II h and k, and Ly α and β (this is mainly a chromospheric model), Vernazza *et al.* (1981, VAL),

their model F of a bright network region is largely based on the spectrum between 400 and 1400 Å (it is mainly a chromosphere and transition-region model), Avrett (1985), his model F′ is a slight modification of model F of Vernazza *et al.* (1981), differing mainly around the temperature minimum region, Ayres *et al.* (1986), their VALP model is an average plage model based on Ca II K (it includes the lower and middle chromosphere), Kučera *et al.* (1991), Kučera (1992), based on profiles of Hα, Hβ, Hγ, He D_3, Ca II H, K and IR triplet lines (their 3 relatively similar models are mainly valid for the chromosphere) and Fontenla *et al.* (1993), improved VAL models (mainly in the upper chromosphere and transition zone) with a new model P corresponding to average plage.

The general temperature stratification of all 1-component models in the photosphere reflects the simple visual impression given by white-light images of the sun. At low spatial resolution faculae are not visible near disc centre, but show up clearly as bright features near the limb, suggesting that in their deeper layers they have a temperature similar to that of the quiet sun, but are warmer in the middle and upper photosphere (always at equal optical depth, cf. Section 5.4.3). Therefore, single component models derived from relatively low spatial resolution observations (worse than a few arc s) are well defined, although they may not describe any portion of the real solar atmosphere in active regions.

5.4.5. Two-Component Models Based on Stokes I

The first simple 2-component model was proposed by Rogerson (1961), based on the continuum contrast between $\mu = 0.1$ and 0.2. Further examples of Stokes I based 2-component models are those of Chapman (1970), derived from the CLV of continuum contrast (at low spatial resolution), Wilson (1971), based on a reinterpretation of Chapman's data, Muller (1975), from the CLV of continuum contrast measured at high spatial resolution, Chapman (1977), from the profiles of ten photospheric lines observed at disc centre with relatively low spatial resolution, Hirayama (1978), from the CLV of the continuum contrast at $\mu \lesssim 0.5$ (spatial resolution of 1″), Koutchmy and Stellmacher (1978), from three Fe I lines plus the continuum contrast value at disc centre given by Koutchmy (1977, high spatial resolution data), Stellmacher and Wiehr (1979), based on high resolution observations of eleven lines and $\langle \delta_c \rangle$ as a function of wavelength (it is basically a modified version of the Koutchmy-Stellmacher model), Chapman (1979), which is the Chapman (1977) model extended to include the effects of a magnetic field on the pressure balance (Wilson depression), Chapman (1981), an extension of Chapman's (1979) model into the chromosphere, Ayres *et al.* (1986), their FLUXT model is based on profiles of the Ca II K line and of CO rotation-vibration bands in active and quiet regions (low spatial resolution data, mainly a chromospheric model), and, finally, Walton (1987), based on the low spatial resolution infrared continuum contrast at $\mu \approx 1$ (a diagnostic that was also taken into account by Chapman 1977, 1979), eight photospheric lines measured at two disc positions and the Mg I b line wings (low spatial resolution data). Note that the models of

Koutchmy and Stellmacher (1978) and of Stellmacher and Wiehr (1979) are actually 3-component models, since the granules and the intergranular lanes are treated separately. Also, Koutchmy and Stellmacher claim to take the expansion of the field with height into account. Their procedure for doing so, however, is not apparent from their paper, since they do not calculate profiles along multiple rays, in contrast to Walton (1987), whose models must be considered 2-D models. Walton also takes the presence of neighbouring flux tubes into account when calculating line profiles close to the limb.

All the 2-component (and 2-D) models described above show appreciably higher temperatures in the middle and upper photospheric layers of their magnetic component than the 1-component models. This is not too surprising, since in the 2-component models the observed line weakening and the continuum enhancement near the limb are assumed to be produced entirely within the small fraction of the surface covered by the magnetic features. Around the height at which most of the lines used to derive the models are formed ($-2.5 \lesssim \log\tau \lesssim -1.5$), the Stokes I based 2-component models give reasonably similar $T(\tau)$, given the uncertainty in the filling factor, a free parameter in all such models. A selection of Stokes I based 2-component models is plotted in Figure 5.4. The difference between the dashed (Chapman) and the dot-dashed (Walton) curves in Figure 5.4 illustrates the effect of changing the assumed filling factor, since Walton (1987) was also able to obtain a good fit to his data with a model very similar to Chapman's simply by increasing the assumed value of α from 0.1 to 0.2.

In the lower photosphere, however, the 2-component models differ substantially from each other. In these layers they basically reflect the disc centre $\langle\delta_c\rangle$ values selected by the modellers. Models based on low $\langle\delta_c\rangle$ (e.g. Chapman 1970, 1977, 1979, Ayres *et al.* 1986, Walton 1987) have a temperature close to the quiet sun value at $\tau = 1$, while models based on high $\langle\delta_c\rangle$ (e.g. Koutchmy and Stellmacher 1978, Stellmacher and Wiehr 1979) have a very high temperature in their lower layers.

Note that some of the differences between the various models are due to different assumptions about the local non-magnetic atmosphere (cf. Section 4.6.2). Furthermore, Frazier (1977) points out that observations of $\langle\delta_c\rangle$ tend to select regions bright in the continuum, while observations of Stokes V line weakening tend to select regions bright in the lines. He warns that since the two types of regions are not the same (cf. Frazier 1971), models based on the two types of data are also expected to differ from each other.

In summary, Stokes I based 2-component models differ considerably from each other, depending on the assumed filling factor and continuum contrast. However, all models predict a considerable enhancement of temperature over the quiet sun value at equal τ in the middle and upper photosphere.

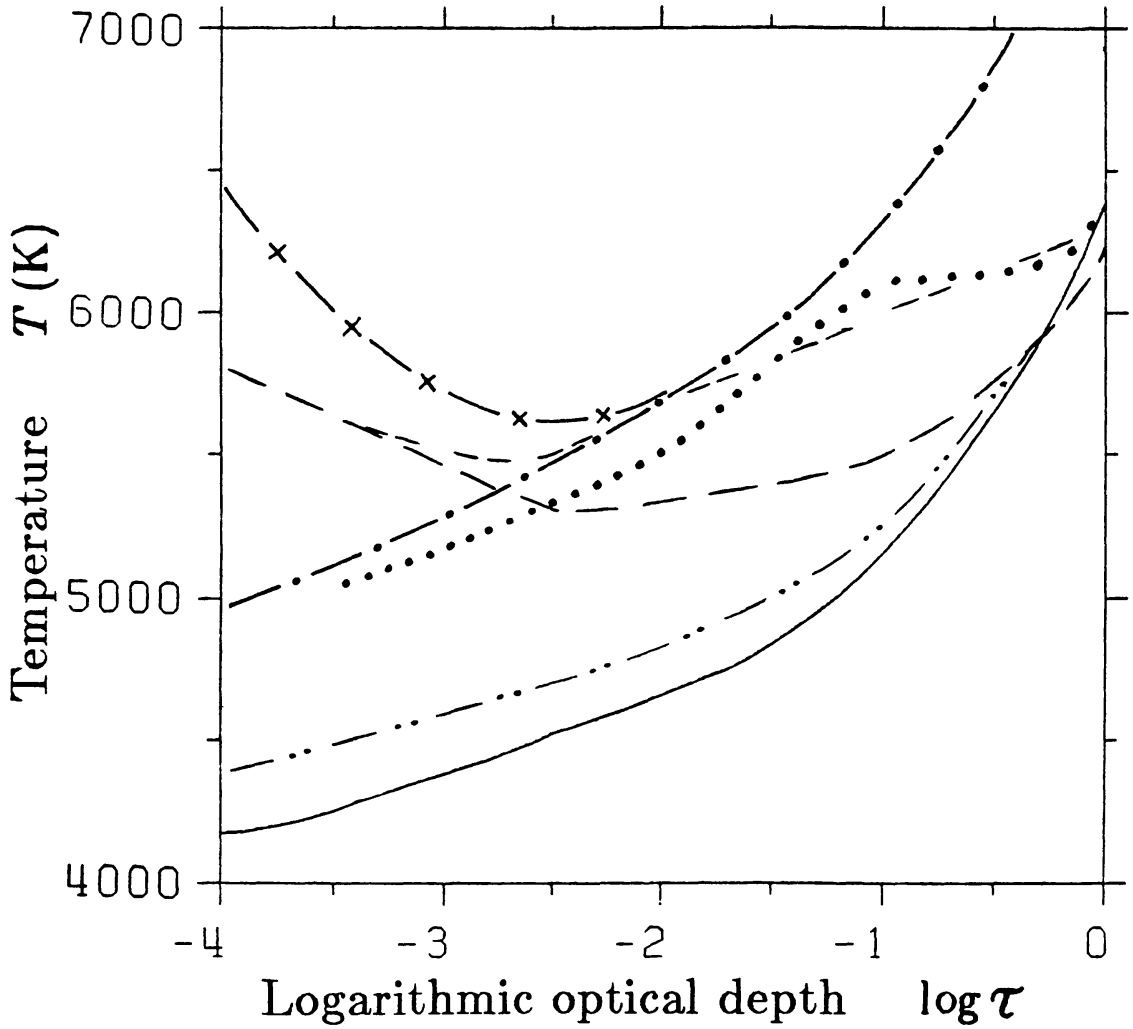

Fig. 5.4. Stratification of the temperature, T, of empirical facular models based on Stokes I vs. logarithmic continuum optical depth. Quiet sun (HSRA, Gingerich *et al.* 1971): solid line. 1-component model of Shine and Linsky (1974): —— · · ——, 2-component models of Chapman (1977): —— ——, Walton (1987): — — — —, Hirayama (1978): · · · · ·, Koutchmy and Stellmacher (1978): —— × ——, Stellmacher and Wiehr (1979): —— · —— (from Solanki 1990).

5.4.6. Models Based on Stokes V

The first model based on Stokes V observations is due to Stenflo (1975). He used magnetograms in Fe I 5233 Å, Fe I 5247.1 Å and Fe I 5250.2 Å to simultaneously determine the temperature and the magnetic field strength, i.e. he combined the 'magnetic' line ratio introduced by Stenflo (1973) with the 'thermal' line ratio of Harvey and Livingston (1969). In accordance with the low resolution observations available at that time he used a δ_c close to unity. At the level of line formation the model of Stenflo (1975) is rather similar to the more recent models of Solanki (1986) and Keller *et al.* (1990a). The $T(\tau)$ stratifications of these models are plotted in Figure 5.5. The models of Solanki (1986) satisfy selected line parameters of approximately two hundred Stokes V profiles of Fe I and II lines. The models of Keller *et al.* (1990a) are based on the inversion (non-linear least-squares fit) of

the Stokes V parameters of ten lines (see Section 4.9). They calculated both 1-D and 2-D models, which result in almost identical temperature stratifications. Since the models of Solanki (1986) and Keller *et al.* (1990a) are sufficiently similar, the following remarks are valid for both of them. These models also satisfy the CLV of the σ-π asymmetry of the Stokes Q profiles of Fe I 5250.2 Å and Fe I 5247.1 Å (Solanki *et al.* 1987) and the CLV of the Stokes V profiles of numerous Fe I and II lines (Pantellini *et al.* 1988). In spite of the effort put into them, these models are only reliable in the range $-3 \lesssim \log\tau \lesssim -1$. In particular, in their deeper layers they are based only on continuum contrast measurements (cf. Solanki and Steenbock 1988), mainly those of Muller and Keil (1983). Therefore, in these layers they suffer from the same problems as the Stokes I based models. Only with the use of high excitation C I lines has it now become possible to construct empirical models of magnetic elements that are completely independent of measured δ_c or $\langle\delta_c\rangle$ values. The results obtained from these lines suggest that the temperature in the lower part of the models of Solanki (1986) and Keller *et al.* (1990a) is probably too high, at least for the plage models.

The Stokes V based modelling has firmly established that the temperature within the unresolved magnetic feature is a function of filling factor. This was first noticed by Solanki and Stenflo (1984) from spectra of five solar regions and confirmed for the same data set, but using more detailed analyses, by Solanki and Stenflo (1985), Solanki (1986) and Keller *et al.* (1990a). Zayer *et al.* (1990) inverted twenty-three Stokes V spectra of Fe I 5247.1 Å, 5250.2 Å and 5250.6 Å. The first and third lines may be used to form a thermal line ratio. In agreement with the earlier investigations they found that the temperature at the height of line formation decreases steadily with increasing filling factor. As mentioned in Section 5.4.2, the α dependence of the temperature reaches right down to the continuum forming layers. The possibility of a continuous range of temperature models as a function of α was first suggested by Frazier (1970), but his data could not distinguish between changes in the magnetic and in the non-magnetic components of an active region. Hirayama (1978) has also proposed different temperature stratifications for 'facular granules' in regions with different levels of activity. Finally, Gopasyuk and Severny (1983) had noticed a difference similar to that seen by Solanki and Stenflo (1984) between temperature diagnostics in 'quiet' (low filling factor) and 'active' (high filling factor) regions. However, instead of attributing the difference to a temperature variation, they suggested that it may have to do with differences in abundances. Unlike the more recently used diagnostics, theirs, based on the comparison between lines of different elements, could not distinguish between the two possibilities.

The similarity between the models of Keller *et al.* (1990a) and Solanki (1986) in the range of heights in which they are both based on Stokes V observations suggests that the Stokes V based models do indeed overcome some of the main disadvantages of Stokes I based models. The remaining limitations common to both sets of models are the assumption of LTE and that they are based on relatively

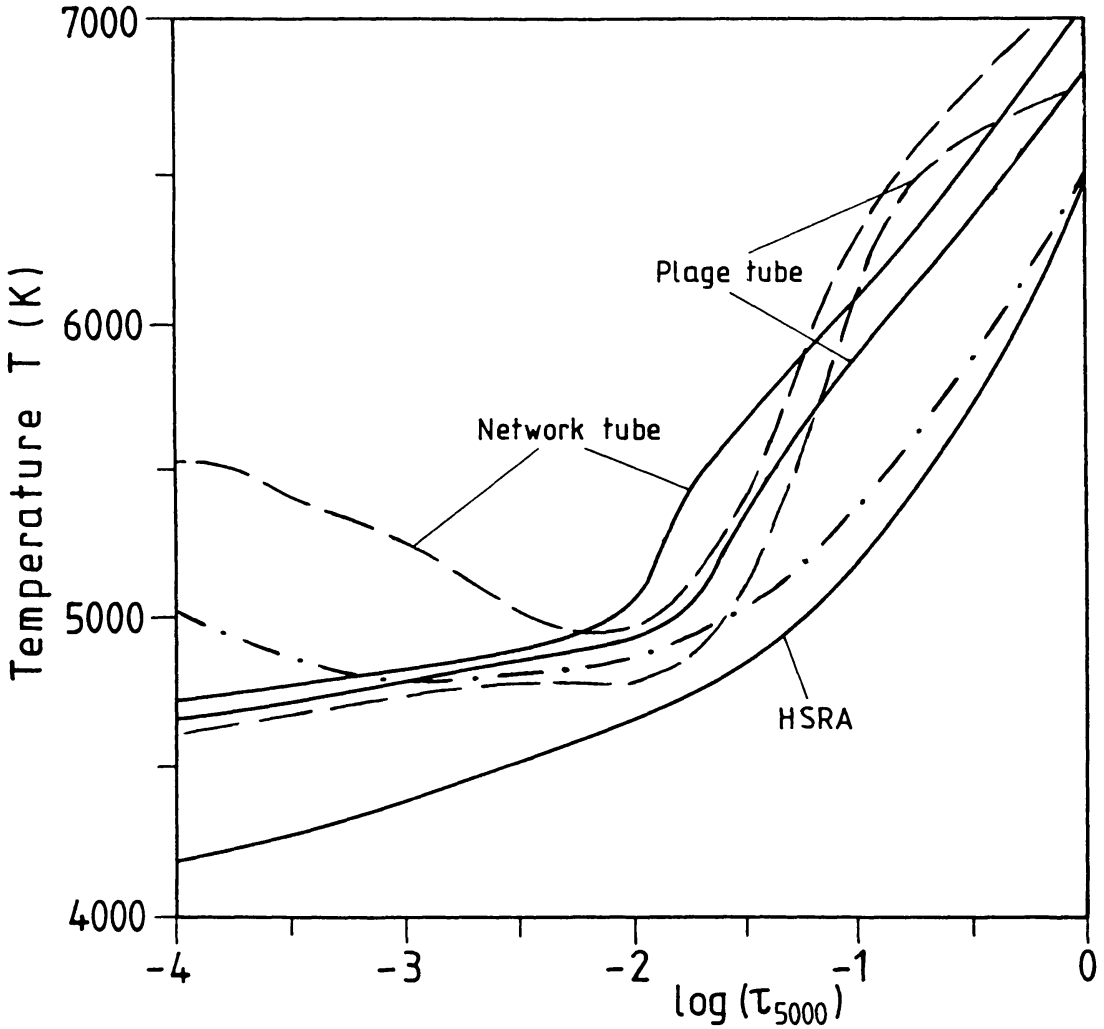

Fig. 5.5. Temperature stratification of empirical models of small-scale magnetic features based on Stokes V and of a quiet-sun reference atmosphere (marked HSRA). Model of Stenflo (1975): dot-dashed curve, models of Solanki (1986): solid curves, models of Keller *et al.* (1990a): dashed curves. Where separate models for the network and for plages exist these have been marked (from Solanki 1990).

low spatial resolution data with contributions from many, not necessarily identical magnetic features. Individually, each of the models has some additional shortcomings. The models of Solanki (1986) are based on a 'chi-by-eye' fit to the data, and the exact run of the temperature is consequently somewhat subjective. The Keller *et al.* (1990a) models, on the other hand, are based on only 10 lines, so that blends may affect the results to a larger extent. Another possible source of uncertainty is the interpolation using cubic splines between the five grid points of the atmosphere used for the least-squares fitting. Cubic splines are known to undulate excessively in some cases and may be responsible for the 'rounder' appearance of the Keller *et al.* (1990a) models compared to the Solanki (1986) models. This suspicion is strengthened by the knowledge that a reduction of the number of grid points to three leads to much larger 'oscillations' in the temperature profile (Keller

1988). Obviously, a new set of models is required that is based on a least-squares fit, interpolates between the grid points using either splines under tension, Akima's or Steffen's (1991) interpolation techniques, assumes 2-D geometry, combines the Stokes V profiles of the C I lines and a substantial number (20–40) of Fe lines.

One of the interesting features of the Stokes V based models is the dip in $T(\tau)$ around $\log\tau = -2$. The causes of this dip are still unclear. Holweger (private communication 1986) has proposed that the dip is an artifact of the neglected horizontal temperature variation within each magnetic element, or from one magnetic element to the next. In the presence of such variations the Fe I lines are preferably formed in the cooler parts of the atmosphere, while the Fe II lines are relatively unaffected. In models not allowing any horizontal variation of T within the magnetic features (or from one magnetic feature to another), the horizontally coexisting hot and cold temperatures must be redistributed vertically. The vertical redistribution of the horizontal temperature variation is aided by the fact that Fe I lines are, on average, formed higher in the atmosphere than the Fe II lines (e.g. Larsson *et al.* 1991). Another possible source of the $T(\tau)$ dip, namely departures from LTE, can probably be ruled out (Bruls and Solanki 1992b).

Nevertheless, the importance of NLTE effects in a 2-D flux tube model with hot walls has been demonstrated by Stenholm and Stenflo (1977, 1978) using a 2-level atom. They showed that lines whose formation is dominated by scattering processes (collisional thermalization parameter $\epsilon \ll 1$) can be considerably weakened, even if the flux tube interiour at a given optical depth τ is no hotter than the quiet sun surrounding it at equal τ. This is particularly true for lines whose formation height in the flux tubes lies below the $\tau = 1$ level of the quiet sun. In a complementary investigation Solanki and Steenbock (1988) used only a 1-D flux tube model, but a comprehensive iron model atom to study the influence of the temperature stratification on the magnitude of the departures from LTE. They found that for empirically determined temperature stratifications the departures from LTE due to overionisation of Fe° to Fe^{+} are larger within flux tubes than in the quiet sun. The lines calculated in NLTE are weaker than those calculated in LTE, so that NLTE effects tend to mimic higher temperatures. The magnitude of the departures from LTE of Fe lines depends on the brightness, i.e. the temperature of the walls and the bottom of the magnetic feature relative to the temperature at the level of line formation. The larger this difference, the stronger the NLTE effects.

In summary, models using Stokes V overcome some, but not all, of the shortcomings of Stokes I based models. Different Stokes V modelling approaches give relatively similar models. The temperature inside flux tubes is seen to decrease with increasing filling factor. NLTE effects are important.

5.4.7. Recent Empirical Models of the Chromospheric Layers of Magnetic Features
One important consequence of neglecting NLTE effects is that the present empirical models based on Stokes V cannot reproduce the onset of the chromospheric temperature rise. A first step towards remedying this deficiency is to calculate NLTE

Stokes profiles in models of flux tubes including a chromospheric temperature rise. Such calculations have been carried out for Fe I and II lines in simple 2-D models (thin tube approximation and 1.5-D radiative transfer). Line ratios and the V profile shapes of the strongest iron lines (in particular of Fe II 4923 Å) suggest that the chromosphere starts 200–300 km deeper within solar magnetic flux tubes than in the average quiet sun (Bruls and Solanki 1992a,b). A much deeper onset of the chromospheric temperature rise can be ruled out by the profile shapes.

So far, no model of the temperature structure of the middle or upper chromosphere is based on Stokes V observations, partly due to the rarity of observed Stokes V spectra of chromospheric lines outside sunspots. Such observations have, to my knowledge, been published only by Stenflo *et al.* (1984a, Mg I b and Na I D lines) and Martínez Pillet *et al.* (1990, Ca II H and K), cf. Lites *et al.* (1987) and Murphy (1990), who observe Mg I b_2 in sunspots. The 1-component models of active region chromospheres have been listed in Section 5.4.4. Similarly, in Section 5.4.5 the 2-component models of Chapman (1981) and Ayres *et al.* (1986) have been mentioned. The flux tube components of both these models are relatively similar and very hot in the chromosphere. The Ayres *et al.* (1986) flux tube, when combined with a very cool atmosphere without a chromospheric temperature rise, can simultaneously reproduce spatially averaged observations of Ca II K and CO vibration-rotation band lines, in both quiet and active regions simply by changing the filling factor. However, the validity of 2-component models is questionable in the chromosphere. The observed magnetic canopies in the lower chromosphere (e.g. Jones 1985, cf. Section 5.6.2) highlight the need for 2-D models of the chromospheric magnetic and thermal structure.

Recently, Solanki *et al.* (1991) have combined a wide variety of Ca II K observations to constrain the temperature within the magnetic part of the chromosphere in 2-D flux tube models, which also reproduce the observations of low-lying canopies (cf. Solanki and Steiner 1990). They find a considerably lower temperature in the magnetic component than suggested by the previous 2-component models of Chapman (1981) and Ayres *et al.* (1986). Due to the height-independent filling factor in the 1-D models, most of the Ca II core emission must come from a small fraction of the atmosphere, which must be correspondingly hot in order to reproduce the spatially averaged profiles. In 2-D models the canopy also contributes to the Ca II K emission, so that a lower temperature is sufficient to reproduce the observations.

In summary, it is possible to reproduce a wide variety of chromospheric observations and to constrain the chromospheric temperature in flux tubes using models of hot, expanding flux tubes embedded in a cool non-magnetic atmosphere. The chromospheric temperature enhancement begins 200–300 km deeper within magnetic elements than in the quiet sun.

5.4.8. Theoretical Investigations

The calculation of a quantitatively correct thermal structure within small-scale magnetic features from first principles is one of the most complex undertakings

in the theory of solar magnetic fields. Although the general form of the energy equation is relatively clear (Equation 3.5), the correct treatment of the energy transport by radiation, convection, oscillations and waves in three dimensions, as well as the presence of a sharp magnetic boundary make the general solution of the problem prohibitive. Instead, numerous simplified aspects of the problem have been investigated and solved. They involve simplifying the geometry (by assuming axial or translational symmetry), or the energy equation, or, most commonly, both.

Common simplifications of the energy equation include neglecting dynamic effects ($\mathbf{v} = 0$ and $\partial/\partial t = 0$, Spruit 1976, 1977, Steiner 1990, cf. Steiner and Stenflo 1990), neglecting radiation ($\nabla \mathbf{F}_R = 0$, e.g. Unno and Ribes 1985), neglecting resistive effects ($\eta = 0$, this is done by almost all investigators, but see, e.g., Hirayama 1992), or neglecting all dissipative processes, i.e. using the adiabatic approximation given in Equation (3.14). As discussed by Schüssler (1986), resistive effects only become important at scales smaller than 3–10 km, i.e., they only play a role in a boundary layer of this thickness at the edges of the magnetic elements. Consequently, they can significantly affect the evolution only of magnetic fragments with diameters smaller than a few times this value, since the ratio of the field-bearing volume of the flux tube to the area of its surface (at which the dissipation takes place) increases approximately linearly with the size of the tube. The adiabatic approximation has often been used when investigating flux tube dynamics, e.g. the convective collapse (Parker 1978, Webb and Roberts 1978, Spruit 1979, Spruit and Zweibel, 1979, Hasan 1984), or flux tube waves (Defouw 1976, Roberts and Webb 1978, 1979, Spruit 1982, Solanki and Roberts 1990, 1992). Time dependent effects have been neglected by investigators studying stationary flows (e.g. Unno and Ribes 1979, Ribes *et al.* 1985, Hasan and Schüssler 1985).

Finally, numerous approximations have been made of the radiative contribution to the energy transport. One of the simplest of these is to assume that the fluxtube is optically thin, i.e. its width is small compared to the photon mean free path (Ferrari *et al.* 1985, Kalkofen *et al.* 1986). Then the flux tube temperature is close to that of its surroundings at equal geometrical depth. Another simple approach is to apply Newton's law of cooling, i.e. the formula for the radiative relaxation time t_R derived by Spiegel (1957) (cf. Unno and Spiegel 1966) adapted to discrete flux tubes,

$$t_R = \frac{c_v}{16\kappa\sigma T^3}(1 - \kappa\rho R \operatorname{arc\,cot} \kappa\rho R)^{-1}. \tag{5.2}$$

Here κ is the Rosseland mean opacity, σ is the Stefan-Boltzmann constant, ρ is the gas density and R is the radius of the flux tube.

Tests of the validity of this formula using 2-D radiative transfer have been carried out by Trujillo-Bueno and Kneer (1987a), but see also Kneer (1986), Trujillo-Bueno and Kneer (1987b), Kneer and Trujillo-Bueno (1987). The Spiegel formula has been applied to flux tubes by, e.g., Webb and Roberts (1980a,b), Hasan (1985), Venkatakrishnan (1985) and Hasan and Kneer (1986). Only the horizontal

exchange of radiation across the sharp flux tube boundary is taken into account, so that the very important vertical radiative transfer is completely neglected in this approximation. Venkatakrishnan (1985) has also included a simple vertical energy transport. The 2-D diffusion approximation (Equation 3.12) has been used by Spruit (1976, 1977), Deinzer *et al.* (1984a,b), Knölker *et al.* (1987) and Knölker and Schüssler (1988). This approximation is quite reliable in the parts of the model that are optically thick to continuum radiation (i.e. below the $\tau = 1$ surface), but departs considerably from the results of a 2-D radiative transfer above the $\tau_c = 1$ level (compare e.g. Deinzer *et al.* 1984b with Grossmann-Doerth *et al.* 1989b). Hasan (1988, 1991) and Massaglia *et al.* (1989) have used the Eddington approximation to describe the radiation in a thin flux tube.

Radiative transfer in a 2-D grey atmosphere having a slab geometry has been carried out by Grossmann-Doerth *et al.* (1989b), Knölker *et al.* (1991), Fabiani Bendicho *et al.* (1992) and Pizzo *et al.* (1993). A non-grey radiative transfer in an axially symmetric flux tube has been performed by Steiner (1990), cf. Steiner and Stenflo (1990). He used the opacity distribution functions (ODFs) of Kurucz (1979) to describe the frequency dependence of the opacity, thus taking departures from greyness into account. Finally, Nordlund (1983, 1985b, 1986) and Nordlund and Stein (1989, 1990) carry out a full 3-D radiative transfer. It is non-grey, although only four frequency bins are considered. For fully dynamic models a significantly more complex approach than that of Nordlund would be prohibitively expensive. His approach gives very similar results to the more complex ODF-based technique (Steiner, private communication 1992).

Consider now the various components contributing to the energy transport in and around small flux tubes. In the sub-photospheric layers of the non-magnetic surroundings the energy transport is dominated by convection (granulation, cf. Spruit *et al.* 1990 for a review). At sufficient depth the magnetic field strength in the flux tube no longer exceeds the equipartition value (i.e. $B \lesssim \sqrt{4\pi\rho}\, v$, since the convective collapse is only effective near the solar surface, cf. Section 5.7.3), so that the convection there is practically unaffected by the magnetic field. Closer to the surface the convection is affected by the presence of the surface itself, i.e. radiation becomes increasingly important. In regions of sufficiently high magnetic flux, the convection is also influenced by the field and the properties of the granulation near the solar surface are substantially changed. For example, granules live much longer in magnetic regions (Nordlund and Stein 1989, 1990, cf. Title *et al.* 1989, 1992) and their appearance is also 'abnormal' (Dunn and Zirker 1973, Title *et al.* 1992), with a smaller brightness contrast between the up- and downflowing parts (Brandt and Solanki 1990).

The influence of the magnetic field on the granulation is two-fold. Firstly, the magnetic features provide a semi-rigid frame within which convection can take place. Thus they insulate the granules from each other. By impeding the formation of exploding granules this effect probably leads to the extended lifetime of granules in active regions. Secondly, magnetic features affect the thermal structure of the

granulation by absorbing energy from the surrounding granules in the form of radiation (Zwaan 1967). The lower gas density within the tubes implies the presence of a Wilson depression, i.e. a lowered $\tau = 1$ level. Photons entering the tubes through the side walls above the internal $\tau = 1$ level, but below the external $\tau = 1$ level have a greatly enhanced probability of escape relative to similar photons in a completely field free medium (Spruit 1976). Consequently, the flux tubes increase the surface across which the photons can escape. They change the direction of the radiative flux (e.g. Kalkofen *et al.* 1989, Fabiani Bendicho *et al.* 1992) and cool the convective atmosphere in their immediate vicinity (Spruit 1976, 1977, Deinzer *et al.* 1984b). A minor part of the net energy passed from the granulation into the tubes is in the form of kinetic energy. The tubes are buffeted by the changing flow pattern of the granulation and possibly by shock waves (e.g. Cattaneo *et al.* 1990, Malagoli *et al.* 1990, Steffen 1991, Steffen and Freytag 1991). Such buffeting can excite longitudinal tube and transverse kink modes. Whirl flows around individual flux tubes can excite torsional Alfvén waves. Energy is passed by these excitations from the granulation into the flux tubes, where it is transported to higher layers which are additionally heated. Therefore, small magnetic features not only increase the amount of energy leaking out of the solar atmosphere from the lower photosphere, they also increase the radiation from higher layers by heating these [either through the absorption of the increased radiative flux (see Section 5.4.9), the dissipation of waves, or the reconnection of field lines]. The heating in the higher photospheric layers becomes visible through the weakening of the spectral lines and partly as an increased continuum contrast near the limb.

Within the flux tubes the convection is suppressed to a large extent by the magnetic field (see Knölker and Schüssler 1988 for a detailed discussion). The vertical energy flux is thus transported mainly by radiation, although overstable oscillations, waves, oscillatory convection and Rayleigh-Taylor instabilities also contribute. Deinzer *et al.* (1984b) and Knölker *et al.* (1987) have shown that in narrow flux tubes the vertical energy flux above $\tau = 1$ is practically independent of the level of suppression of convection, since the horizontal radiative flux can compensate any missing vertical convective flux. In larger flux tubes the horizontal optical depth is too large and the complete suppression of convection leads to density inversions and a Rayleigh-Taylor instability (Knölker and Schüssler 1988). The horizontal energy flux in the lower photospheric layers of flux tubes is dominated by radiation streaming in through the hot or warm flux tube walls (Zwaan 1967). Higher in the atmosphere, where the interiour of the tube may become hotter than the non-magnetic surroundings at equal geometrical height (see below), the arrow of the horizontal radiative flux is expected to be reversed, so that radiation flows from the flux tubes into the surrounding atmosphere (e.g. Fabiani Bendicho *et al.* 1992).

The complexity of self-consistently calculating the thermal structure of small magnetic elements should by now be obvious. To determine the thermal structure in the lower and middle photosphere it is necessary to include at least the

effects of convection and of multi-dimensional non-grey radiative transfer in LTE. For upper photospheric and chromospheric layers the multidimensional radiative transfer must include NLTE effects and the dissipation of waves must be taken into account. Many of the necessary steps towards an understanding of energy transport mechanisms have been undertaken, but so far no single model has included all energy transport mechanisms.

5.4.9. Calculated Flux Tube Thermal Profiles and Comparison with Observations
The first models to incorporate convective and radiative energy transport in small flux tubes (Spruit 1976, 1977) revealed the importance of the hot walls for the emerging continuum radiation. Although radiation was treated only in the diffusion approximation and convection was approximated by the mixing length formalism, Spruit's models, for a carefully chosen mix of flux tube sizes, produced a CLV of the continuum intensity that is relatively close to the observed CLV.

The calculated CLV of $\langle \delta_c \rangle$ is understood as follows. The suppression of convection in the interiour of the tube contributes to a reduction of the total vertical energy flux there. However, due to the rapid increase of temperature with depth (the non-magnetic stratification is superadiabatic), the walls of the tube are hot and bright, i.e. a large amount of radiation streams in from the sides. Now, if the tube is sufficiently narrow not to be completely optically thick to horizontal radiation near its vertical $\tau_c = 1$ level, the influx of radiation from the side can heat it sufficiently to produce a hot bottom (i.e. $\tau_c = 1$ level) in the flux tube (Spruit 1976, Deinzer *et al.* 1984b, Ferrari *et al.* 1985, Kalkofen *et al.* 1986, Knölker *et al.* 1987). However, unless the tube is completely optically thin, i.e. narrower than the horizontal internal photon mean free path (Ferrari *et al.* 1985, Kalkofen *et al.* 1986), the temperature at equal geometrical height near the vertical $\tau_c = 1$ level within the tube remains lower (by up to a few 1000 K) than in its surroundings. Due to the increased horizontal optical depth in a larger tube, its bottom remains relatively cool, although the walls are still quite warm (Spruit 1976, Knölker and Schüssler 1988). For small tubes δ_c is highest near disc centre, since the bright bottom (brighter than the walls, since it lies deeper) is unobscured. As μ decreases foreshortening lowers the visibility of the discward wall, while the limbward wall becomes more visible. At somewhat larger μ the hot bottom begins to be obscured, although some of the intensity decrease is initially compensated by the increasing visibility of the limbward wall. At sufficiently small μ, however, the limbward wall also begins to be obscured and δ_c then decreases rapidly for smaller μ. Obviously, the μ value at which the limbward wall begins to be obscured decreases with increasing ratio of flux-tube diameter to Wilson depression, i.e. with increasing flux-tube size.

Observations generally show an increase in δ_c towards the limb until at least $\mu = 0.2$. Small flux tubes ($d \lesssim 200$–300 km) without mechanical heating and with radiation treated in the diffusion approximation cannot reproduce the observed CLV of δ_c (Spruit 1976, Caccin and Severino 1979, Chapman and Gingell 1984,

Deinzer *et al.* 1984b). Qualitatively the correct behaviour is shown by somewhat larger magnetic structures (Spruit 1976, Knölker and Schüssler 1988), or by 'hot cloud' models (e.g. Rogerson 1961, Ingersoll and Chapman 1975, Deinzer *et al.* 1984b, Schüssler 1987, Knölker *et al.* 1991, Steiner 1990, cf. Steiner and Stenflo 1990). Note that the hot cloud model works best if a number of flux tubes are present along the line of sight and the hot clouds overlap (Schüssler 1987, Knölker *et al.* 1991). Larger tubes and hot cloud models of small flux tubes differ, however, in their δ_c signal at disc centre. Whereas hot cloud models predict large δ_c at $\mu = 1$, large tubes are expected to be dark there ($\delta_c < 1$, Knölker and Schüssler 1988).

Near disc centre the introduction of a proper radiative transfer does not significantly affect the continuum brightness (Grossmann-Doerth *et al.* 1989b). However, the CLV of δ_c is changed, since a proper 2-D radiative transfer uncovers a new and important effect, the illumination of the upper photosphere by the bottom of the flux tube. If the bottom of the flux tube is hot, then the radiation coming from there and from the walls can be sufficiently intense to heat the middle and upper photospheric layers of the flux tube to a higher temperature than its surroundings at equal geometrical height (Grossmann-Doerth *et al.* 1989b, Steiner 1990, cf. Steiner and Stenflo 1990). Thus, radiation by itself can produce a rudimentary hot cloud. The empirical models of Keller *et al.* (1990a) and Zayer *et al.* (1990) exhibit a qualitatively similar temperature stratification, although quantitative differences still exist. This can be seen in Figure 5.6, in which the two empirical models of Keller *et al.* and the theoretical models of Steiner (1990) and Grossmann-Doerth *et al.* (1989b) are plotted.

Note that for the theoretical models only the temperature along the flux tube axis is plotted. In contrast to the empirical models, these models allow for a horizontal variation of the temperature. In the upper photosphere the theoretical models are cooler than the empirical ones. Although the reliability of the empirical models decreases close to the temperature minimum, the figure still suggests that a further heating component is missing in the theoretical models. This conclusion is underlined when considering the results of recent NLTE modelling, which suggest that the chromospheric temperature rise occurs at a deeper level within flux tubes (Bruls and Solanki 1992a,b). Thus, although the illumination effect can produce a 'warm cloud', it is unable to produce as hot a cloud as required by the observations of Stokes V profiles. However, even the 'warm cloud' models of Steiner (1990, cf. Steiner and Stenflo 1990) and Knölker *et al.* (1991) improve the correspondence of the calculated to the observed CLV of δ_c considerably. The need to take the geometry of the flux tubes or slabs into account explicitly by varying the viewing angle of flux slabs (Knölker *et al.* 1991) or considering rays outside the plane of symmetry of flux tubes (e.g. Bünte *et al.* 1991, 1992b) when calculating the continuum intensity should not be underestimated, particularly for small μ. Finally, it is possible that a proper correspondence to the observed CLV can only be achieved if the calculated $\delta_c(\mu)$ of flux tubes of different sizes is combined.

Note also, that the temperature in the deeper layers of the plotted empirical

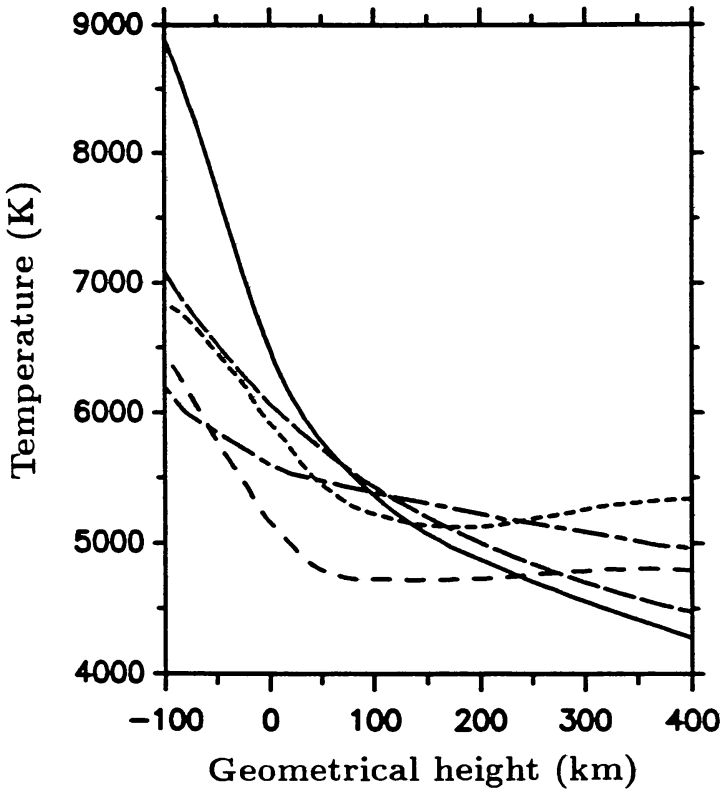

Fig. 5.6. Comparison between the temperature stratifications of theoeretical and empirical models. Plotted is temperature, T, at the flux tube axis vs. geometrical height of the models derived empirically by Keller *et al.* (1990a) from data obtained in an active region plage (– – –) and in a network region (- - - - -), the theoretical model of Steiner (1990, —— ——) and of Grossmann-Doerth *et al.* (1989b, —— - ——). The solid curve is a quiet sun model (from Keller *et al.* 1990a).

models is too high to reproduce the C I lines. The question of how the relatively small δ_c values suggested by the C I lines can be reconciled with the theoretical models is still open. It appears that either flux tubes are relatively large on average (diameters $\gtrsim$ 300–400 km), or they have a broad boundary layer (with a gradual decrease of the field strength over half the diameter of the tube), or that the close packing of many tubes gives rise to a low δ_c value. The second suggestion gives rise to conflicts with other observations, particularly of the field strength, and it is unclear whether densely packed small flux tubes can lower δ_c sufficiently for realistic α (Schüssler, private communication 1992). The model calculations of Knölker and Schüssler (1988) and the observations of Keller (1992a) support the first explanation. Again, probably a mixture of the flux tube sizes, with the average size depending on filling factor, fits the observations best.

Figure 5.6 also illustrates the importance of taking departures from greyness into account. Steiner (1990, cf. Steiner and Stenflo 1990) solves the non-grey radiative transfer for thousands of frequency points, while the Grossmann-Doerth *et al.* (1989b) model is grey. As expected, the Steiner model is cooler and more reliable in the upper layers than the Grossmann-Doerth *et al.* model. In the deeper

layers the relative reliability of the models is reversed, since the Grossmann-Doerth *et al.* model takes convection into account in much greater detail.

In the higher layers any self-consistent model must include departures from LTE into the radiative transfer, ideally in the detail achieved by Anderson (1989) for the quiet sun, but in 2 or 3 dimensions. Cooling by CO may also play a significant role (Ayres 1981, 1990, 1991, Ayres *et al.* 1986, Hasan and Kneer 1986, Massaglia *et al.* 1988, Ayres and Brault 1990), particularly in NLTE models (Anderson 1989). Unlike the strong lines of the iron group elements, the CO vibration-rotation band lines do not depart significantly from LTE (Ayres and Wiedemann 1990) and can become the dominant coolant in the lower chromosphere. The dependence of the relative effectiveness of CO as a coolant on the description of the radiative transfer of the iron lines can be judged by comparing the NLTE models of Anderson (1989) and Anderson and Athay (1989) with the LTE models of Kurucz (1991a,b). CO cooling may be less important inside flux tubes than in the non-magnetic atmosphere. This has partly to do with the evacuation of flux tubes (Massaglia *et al.* 1988) and partly with the presence of additional mechanical heating in them, which may always keep the temperature at a level at which CO does not form.

Only individual aspects of mechanical energy transport and heating due to waves in the upper photosphere and the chromosphere have been studied. In two of the most relevant studies Herbold *et al.* (1985) and Ulmschneider *et al.* (1991) have studied the effects on the flux tube thermodynamic structure of a prescribed flux of acoustic tube-mode and kink-mode wave energy, respectively. For sufficiently large energy fluxes the above-mentioned investigators can produce realistic chromospheres with such waves. The heating produced by non-magnetic acoustic waves has been studied in greater detail (e.g. Muchmore and Ulmschneider 1985 and Muchmore *et al.* 1989, cf. Ulmschneider 1991) and is qualitatively, but not quantitatively similar. More about waves in flux tubes is to be found in Section 5.5.6. In view of the complexity of calculating wave phenomena in sufficient detail it may, for many purposes be adequate to approximate their influence on the energy balance by introducing a source term of a representative form into the energy equation, as done, e.g., by Anderson and Athay (1989).

Finally, Hirayama (1992) has considered Joule heating in the resistive boundary layer of a flux tube. He estimates that near the temperature minimum Joule heating can raise the temperature by 300 K.

In summary, many of the main observational diagnostics of the temperature structure within flux tubes can be qualitatively reproduced by the best current theoretical models. Until now the addition of new terms into the energy equation, or the improved treatment of existing terms has generally led to a new level of understanding. The need for the inclusion of additional physics into the theoretical treatment of the energy balance, in particular of the upper photosphere and of the chromosphere, is still acute.

5.5. Velocity Structure

5.5.1. Stationary Flows seen in Stokes I

Faculae have long been known to be associated with redshifts of 0.2–0.5 km s^{-1} in the wings of Stokes I, relative to profiles observed in the quiet sun (e.g. Servajean 1961, Simon and Leighton 1964, Beckers and Schröter 1968a,b, Deubner 1968, Tannenbaum *et al.* 1969, Frazier 1970, Howard 1971, 1972, Sheeley 1971, Simon and Zirker 1974, Skumanich *et al.* 1975, Tarbell and Title 1977, Frazier and Stenflo 1978). Most of these measurements were carried out with a Babcock-type magnetograph used in velocity mode (i.e. without polarization optics) and the redshifts were generally interpreted as manifestations of downflows within the magnetic features. Skumanich *et al.* (1975) and Frazier and Stenflo (1978) even find a proportionality between flow velocity and $\langle B \rangle$. If extrapolated to the true field strength $B(\gtrsim 1$ kG) this would give an intrinsic velocity of 1.5–3 km s^{-1} within the magnetic elements. Since such large velocities are not seen in Stokes V shifts, Frazier and Stenflo argued that the downflows are to a large part concentrated outside the magnetic features (cf. Stenflo 1976). They have, in the meantime, proved to be correct.

More recently, observations of complete Stokes I line profiles have shown that the 'redshifts' of the line wings are mainly caused by a decrease in the line asymmetry (i.e. a decrease in the 'C'–shape of the line bisector, see below for references) and that shifts of the line core are generally $\lesssim 200$ m s^{-1}. It is still not completely clear what the sign of the shift of the line core is. E.g. Kaisig and Schröter (1984) found the cores of six lines to be blueshifted by 50–250 m s^{-1} relative to the quiet sun profiles. Similarly, Keil *et al.* (1989) found the line core of Fe I 5434 Å ($g = 0$) to be blueshifted by approximately 150 m s^{-1} in some parts of an active region ($\langle B \rangle > 200$ G). Their observed dependence of shift on polarity, however, is rather disturbing. Among the studies that find no core shifts, Beckers and Taylor (1980) have compared the CLVs of the line shifts in the network, in plages and in the quiet sun. They find no obvious differences. Cavallini *et al.* (1988) find a slight blueshift (50 m s^{-1}) in Ca I 6162.2 Å, but no visible shifts relative to the quiet sun in three Fe I lines. Finally, Miller *et al.* (1984) and Dara *et al.* (1987) see no difference between the velocity in magnetic and in non-magnetic regions in the network. Miller *et al.* set an upper limit of 50 m s^{-1} on network line-core shifts. Immerschitt and Schröter (1989) find a small blueshift (< 50 m s^{-1}) but conclude that it is not significant. Finally, we have the observations showing (small) redshifts. Livingston (1982) found active region profiles to be redshifted by < 50 m s^{-1}. Cavallini *et al.* (1985, 1987) find redshifts $\lesssim 100$ m s^{-1} in three Fe I lines, Brandt and Solanki (1990) find relative redshifts of 50–120 m s^{-1} in active regions ($\alpha \lesssim 15\%$) from nineteen spectral lines, Brandt and Steinegger (1990) find redshifts up to 250 m s^{-1} from a larger sample of lines and Kneer and Von Uexküll (1991) obtain redshifts of 300 ± 200 m s^{-1} in a spectrogram obtained under good seeing.

The current thinking is that the behaviour of the Stokes I asymmetry mainly reflects changes in the granular convection caused by magnetic fields. Such changes are also clearly visible in filtergrams as 'abnormal granulation', i.e. granulation with abnormally low contrast and consequently ill defined granular cells with abnormally long lifetimes (Dunn and Zirker 1973, Title *et al.* 1989, 1990a,b). Due to the generally limited magnetic filling factor, the properties of the magnetic features hardly affect the Stokes I asymmetry and shift significantly. Exceptions to this interpretation may have been observed in some cases, mainly at very high spatial resolution. For example, Börner and Kneer (1992) see a downflow in a small bright element bordering a sunspot. They interpret this as a small flux tube connected by a loop to the sunspot and the downflow as a continuation of the Evershed flow of the sunspot.

5.5.2. Stationary Flows seen in the Stokes V Zero-Crossing Wavelength

A more direct indicator of flows within the magnetic features is the zero-crossing wavelength λ_V of Stokes V. Older observations of λ_V showed sizeable downflows ranging up to 1.6 km s^{-1}. Much of this work was done with the line-centre-magnetogram technique, introduced by Gionavelli and Ramsay (1971) and extensively applied by Giovanelli and Brown (1977) and Giovanelli and Slaughter (1978), amongst others. It is based on the idea that for an *antisymmetric* Stokes V profile, the signal disappears if the single magnetograph slit used is centred at λ_V. Any shift of λ_V with respect to the slit position produces a signal whose strength is a measure of the shift. Its weakness is that asymmetric Stokes V profiles produce spurious shifts. For photospheric spectral lines this technique gives λ_V shifts of 0.5 km s^{-1}. For stronger lines, with cores formed in the chromosphere, the shift disappears. Other measurements have also shown λ_V shifts. For example the Stokesmeter data of Harvey *et al.* (1972) and the magnetograms of Stenflo (1973) suggested downflows of 0.5 km s^{-1} (cf. Stenflo 1976). Harvey (1977a) published an observed λ_V shift of Fe I 15648.5 Å of 1.6 km s^{-1}. Wiehr (1985) found values ranging from 0 to 2 km s^{-1} for Fe I 8468.4 Å and Scholier and Wiehr (1985) also found downflows in the majority of the spectra analysed by them.

More recently, evidence against the presence of λ_V shifts has accumulated. Investigators not finding any significant λ_V shift are: Stenflo and Harvey (1985), in Stokes V profiles of 5250.2 Å observed in regions with different filling factors, Brants (1985b), in high spatial resolution spectra of Fe I 6302.5 Å in an emerging flux region (however, his accuracy is only $\pm$ 0.5 km s^{-1}), Solanki (1986), in the Stokes V profiles of hundreds of Fe I and II and of Mg I b_1 and b_2, Stenflo *et al.* (1987a), in the CLV of λ_V of four lines near 5250 Å, Wiehr (1987), in the CLV of 6301.5 Å and 6302.5 Å, Wiehr and Lustig (1989), in time series of the same lines, Muglach and Solanki (1991, 1992), in the V profiles of all the unblended Fe I lines in the infrared H-band (1.5–1.8 μm), and finally Fleck (1991) and Fleck and Deubner (1991), in high spatial resolution time series of 6301.5 Å and 6302.5 Å Stokes V profiles.

Spatially localized snapshots of λ_V often show sizeable blue or redshifts relative to the local Stokes I. A part of the relative shifts may have to do with the strong variability of the wavelength of the Stokes I profile (Fleck 1991). When averaged over spatial position (Solanki and Pahlke 1988), or time (Fleck 1991) the λ_V shifts in general become less than approximately 0.2–0.3 km s^{-1}, both when compared to laboratory wavelengths (Solanki 1986) or to local Stokes I profiles, if the relevant corrections for solar rotation, convective blueshift, etc. have been carried out (e.g. Stenflo and Harvey 1985, Solanki 1986, Muglach and Solanki 1992). This is true for all lines formed between the low photosphere (infrared H-band Fe I lines) and the lower to middle chromosphere (Mg I b 5172.7 Å and 5183.6 Å). As pointed out by Solanki (1986) these observations do not contradict the large flows (10–20 km s^{-1}) observed in the C IV doublet in the transition zone of active regions (e.g. Dere *et al.* 1981, Feldman *et al.* 1982), even in the presence of extensive magnetic canopies, such as those proposed by Gabriel (1976), or Solanki and Steiner (1990) and observed by Giovanelli (1980).

How can the contradiction between the older and the newer measurements of downflow velocity be explained? The main difference between the observations that show downflows and those that do not is that the former have a lower *spectral* resolution. Since Stokes V profiles of almost all spectral lines are asymmetric, with stronger blue wings than red wings near disc centre (Section 5.5.3), spectral smearing tends to shift the zero-crossing wavelength towards the red, thus simulating a downflow (Solanki and Stenflo 1986). The magnitudes of the redshifts observed by, e.g. Giovanelli and Slaughter (1978) and Wiehr (1985) can be reproduced by smearing Stokes V profiles observed with high spectral resolution (FTS data) by an amount appropriate to the instrumental parameters relevant to the downflow observations (Solanki and Stenflo 1986).

This explanation works for all observations showing redshifts, except those of Scholier and Wiehr (1985) and those involving the Fe I 15648.5 Å line. The predominance of redshifts observed by Scholier and Wiehr (1985) turns out to be a selection effect. A larger sample of their observations was analysed by Solanki and Pahlke (1988). They found that averaged over all the profiles no net shift greater than 200 m s^{-1} is visible.

Therefore, only the Fe I 15648.5 Å line remains, with its chequered history of λ_V shifts. Harvey (1977a) found a zero-crossing redshift of 2.2 km s^{-1} with respect to the local Stokes I wavelength of this line. The convective blueshift affecting the Stokes I profile (Nadeau 1988) reduces the actual λ_V redshift to 1.6 km s^{-1}. This value played a pivotal role in the compilation of redshifts by Giovanelli and Slaughter (1978). The next measurement of this line was published ten years later by Stenflo *et al.* (1987). At $\mu \approx 1$ they found a redshift of 1.1 km s^{-1} with respect to the local Stokes I. Although much smaller than the value measured by Harvey, this observation still suggested a downflow of approximately 0.5 km s^{-1} within magnetic features. Muglach and Solanki (1991, 1992), however, have demonstrated that if all the unblended lines in the H-band are considered,

then no residual downflow larger than 0.3 km s^{-1} is found in magnetic features. They also showed that for the Fe I 15648.5 Å line, the error in the λ_V position is particularly large by virtue of its large Zeeman splitting and the resulting minute $dV/d\lambda$ at λ_V. Thus, a line which is a good magnetic diagnostic is not always a good velocity diagnostic, or, in other words, you can't win em all! For the high S/N observations of Stenflo *et al.* (1987b) an uncertainty of approximately 0.6 km s^{-1} is deduced for the λ_V of this line. For the lower S/N observations of Harvey (1977a) the uncertainty is proportionally larger.

Rüedi *et al.* (1992b) observed an upflow and a lower field strength in one polarity close to the neutral line of an active region and a downflow coupled to a higher field strength in the other polarity. This is exactly the signature predicted by siphon flow models (Section 5.5.4). Rüedi *et al.* (1992a), using 1.5 μm lines, also noticed the presence of relative shifts between the Stokes V profiles of 2 magnetic components in the same spatial element. The origin and implications of these shifts, which are seen only in a minority of the spectra, is still unclear.

In conclusion, there is currently no compelling observational evidence for the presence of stationary flows within the majority of the small-scale magnetic features. It is to be expected, however, that stationary flows are present under some circumstances. Siphon flows, such as those detected by Rüedi *et al.* (1992b), fall under this category.

5.5.3. Stationary Flows Diagnosed from the Stokes V Asymmetry

Another diagnostic of stationary flows is the blue-red asymmetry of Stokes V. Stenflo *et al.* (1984a) discovered that Stokes V profiles observed in faculae and the network near $\mu = 1$ are strongly asymmetric. Both the area, A_b, and the amplitude, a_b, of the blue Stokes V wing differ from the red wing area, A_r, and amplitude, a_r, respectively. Quantitatively, this asymmetry is expressed by the relative amplitude δa and area δA asymmetry (see Section 4.7.2 for their definitions). Close to solar disc centre both δa and δA are positive for most Fe I (Solanki and Stenflo 1984) and Fe II lines (Solanki and Stenflo 1985). For the weakest lines noise and blends do not allow the exact asymmetry to be determined, while the strongest lines do not appear to show a significant δA. For the stronger lines $\delta a > \delta A$.

These results have been confirmed for smaller samples of lines, but for many more solar regions by Stenflo and Harvey (1985), Wiehr (1985), Scholier and Wiehr (1985), Zayer *et al.* (1990), Fleck (1991) and Dara *et al.* (1991). Lines in the infrared H-band are also asymmetric in the same sense as the lines in the visible, but the magnitude of the asymmetry is smaller (Muglach and Solanki 1991, 1992). Closer to the limb both δa and δA change sign, i.e. the red Stokes V wing becomes stronger than the blue wing, as illustrated in Figure 5.7 (Stenflo *et al.* 1987a, Pantellini *et al.* 1988). The observed CLV of δA has been used by Mürset *et al.* (1988) to reproduce the broad-band circular polarization measured by Kemp *et al.* (1987). The measurements of Kemp *et al.* therefore represent an independent confirmation of the direct measurements of δA.

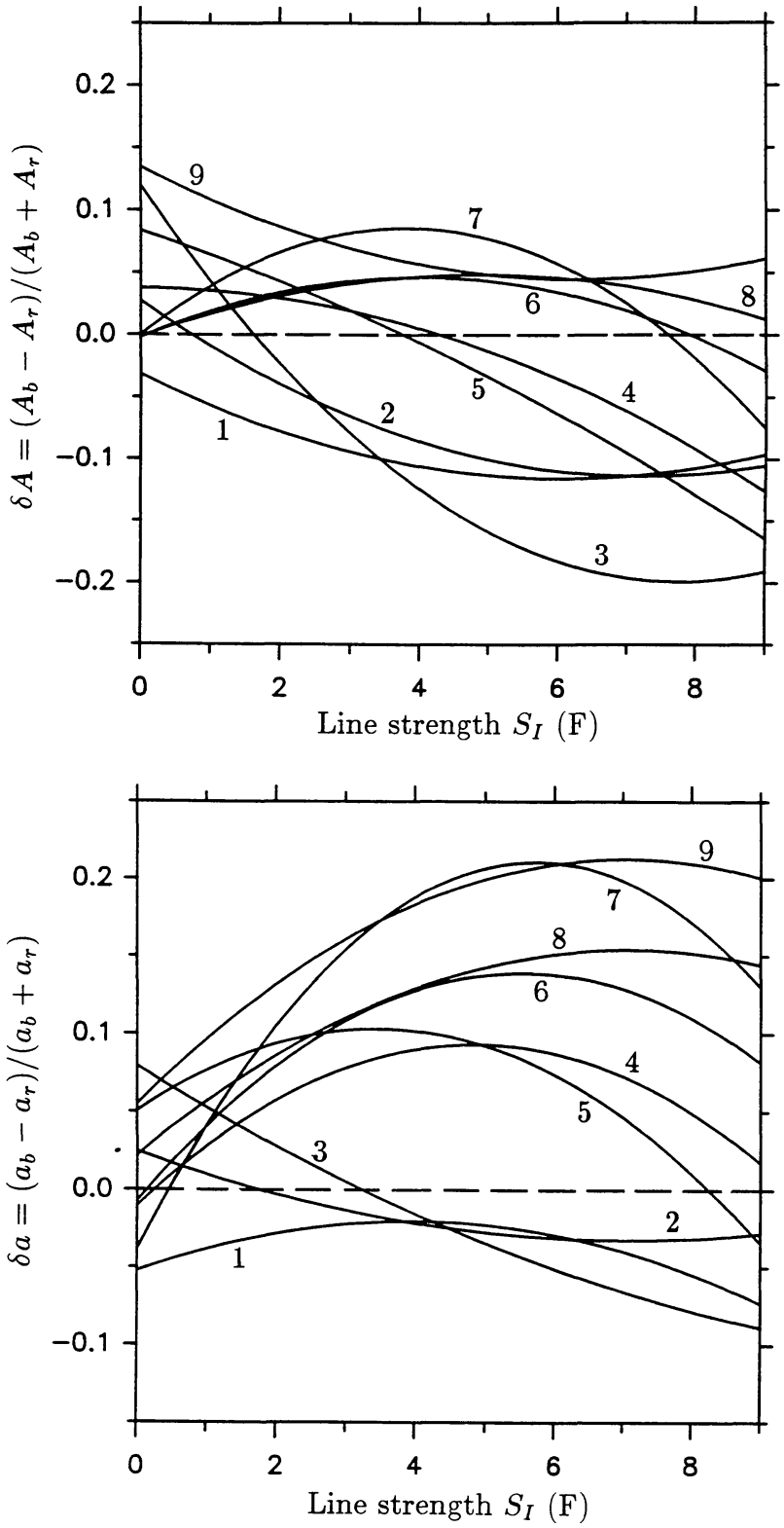

Fig. 5.7. Stokes V asymmetry as a function of line strength, S_I. Each curve represents the asymmetry, for different spectral lines, measured in a given solar region. The regions are numbered according to their limb distance, with region 1 being closest to the limb ($\mu \approx 0.16$) and region 9 being closest to disc centre ($\mu = 0.98$). The curves are second-order polynomial fits to the approximately 180 data points (spectral lines) per observed region. **(a)** Relative area asymmetry δA, **(b)** relative amplitude asymmetry δa (from Pantellini *et al.* 1988).

Well before the first observations of asymmetric Stokes V profiles outside of sunspots, Illing *et al.* (1975) had already proposed a combination of magnetic field and velocity gradients to explain the broad-band circular polarization observed in sunspots (Illing *et al.* 1974a,b, 1975). Grigorjev and Katz (1975) also calculated Stokes V profiles in the presence of velocity gradients, but paid no particular attention to the blue-red asymmetry. They were more interested in understanding the crossover effect in sunspot penumbrae, i.e. the presence of V profiles with 3 or more lobes near the polarity inversion line (e.g. Grigorjev and Katz 1972, Golovko 1974, Sánchez Almeida and Lites 1992). Gradients of a cospatial velocity and magnetic field have been relatively successful in reproducing selected line parameters (δA, λ_V) at disc centre of a number of lines, if a velocity decreasing with height and a magnetic field increasing with height is assumed (Sánchez Almeida *et al.* 1988b, 1989, 1990). Both theory and observations, however, constrain the field strength to decrease with height in the main body of the flux tubes (Sections 5.1.3 and 5.1.5). If this constraint is accepted then the asymmetry and the absence of a λ_V shift cannot be simultaneously reproduced by flows within the magnetic features (Solanki and Pahlke 1988).

Van Ballegooijen (1985b) pointed out that downflows outside the magnetic elements can also produce an asymmetry in Stokes V, if the expansion of the magnetic features with height is taken into account, so that some rays pass through both magnetic and non-magnetic parts of the atmosphere. Grossmann-Doerth *et al.* (1988b, 1989a) showed that such downflows do not produce any zero-crossing shift (Section 4.7). Solanki (1989) was able to reproduce the δA values of four widely different lines without shifting λ_V using a thin tube model of a flux tube surrounded by a downflow. The observations require downflow velocities of 1–2 km s^{-1} in the immediate surroundings of magnetic features. In addition, the surroundings must be approximately 200–300 K cooler than the average quiet sun, highly suggestive of intergranular lanes. The observed δa values have so far not been reproduced by any models incorporating only stationary flows (see Section 5.5.5 for more on the modelling of δa).

Finally, the CLV of δA has been modelled by Bünte *et al.* (1991, 1992b) and by Knölker *et al.* (1991). The latter authors analyse the Stokes V profiles resulting from dynamical flux tube models incorporating a convective cell that resembles a granule in the surroundings of the flux tube. They find that the asymmetry of the calculated Fe I 5250.2 Å line changes sign near $\mu = 0.4$, in accordance with the observations. Bünte *et al.* (1991, 1992b) used hydrostatic models of flux tubes with an external velocity field (Bünte 1989) that is allowed to assume different forms. They could reproduce the observations only for a relatively sophisticated model incorporating overturning convective cells having hot up- and cool downflows, with the flux tubes positioned in their downflowing parts. Figure 5.8 shows observed (squares) and calculated (curves) δA values of Fe I 5250.2 Å. The three curves correspond to models with slightly different velocity fields.

In summary, the δA observed in magnetic elements appears to be a product of the

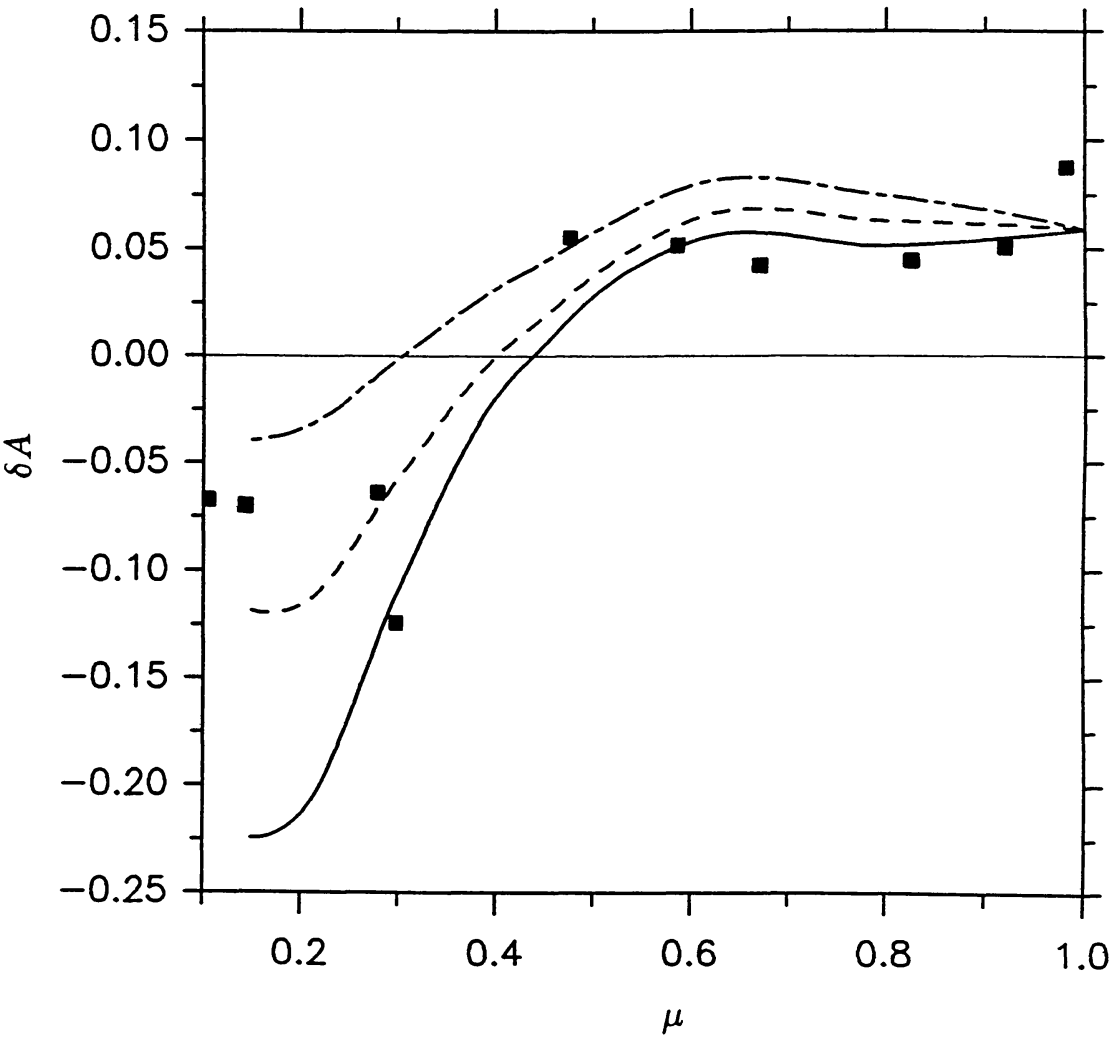

Fig. 5.8. Centre-to-limb variation of Stokes V area asymmetry, δA, of Fe I 5250.2 Å. The filled squares are values observed by Stenflo *et al.* (1987a), the three curves correspond to δA values of synthetic profiles arising from three slightly different models. Each model is composed of a periodic array of flux tubes embedded in a granule-like velocity field with cool downflows near the flux tubes and warm upflows further away from them. The dot-dashed curve results for suppressed, the solid curve for enhanced horizontal velocities (from Bünte *et al.* 1991).

granulation surrounding the magnetic elements. Conversely, δA can constrain the velocity and the temperature of the convection in active regions. It has the potential of becoming a powerful diagnostic of the properties of 'abnormal granulation'. Note that the 5250.2 Å line is not the most sensitive to the details of the granular structure. Bünte *et al.* (1992b) have found that δA of 5083.3 Å reacts more strongly to changes in the model. Their model also turns out to be too simple to quantitatively reproduce the CLV of δA of both lines, although it gives the correct qualitative dependence.

5.5.4. Theoretical Investigations of Steady Flows in Flux Tubes

Different theoretical aspects of steady flows within magnetic flux tubes (or slabs) have been investigated by Giovanelli (1977), Durrant (1977), Unno and Ribes (1979), Hasan and Schüssler (1985), Ribes *et al.* (1985), Schüssler (1986) and Henoux and Somov (1990). 'Steady' flows of limited duration are also predicted by theories of the convective collapse mechanism (e.g. Parker 1978, Spruit 1979, Hasan 1983, 1984, 1985). Here only the velocities are of interest. More details on the collapse mechanism are given in Section 5.7.3. The theoretical results have, like the observations, been somewhat controversial. An inflow through the walls of the flux tubes is required to support a stationary downflow, since otherwise the flux tubes would, due to the rapid drop in density with height, quickly drain the chromosphere and corona of all their material. Giovanelli (1977) claimed that near the temperature minimum the gas is sufficiently neutral to flow more or less freely across the field lines into the flux tubes and thus feed the downflows observed in the 1970s. However, in order to explain the rapid increase of downflow velocity with depth (observed by Giovanelli and Slaughter 1978) and fulfill mass conservation, a massive inflow of material is required throughout the photosphere. Durrant (1977) used this as an arguments against downflows within flux tubes. He has been supported by Hasan and Schüssler (1985), Schüssler (1986) and Henoux and Somov (1990), who reconsidered the diffusion coefficient which governs the entry of gas through the side walls of a flux tube. They concluded that the magnitude of the downflow that can be supported in this way is of the order of 1–10 m s^{-1}, i.e. 2–3 orders of magnitude smaller than the values observed by Giovanelli and Slaughter (1978).

Thus, the presence of measurable stationary net downflows of long duration in the majority of the magnetic elements is not supported by theory. However, transient downflows are by no means ruled out. In particular during the convective collapse phase downflows reaching peak velocities between 600 m s^{-1} (Hasan 1984) and 9 km s^{-1} (Hasan 1983) at the solar suface have been theoretically predicted. The larger number results when the lower boundary of the model is opened and material is allowed to flow out of the computational domain freely. The considerably smaller downflows found by Hasan (1984, 1985) during the initial collapse phase (with a closed lower boundary) are not very different in magnitude from the downflow phases of the subsequently excited overstable oscillations.

One way of producing stationary flows (with up- and downflows of similar magnitude) in magnetic flux tubes, without running into problems with mass conservation, is through siphon flows. A difference in gas pressure between the two foot points of a loop (e.g. due to different field strengths) drives such a flow, which then attempts to equalize the field strengths in the two foot points. Siphon flows in an extended field were first studied by Meyer and Schmidt (1968), in connection with the Evershed effect in sunspots (e.g. Evershed 1909, St John 1913, Schröter 1965a,b, Bhatnagar 1967, Küveler and Wiehr 1985). Siphon flows in isolated tubes (bent over to form loops) have more recently been investigated in great detail by

Thomas (1988), Montesinos and Thomas (1989), Thomas and Montesinos (1990, 1991) and Degenhardt (1989, 1991).

The influence of stationary flows on the thermodynamic and magnetic structure of flux tubes has been studied by Unno and Ribes (1979) and by Hasan and Schüssler (1985). Downflows are found to be efficient heaters of the atmosphere within flux tubes. See also Ribes *et al.* (1985), who calculated the spectral signatures of such flows, and Degenhardt (1991), who included the radiative exchange with the surroundings (using Newton's law of cooling) in models of siphon flows.

Downflows in the surroundings of flux tubes, respectively slabs, are predicted by Nordlund (1983, 1985b, 1986), Deinzer *et al.* (1984b), Nordlund and Stein (1989, 1990), Grossmann-Doerth *et al.* (1989b) and Knölker *et al.* (1991). The velocity of the integranular downflow lanes in which the flux tubes are embedded (cf. Sect 5.6.3) is enhanced near the solar surface by radiation losses into the evacuated flux tubes. These losses lead to a cooling of the non-magnetic material adjacent to the tubes, which, due to the proportionality of pressure scale height to temperature, produces a horizontal pressure disequilibrium near the surface. This pressure gradient drives a horizontal flow directed towards the tubes which is redirected downwards by the flux tube boundary and the loss of buoyancy of the cooled gas (Deinzer *et al.* 1984b). The peak velocities found in the downflow surrounding the tubes can reach 6 km s^{-1} if the numerical viscosity is reduced sufficiently (Knölker *et al.* 1991).

In conclusion, theory and numerical modelling predict a virtual absence of long term downflows within the flux tubes, but substantial downflows in their vicinity, in good agreement with the observations.

5.5.5. Observations of Non-Stationary Velocities

There are basically three diagnostics currently supporting the presence of non-stationary velocities in magnetic elements: time-series of λ_V, line widths of Stokes V and Stokes I, and the Stokes V amplitude asymmetry δa.

The most direct of these, time-series of λ_V, have so far only uncovered oscillations or waves with a period close to five minutes and an amplitude of 0.2–0.3 km s^{-1} in photospheric spectral lines (Giovanelli *et al.* 1978, Wiehr 1985, Fleck 1991, Fleck and Deubner 1991, Keller 1992b).* The amplitude increases with height and reaches 0.75 km s^{-1} in Hα. Since the velocity fluctuations in the chromospheric Mg I b 5183 Å line occur later (by 18 s on average) than in the photospheric Fe I 5166 Å line, Giovanelli *et al.* (1978) conclude that the waves are propagating upwards with a phase velocity of approximately 100 km s^{-1}. Roberts (1983) has identified these with longitudinal tube waves (sausage mode, Section 3.4) in the presence of radiative damping. The waves within the magnetic elements (as seen in

* A possible exception is Severny (1967), who finds some evidence of oscillations of the magnetograph signal with periods of 80 s and 7–9 minutes. However, he finds no evidence for such periods in the velocity signal and also sees no fixed phase relation between the oscillations seen in Fe I 5250.2 Å and Ca I 6103 Å, which is suggestive of noise or some instrumental effect.

Stokes V) are almost in phase with the waves in the non-magnetic atmosphere (as seen in Stokes I, Giovanelli *et al.* 1978, Wiehr 1985, Wiehr and Lustig 1989), so that either the coupling between the internal and external atmospheres is extremely strong, or both waves have a common excitation mechanism. The spatial resolution of the observations varies between $1''$ and $8''$, but the results appear to be relatively spatial resolution independent within this range of resolutions.

Oscillations with similar periods have also been observed in the Stokes V amplitude by Tanenbaum *et al.* (1971) and Dara *et al.* (1987). They either reflect the temperature perturbations associated with the velocity oscillations (e.g. in longitudinal tube waves, Herbold *et al.* 1984, Solanki and Roberts 1992) or instrumental effects, and are unlikely to represent actual changes in the magnetic flux, as suggested, possibly somewhat prematurely, by Dara *et al.* (1987).

Measurements of Stokes I time series, power and phase spectra also suggest some differences between active regions and the magnetic network on the one hand and the supergranule cell interiours on the other (e.g. Orrall 1966, Howard 1967, Mein 1971, Liu and Sheeley 1971, Bhatnagar and Tanaka 1972, Lites *et al.* 1982, Damé *et al.* 1984, Kneer and Von Uexküll 1985, 1986, Von Uexküll *et al.* 1989, Deuber and Fleck 1990, Title *et al.* 1992), although some observers do not find any significant differences (Mein and Mein 1976, Mein 1977). Low frequency oscillations ($\nu \lesssim 2.5$ mHz, i.e. periods $\gtrsim 6.5$ minutes) are more prominent in plage and network, while higher frequencies are considerably stronger in the cell interiours, in particular the three minute peak (which was not noticed in Stokes V, Fleck 1991). The power in the 5 minute oscillations is significantly lower in network and plages than in the quiet sun. There are also considerable differences in the phase spectra (see Deubner and Fleck 1990 for details). However, the direct relation of such observations to mass motions within magnetic structures like flux tubes and canopies is difficult to establish.

The widths of the I_V (integrated V profiles, Section 2.4) and of the V profiles of relatively Zeeman-insensitive lines suggest that non-stationary velocities with much larger amplitudes than seen in time-series of λ_V are present in magnetic elements (Solanki 1986, Solanki *et al.* 1987, Pantellini *et al.* 1988, Keller *et al.* 1990a, Zayer *et al.* 1990, Muglach and Solanki 1991). Typical rms values of such velocities lie between 1 and 3 km s^{-1}, depending on the spectral line and to some extent on the observed region. A recent NLTE analysis (Bruls and Solanki 1992b) suggests that the Stokes V line widths can be reproduced by rms velocities of between 1.5 and 2 km s^{-1}. The Stokes V profile widths tell us that additional broadening velocities, of a similar magnitude as the 'turbulent velocities' in the quiet sun, are present in magnetic elements. In the quiet sun, however, most of the line broadening comes from the granulation (Nordlund 1984a), which is, of course, not present within the magnetic features. Therefore, the broadening must be due to an oscillatory or wave-like velocity field, or due to the presence of stationary up- and downflows within different spatially unresolved magnetic elements (e.g. siphon flows on small scales, as suggested by Degenhardt and Kneer 1992).

The Stokes I profiles also support the large observed Stokes V widths. Cavallini *et al.* (1988), Immerschitt and Schröter (1989) and Brandt and Solanki (1990) find an increase in line width with increasing activity, respectively magnetic flux. This may be due to larger rms velocities in active regions, although Brandt and Solanki (1990) do point out that a generally lower temperature in the non-magnetic part of active regions may also produce such an effect. The reduction in rms granular velocities in active regions, deduced by Nesis *et al.* (1989), Günther and Mattig (1991) and Title *et al.* (1992) from high spatial resolution observations of line shifts and by Hanslmeier *et al.* (1991) from line bisectors, implies that any enhanced velocities in active regions must be distributed on small horizontal scales (within the magnetic elements?).

The velocity amplitudes near the limb are almost the same as near disc centre (Solanki *et al.* 1987, Pantellini *et al.* 1988), suggesting that transverse wave modes (e.g. kink mode, torsional Alfvén mode) are just as strongly excited as longitudinal modes (e.g. sausage mode, overstable oscillations). Another possible source of horizontal velocity visible in Stokes V is the motion of complete magnetic elements that are continually being shuffled around by the evolving granulation. It is still unclear, however, what magnitude this effect is expected to have. Whereas Title *et al.* (1990a) mention *maximum* velocities of 3 km s^{-1} (but give no average value), Zirin (1985) reports an *average* horizontal velocity of only 0.06 km s^{-1}. His spatial resolution, however, is considerably lower, and he may well be missing much of the motion taking place on a small scale. De Boer and Kneer (1992) and Title *et al.* (1992) mention the presence of strong horizontal motions of facular bright points, but give no numbers.

There is some evidence that the velocity amplitudes derived from the Stokes V widths decrease slightly with filling factor (Zayer *et al.* 1990). This is suggestive of a decrease in the excitation of tube waves and oscillations in regions with large filling factors, a view consistent with the increased lifetimes of granular cells in active regions (Title *et al.* 1989). Finally, velocity amplitudes derived from Stokes V profiles of lines in the infrared H-band, formed deeper in the atmosphere, are similar to those derived from lines in the visible (Muglach and Solanki 1991).

The final parameter indicating non-stationary velocities in magnetic features is δa. Although Solanki (1989) could reproduce the observed δA values with an external downflow (Section 5.5.3), he was unable to reproduce the $\delta a/\delta A$ ratio. The δa values of the synthetic profiles were too small. He was able to increase the $\delta a/\delta A$ ratio by introducing, in an extremely simple model, an oscillatory motion with different weights for the upflowing and downflowing components. Solanki and Roberts (1992), however, have found that the $\delta a/\delta A$ ratio of Fe I and II lines cannot be simultaneously reproduced if they consider a more sophisticated model, namely a linear tube wave calculated in the thin tube approximation. This appears to rule out mechanisms of enhancing δa relative to δA that are based on a temperature-velocity correlation. Grossmann-Doerth *et al.* (1991) have, therefore, considered the influence of a simple representation of a non-linear wave with different up-

and downflow velocity amplitudes. They can roughly reproduce the δA, δa and λ_V values of five spectral lines observed near disc centre, if the upflow velocity is a factor of 3–4 smaller than the downflow velocity, whose amplitude may range from 2 to 4 km s^{-1}. Of course, their model also includes a downflow outside the flux tube.

Degenhardt and Kneer (1992) favour a superposition of differently directed siphon flows in different flux tubes as a method of enhancing δa. Basically, their proposal boils down to a correlation between field strength and velocity. Another mechanism that may enhance δa, but which has not yet been analysed in detail, is the superposition of waves or oscillations with a distribution of amplitudes and/or phases across the cross-section of a magnetic element. Such oscillations have been seen in the self-consistent model calculations of Knölker *et al.* (1991).

In summary, some diagnostics indicate the presence of broadening velocities up to 3 km s^{-1} (both Stokes V line broadening and δa give similar velocity amplitudes), but λ_V time series only show rather low amplitude perturbations. It appears that besides low amplitude tube waves excited by the global five minute oscillations, other oscillations or waves are also present in magnetic features, but not visible in λ_V due to one or more of the following reasons: a) Many flux tubes with tube waves having different phases are present in the resolution element of a given observation. However, unless the flux tubes are very small ($d \lesssim 0.1 - 0.2''$) some residual signal of such waves should be visible in the high resolution observations of Fleck (1991). b) The tube waves have a very short wavelength (and consequently also a short period). If it becomes smaller than the half-width of the Stokes V contribution function of a particular line, the waves become invisible in the λ_V time series of that line (Solanki and Roberts 1992). The observational constraint that the time-averaged λ_V is close to the rest wavelength restricts the properties of any short period waves considerably. c) Finally, it is possible that the dynamical thin tube approximation breaks down and most of the power is present in higher order modes having multiple nodes or at least different phases across the cross-section of the tube (cf. Section 5.5.6). Such waves are extremely difficult to detect, due to the cancellation of phases when averaging over even a single flux tube.

5.5.6. Theoretical Studies of Non-Stationary Velocities in Flux Tubes

The literature on all aspects of non-stationary velocities, particularly waves, in and around flux tubes is very extensive and only a selection is briefly reviewed here. The theory of wave excitation, propagation and dissipation in flux tubes has been reviewed by Spruit (1981a), Spruit and Roberts (1983), Roberts (1984, 1986, 1990), Thomas (1985), Hollweg (1986, 1990, 1991), Ulmschneider and Muchmore (1986), Hammer (1987), Ryutova (1990), Davila (1991), Musielak (1991) and Stein and Nordlund (1991). Much of the theory has been developed in the framework of the thin-tube approximation. The theory of acoustic wave propagation and heating has been reviewed by Ulmschneider (1991).

Linearized waves in isolated (thin or thick) flux tubes with or without gravity have been studied among others by Defouw (1976), Ryutov and Ryutova (1976), Roberts and Webb (1978, 1979), Wilson (1979, 1980a,b, 1981a), Parker (1979a), Wentzel (1979b), Webb and Roberts (1980a,b) Spruit (1982), Rae and Roberts (1982), Roberts (1983), Edwin and Roberts (1983), Bogdan (1984, 1987a,b), Cally (1985, 1986), Davila (1985), Bogdan and Zweibel (1987), Abdelatif (1988), Anton (1989), Ryutova (1988), Evans and Roberts (1989), Ferriz Mas and Schüssler (1989) and Ferriz Mas *et al.* (1989).

The perturbations to the stationary state have generally been assumed to be adiabatic. Exceptions are: Webb and Roberts (1980a,b) and Roberts (1983), who include radiative damping, as approximated by Spiegel's (1957) formula for Newton's law of cooling (cf. Sect 5.4.8). The plasma is always assumed to be inviscid and perfectly conducting.

In the unstratified case the linear wave modes are well understood, even for thick flux tubes (cf., e.g., Thomas 1985). A thick tube has a purely torsional Alfvén mode as the only truly incompressible mode. An infinite number of compressible modes are possible which differ mainly in their radial dependences that, not surprisingly in cylindrical coordinates, are described by Bessel functions. In contrast to thin tubes, which know only a single longitudinal mode, thick tubes have fast and slow magnetoacoustic modes that may exist as body or as surface modes. The former are radially propagating within the tube and radially evanescent outside it. See Wilson (1980b), Spruit (1982), Edwin and Roberts (1983) or Evans and Roberts (1989) for their dispersion relation. The latter are radially evanescent both outside and inside the tube and have their maxima at the flux tube boundary; see Wentzel (1979b), Wilson (1980b) or Edwin and Roberts (1983) for the dispersion relation. Another difference between thin and thick tube modes is that in thick tubes the transverse wave mode is compressible, while in thin tubes it is Alfvén-like (kink mode). Note also that in the absence of gravity there is no cutoff frequency for waves propagating along the tube. In the presence of gravity only the thin tube case has been studied in detail. The basic wave modes of a thin flux tube in a stratified atmosphere have been described in Section 3.4.

The propagation of a wave pulse in a flux tube has been investigated by Rae and Roberts (1982), who found the formation of a wake behind the initially excited pulse. Wave propagation in a twisted flux tube has been considered by Bogdan (1984) and waves in a uniform distribution of magnetic flux tubes by Bogdan (1987a,b) and Bogdan and Zweibel (1987). Spruit (1984) has followed the propagation of transverse waves along a series of merging flux tubes.

The wave modes in flux *slabs* have been studied by e.g. Cram and Wilson (1975), P.R. Wilson (1978a,b), Roberts (1981b) and Edwin and Roberts (1982). The related problem of surface waves at a magnetic interface has been investigated by, e.g., Parker (1974) for the incompressible case and more generally by Wentzel (1979a), Roberts (1981a), Miles and Roberts (1989, 1992) and Miles *et al.* (1992). For a review see Roberts (1991).

Qualitatively new results are obtained from even weakly non-linear calculations. Roberts and Mangeney (1982) showed that in a homogeneous flux slab the slow sausage mode is described by the so-called Benjamin-Ono equation which allows soliton solutions. Roberts (1985) has derived the non-linear equation describing sausage modes in flux tubes (Leibovich-Roberts equation) and shown that it may have solitary solutions. The properties of the equation have been further studied by Bogdan and Lerche (1988) and numerical solutions have been found by Weisshaar (1989), cf. Molotovshchikov and Ruderman (1987). Another effect of non-linearity is the presence of shocks for waves with sufficiently large amplitudes. The properties of shocks in flux tubes have been investigated analytically by Ferriz Mas and Moreno Insertis (1987) and Ferriz Mas (1988, 1990) and numerically (including gravity, radiation, etc., but neglecting the elasticity of the magnetic field) by Herbold *et al.* (1985) and Ulmschneider *et al.* (1987). The non-linear development of a transverse mode similar to the kink mode has been numerically investigated by Ulmschneider *et al.* (1991) and that of the Alfvén mode by Hollweg *et al.* (1982). Ulmschneider *et al.* (1991) find that a transverse wave, excited by purely horizontal foot-point shaking, in turn excites a longitudinal wave. Suematsu *et al.* (1982), Shibata and Suematsu (1982), Hollweg (1982) and Sterling and Hollweg (1988) have argued that a non-linear sound-wave pulse guided by a flux tube, upon impinging on the transition zone can lift it to higher levels and produce a spicule, cf. Shibata (1982) and Cheng *et al.* (1991). Similarly, Shibata *et al.* (1982) have proposed that magnetically guided sound pulses are the origin of surges. Haerendel (1992), on the other hand, proposes that it is weakly damped Alfén waves which drive spicules. Finally, non-linear calculations of flux-tube oscillations and standing waves have been carried out by Hasan (1984, 1985, 1986), Venkatakrishnan (1985) and Knölker *et al.* (1991).

How are the waves damped and dissipated? For compressible modes (electromagnetic) radiative damping is probably the most important damping mechanism. The proper inclusion of radiative damping requires a coupling of the radiative transfer into the energy equation. This step has been carried out in full detail only by Herbold *et al.* (1985), Ulmschneider *et al.* (1987, 1991) and Knölker *et al.* (1991). Herbold *et al.* (1985) and Ulmschneider *et al.* (1987) consider acoustic tube waves, i.e. purely acoustic waves guided by a rigid tube, and include NLTE effects in the 1-D radiative transfer. Knölker *et al.* (1991) restrict themselves to a grey atmosphere in LTE, but carry out a full 2-D radiative transfer in an elastic flux tube. At a somewhat simpler level, Massaglia *et al.* (1989) and Hasan (1990) have coupled oscillations with a radiation field calculated in the Eddington approximation. Finally, Newton's law of cooling has been applied by Webb and Roberts (1980a,b), Roberts (1983), Hasan (1985, 1986) and Venkatakrishnan (1985).

Compressible wave modes may also be damped by exciting acoustic waves in the non-magnetic surroundings of flux tubes, i.e. by acoustic radiative damping. As long as the phase speed ω/k of the tube modes is lower than the external sound speed, waves excited in the external medium by the passage of the internal waves

are evanescent and cannot transport any energy away from the tube. However, as first pointed out by Ryutov and Ryutova (1976), if the internal phase velocity is larger than the external sound speed, the vibrations of the tube may excite sound waves in the environment that propagate away from the tube and carry energy with them. These "leaky" modes of the tube have also been studied by Roberts and Webb (1979), Spruit (1982), Davila (1985) and Cally (1986).

In contrast to damping mechanisms by which the energy in a wave is converted into energy in another (acoustic or electromagnetic) wave and may be transported away, dissipation mechanisms are local and lead to a heating of the local plasma. The viscosity and the resistivity of the plasma are mainly responsible for the dissipation of the energy in the wave modes of a flux tube. However, they become efficient only at relatively small length scales corresponding to a few km in the photosphere. Various processes can produce such length scales in the presence of waves. Examples are shock formation (e.g. Herbold *et al.* 1985, Ulmschneider *et al.* 1987), resonant absorption (Ionson 1978, cf. the review by Davila 1991) and phase mixing (e.g. Heyvaerts and Priest 1983, Lee and Roberts 1986, but see also Parker 1991). Shocks are important for the truly compressible modes (e.g. longitudinal waves in thin tubes) in a stratified atmosphere, while resonant absorption and phase mixing act on Alfvénic waves in non-uniform magnetic fields.

How are flux-tube waves and oscillations excited? The basic excitation mechanisms according to current thinking are overstability, coupling to the global p-modes, buffeting by granulation (turbulent excitation) and, for torsional Alfvén waves, interaction with whirl flows. Overstability has been studied by, e.g., Hasan (1986), the scattering and absorption of p-modes by small flux tubes by, e.g., Bogdan and Zweibel (1987), Bogdan (1989), Goldreich *et al.* (1991), Rosenthal (1992), cf. Spruit and Bogdan (1992). MHD wave excitation by turbulence has been studied in a row of papers by Musielak, Rosner and Ulmschneider and reviewed by Musielak (1991). Schüssler (1986) has pointed out that torsional Alfvén modes can be excited by whirl flows surrounding the flux tubes. If the surface of a flux tube is rough, as it is expected to be in nature, then the flows can transfer momentum and energy into the Alfvén waves. Schüssler (private communication 1991) has studied the response of the flux tube atmosphere to a thermal disturbance near the $\tau = 1$ level and finds that a standing wave mode is produced with a period of 4 minutes, similar to the period found in simulations of the non-magnetic atmosphere. Venkatakrishnan (1986b) has studied the non-linear response of a flux tube of fixed "length" to external pressure fluctuations and finds that large amplitude velocity oscillations can result when the frequency of the imposed fluctuations equals the resonance frequency of the tube. Hasan (1984, 1985) found that a convective collapse leads to overstability, as first suggested by Spruit (1979). Hasan followed the non-linear development of the overstable oscillations through a number of periods. They soon reach an almost constant amplitude and possess a period of approximately 20 minutes. The horizontal exchange of radiation has been invoked as the driver of overstable oscillations (e.g. Roberts 1976).

Musielak and Rosner (1987, 1988) first considered the turbulent excitation of MHD waves in a stratified, but otherwise uniform magnetic field. From comparisons with observations of X-ray fluxes on cool stars (Vaiana *et al.* 1981, Rosner *et al.* 1985), they concluded that the wave luminosity produced in this manner is grossly insufficient to explain the observations. Musielak *et al.* (1987, 1989) then considered the excitation of waves in flux tubes by turbulence in the non-magnetic atmosphere surrounding the tubes (they assumed zero turbulence inside), with particular emphasis on longitudinal waves. Again they found that the wave energy fluxes produced in this manner are too low by two orders of magnitude to heat the lower chromosphere, where these waves are expected to dissipate through shocks (Herbold *et al.* 1985). Finally, Musielak *et al.* (1990) investigated the turbulent excitation of the transverse tube mode (kink mode). They again compared energy flux transported by the wave with cool-star X-ray fluxes and found that they could roughly reproduce the observed magnitude and the range of observed fluxes. Their work strongly supports the notion that kink mode waves are more important for the energetics of the outer atmosphere than other wave modes. Other arguments in favour of the kink mode have been presented by Spruit (1981b) and Thomas (1985). Spruit compared the cutoff frequencies of longitudinal and transverse tube modes, i.e., ω_{CT} and ω_{CK}, respectively. Both frequencies may be expressed in terms of the acoustic cutoff frequency ω_{CS},

$$\omega_{CT}^2 = 4\omega_{CS}^2 \left(\frac{2}{\gamma\beta + 2}\right) \left(\frac{\beta}{2}\left(\frac{\gamma - 1}{\gamma}\right) + \frac{9}{16} - \frac{1}{2\gamma}\right) \tag{5.3}$$

and

$$\omega_{CK}^2 = \frac{\omega_{CS}^2}{2\gamma(2\beta + 1)}, \tag{5.4}$$

where γ is the ratio of heat capacities and $\beta = 8\pi p/B^2$. For $\gamma = 5/3$ and $\beta = 1$, the cutoff of the longitudinal mode (tube mode) is $\omega_{CT} = w_{CS}$, while $\omega_{CK} = 0.32\omega_{CS}$. Since in the photosphere $\omega_{CS} \approx 3 \times 10^{-2}$ s^{-1} $\approx \omega_{CT}$ (corresponding to a period of 200 s) this implies that $\omega_{CK} \approx 9.6 \times 10^{-3}$ s^{-1} (period of 650 s). As pointed out by Spruit, the typical lifetimes of granules (5–10 minutes, e.g. Title *et al.* 1989) correspond approximately to $1/\omega_{CK}$, but are considerably longer than $1/\omega_{CT}$. Spruit concludes that granules can therefore excite propagating transverse waves rather efficiently, but longitudinal waves only very inefficiently. Even for an average β of approximately 0.3, suggested by the investigation of Rüedi *et al.* (1992a), $\omega_{CK} \approx 0.43\omega_{CS}$ remains well below $\omega_{CT} \approx 1.2\omega_{CS}$. However, the work of Ulmschneider *et al.* (1991) has demonstrated that an initially excited transverse wave produces a longitundinal mode after some time, so that above some height both are probably present at similar amplitudes.

In summary, wave propagation, damping and dissipation in flux tubes, particularly in thin flux tubes, is well studied. The excitation of these waves is somewhat

less well investigated, so that the relative amount of energy in the different wave modes is not yet clear, although it is argued that kink mode waves are more easily excited by granular buffeting than longitudinal waves.

5.6. Size, Shape and Distribution

5.6.1. Sizes

Although the size spectrum of sunspots is relatively well studied (e.g. Bogdan *et al.* 1988), less is known about the sizes of the smallest magnetic elements (flux tubes) and of weak field patches. Early observations indicated sizes greater than $1''$. For example, Beckers and Schröter (1968a) found knots to be $1.3''$ in diameter and Simon and Zirker (1974) also found relatively large patches of field with diameters of 1–$3''$. Later observations have often not supported their conclusions. Thus, Tarbell and Title (1977) found that in spite of their spatial resolution of $1.5''$, they still obtained $B/\langle B\rangle$ ratios of 3–12 (i.e. $0.08 \lesssim \alpha \lesssim 0.3$) and concluded that Simon and Zirker mistook clusters of magnetic elements for single ones. On the other hand, Dara-Papamargaritis and Koutchmy (1983) find results similar to those of Simon and Zirker (1974).

The smallest observed magnetic features are smaller than $0.3''$ according to Ramsey *et al.* (1977). The limit is set by seeing. Recently, Keller (1992a) finds from speckle reconstructions that the smallest magnetic features have diameters smaller than or equal to $0.27''$, the diffraction limit of the Swedish Solar Tower. Indirect determinations, based on the smallest measured flux, give minimum diameters of 390–550 km (Wiehr 1979, derived from a measured minimum flux of 2.4×10^{18} Mx, assuming a field strength of 1000–2000 G) and 35–130 km (Wang *et al.* 1985, from a minimum measured flux of one to several times 10^{16} Mx if the fields are in kG form). The Wang *et al.* limit is set by the sensitivity of their instrument, while Wiehr claims that his limit is solar. However, Zirin (1987) cites the value found to be the minimum by Wiehr (1979), 2.4×10^{18} Mx, as the *typical* flux in small magnetic features. There is also some doubt concerning the diameters deduced from the flux measurements of Wang *et al.* (1985). They followed cancelling magnetic features to the limit of their visibility. If, as is generally assumed (cf. Sect 5.7), cancellation implies the removal of flux from the photosphere, then the final flux at the end of a cancellation process may well be zero. It makes little sense to ascribe an area to the visible flux during the final stages of the cancellation process (e.g. during the submergence of a loop).

Another indirect, but still Stokes V based, determination of the size of small magnetic features is due to Zayer *et al.* (1989). From an analysis of the Fe I 15648.5 Å line at a sufficiently large limb distance, they concluded that the widths of the magnetic features in the observed region must lie between 60 and 300 km, depending on the assumed geometry of the magnetic element. Unfortunately, there are a number of assumptions and simplifications in their analysis and their result must be treated with caution. For example, they make simplifications in the assumed geometry (e.g. in cylindrical geometry only the central plane is considered), and

they implicitly assume a relatively thick flux-tube boundary, over which the field strength decreases to zero. If the boundary layer thickness is substantially reduced, then the behaviour of the line at small μ values can be significantly affected. Such indirect techniques may well have a potential for the future, but have to be developed further first.

Another approach is to determine the sizes of proxy indicators of the magnetic field. If we assume an exact correlation between the numbers and sizes of magnetic elements and white-light facular points, then sizes become easier to study. Facular points are usually observed to be smaller than 250 km (Mehltretter 1974, Spruit and Zwaan 1981, Muller and Keil 1983) and many more with sizes smaller than the best spatial resolution of 150–200 km may lie undetected. In a quiet network region Muller and Keil (1983) found a mean size (after correcting for atmospheric and telescope-induced smearing) of approximately $0.2''$, with only very few points being larger than $0.5''$. In an active region Von der Lühe (1987) found a bright structure with a width less than 100 km after speckle-interferometric reconstruction. Harvey (1972) and Harvey and Breckinridge (1973) had earlier found evidence for features with scales of 0.2–$0.4''$ in faculae from wave-front division and speckle interferometry, respectively.

Spruit and Zwaan also infer the presence of such small elements from estimates of the effects of seeing. From the average magnetic flux per bright point, Mehltretter (1974) was able to derive an average size (the magnetogram had considerably lower spatial resolution than his filtergram). Assuming $B = 1000$ G the *average* diameter turns out to be 200 km, for $B = 1500$ G it becomes 170 km. Note that although this estimate is also based on the assumption that all bright points are magnetic and vice versa, unlike the other size determinations based on bright points it does not assume that the size of the bright points is identical to that of the magnetic elements. In an active region Spruit and Zwaan (1981) have found sizes to range between their best resolution of $0.3 - 0.4''$ (bright facular points) and $4''$ (dark pores). Spruit and Zwaan (1981) assumed that structures of intermediate size exist, but are not easily visible, since they have the same brightness as the quiet photosphere.

It must be cautioned that, although there is a good correlation between bright points and magnetic flux in relatively quiet regions (Mehltretter 1974), the exact relation, particularly in active regions, is still unclear. Recall, e.g., the brightness vs. spatially averaged field strength curves of Frazier (1971), or the dependence of δ_c on the size of the magnetic elements (Keller 1992a) and on the magnetic filling factor (Solanki and Brigljević 1992, Section 5.4.2). Therefore, sizes derived from brightness structures should be quoted with care.

Spruit and Zwaan (1981) have proposed a subdivision of small-scale magnetic features into three categories according to their magnetic fluxes. Features with fluxes less than 10^{18} Mx correspond to what may be called magnetic elements or magnetic points, for fluxes of 10^{18}–10^{19} Mx the features are termed magnetic knots and, finally, features with fluxes greater than 10^{19} Mx are seen as pores. The existence of magnetic elements and of pores is undoubted. Schüssler (1984) and

Knölker and Schüssler (1988), however, have argued against the interpretation of magnetic knots as intermediate sized flux tubes, with fluxes between 10^{18} and 10^{19} Mx.

The argument of Schüssler (1984) is based on stability considerations. Whereas larger magnetic features with fluxes greater than 1–6 $\times$ 10^{19} Mx (pores, sunspots) are stabilized against the fluting or interchange instability by the extremely strong expansion of the field and the resulting buoyancy of the tubes (Meyer *et al.* 1977), this mechanism does not work for smaller tubes. Schüssler (1984), and later Steiner (1990) for more sophisticated models, showed that a whirl flow of approximately 2 km s^{-1} can stabilize sufficiently small magnetic flux concentrations ($\Phi \lesssim 1 - 5 \times 10^{17}$ Mx). Schüssler (1984) was unable to find any mechanism stabilizing tubes of intermediate size, i.e. tubes corresponding to magnetic knots, against fluting. Schüssler (1986) argued that such a tube would break up into smaller magnetic elements within an Alfvén transit time of one minute. The resulting elements could then be individually stabilized by whirl flows. As pointed out by Schüssler (1990) the equations for the magnetic field and for vorticity are formally the same. Therefore, it is to be expected that flux tubes and the vortical flows needed to stabilize them are concentrated at the same positions. The 3-D calculations of Nordlund (1985a) exhibit strong vortical flows in the narrow downflowing fingers of the granular velocity field, due mainly to the conservation of angular momentum (bathtub effect). Vortices are observationally accessible only on the larger mesogranular scale (Brandt *et al.* 1988, Simon and Weiss 1989).

The argument of Knölker and Schüssler (1988) against magnetic knots as single magnetic structures rests on MHD model calculations of structures of this size (at least in one direction, their models being in slab geometry). They find that such structures are much darker and cooler than empirical models of magnetic features. From this they conclude that the average size of the magnetic features is small (diameters $\lesssim$ 200–300 km), even in regions with a high magnetic filling factor. Due to the lower δ_c values recently observed by Solanki and Brigljević (1992) and Keller (1992a) in active regions, the model calculations of Knölker and Schüssler are no longer too cool in the lower photosphere. Differences between the calculations and the observations in the upper photosphere are less critical, since they can be explained by the lack of mechanical heating (and also a proper radiative transfer) in the theoretical models.

Therefore, the main argument against the existence of magnetic knots is their instability to fluting. It may be that the importance of this instability decreases substantially in regions with large filling factors, when the intergranular lanes are almost completely filled with magnetic field. A bundle of field lines breaking away from one flux tube will soon find itself being pushed towards and merged with the same or another flux tube. Thus, a dynamical equilibrium is expected with magnetic features constantly changing shape and exchanging flux, as suggested by the 3-D simulations of Nordlund (1983, 1986). The size distribution of magnetic features resulting from this picture depends on the filling factor. For large filling

factors the presence of knot-sized magnetic features may well be unavoidable.

This scenario is supported by the recent calculations of fluting instability carried out by Bünte *et al.* (1992a). They find that tubes whose field satisfies the complete magnetohydrostatic force balance equation (including all tension terms) are considerably more stable to fluting than the simpler thin tubes considered by Schüssler (1984). Although the instability is strongest for tubes of intermediate size, even these can be stabilized by a whirl flow of up to 2 km s^{-1} (evacuated tubes) according to Bünte *et al.* (1992a). Thus, there is currently no convincing argument against the existence of flux tubes of all sizes, although the sensitivity of the fluting instability to the details of the atmospheric structure (Bünte *et al.* 1992a) suggests that the last word on this subject has not yet been spoken.

From a theoretical point of view the minimum size of flux tubes is best discussed by considering the two paths by which a small flux tube may be created. The first involves the convective collapse of initially relatively weak fields, the second the breaking away of a small tube from a larger one through fluting. In the first case, a critical minimum diameter is reached when the horizontal optical depth across the tube becomes of order unity. Then the radiation couples the interiour of the tube completely with the surroundings and inhibits the cooling required to initiate a convective collapse (Schüssler 1986, Venkatakrishnan 1986a). In the lower photosphere the critical diameter corresponds to a few kilometers. The second path also yields a critical diameter of a couple of kilometers (Schüssler 1990). At such scales ohmic diffusion becomes relevant and the flux tubes disperse into patches of weak field.

Finally, there is the question of the sizes of weak field patches. If the intranetwork field is assumed to be weak, then the true sizes of the individual intranetwork field elements depends critically on the assumed field strengths, which are uncertain by a factor of 100 (are intranetwork field strengths 10 G or 1000 G?). Another approach has been to set upper limits on sizes of patches by assuming that only a single weak-field patch is present within the spatial resolution element of spectra of the Fe I 15648.5 Å line obtained by Livingston (1991, cf. Section 5.1.4). Diameters derived in this manner range from 400 km to 2000 km. However, it is easily possible that smaller weak-field patches have escaped detection due to the limited sensitivity of the observations. For example, Kitt Peak magnetograms show intranetwork features that have 10-100 times less flux than the smallest weak-field features visible in the infrared spectra.

In conclusion, flux tubes come in a range of sizes. The smallest still lie below the best achievable spatial resolution, the largest are sunspots. Theoretically, a limit of a few 10s of km can be set on the smallest possible flux tubes with kG fields. There is currently no compelling observational or theoretical evidence against a continuous distribution of sizes. The peak of the size distribution appears to shift towards larger flux tubes in regions with large filling factors.

5.6.2. Shapes

Pores, with diameters of a couple of arc s exhibit the same richness of shape as sunspots, with almost circular examples coexisting with extremely elongated or complex ones. Magnetic elements (knots), being closer to the spatial resolution limit in size, do not divulge the secrets of their outlines easily. Facular points appear round, suggesting flux tubes, but some brightness structures reconstructed from speckle interferometry are considerably elongated (Von der Lühe 1987), reminiscent of flux slabs. However, this is not necessarily so. The speckle reconstructed images of De Boer and Kneer (1992) suggest that elongated structures often break down into rows of bright points. Finally, Keller (1992a), in his reconstructed image, finds both round and elongated magnetic structures. Keller (private communication 1992) finds an example of an elongated structure in the brightness image, which breaks up into points in the magnetic image.

The vertical shape of magnetic elements is easier to determine. Due to magnetic flux conservation the field must expand with height in order to compensate for the measured decrease in field strength (e.g. Equation 3.24 in the thin tube approximation). The exact amount of the expansion depends on the size of the magnetic feature, on the horizontal variation of the gas pressure within the tube, on the ratio of the internal to external pressure scale height and on the filling factor at some fiducial height (Pneuman *et al.* 1986, Steiner and Pizzo 1989, Solanki and Steiner 1990).

The expansion, on a larger scale, has been directly observed by Harvey and Hall (1971), Giovanelli (1980), Giovanelli and Jones (1982), in active regions and Jones and Giovanelli (1983), in quiet unipolar regions. Magnetograms in lines formed in the chromosphere (e.g. He I 10830 Å, Harvey and Hall, or Ca II 8542 Å, Giovanelli and Jones), and partly the upper photosphere, show considerably larger structures than magnetograms in middle or lower photospheric lines. The observations were interpreted by Giovanelli and Jones as representing magnetic canopies, i.e. almost horizontal field lines overlying a mainly field-free atmosphere, with a lower boundary in the upper photosphere in active regions (where the magnetic filling factor is large) and in the lower chromosphere in quiet regions (with low magnetic flux density). Note that some of the canopies observed in active regions, mainly the very low ones, probably are sunspot superpenumbrae (Giovanelli and Jones 1982, Giovanelli 1982, Solanki *et al.* 1992b) and are not directly related to the expansion of magnetic elements. The observations and their interpretations have been reviewed by Jones (1985).

Other observations also indicate the expansion of magnetic features. For example, expanding flux tubes are the most promising and natural geometry in which to explain the observed Stokes V asymmetry (Section 5.5.3), or the higher a brightness structure is formed in the atmosphere, the larger it becomes (e.g. Hale and Ellerman 1903, Simon and Noyes 1971, Dunn and Zirker 1973, Athay 1986). MacKinnon and Brown (1989, 1990) have made use of the observed limb brightening of solar flares at γ-ray energies larger than 10 MeV (Rieger *et al.* 1983, Vestrand *et al.*

1987) to set some limits on the expansion of the field between the photosphere and the corona. Although the method is rather indirect, it suggests that most of the field expansion occurs in the photosphere and chromosphere. There is some evidence in their analysis, again indirect, against magnetic canopies. However, this may have to do with the assumption of a horizontally constant field (except at the magnetic to non-magnetic interface), a condition that is patently not fulfilled by MHD models of canopies (Solanki and Steiner 1990).

A combination of theoretical ideas on the stability of magnetic features and the observational evidence that magnetic elements are concentrated into the elongated dark intergranular lanes suggests the following picture of the shape of magnetic elements: In and below the lower photosphere any flux sheet (i.e. slab) gets quickly torn into shreds due to its considerable instability to fluting. Therefore, the magnetic elements are expected to resemble flux tubes in these layers. With increasing height in the atmosphere the expanding field of each element begins to merge with that of its nearest neighbours. These probably are located in the same intergranular lane, so that over a certain height range (middle and upper photosphere, depending somewhat on the average field strength) the fields have merged along the intergranular lanes, but have not expanded sufficiently to merge across the body of the granule. In this height range flux slabs probably correspond more closely to reality. Yet higher in the atmosphere the field expands rapidly, forming a magnetic canopy and filling all the available space. In essence, this picture suggests the need for detailed 3-D modelling.

5.6.3. Distribution

Small-scale magnetic features are found at all latitudes. They form the plage or facular areas of active regions, and are otherwise concentrated mainly in a network with typical cell sizes of 30'000 km corresponding closely to the boundaries of supergranular velocity cells (e.g. Simon and Leighton 1964, Frazier 1970, Simon *et al.* 1988). Indeed, the boundaries of supergranular cells are best identified in magnetograms or in spectroheliograms taken in Ca II K or in a similar, temperature sensitive line. The exceptions are intranetwork fields, which, as the name suggests, are best seen in the interiours of supergranular cells (Livingston and Harvey 1975, Martin 1984, 1988). However, there is no evidence that they are absent in the network or within active regions. The weak-field component visible in many infrared profiles possibly represents intranetwork fields in the vicinity of strong fields.

In contrast to the quiet network, which is dominated by the supergranular scale, no magnetic voids (or relative voids) of similar size are known in active regions. However, smaller cells with diameters of half the typical supergranular value are defined by the magnetic distribution in active regions (e.g. Ramsey *et al.* 1977, Zwaan 1978). Finally, the third scale on which small magnetic elements appear to from a 'network' is that of the granulation. Magnetic elements are distinctly associated with the dark downflowing intergranular lanes (Title *et al.* 1987a, Solanki 1989, Lundstedt *et al.* 1991, Bünte *et al.* 1991, 1992b), a correlation also found

for the bright points seen in white light and for the filigree (e.g. Mehltretter 1974, Muller 1983, Muller *et al.* 1989). The granulation associated with magnetic features is abnormal (Dunn and Zirker 1973), with reduced contrast (e.g. Immerschitt and Schröter 1988, Brandt and Solanki 1990, Hanslmeier *et al.* 1991), longer granule lifetimes (Title *et al.* 1989), different cell sizes (Title *et al.* 1990a,b) and different cell shapes (Muller *et al.* 1987). The fractal dimension of the magnetic distribution in plages is found to lie between 1.45 and 1.60 (Schrijver *et al.* 1992).

Fields can be distributed on the solar surface in bipolar regions (active regions, ephemeral regions), in large monopolar regions (e.g. monopolar network, enhanced network) and in mixed-polarity regions (parts of the network, intranetwork areas). The number of bipolar (active) regions present on the sun increases rapidly with decreasing area. The smallest clearly defined ones, the ephemeral regions (e.g. Harvey *et al.* 1975, Martin 1990), are also the most numerous (cf. Stenflo 1991c). Unlike the larger active regions, which are confined to the low-latitude sunspot belts, ephemeral regions are found at all latitudes. Even more numerous are small bipolar regions of the intranetwork field, but according to Martin (1988), it is extremely difficult to associate one intranetwork element with a particular element of the opposite polarity. It is even unclear whether most of the field lines emerging within a single intranetwork element connect to a single other element, or are distributed among various elements. The relation between the distribution of magnetic elements and the convection has been studied theoretically by Meyer *et al.* (1979), Schmidt *et al.* (1985) and Nordlund (1983, 1985b, 1986), but see also the flux expulsion calculations reviewed in Section 5.7.3. Meyer *et al.* (1979) and Schmidt *et al.* (1985) have followed flux tubes dragged along by the flow in prescribed cellular velocity fields representing supergranulation in 2-D (Meyer *et al.*) and granulation and supergranulation in specific 3-D (Schmidt *et al.*) geometries. They find that the motion and the final position of the flux tubes depends largely on their flux, both in the granular and the supergranular case. Tubes with fluxes less than 10^{18} Mx are drawn by the flow to the edges of the convection cell (i.e. to the network, respectively the granular downflow lanes). Tubes with fluxes larger than 10^{18} Mx are, on the other hand, drawn towards the centres of the supergranules, respectively granules, and end up in the central upwelling regions.

The result for small magnetic features is confirmed by observations (Title *et al.* 1987a, Solanki 1989). Their result for larger features is somewhat more problematic. It may well be true for sunspots, which are generally surrounded by outflowing moat cells that may correspond to the supergranule in the theoretical calculations (Sheeley and Bhatnagar 1971, Sheeley 1972, Meyer *et al.* 1974). However, outside active regions no concentration of magnetic flux is observed at the centres of supergranules (recall that no supergranular cells are visible inside active regions). Taken at face value, this implies that either the convective flow pattern of supergranules or the flux-tube shape is different from those assumed by the above authors (cf. Parker 1979b), or else only few tubes with a flux larger than approximately 10^{18} Mx exist outside active regions. The latter possibility appears unlikely.

The presence of a large flux tube should considerably affect the granular velocity field and should itself cause the granulation pattern to change (abnormal granulation, see above). This view is supported by Deinzer *et al.* (1984) and Knölker *et al.* (1987), who find that the very presence of a flux tube produces a convective cell with a downflow surrounding the flux tube or slab, due to the inflow of radiation into the (convectively stable) tube. Large tubes, therefore, inherently violate one of the assumptions of Schmidt *et al.* (1985), namely that the convective pattern is not affected by the field. Their results for this case should consequently be treated with caution.

Nordlund (1983, 1985b, 1986) has studied the dynamical evolution of the field in the presence of granules, with the influence of the field on the convection taken into account. He found that the flux was invariably deposited in the intergranular lanes, even for relatively large fluxes, i.e. for sufficient flux to fill the lanes with equipartition fields.

Finally, theoretical studies aimed at deriving the global solar distribution of the magnetic field are largely based on dynamo theories (e.g. Schüssler 1983, Ruzmaikin 1990, Hoyng 1990). The observation and theory of global patterns of the magnetic field are not considered further here.

In summary, small flux tubes are found in bipolar active regions limited to low latitudes and in quiet regions over the whole solar disc. The field is swept by the convective flow to the edges of supergranules and granules, where it is also observed.

5.7. Lifetimes and Evolution

5.7.1. Lifetimes

As argued in Section 4.8.3, it is currently extremely difficult to determine lifetimes of individual magnetic elements due to their small sizes. Ramsey *et al.* (1977) could only set a lower limit of 10 minutes on the lifetimes of the small-scale magnetic structures visible in their high resolution magnetograms. Wang *et al.* (1985) set a lower limit of one hour on the lifetimes of features having the weakest detectable fluxes in their magnetograms. It is easier to determine the lifetimes of conglomerates of magnetic elements, like active regions or network clusters and to assume that they are representative of the lifetimes of the individual magnetic elements. Zwaan (1987) lists the following approximate lifetimes: Large active regions with sunspots ($\Phi = 5 \times 10^{21} - 4 \times 10^{22}$ Mx) live for months, small active regions with no complete spots, but with pores ($\Phi = 1 \times 10^{20} - 5 \times 10^{21}$ Mx) live for days to weeks, while ephemeral active regions ($\Phi = 3 \times 10^{18} - 1 \times 10^{20}$ Mx) live for hours, or at the most for a day. For clusters of magnetic elements at network boundaries Zirin (1985) derived a lifetime of 50–100 h, while Wang *et al.* (1989) find an average value of 90 h. For whole cells of the enhanced magnetic network Wang *et al.* (1991) find a mean lifetime of 70 h. Note that the observations used by Wang *et al.* (1989, 1991) are composites of video magnetograms obtained at two stations (in the USA and in China) to minimize interruptions. Zirin (1987) suggests

that the enhanced network lives considerably longer than the quiet network, but gives no numbers.

The relation of these measured lifetimes to the true lifetimes of individual magnetic elements is not straightforward. Magnetic elements may live considerably longer than a conglomerate can keep its identity. For example, the individual magnetic elements forming a cluster may drift apart and dissolve the cluster, although each element remains intact. However, if a magnetic conglomerate dies by flux cancellation, and this appears to be the most common case (Livi at al. 1985, Martin *et al.* 1985a), then the constituent magnetic elements are also destroyed. Thus, the average lifetime of magnetic elements is not expected to be significantly longer than that of the overlying structures. On the other hand, the overlying structure may well outlive its constituents. For example, individual elements may break up and reform continuously, without producing obvious changes in the overlying magnetic pattern.

A lower limit on the lifetimes of elements of the intranetwork field has been set by Sivaraman and Livingston (1982). They found that all the elements of intranetwork flux in their field-of-view survived their observing span of an hour. I am unaware of an upper limit to the lifetime in the literature.

Another approach to measuring lifetimes is to consider easier to observe proxy indicators. In the most relevant such investigations Mehltretter (1974) and Zachariadis (1987) found that bright facular points live only 5–15 minutes, while Muller (1983), Muller and Mena (1987) and Muller and Roudier (1992) found an average lifetime of 17–20 minutes. Similarly, Waldmeier (1940) set a lower limit of two hours and Hirayama (1978) estimated a lifetime of approximately four hours for the larger 'facular granules' observed near the solar limb. However, brightenings and fadings are thermodynamic effects. It is unknown to what extent they are associated with drastic changes of the (presumably) associated magnetic fields. Interestingly, both Muller and Hirayama find evidence that bright features tend to reappear at or near the position previously occupied by a predecessor. This observation supports the interpretation that the lifetimes of bright features give a 'thermodynamic lifetime' that is unrelated to the 'magnetic lifetime'.

Theory makes no quantitative predictions regarding the lifetimes of magnetic elements, which is not surprising in view of the many unknowns. It has even been suggested that it may be senseless to as much as define a lifetime (Nordlund 1985b, 1986), since the magnetic structures keep changing shape and position, breaking apart and merging. More on theoretical ideas related to lifetimes may be found in Section 5.7.5.

Schüssler (1990) has combined observational and theoretical constraints to estimate the minimum lifetime of magnetic elements. Pivotal parameters are the relative fluxes in strong and weak field form. Frazier and Stenflo (1972) estimate that at least 90% of the magnetic flux is in strong-field form. This is confirmed by observations at 1.5 μm, from which a value of approximately 90% is found (Rabin 1992b, Rüedi *et al.* 1992a, cf. Section 5.1.4). If all the weak flux is assumed to be

either undergoing convective collapse, or is being created from the strong field of a dissolving flux tube, then an estimate of the time scales of convective collapse and dissolution provides a minimum lifetime of strong field flux features. Taking a time-scale of 2–5 minutes for the convective collapse (Hasan 1985, Nordlund 1986) and one minute for destruction (Schüssler 1986), a lower limit of 30–60 minutes is obtained. The longer that concentration and dissolution take, the longer the estimate of lifetime becomes. The absence of major downflows in most of the weak field patches seen in the 15648.5 Å line, contrary to the expectations of convective collapse, suggests that either the ratio of formation to destruction timescales must be much smaller than the values used, or a significant amount of the weak field must be present in a relatively stable form. Assuming the cited convective collapse and destruction time-scales to be correct, the infrared results suggest that the minimum lifetime estimate can be increased to well over an hour.

In conclusion, the lifetimes of the small-scale magnetic features are unknown, although they are estimated to live for at least an hour. The lifetime of conglomerates of magnetic elements increases with the amount of flux they contain.

5.7.2. Formation of Magnetic Features: Observations

This subject has been reviewed by Zwaan (1978, 1985, 1987), Brants (1985c), Schüssler (1990) and Spruit *et al.* (1991). The creation of small-scale solar magnetic features begins with the eruption of flux through the solar surface. The observational signature of an emerging flux region (EFR) is the appearance of an initially small bipolar plage with a dark patch between the poles (Sheeley 1969). The poles drift steadily apart with velocities ranging from 0.2 to 1.0 km s^{-1} (e.g. Harvey and Martin 1973, Chou and Wang 1987 and Tarbell *et al.* 1989).* In the core of Hα an arch filament system connecting the plages of opposite polarity is seen to form (Zwaan 1978). In white light mutually aligned abnormally dark intergranular lanes living for approximately ten minutes are seen (e.g. Brants and Steenbeck 1985, Tarbell *et al.* 1989). It is expected that the field strength of the erupting field is well below the kG values observed in mature magnetic elements. Unfortunately, there is no clear evidence for this, although Brants (1985a,b), using data not ideal for the purpose, estimates field strengths near 500 G, a value close to the equipartition field strength near the top of the convection zone. He also presents evidence for highly inclined fields associated with emerging flux. Zwaan (1978) has pointed out that since the spatially averaged field strength during the eruption is often quite large, the true pre-eruption field strength cannot be less than a few hundred G.

Just prior to the appearance of the bipole, a transient upflow has been observed (Bruzek 1967, Frazier 1972, Brants 1985a, Tarbell *et al.* 1989). Shortly after the end of the brief upflow phase, a downflow sets in, with peak velocities reaching 1 km s^{-1} (Tarbell *et al.* 1989) or 1.5–2 km s^{-1} (Kawaguchi and Kitai 1976, Zwaan *et*

* According to Sheeley (1969) and Harvey and Martin (1973), the expansion rate in the first few minutes of development of pairs of CN bright points or ephemeral active regions is on the order of 5 km s^{-1}.

al. 1985, Brants 1985a, cf. Zwaan 1987). It is plausible to assume that the observed downflows represent the draining of mass down the legs of the magnetic loop after its emergence (Frazier 1972, Brants 1985b). Note, however, that Brants (1985b) sees downflows mainly in Stokes I and not in Stokes V, suggesting that they may be concentrated outside the magnetic features. Tarbell *et al.* (1989) see the upflow only in the dark central part of the emerging bipole, while the downflow is located mainly in the bright endpoints of the bipole.

Not all small-scale magnetic features appear to be created through the emergence of new flux. A fraction may be the end result of the decay by fragmentation of larger magnetic features, e.g. sunspots (Gokhale and Zwaan 1972, Harvey and Harvey 1973, Stenflo 1976, Brickhouse and LaBonte 1988). Decaying sunspots are surrounded by mixed polarity moving magnetic features (MMFs), with a slight dominance of the sunspot's polarity (Harvey and Harvey 1973), that are moving away from the sunspot with velocities between 0.5 and 1.5 km s^{-1} (cf. Muller and Mena 1987), possibly due to the moat cell surrounding it (Brickhouse and LaBonte 1988). The MMFs transport net magnetic flux away from the sunspot at approximately the same rate as the decaying sunspot loses it. The lognormal distribution of sunspot umbral sizes (Bogdan *et al.* 1988) is consistent with the hypothesis that smaller umbrae are formed by the fragmentation of large ones. Lee (1992), on the other hand, argues (based on the relatively radial alignment of MMFs to the sunspot, with the pole of opposite polarity being closer to the sunspot) that MMFs carry no net flux away from sunspots and thus are not associated with their decay (he does not actually measure magnetic fluxes, though). Some of the larger magnetic features, and this includes not only sunspots, are formed by the opposite process, i.e. the coalescence of smaller features to form larger ones (e.g. Vrabec 1971, 1974, Smithson 1973, Schoolman 1973, Kömle 1979, Martin 1984, 1988, 1990, Wang and Zirin 1992). Finally, Muller and Roudier (1992) find that network bright points appear when they are compressed between converging granules. It remains unclear whether the magnetic field is also concentrated by the converging granules or whether these only lead to a transient brightening.

No firm evidence for the emergence of flux in the intranetwork regions is available, since no bipoles showing the signature of emergence have yet been observed. According to Martin (1984) the elements or fragments of the intranetwork field appear seemingly spontaneously. This apparent contradiction of Maxwell's equations may have a similar solution as the apparent spontaneous disappearance of flux noted by various authors (see Section 5.7.4). It has probably to do with processes that increase the visibility of the field at the time of its seemingly spontaneous appearance.

According to Martin (1988) the intranetwork field elements flow in approximately radial patterns from their probable birthplace, the supergranule cell interiours, to the boundaries. There they either coalesce with or cancel the network field already present. In contrast, Zirin (1985) claims that most intranetwork elements show a random motion. The magnetic features in the network and in active regions

are also in constant motion (Simon *et al.* 1988), following the dictates of the convection either at the surface or at their anchoring depth. According to Zirin (1985) network elements move much less than elements of the intranetwork field: 0.06 km s^{-1} vs. 0.35 km s^{-1} on average. Ephemeral active regions (Harvey *et al.* 1975) are relatively fast movers, with a pole separation velocity of 0.5 km s^{-1}. Cancelling (or merging) fields are drawn together at a similar rate of 0.3–0.5 km s^{-1} (Zirin 1987). From molecular CN observations Sheeley (1971) concludes that magnetic elements move horizontally over short distances at a rate of approximately 1 km s^{-1}. Ca II mottles forming the network exhibit an rms velocity of 0.15 km s^{-1}, due probably to the supergranular flow pattern (Schröter and Wöhl 1975). Finally, at very high spatial resolution De Boer and Kneer (1992) also find the smallest bright features to be in constant motion.

Interestingly, according to Zirin (1987) the amount of flux emerging in the form of intranetwork fields is one hundred times larger than in ephemeral regions and 10^4 times larger than the flux in sunspots. The consequences of such a predominance of flux emergence at small scales have been discussed by Stenflo (1991c, 1992).

In summary, small-scale magnetic features are formed either following the emergence of new magnetic flux (seen as an expanding bipole) or by breaking away from larger magnetic featuers, e.g. sunspots.

5.7.3. Formation of Magnetic Features: Theory

The solar dynamo is expected to generate a horizontal (toroidal) magnetic flux system near the bottom of the solar convection zone. An instability in this system can lead to the buoyant rise of a bundle of magnetic flux tubes towards the solar surface (Parker 1955, Spruit and Van Ballegooijen 1982, Moreno Insertis 1986, Chou and Fisher 1989, Caligari 1992, Moreno Insertis *et al.* 1992, cf. Moreno Insertis 1992 for a review). As a flux tube floats up it is deformed into a loop shape and a part of its mass drains down its legs. However, the time-scale of the rise of the tube (convective time-scale) is short compared to the time scale of its drainage, so that mass per unit flux is conserved and the tube is hardly evacuated at all. Therefore, it must expand strongly to remain in pressure balance, leading to a strong decrease of the field strength with height, so that, if nothing else happens, the field finally emerges with a strength well below the equipartition value (Moreno Insertis 1986, Chou and Fisher 1989, cf. below).

Although such calculations of the buoyant rise of flux tubes cannot reproduce the surface field strengths, they can roughly reproduce formation times and sizes of active regions. Van Ballegooijen (1984) has invoked the vertical component of the Reynold's stress $\langle \rho_e v_{ez}^2 \rangle$ (where ρ_e = external density, v_{ez} = vertical component of external velocity, $\langle\ \rangle$ = averaging over a horizontal surface) of the external medium as a means of reducing the drop in field strength between the bottom and the top of the convection zone. By assuming the flux tube to be free of convection (cf. the flux expulsion process described below), he succeeds in limiting the drop in the field from the equipartition value B_{eq} at the bottom of

the convection zone to approximately $0.6B_{\rm eq}$ at a depth of 1000 km below the surface. Here, $B_{\rm eq} = \sqrt{4\pi\rho v^2}$ is derived by setting the magnetic energy density $B^2/8\pi$ equal to the kinetic energy density $\rho v^2/2$. $B_{\rm eq}$ should not be mistaken with what stellar astronomers sometimes call an "equipartition field" (e.g. Saar 1990), which actually corresponds to $B_{\rm max}$ in Equation (5.1). Chou and Fisher (1989) also estimate the influence of the turbulent motions in the convection zone and conclude, in contrast to Van Ballegooijen, that these have little effect on the resulting field strengths.

Another mechanism that concentrates the field to the equipartition value is the interaction of B and convection. As pointed out by Parker (1963), and studied in greater detail by e.g. Weiss (1966, 1981a,b), Galloway *et al.* (1977), Galloway and Weiss (1981), Hurlburt *et al.* (1984), Hurlburt and Toomre (1988), cf. reviews by Proctor and Weiss (1982), Hurlburt and Weiss (1987), and Hughes and Proctor (1988), overturning convective cells sweep an initially homogeneous field into regions between the cells within a couple of turnover times. Flux in the cell centre is removed in this process by local reconnection between field lines. The magnetic field continues to be concentrated and locally enhanced until the Lorentz force $\mathbf{j} \times \mathbf{B}$ becomes sufficiently strong to locally inhibit the flow, i.e. until it reaches its equipartition value. Thus the field and the convection appear to mutually expell each other. Parker (1984b) has proposed that the expulsion process leads to an energetically favourable configuration, since it minimizes interference between the magnetic field and convective motions.

The 3-D calculations of Nordlund (1983, 1985b) also illustrate the flux expulsion process and show how an initially homogeneous field is swept into and concentrated in the intergranular lanes. The vertical component of the vorticity shares the same fate. As pointed out by Schüssler (1990) this has to do with the formal identity of the equations of motion for B and $\nabla \times \mathbf{v}$ (cf. Nordlund 1985a).

The actual erruption process of a loop of flux through the solar surface has been modelled by Shibata (1980), Shibata *et al.* (1989a, b, 1990, 1992) and Nozawa *et al.* (1992). In these calculations the mass at the top of the loop is pushed up with a velocity of a few 100 m s^{-1} in the photosphere. This may possibly correspond to the observed blueshift seen in the first phase of flux emergence. Later, the calculations show a considerable downflow along the legs of the loop (as first suggested by Nordlund 1977). Shibata *et al.* (1992) pay particular attention to the interaction between the emerging flux and an overlying magnetic canopy. They propose that the jets and shocks formed by the reconnection of the two field components are the underlying cause of UV microflares (Porter *et al.* 1987) and x-ray bright points often associated with emerging magnetic flux.

The field strengths produced by the flux expulsion process are still too small compared to the observed values. Convection, however, has another ace in hand to concentrate the field even more: the convective instability, leading to a convective collapse of the field. The convective collapse has been reviewed by Schüssler (1990, 1992) and Thomas (1990).

The basis for the instability is the superadiabatic effect (Parker 1978). Let us start with a patch of relatively weak field that still allows some convective motions to occur within its confines. An adiabatic downflow within the magnetic patch makes it cooler than its superadiabatically stratified surroundings. A lower temperature implies a lower pressure scale height (Equation 3.20), so that the gas pressure in the photosphere and the uppermost part of the convection zone is reduced. The field is then pressed together by the inwards flowing gas, causing the magnetic pressure to increase until it cancels the gas pressure deficit. The whole process can become a runaway, driving a convective instability (Webb and Roberts 1978, Spruit and Zweibel 1979, Unno and Ando 1979), which can enhance the field strength even more. However, note that the bulk of the field compression is limited to the photospheric and immediately sub-photospheric layers.

How can the process be stopped? Spruit (1979) and Spruit and Zweibel (1979) suggest that a field with a strength above a critical value inhibits convection sufficiently to become stable. Nordlund (1984), on the other hand, has argued that if the lower boundary is kept open, then mass will continue to drain down (moving matter down in a gravitational field lowers the energy) and no stable equilibrium can be reached. Further evidence and arguments in support of his argument have been provided by Webb and Roberts (1978), Hasan (1986) and Schüssler (1990). The contrast between the huge downflows found by Venkatakrishnan (1983) and Hasan (1983), with an open lower boundary, and the oscillatory steady state reached by the calculations of Hasan (1984, 1985), with a closed lower boundary, also provide support for Nordlund's argument. The lower boundary condition appears to be crucial to the type of end state reached. The sun appears to have chosen a closed lower boundary, but it remains unclear why (see Schüssler 1990).

Another problem is that the assumption of adiabaticity is a very poor one near the solar surface, where radiative effects become important. So far the calculations of convective collapse have included only a very schematic radiative transfer, either in the form of the Spiegel (1957) formula for horizontal radiative exchange, i.e. Newton's law of cooling (Equation 5.2), or of a crude vertical radiative exchange (Venkatakrishnan 1985), or of radiative transfer in the Eddington approximation (Massaglia *et al.* 1989).

Inspite of these shortcomings and loose ends, the various convective collapse calculations have produced a number of interesting results. Spruit and Zweibel (1979) found that thin tubes with a depth-independent plasma β are convectively stable for $\beta \lesssim 1.8$, while Spruit (1979) obtained field strengths of 1280–1650 G at $z = 0$ ($\tau = 1$ in the average non-magnetic atmosphere) in the collapsed state. These values are in good agreement with observations, although the observed field strengths tend to cluster near the upper end of the predicted range, between 1400 G and 1700 G. Hasan (1984, 1985) found an oscillatory (even slightly overstable) end state with a mean field strength of 1250 G at 50 km below $z = 0$. His initial field strength was 800 G. Spruit (1979) had earlier predicted such oscillations. Finally, the 3-D calculations of Nordlund (1983, 1986) follow the field through both the flux

expulsion and the convective collapse phase. Unfortunately, the limited horizontal resolution of his spatial mesh, corresponding to 190 km, does not allow him to follow the fields to their fully concentrated state. Therefore, his results, although very exciting at a qualitative level, do not allow a quantitative comparison with observed field strengths.

So far, direct observational evidence of the convective collapse is missing, although Wiehr (1985) claims to have observed its signal. He saw strongly asymmetric, highly redshifted Stokes V profiles in an isolated Ca II K plage. After a few minutes the Stokes V profiles relaxed to unshifted, almost antisymmetric profiles. This observation does sound interesting, but the concurrent *reduction* of the apparent flux by a factor of 3 in as many minutes suggests that it should be treated with great caution. His λ_V values may be corrupted by the low spectral resolution, as mentioned in Section 5.5.2.

In conclusion, after the emergence of new flux in the form of an errupting loop, the surface magnetic field is first concentrated by interaction with convection (flux expulsion) until it reaches a field strength of 400–800 G. Then, in a second step, the field strength is enhanced by the convective collapse (a convectively unstable downflow within the field) until it reaches values that are in good agreement with the measured kG fields.

5.7.4. Destruction of Magnetic Features: Observations

The most common signature of the removal of magnetic flux from the solar surface, both in the quiet sun and in active regions is cancellation (e.g. Martin *et al.* 1985a,b, Livi *et al.* 1985, Wang *et al.* 1988, Martin 1990). During this process magnetic features of opposite polarity approach each other, merge together and disappear, i.e. their fluxes cancel each other. Interpretations of such events in terms of submergence of magnetic loops, or reconnection above or below the solar surface have been given by Zwaan (1978, 1987) and Priest (1987), cf. Section 5.7.5.

Observations in an active region by Rabin *et al.* (1984) support simple submergence of the flux, without prior reconnection. Howard (1992), from the difference between the rotation rates of following and leading polarities of active regions during their development and decay phases, also concludes that at least part of their flux is retracted. There is, however, also an observational case for processes involving reconnection. For example, Martin (1984) finds that none of the ephemeral regions observed by her ever contracted and submerged again. They always cancelled with previously unrelated fields, which can only lead to submergence after reconnection has taken place. It may well be that simple submergence is commom in large, relatively ordered regions, like simple active regions, where the same loop that emerged during the formation of the active region is retracted again. Processes involving reconnection prior to submergence, on the other hand, are expected to be most common in complex active regions and in mixed polarity regions of the quiet sun. Such processes may, however, also be common in the unipolar network and enhanced network, if most of the flux removal there is due to cancellation with

intranetwork field fragments, which are always of mixed polarity.

There exists also another class of observations showing the disappearance of magnetic flux in small, relatively isolated unipolar magnetic features, with no apparent signs of cancellation with opposite polarity flux (Wilson and Simon 1983, Simon and Wilson 1985, Topka *et al.* 1986). Similar observations also exist for the disappearance of the flux in sunspots (Wallenhorst and Howard 1982, Wallenhorst and Topka 1982). The most straightforward interpretation of such observations is diffusion of the concentrated field into a larger patch of weak field which would then escape detection due to the finite sensitivity of the used detectors. Other explanations, like changes in the temperature and brightness of magnetic structures (Stenflo 1984a, Grossmann-Doerth *et al.* 1987) are just as reasonable. Since Martin *et al.* (1985a) and Livi *et al.* (1985) do not see any signs of such a process in their very sensitive magnetograms, the disappearance of a single polarity could well be an artifact of insufficient sensitivity to the magnetic flux (Martin 1988). These alternative explanations of flux disappearance observations are a reminder that all observations of magnetic evolution only show the evolution of Stokes V and the interpretation in terms of fluxes is based on a number of additional assumptions.

Howard (1991) has quantitatively studied flux changes in active regions based on the daily Mt. Wilson magnetograms (cf. Howard and LaBonte 1981). He finds that the average rate of unsigned flux increase and decrease is about the same (his curve resembles a Gaussian with a half-width of approximately $5 \times 10^{20} - 1 \times 10^{21}$ Mx/day). Note that the diffusion of fields also contributes to these rates. The qualitative picture often suggested that active regions appear quickly and decay slowly does not appear to be borne out quantitatively, at least as far as the magnetic flux is concerned.

5.7.5. Destruction of Magnetic Features: Theory

We must distinguish between two distinct ways in which magnetic elements may be destroyed, namely processes that remove magnetic flux from the solar surface and processes that do not. The former are related to cancellation events. If the two cancelling polarities were previously connected then the observed cancellation simply implies the submergence of a flux loop below the surface. This process has also been called flux retraction, since a loop that initially emerged through the surface is pulled back down again. If the cancelling polarities were previously unconnected then the submergence must be preceded by field-line reconnection. Flux cancellation in merging features is expected to be seen only if the reconnection takes place at or above the solar surface. The energy release due to the reconnection may then be directly visible as a local brightening in the relevant atmospheric layers. No flux is removed directly due to the reconnection. Only the subsequent submergence of the Ω loop formed by the reconnection leads to flux removal. However, submergence requires that the initially formed loop is not too large, since the tension forces which act to draw the loop below the surface only become effective if the footpoint separation is less than a few scale heights (Parker 1979a,

Chapter 8). This relatively strong requirement is likely to be fulfilled only by small loops with footpoints consisting of at the most a few photospheric flux tubes, if the separation between the two polarities is of the same order as their diameters at the surface. The expected observational signature of submergence is consistent with the cancellation events seen by Martin and co-workers with the Big Bear video magnetograph.

If reconnection takes place below the surface and the energy release is hidden by the optically thick gas above it, then the two polarities at the solar surface become connected by a U–shaped loop (Spruit *et al.* 1987). Magnetic buoyancy and magnetic tension forces both act in the same direction and make the U–loop float inexorably upwards. A substantial amount of mass may be trapped in the loop. Mass conservation and the strong decrease in density with height lead to the expansion of the tube as it rises. The field strength decreases correspondingly. If the reconnection takes place at sufficient depth, the surface field may become weak enough to be compatible with the field strengths deduced from the weak field component of the 15648.5 Å line and may be one of the sources of the intranetwork field. Observationally, the formation and rise of a U–loop is expected to be difficult to recognize. The visible signs are expected to be two concentrations of opposite magnetic polarity, possibly initially separated by a large distance, each of which diffuses into a patch of weak field as they approach each other, before finally fading away completely as the U–loop passes out of the photosphere.

The loss of flux from the solar surface has been reviewed by Zwaan (1978, 1987), Parker (1984a, 1986), Spruit *et al.* (1987, 1991) and Priest (1987). For a description of the theory of reconnection see Priest and Forbes (1986).

The life of an individual magnetic element is not only limited by processes that cause the flux to disappear from the solar surface. A magnetic feature can also break apart into smaller fragments, or coalesce together with other elements into a larger magnetic feature. In regions with locally a single polarity this may well be the dominant cause of death. The 3-D calculations of Nordlund (1983, 1986) show an almost uninterrupted rearrangement of magnetic flux in the intergranular lanes. In his simulations the lifetimes of the individual magnetic features, if they can be distinguished from each other at all, are similar to the granular lifetimes. The passivity with which the magnetic flux reacts to granular dynamics in his calculations may, however, have to do with the low spatial resolution (coarse spatial grid) of his simulations and the resulting small field strengths.

The most efficient and therefore dominant way of destroying a magnetic feature is by destabilising it. One of the proposed instabilities is the Kelvin-Helmholtz instability caused by a shear between the flow in the external and the internal medium (Schüssler 1979, Tsinganos 1980). Such shear flows are almost certainly present at the boundaries of magnetic elements. The other instability that may lead to the demise of a small magnetic feature is the fluting or interchange instability (Parker 1975b). Although pores and sunspots are stable near the solar surface due to magnetic buoyancy and the very rapid expansion of the field (Meyer *et al.*

1977), smaller flux tubes can only be stabilized if they are situated at the centre of strong whirl flows (Schüssler 1984, Steiner 1990, Bünte *et al.* 1992a). If for some reason, e.g. a change in the surrounding granulation, the whirl flow ceases, the tube is disrupted within an Alfvén travel time, i.e. in less than one minute (Schüssler 1986).

If the tubes are below a critical size, corresponding to approximately 10 km near the solar surface, they become optically thin to the horizontal radiation field. Then the internal temperature and thus the pressure scale height approach the respective external values. The pressure difference in the photosphere is thereby reduced and the field strength is lowered (i.e. raising the temperature undoes what lowering the temperature prior to the convective collapse initially produced). Thus, the finally expected field strength for such minute elements is close to the equipartition value. If the fragments produced by an instability are even smaller ($\lesssim$ 1 km) then ohmic diffusion can lead to a spreading (and weakening) of the field, so that the fragments finally lose their identity. For larger fragments ohmic diffusion is ineffective (cf. Spruit *et al.* 1991). Larger tubes can, however, also be returned to their original diffuse, weak-field state if a sufficiently large upflow takes place within them (anti-convective collapse). Such an upflow may be the result of a particularly vehement upflowing phase of an overstable oscillation.

None of the processes described in this section is expected to produce field strengths significantly below the equipartition value, since the omnipresent granulation tends to reconcentrate the field in the intergranular lanes (flux expulsion). Lower field strengths may be possible within the bodies of supergranules where the average magnetic field strength is very small. A tangled magnetic field component of variable strength is also expected to be produced in a truly turbulent atmosphere.

The scenarios for the death of individual magnetic features have been sketched in greatest detail by Schüssler (1990, 1992) and Spruit *et al.* (1991).

In conclusion, flux tubes are destroyed in mainly two ways, by the submergence of a flux loop below the surface (with or without prior reconnection) and by the return of the magnetic flux to a weak field state. This can be achieved by shredding of flux tubes into smaller entities by either the fluting or the Kelvin-Helmholtz instabilities, by an inverse convective collapse (i.e., a strong upflow in the flux tube), or by the formation of U-loops.

6. Conclusion

The last decades have seen substantial progress on many aspects of theory and observations of small-scale solar magnetic fields. However, the number of unanswered questions, many of them basic to our understanding of solar and stellar activity, is still large. Below I present a subjective selection of such open questions, in no particular order. It has greatly profited from the list compiled by Simon (1990), whose perusal I recommend. Some of the questions will hopefully be answered soon, the answers to others may have to await a new generation of solar physicists,

instruments and computers.

1. What is the size spectrum of magnetic features? Is there a continuous spectrum from magnetic elements to sunspots? How large are the smallest discrete magnetic features?
2. How does the internal temperature of magnetic features vary with their size, packing density, etc?
3. Do magnetic elements have definite lifetimes, or are they in a state of constant decay and renewal? If they have definite lifetimes, how long are these?
4. Are small magnetic features bounded by current sheets? If so, then what is its thickness?
5. Are magnetic elements elongated (slabs), round (tubes), or simply irregular?
6. If magnetic elements (or at least some of them) can be described by flux tubes, then are these flux tubes twisted? Is any such twist stationary or dynamic?
7. How do field strength and temperature within magnetic features vary as a function of height and radial distance from their centre?
8. What is the relative importance of different forms of energy transport in magnetic features?
9. How strongly are magnetic elements (flux tubes) inclined towards the horizontal? Are the inclinations random or aligned on a larger scale? Is the inclination transient or almost permanent? What causes any such inclination or alignment?
10. What is the magnetic field strength in the chromosphere in regions of different photospheric filling factor? How large are magnetic inhomogeneities in the chromosphere?
11. How common are magnetic canopies in the upper photosphere or the lower chromosphere?
12. How can the spatial structuring and filamentation seen in chromospheric lines (e.g. in Hα or in Ca II H and K) be explained in the presence of magnetic canopies?
13. Do molecular CO clouds exist? What fraction of the lower chromosphere do they cover? Where are they located relative to the magnetic features?
14. What are the wave modes of a thick tapered tube in the presence of gravity?
15. How are the different wave modes excited and how are they dissipated in magnetic features?
16. What are the energy fluxes transported by the various wave modes?
17. Are siphon flows across magnetic neutral lines common? Are they restricted only to small loops?
18. Are small magnetic features surrounded by whirl flows? Can these stabilize the flux tubes against fluting?
19. Are the strong fields in magnetic elements produced by a convective collapse?
20. Does the convective collapse invariably lead to an overstably oscillating final state?

21. What is the state of the magnetic field at the moment of its eruption through the solar surface?
22. What causes the disappearance of magnetic flux from the solar surface?
23. How do emerging and pre-existing fields interact?
24. What does the motion of individual magnetic features on the solar surface look like and how can it be described?
25. What is the nature of abnormal granulation?
26. What is the turbulent spectrum of the tangled or turbulent magnetic field component? How is it formed?
27. What is the true amount of magnetic flux in weak-field form? What is the nature of the weak fields seen in the 1.5648 μm line?
28. Do fields with strength below the equipartition value (400–800 G) exist on the sun (excluding turbulent fields), or, what is the true field strength of the intranetwork or inner-network fields? What is the nature of these fields?
29. How are spicules related to magnetic features?
30. How can the centre-to-limb variation and the wavelength dependence of the facular continuum contrast be explained?
31. How do small-scale magnetic features affect the global solar luminosity?
32. Do any differences between the elemental abundances of magnetic and of non-magnetic regions on the sun exist in photospheric layers? If so, why?
33. How large are horizontal transfer effects in spectral lines? How do they affect lines formed in magnetic elements?

Acknowledgements

Discussions with many colleagues have substantially increased my understanding of the subject matter presented here. Numerous older reviews have not only helped me to find the relevant literature, but have also clarified many problems. Notable are reviews by Landi Degl'Innocenti, Parker, Priest, Roberts, Schüssler, Spruit, Stenflo, Thomas and Zwaan. M. Faurobert-Scholl and O. von der Lühe have read and vastly improved Sections 2.5 and 4.8, respectively. U. Grossmann-Doerth, M. Schüßler and J.O. Stenflo have, through their comments, raised this overview from a state of chaos to a semblence of coherency. The critical comments of C.U. Keller to Section 5 have been very helpful.

References

Abdelatif, T.E.: 1988, *Astrophys. J.* **333**, 395
Abdussamatov, H.I., Krat, V.A.: 1969, *Solar Phys.* **9**, 420
Acton, D.S.: 1989, in *High Spatial Resolution Solar Observations*, O. von der Lühe (Ed.), National Solar Obs., Sunspot, NM, p. 71
Acton, D.S.: 1990, Ph.D. Thesis
Akima, H.: 1970 *JACM* **17**, 589
Akimov, L.A., Belkina, I.L., Dyatel, N.P.: 1982, *Sov. Astron.* **26**, 334
Akimov, L.A., Belkina, I.L., Dyatel, N.P.: 1984, *Sov. Astron.* **28**, 310

Akimov, L.A., Belkina, I.L., Dyatel, N.P., Marchenko, G.P.: 1987, *Sov. Astron.* **31**, 64.
Alfvén, H.: 1967, in *Magnetism and the Cosmos*, W. Hindmarsh, F. Lowes, P. Roberts, and S. Runcorn (Eds.), Oliver and Boyd, Edinburgh, p. 246
Anderson, L.S.: 1989, *Astrophys. J.* **339**, 558
Anderson, L.S., Athay, R.G.: 1989, *Astrophys. J.* **346**, 1010
Anton, V.: 1989, Ph.D. Thesis, Universität Göttingen
Anzer, U., Galloway, D.J.: 1983, *Monthly Notices Royal Astron. Soc.* **203**, 637
Arena, P., Landi Degl'Innocenti, E., Noci G.: 1990, *Solar Phys.* **129**, 259
Athay, R.G.: 1986, in *Physics of the Sun, Vol. II*, P.A. Sturrock et al. (Eds.), Reidel, Dordrecht, p. 51
Audic, S.: 1991, *Solar Phys.* **135**, 275
Auer, L.H., Heasley, J.N.: 1978, *Astron. Astrophys.* **64**, 67
Auer, L.H., Heasley, J.N., House, L.L.: 1977, *Solar Phys.* **55**, 47
Auffret, H., Muller, R.: 1991, *Astron. Astrophys.* **246**, 264
Avrett, E.H.: 1985, in *Chromospheric Diagnostics and Modelling*, B.W. Lites (Ed.), National Solar Obs., Sunspot, NM, p. 67
Avrett, E.H.: 1992, in *Infrared Solar Physics*, D. Rabin, J. Jefferies (Eds.), Kluwer, Dordrecht, *IAU Symp.* **154**, in press
Avrett, E.H., Fontenla, J.M., Loeser, R.: 1992, in *Infrared Solar Physics*, D. Rabin, J. Jefferies (Eds.), Kluwer, Dordrecht, *IAU Symp.* **154**, in press
Ayres, T.R.: 1981, *Astrophys. J.* **244**, 1064
Ayres, T.R.: 1990, in *Solar Photosphere: Structure, Convection and Magnetic Fields*, J.O. Stenflo (Ed.), Kluwer, Dordrecht, *IAU Symp.* **138**, 23
Ayres, T.R., Linsky, J.L.: 1976, *Astrophys. J.* **205**, 874
Ayres, T.R., Testerman, L., Brault, J.W.: 1986, *Astrophys. J.* **304**, 542
Ayres, T.R., Wiedemann, G., R.: 1989, *Astrophys. J.* **338**, 1033
Babcock, H.W.: 1947, *Astrophys. J.* **105**, 105
Babcock, H.W.: 1951, *Astrophys. J.* **114**, 1
Babcock, H.W.: 1963, *Ann. Rev. Astron. Astrophys.* **1**, 41
Babcock, H.W., Babcock, H.D.: 1952, *Publ. Astron. Soc. Pacific* **64**, 282
Babcock, H.W., Babcock, H.D.: 1955, *Astrophys. J.* **121**, 349
Bachmann, G.: 1991, *Astron. Nachr.* **312**, 257
Badalyan, O.G.: 1968, *Soln. Dannye* **5**, 105
Badalyan, O.G., Prudkovskii, A.G.: 1973, *Sov. Astron.* **17**, 356
Balasubramaniam, K.S., Venkatakrishnan, P., Bhattacharya, J.C.: 1985, *Solar Phys.* **99**, 333
Balasubramaniam, K.S., West E.A.: 1991, *Astrophys. J.* **382**, 699
Balthasar, H.: 1984b, *Solar Phys.* **93**, 219
Banwell, C.N.: 1972, *Fundamentals of Molecular Spectroscopy*, McGraw-Hill, London
Basri, G.S., Linsky, J.L., Bartoe, J.–D.F., Brueckner, G.E., Van Hoosier, M.G.: 1979, *Astrophys. J.* **230**, 924
Basri, G.S., Marcy, G.W.: 1988, *Astrophys. J.* **330**, 274
Beckers, J.M.: 1969a, *Solar Phys.* **9**, 372
Beckers, J.M.: 1969b, *Solar Phys.* **10**, 262
Beckers, J.M.: 1969c, *A Table of Zeeman Multiplets*, AFCRL–69–0115
Beckers, J.M.: 1976, in *Physics of Solar Planetary Environments*, D.J. Williams (Ed.), American Geophysical Union, Washington, D.C., p. 89
Beckers, J.M.: 1981, in *The Sun as a Star*, S.D. Jordan (Ed.), CNRS/NASA-Publication, NASA SP-450, p. 11
Beckers, J.M., Milkey, R.W.: 1975, *Solar Phys.* **43**, 289
Beckers, J.M., Schröter, E.H.: 1968a, *Solar Phys.* **4**, 142
Beckers, J.M., Schröter, E.H.: 1968b, *Solar Phys.* **4**, 165
Beckers, J.M., Schröter, E.H.: 1969, *Solar Phys.* **10**, 384
Beckers, J.M., Schultz, R.B.: 1972, *Solar Phys.* **27**, 61
Beckers, J.M., Taylor, W.R.: 1980, *Solar Phys.* **68**, 41
Bernasconi, P.: 1992, Diplomarbeit, ETH, Zürich
Bommier, V., Landi Degl'Innocenti, E., Leroy, J.-L., Sahal-Bréchot S.: 1992, in *Methods of Solar*

and Stellar Magnetic Field Determination, M. Faurobert-Scholl, H. Frisch, N. Mein (Eds.), Obs. de Paris, Meudon, p. 211
Bhatnagar, A.: 1967, *Kodaikanal Obs. Bull.* **180**, A13
Bhatnagar, A., Tanaka, K.: 1972, *Solar Phys.* **24**, 87
Biémont, E.: 1992, in *Infrared Solar Physics*, D. Rabin, J. Jefferies (Eds.), Kluwer, Dordrecht, *IAU Symp.* **154**, in press
Blackwell, D.E., Ibbetson, P.A., Petford, A.D., Shallis, M.J.: 1979a, *Monthly Notices Royal Astron. Soc.* **186**, 633
Blackwell, D.E., Petford, A.D., Shallis, M.J.: 1979b, *Monthly Notices Royal Astron. Soc.* **186**, 657
Blackwell, D.E., Petford, A.D., Shallis, M.J., Simmons, G.J.: 1980, *Monthly Notices Royal Astron. Soc.* **191**, 445
Blackwell, D.E., Petford, A.D., Shallis, M.J., Leggett, S.: 1982a, *Monthly Notices Royal Astron. Soc.* **199**, 21
Blackwell, D.E., Petford, A.D., Shallis, M.J., Simmons, G.J.: 1982b, *Monthly Notices Royal Astron. Soc.* **199**, 43
Blackwell, D.E., Petford, A.D., Shallis, M.J., Simmons, G.J.: 1982c, *Monthly Notices Royal Astron. Soc.* **201**, 595
Blackwell, D.E., Menon, S.L.R., Petford, A.D.: 1982d, *Monthly Notices Royal Astron. Soc.* **201**, 602
Blackwell, D.E., Menon, S.L.R., Petford, A.D.: 1982e, *Monthly Notices Royal Astron. Soc.* **201**, 611
Blackwell, D.E., Menon, S.L.R., Petford, A.D.: 1983, *Monthly Notices Royal Astron. Soc.* **204**, 883
Blackwell, D.E., Booth, A.J., Menon, S.L.R., Petford, A.D.: 1986a, *Monthly Notices Royal Astron. Soc.* **220**, 289
Blackwell, D.E., Booth, A.J., Menon, S.L.R., Petford, A.D.: 1986b, *Monthly Notices Royal Astron. Soc.* **220**, 303
Blackwell, D.E., Booth, A.J., Haddock, D.J., Petford, A.D., Leggett, S.K.: 1986c, *Monthly Notices Royal Astron. Soc.* **220**, 549
Bogdan, T.J.: 1984, *Astrophys. J.* **282**, 769
Bogdan, T.J.: 1987a, *Astrophys. J.* **318**, 888
Bogdan, T.J.: 1987b, *Astrophys. J.* **318**, 896
Bogdan, T.J.: 1989, *Astrophys. J.* **345**, 1042
Bogdan, T.J., Gilman, P.A., Lerche, I., Howard, R.: 1988, *Astrophys. J.* **327**, 451
Bogdan, T.J., Lerche, I.: 1988, *Quat. Applied Maths.* **46**, 365
Bogdan, T.J., Zweibel, E.G.: 1987, *Astrophys. J.* **312**, 444
Bommier, V., Landi Degl'Innocenti, E., Leroy, J.-L., Sahal-Bréchot S.: 1992, in *Methods of Solar and Stellar Magnetic Field Determination*, M<. Faurobert-Scholl, H. Frisch, N. Mein (Eds.), Obs. de Paris, Meudon, p. 211
Börner, P., Kneer, F.: 1992, *Astron. Astrophys.* **259**, 307
Borra, E.F., Edwards, G., Mayor, M.: 1984, *Astrophys. J.* **284**, 211
Brandt, P.N., Scharmer, G.B., Ferguson, S., Shine, R.A., Tarbell, T.D., Title, A.M.: 1988, *Nature* **335**, 238
Brandt, P.N., Erasmus, D.A., Kusoffsky, U., Righini, A., Rodriguez, A., Engvold, U.: 1989, LEST Techn. Report No. 38.
Brandt, P.N., Solanki, S.K.: 1990, *Astron. Astrophys.* **231**, 221
Brandt, P.N., Steinegger, M.: 1990, in *Solar Photosphere: Structure, Convection and Magnetic Fields*, J.O. Stenflo (Ed.), Kluwer, Dordrecht, *IAU Symp.* **138**, 41
Brants, J.J.: 1985a, *Solar Phys.* **95**, 15
Brants, J.J.: 1985b, *Solar Phys.* **98**, 197
Brants, J.J.: 1985c, *Ph.D. Thesis*, University of Utrecht
Brants, J.J., Steenbeck, J.C.M.: 1985, *Solar Phys.* **96**, 229
Brants, J.J., Zwaan, C.: 1982, *Solar Phys.* **80**, 251
Brault, J.W., Noyes, R.W.: 1983, *Astrophys. J.* **269**, L61
Braun, D.C., Duvall Jr., T.J., LaBonte, B.J.: 1987, *Astrophys. J.* **319**, L27
Braun, D.C., Duvall Jr., T.J., LaBonte, B.J.: 1988, *Astrophys. J.* **335**, 1015
Braun, D.C., Duvall, T.L., Jr., La Bonte, B.J., Jefferies, S.M., Harvey, J.W., Pomerantz, M.A.: 1992, *Astrophys. J.* **391**, L113

Brickhouse, N.S., La Bonte, B.J.: 1988, *Solar Phys.* **115**, 43
Browning, P.K., Priest, E.R.: 1982, *Geophys. Astrophys. Fluid Dyn.* **21**, 237
Browning, P.K., Priest, E.R.: 1983, *Astrophys. J.* **266**, 848
Bruls, J.H.M.J., Lites, B.W., Murphy, G.A.: 1991, in *Solar Polarimetry*, L. November (Ed.), National Solar Observatory, Sunspot, NM, p. 444
Bruls, J.H.M.J., Solanki, S.K.: 1992a, in *Cool Stars, Stellar Systems and the Sun, VII*, M.S. Giampapa, J.A. Bookbinder (Eds.), Astron. Soc. Pacific Conf. Ser., Vol. 26, p. 512
Bruls, J.H.M.J., Solanki, S.K.: 1992b, *Astron. Astrophys.*
Bünte, M.: 1989, Diplomarbeit, ETH Zürich
Bünte, M., Steiner, O., Solanki, S.K.: 1991, in *Solar Polarimetry*, L. November (ed.), National Solar Obs., Sunspot, NM, p. 468
Bünte, M., Steiner, O., Pizzo, V.: 1992a, *Astron. Astrophys.* **268**, 299
Bünte, M., Solanki, S.K., Steiner O.: 1992b, *Astron. Astrophys.* **268**, 736
Caccin, B., Falciani, R., Donati-Falchi, A.: 1974, *Solar Phys.* **35**, 41
Caccin, B., Gomez, M.T., Marmolino, C., Severino, G.: 1977, *Astron. Astrophys.* **54**, 227
Caccin, B., Severino, G.: 1979, *Astrophys. J.* **232**, 297
Caligari, P.: 1991, Diplomarbeit, Universität Freiburg
Cally, P.S.: 1985, *Aust. J. Phys.* **38**, 825.
Cally, P.S.: 1986, *Solar Phys.* **103**, 27.
Cally, P.S.: 1991, *J. Comp. Phys.* **93**, 411
Carlsson, M., Rutten, R.J., Shchukina, N.G.: 1992, *Astron. Astrophys.* **253**, 567
Carlsson, M., Scharmer, G.B.: 1985, in *Chromospheric Diagnostics and Modelling*, B.W. Lites (Ed.), National Solar Obs., Sunspot, NM, p. 137
Carlsson, M., Stein, R.F.: 1992, *Astrophys. J.* **397**, L59
Carter, C.S., Snodgrass, H.B., Bryja, C.: 1992, *Solar Phys.* **139**, 13
Cattaneo, F., Hurlburt, N.E., Toomre, J.: 1990, *Astrophys. J.* **349**, L63
Cavallini, F., Ceppatelli, G., Righini, A.: 1985, *Astron. Astrophys.* **143**, 116
Cavallini, F., Ceppatelli, G., Righini, A.: 1987, *Astron. Astrophys.* **173**, 155
Cavallini, F., Ceppatelli, G., Righini, A.: 1988, *Astron. Astrophys.* **205**, 278
Chandrasekhar, S.: 1950, *Radiative Transfer*, Clarendon Press, Oxford
Chang, E.S. 1984, *J. Phys. B: Atom. Mol. Phys.* **17**, L11
Chang, E.S. 1987, *Phys. Scripta* **35**, 792
Chang, E.S.: 1992, in *Infrared Solar Physics*, D. Rabin, J. Jefferies (Eds.), Kluwer, Dordrecht, *IAU Symp.* **154**, in press
Chang, E.S., Avrett, E.H., Mauas, P.J., Noyes, R.W., Loeser, R.: 1991, *Astrophys. J.* **379**, L79
Chang, E.S., Noyes, R.W.: 1983, *Astrophys. J.* **275**, L11
Chapman, G.A.: 1970, *Solar Phys.* **14**, 315
Chapman, G.A.: 1974, *Astrophys. J.* **191**, 255
Chapman, G.A.: 1977, *Astrophys. J. Suppl. Ser.* **33**, 35
Chapman, G.A.: 1979, *Astrophys. J.* **232**, 923
Chapman, G.A.: 1981, in *Solar Active Regions*, F.Q. Orall (ed.), Colorado University Press, p. 43
Chapman, G.A., Gingell, T.A.: 1984, *Solar Phys.* **91**, 243
Chapman, G.A., Klabunde, D.P.: 1982, *Astrophys. J.* **261**, 387
Chapman, G.A., Sheeley, Jr., N.R.: 1968, *Solar Phys.* **5**, 442
Cheng, J.: 1992, *Astron. Astrophys.* **264**, 243
Cheng, Q.-Q., Ulmschneider, P., Korevaar, P.: 1991, in *Mechanisms of Chromospheric and Coronal Heating*, P. Ulmschneider, E. Priest, R. Rosner (Eds.), Springer-Verlag, Berlin, p. 350
Chou, D.-Y., Fisher, G.H.: 1989, *Astrophys. J.* **341**, 533
Chou, D.-Y., Wang, H.: 1987, *Solar Phys.* **110**, 81
Choudhuri, A.R.: 1990, *Astron. Astrophys.* **239**, 335
Choudhuri, A.R., Auffret, H., Priest, E.R., 1992, preprint
Choudhuri, A.R., Gilman, P.A.: 1987, *Astrophys. J.* **316**, 788
Cook, J.W., Ewing, J.A.: 1990, *Astrophys. J.* **355**, 719
Cook, J.W., Brueckner, G.E., Bartoe, J.–D.F.: 1983, *Astrophys. J.* **270**, L89
Cowley, C.R.: 1990, *Astrophys. J.* **348**, 328

Craig, I.J.D., Brown, J.C.: 1986, *Inverse Problems in Astronomy. A Guide to Inversion Strategies for Remotely Sensed Data*, Adam Hilger, Bristol
Cram, L.E., Wilson, P.R.: 1975, *Solar Phys.* **41**, 313
Damé, L., Gouttebroze, P., Malherbe, J.-M.: 1984, *Astron. Astrophys.* **130**, 331
Dara, H.C., Alissandrakis, C.E., Koutchmy, S.: 1987, *Solar Phys.* **109**, 19
Dara, H.C., Alissandrakis, C.E., Koutchmy, S.: 1991, in *Solar Polarimetry*, L.J. November (Ed.), National Solar Obs., Sunspot, NM., p. 257
Dara-Papamargaritis, H., Koutchmy, S.: 1983, *Astron. Astrophys.* **125**, 280
Darvann, T.A., Koutchmy, S.: 1992, in *Infrared Solar Physics*, D. Rabin, J. Jefferies (Eds.), Kluwer, Dordrecht, *IAU Symp.* **154**, in press
Davila, J.M.: 1985, *Astrophys. J.* **291**, 328
Davila, J.M.: 1991, in *Mechanisms of Chromospheric and Coronal Heating*, P. Ulmschneider, E. Priest, R. Rosner (Eds.), Springer-Verlag, Berlin, p. 464
De Boer, C.R., Kneer, F.: 1992, *Astron. Astrophys.* **264**, L24
Defouw, R.J.: 1976, *Astrophys. J.* **209**, 266
Degenhardt, D.: 1989, *Astron. Astrophys.* **222**, 297
Degenhardt, D.: 1991, *Astron. Astrophys.* **248**, 637
Degenhardt, D., Kneer, F.: 1992, *Astron. Astrophys.* **260**, 411
Degenhardt, D., Wiehr, E.: 1992, *Astron. Astrophys.* **252**, 821
Degiacomi, C.G., Kneubühl, F.K., Huguenin, D.: 1985, *Astrophys. J.* **298**, 918
Deinzer, W.: 1965, *Astrophys. J.* **141**, 548
Deinzer, W., Hensler, G., Schüssler, M., Weisshaar, E.: 1984a, *Astron. Astrophys.* **139**, 426
Deinzer, W., Hensler, G., Schüssler, M., Weisshaar, E.: 1984b, *Astron. Astrophys.* **139**, 435
Del Toro Iniesta, J.C., Semel, M., Collados, M., Sánchez Almeida, J.: 1990a, *Astron. Astrophys.* **227**, 591
Del Toro Iniesta, J.C., Collados, M., Sánchez Almeida, J., Martínez Pillet, V., Ruiz Cobo, B.: 1990b, *Astron. Astrophys.* **233**, 570
De Martino, S.: 1986, *Diplomarbeit*, ETH, Zürich
Deming, D., Hillman, J.J., Kostiuk, T., Mumma, M.J., Zipoy, D.M.: 1984, *Solar Phys.* **94**, 57
Deming, D., Boyle, R.J., Jennings, D.E., Wiedemann, G.: 1988, *Astrophys. J.* **333**, 978
Deming, D., Hewagama, T., Jennings, D.E., Osherovich, V., Wiedemann, G., Zirin, H.: 1990, *Astrophys. J.* **364**, L49
Deming, D., Hewagama, T., Jennings, D.E., Wiedemann, G.: 1991, in *Solar Polarimetry*, L. November (Ed.), Natinal Solar Obs., Sunspot, NM, p. 341
Deming, D., Hewagama, T., Jennings, D.: 1992a, in *Infrared Solar Physics*, D. Rabin, J. Jefferies (Eds.), Kluwer, Dordrecht, *IAU Symp.* **154**, in press
Deming, D., Jennings, D.E., McCabe, G., Noyes, R., Wiedemann, G., Espanak, F.: 1992b, *Astrophys. J.* **396**, L53
Démoulin, P.: 1990, in *Advances in Solar System MHD*, E.R. Priest (Ed.), Cambridge University Press,
Deubner, F. L.: 1968, in *Structure and Development of Solar Active Regions*, K.O. Kiepenheuer (Ed.), Reidel, Dordrecht, *IAU Symp.* **35**, 230
Deubner F.-L., 1974, *Solar Phys.* **39**, 31
Deubner, F.L.: 1975, *Osserv. Mem. Oss. Astrofis. Arcetri* **105**, 39
Deubner F.-L., Fleck B., 1989, *Astron. Astrophys.* **213**, 423
Deubner, F. L., Fleck, B.: 1990, *Astron. Astrophys.* **228**, 506
Dravins, D.: 1982, *Ann. Rev. Astron. Astrophys.* **20**, 61
Dravins, D., Lindegren, L., Nordlund, Å.: 1981, *Astron. Astrophys.* **96**, 345
Dunn, R.B.: 1985, *Solar Phys.* **100**, 1
Dunn, R.B., Zirker, J.B.: 1973, *Solar Phys.* **33**, 281
Durrant, C.J.: 1977, in *Highlights in Astronomy*, E.A. Müller (Ed.), Vol. 4, part II, p. 267
Edwin, P.M., Roberts, B.: 1982, *Solar Phys.* **76**, 239
Edwin, P.M., Roberts, B.: 1983, *Solar Phys.* **88**, 179
Edwin, P.M., Roberts, B.: 1986, *Wave Motion* **8**, 151
Elste, G.: 1985, in *Theoretical Problems in High resolution Solar Physics*, H.U. Schmidt (Ed.), Max

Planck Institut für Astrophysik, München, p. 185
Emonet, Th.: 1992, Diplomarbeit, ETH, Zürich
Evans, D.J., Roberts, B.: 1989, *Astrophys. J.* **348**, 346
Evans, J.C., Ramsey, L.W., Testerman, L.: 1975, *Astron. Astrophys.* **42**, 237
Evans J.W., Michard R., 1962, *Astrophys. J.* **136**, 493
Evershed, J., 1909, *Monthly Notices Royal Astron. Soc.* **69**, 454
Fabiani Bendicho, P., Kneer, F., Trujillo Bueno, J.: 1992, *Astron. Astrophys.* **264**, 229
Fang, C., Mouradian, Z., Banos, G., Dumont, S., Pecker, J.C.: 1984, *Solar Phys.* **91**, 61
Farmer, C.B., Norton, R.H.: 1989, *A High Resolution Atlas of the Infrared Spectra of the Sun and the Earth Atmosphere from Space. Vol 1. The Sun*, NASA Reference Publication 1224
Faurobert-Scholl, M.: 1991, *Astron. Astrophys.* **246**, 469
Faurobert-Scholl, M.: 1992a, *Astron. Astrophys.* **258**, 521
Faurobert-Scholl, M.: 1992b, *Astron. Astrophys.* in press
Faurobert-Scholl, M.: 1992c, in *Methods of Solar and Stellar Magnetic Field Determination*, M. Faurobert-Scholl, H. Frisch, N. Mein (Eds.), Obs. de Paris, Meudon, p. 147
Feldman, U., Cohen, L., Doschek, G.A.: 1982, *Astrophys. J.* **255**, 325
Ferrari, A., Massaglia, S., Kalkofen, W., Rosner, R., Bodo, G.: 1985, *Astrophys. J.* **298**, 181
Ferriz Mas, A.: 1988, *Phys. Fluids* **31**, 2583
Ferriz Mas, A.: 1990, in *Physics of Magnetic Flux Ropes*, C.T. Russell, E.R. Priest, L.C. Lee (Eds.), Geophysical Monograph 58, American Geophys. Union, Washington, DC, p. 107
Ferriz Mas, A., Moreno Insertis, F.: 1987, *Astron. Astrophys.* **179**, 268
Ferriz Mas, A., Schüssler, M.: 1989, *Geophys. Astrophys. Fluid Dyn.* **48**, 217
Ferriz Mas, A., Schüssler, M.: 1992, *Geophys. Astrophys. Fluid Dyn.* in press
Ferriz Mas, A., Schüssler, M., Anton, V.: 1989, *Astron. Astrophys.* **210**, 425
Fiedler, R.A.S., Cally, P.S.: 1990, *Solar Phys.* **126**, 69
Fleck, B.: 1991, *Rev. Mod. Astron.* **4**, 90
Fleck, B., Deubner, F.-L.: 1991, in *Mechanisms of Chromospheric and Coronal Heating*, P. Ulmschneider, E.R. Priest, R. Rosner (Eds.), Springer, Berlin, p. 19
Foing, B., Bonnet, R.M.: 1984, *Astrophys. J.* **279**, 848
Foing, B., Bonnet, R.M., Brunner, M.: 1986, *Astron. Astrophys.* **162**, 292
Fontenla, J.M., Avrett, E.H., Loeser, R.: 1993, *Astrophys. J.* in press Foukal, P., Duvall, T. Jr.: 1985, *Astrophys. J.* **296**, 739
Foukal, P., Duvall, T. Jr., Gillespie, B.: 1981, *Astrophys. J.* **249**, 394
Foukal, P., Fowler, L.: 1984, *Astrophys. J.* **281**, 442
Foukal, P., Lean, J.: 1988, *Astrophys. J.* **328**, 347
Foukal, P., Little, R., Graves, J., Rabin, D., Lynch, D.: 1990, *Astrophys. J.* **353**, 712
Foukal, P., Little, R., Mooney, J.: 1989, *Astrophys. J.* **336**, L33
Frazier E.N., 1968, *Astrophys. J.* **152**, 557
Frazier, E.N.: 1970, *Solar Phys.* **14**, 89
Frazier, E.N.: 1971, *Solar Phys.* **21**, 42
Frazier, E.N.: 1972, *Solar Phys.* **24**, 98
Frazier, E.N.: 1977, in *Highlights of Astronomy*, E.A. Müller (Ed.), Vol. 4, Part. II, p. 255
Frazier, E.N.: 1978, *Astron. Astrophys.* **64**, 351
Frazier, E.N., Stenflo, J.O.: 1972, *Solar Phys.* **27**, 330
Frazier, E.N., Stenflo, J.O.: 1978, *Astron. Astrophys.* **70**, 789
Fredga, K.: 1969, *Solar Phys.* **9**, 358
Fredga, K.: 1971, *Solar Phys.* **21**, 60
Gabriel A.H.: 1976, *Phil. Trans. Roy. Soc. London* **A281**, 339
Galloway, D.J., Proctor, M.R.E., Weiss, N.O.: 1977, *Nature* **266**, 686
Galloway, D.J., Weiss, N.O.: 1981, *Astrophys. J.* **243**, 945
Gary, G.A., Hagyard, M.J.: 1990, *Solar Phys.* **126**, 21
Giampapa, M.S., Golub, L., Worden, S.P.: 1983, *Astrophys. J.* **268**, L121
Gingerich, O., Noyes, R.W., Kalkofen, W., Cuny, Y.: 1971, *Solar Phys.* **18**, 347
Giovanelli, R.G. 1977, *Solar Phys.* **52**, 315.
Giovanelli, R.G.: 1980, *Solar Phys.* **68**, 49

Giovanelli, R.G.: 1982, *Solar Phys.* **80**, 21
Giovanelli, R.G., Brown, N.: 1977, *Solar Phys.* **52**, 27
Giovanelli, R.G., Jones, H.P.: 1982, *Solar Phys.* **79**, 267
Giovanelli, R.G., Ramsay, J.V.: 1971, in *Solar Magnetic Fields*, R. Howard (Ed.), Reidel, Dordrecht, *IAU Symp.* **43**, 293
Giovanelli, R.G., Slaughter, C.: 1978, *Solar Phys.* **57**, 255
Giovanelli, R.G., Livingston, W.C., Harvey, J.W.: 1978, *Solar Phys.* **59**, 49
Glenar, D.A., Reuter, D.C., Deming, D., Chang, E.S.: 1988, *Astrophys. J.* **335**, L35
Gokhale, M.H., Zwaan, C.: 1972, *Solar Phys.* **26**, 52
Goldreich, P., Murray, N., Willette, G., Kumar, P.: 1991, *Astrophys. J.* **370**, 752
Golovko, A.A.: 1974, *Solar Phys.* **37**, 113
Golub, L., Maxson, C., Rosner, R., Serio, S., Vaiana, G.S.: 1980, *Astrophys. J.* **238**, 343
Golub, L., Noci, G., Poletto, G., Vaiana, G.S.: 1982, *Astrophys. J.* **259**, 359
Gopasyuk, S.I., Severny, A.B.: 1983, *Sov. Astron. Lett.* **9**, 65
Gordon, J., Wilkerson, G.: 1981, in *Solar Instrumentation; What's Next?*, R.B. Dunn (Ed.), National Solar Obs., Sunspot, NM, p. 459
Gray, D.F.: 1984, *Astrophys. J.* **277**, 640
Gray, D.F.: 1988, *Lectures on Spectral-Line Analysis: F, G, and K Stars*, The Publisher, Arva, Ontario
Grigorjev, V.M.: 1969, *Solar Phys.* **6**, 67
Grigorjev, V.M., Katz, J.M.: 1972, *Solar Phys.* **22**, 119
Grigorjev, V.M., Katz, J.M.: 1975, *Solar Phys.* **42**, 21
Grigoryev, V.M., Selivanov, V.L.: 1990, in *Physics of Magnetic Flux Ropes*, C.T. Russell, E.R. Priest, L.C. Lee (Eds.), Geophysical Monograph 58, American Geophys. Union, Washington, DC, p. 153
Grossmann-Doerth, U.: 1970, *Solar Phys.* **13**, 287
Grossmann-Doerth, U., Knölker, M., Schüssler, M., Weisshaar, E., 1989b, in *Solar and Stellar Granulation*, R.J. Rutten and G. Severino (Eds.), Kluwer, Dordrecht, p. 481
Grossmann-Doerth, U., Larsson, B., Solanki, S.K.: 1988a, *Astron. Astrophys.* **204**, 266
Grossmann-Doerth, U., Pahlke, K.-D., Schüssler, M.: 1987, *Astron. Astrophys.* **176**, 139
Grossmann-Doerth, U., Schüssler, M., Solanki, S.K.: 1988b, *Astron. Astrophys.* **206**, L37
Grossmann-Doerth, U., Schüssler, M., Solanki, S.K.: 1989a, *Astron. Astrophys.* **221**, 338
Grossmann-Doerth, U., Solanki, S.K.: 1990, *Astron. Astrophys.* **238**, 279
Guenther, E., Mattig, W.: 1991, *Astron. Astrophys.* **243**, 244
Gurtovenko, E.A., Kostik, R.I.: 1981, *Astron. Astrophys. Suppl. Ser.* **46**, 239
Gurtovenko, E.A., Kostik, R.I.: 1982, *Astron. Astrophys. Suppl. Ser.* **47**, 193
Gurtovenko, E.A., Kostik, R.I.: 1989, *Fraunhofer Spectrum and the System of Solar Oscillator Strengths*, Naukova Dumka, Kiev
Haerendel, G.: 1992, *Nature* **360**, 241
Hagyard, M.J.: 1984, Studies of Solar Magnetic Fields During the Solar Maximum Year, NASA Technical Memorandum, TM–86469.
Hagyard M.J.: 1985, (Ed.), *Measurements of Solar Vector Magnetic Fields*, NASA Conf. Publ. 2374
Hagyard, M.J.: 1987, *Solar Phys.* **107**, 239
Hagyard, M.J., Smith Jr. J.B., Teuber, D., West, E.A.: 1984, *Solar Phys.* **91**, 115
Hagyard, M.J., Teuber, D., West, E.A., Tandberg-Hanssen, E., Henze, W., Beckers, J.M., Bruner, M., Hyder, C.L., Woodgate, B.E.: 1983, *Solar Phys.* **84**, 13
Hagyard, M.J., West, E.A., Cumings, N.P.: 1977, *Solar Phys.* **53**, 3
Hale, G.E.: 1908, *Astrophys. J.* **28**, 315
Hale, G.E.: 1922a, *Proc. National Acad. Sci.* **8**, 168
Hale, G.E.: 1922b, *Monthly Notices Royal Astron. Soc.* **82**, 168
Hale, G.E., Ellerman, F.: 1903, *Publ. Yerkes Obs.* **3**, 1
Hall, D.N.B.: 1974, *An Atlas of Infrared Spectra of the Solar Photosphere and of Sunspot Umbrae*, Kitt Peak National Observatory, Contribution No. 556, Tucson, AZ
Hammer, R.: 1987, in *The Role of Fine-Scale Magnetic Fields on the Structure of the Solar Atmosphere*, E.-H. Schröter, M. Vázquez, A.A. Wyller (Eds.), Cambridge University Press, p. 255

Hanle, W.: 1924, *Z. Phys.* **30**, 93
Hanslmeier, A., Mattig, W., Nesis, A.: 1991, *Astron. Astrophys.* **244**, 521
Harvey, J.W.: 1971, in *Solar Activity: Observations and Predictions*, MIT Press, Cambridge, MA, p. 51
Harvey, J.W.: 1972, *Nature* **235**, 90
Harvey, J.W: 1977a, in *Highlights of Astronomy*, E.A. Müller (Ed.), Vol. 4, Part II, p. 223
Harvey, J.W.: 1977b, in *Illustrated Glossary for Solar and Solar-Terrestrial Physics*, A. Bruzek, C.J. Durrant (Eds.), Reidel, Dordrecht, p. 13
Harvey, J.W.: 1983, *Space Sci. Rev.* **34**, 55
Harvey, J.W.: 1985, in *Measurements of Vector Magnetic Fields*, M.J. Hagyard (Ed.), NASA Conference Publication 2374, p. 109
Harvey, J.W.: 1986, in *Small Scale Magnetic Flux Concentrations in the Solar Photosphere*, W. Deinzer, M. Knölker, H.H. Voigt (Eds.), Vandenhoeck & Ruprecht, Göttingen, p. 25
Harvey, J.W., Breckinridge, J.B.: 1973, *Astrophys. J.* **182**, L137
Harvey, J.W., Hall, D.N.B.: 1971, in *Solar Magnetic Fields*, R.F. Howard (Ed.), Reidel, Dordrecht, *IAU Symp.* **43**, 279
Harvey, J.W., Hall, D.: 1975, *Bull. Amer. Astron. Soc.* **7**, 459.
Harvey, J.W., Livingston, W.: 1969, *Solar Phys.* **10**, 283
Harvey, J.W., Livingston, W., Slaughter, C: 1972, in *Line Formation in the Presence of Magnetic Fields*, High Altitude Obs., NCAR, Boulder, CO, p. 227
Harvey, K.L., Harvey, J.W.: 1973, *Solar Phys.* **28**, 61
Harvey, K.L., Harvey, J.W.: 1975, *Solar Phys.* **47**, 233
Harvey, K.L., Harvey, J.W.: 1979, Photospheric Velocity Fields as Indicators of Flare Activity, AFGL-TR-79-0262, Air Force Geophysics Lab.
Harvey, K.L., Harvey, J.W., Martin, S.F.: 1975, *Solar Phys.* **40**, 87
Harvey, K.L., Martin, S.F.: 1973, *Solar Phys.* **32**, 389
Hasan, S.S.: 1983, in *Solar and Stellar Magnetic Fields: Origins and Coronal Effects*, J.O. Stenflo (Ed.), Reidel, Dordrecht, *IAU Symp.* **102**, 73
Hasan, S.S.: 1984, *Astrophys. J.* **285**, 851
Hasan, S.S.: 1985, *Astron. Astrophys.* **143**, 39
Hasan, S.S.: 1986, *Monthly Notices Royal Astron. Soc.* **219**, 357
Hasan, S.S.: 1988, *Astrophys. J.* **332**, 499
Hasan, S.S.: 1990, in *Physics of Magnetic Flux Ropes*, C.T. Russell, E.R. Priest, L.C. Lee (Eds.), Geophysical Monograph 58, American Geophys. Union, Washington, DC, p. 157
Hasan, S.S.:1991, in *Mechanisms of Chromospheric and Coronal Heating*, P. Ulmschneider, E.R. Priest, R. Rosner (Eds.), Springer-Verlag, Berlin, p. 408
Hasan, S.S., Kneer, F.: 1986, *Astron. Astrophys.* **158**, 288
Hasan, S.S., Schüssler, M.: 1985, *Astron. Astrophys.* **151**, 69
Henze, W., Jr., Tandberg-Hanssen, E., Hagyard, M.J., Woodgate, B.E., Shine, R.A., Beckers, J.M., Bruner, M., Gurman, J.B., Hyder, C.L., West, E.A.: 1982, *Solar Phys.* **81**, 231
Herbold, G., Ulmschneider, P. Spruit, H.C. and Rosner, R.: 1985, *Astron. Astrophys.* **145**, 157
Hermans, L.M., Lindsey, C.: 1986, *Astrophys. J.* **310**, 907
Hersé, M.: 1979, *Solar Phys.* **63**, 35
Hewagama, T., Deming, D., Jennings, D.E., Osherovich, V., Wiedemann, G., Zipoy, D., Mickey, D.L., Garcia, H.: 1993, *Astrophys. J.* **3**, Suppl. in press
Heyvaerts, J., Priest, E.R.: 1983, *Astron. Astrophys.* **117**, 220
Hirayama, T.: 1978, *Publ. Astron. Soc. Japan* **30**, 337
Hirayama, T.: 1992, *Solar Phys.* **137**, 33
Hirayama, T., Hamana, S., Mizugaki, K.: 1985, *Solar Phys.* **99**, 43
Hirayama, T., Moriyama, F.: 1979, *Solar Phys.* **63**, 251
Hoang-Binh, D.: 1991, *Astron. Astrophys.* **241**, L13
Hollweg, J.V.: 1982, *Astrophys. J.* **257**, 345
Hollweg, J.V.: 1986, in *Advances in Space Plasma Physics*, B. Buti (Ed.), World Scientific, Singapur, p. 77
Hollweg, J.V.: 1990, in *Physics of Magnetic Flux Ropes*, C.T. Russell, E.R. Priest, L.C. Lee (Eds.),

Geophysical Monograph 58, American Geophys. Union, Washington, DC, p. 23
Hollweg, J.V.: 1991, in *Mechanisms of Chromospheric and Coronal Heating*, P. Ulmschneider, E. Priest, R. Rosner (Eds.), Springer-Verlag, Berlin, p. 423
Hollweg, J.V., Jackson, S., Galloway, D.: 1982, *Solar Phys.* **75**, 35.
Holweger, H.: 1967, *Z. Astrophys.* **65**, 365
Holweger, H.: 1979, in *Proc. 22nd Liège International Astrophys. Symp.*, Inst. d'Astrophysique, Liège, p. 117
Holweger, H., Müller, E.A.: 1974, *Solar Phys.* **39**, 19
Holweger, H., Gehlsen, M., Ruland, F.: 1978, *Astron. Astrophys.* **70**, 537
Howard, R.: 1967, *Solar Phys.* **2**, 3
Howard, R.: 1971, *Solar Phys.* **16**, 21
Howard, R.: 1972, *Solar Phys.* **24**, 123
Howard, R.F.: 1991, *Solar Phys.* **131**, 239
Howard, R.F.: 1992, *Solar Phys.* **142**, 47
Howard, R.F., Bhatnagar, A.: 1969, *Solar Phys.* **10**, 245
Howard, R.F., La Bonte, B.: 1981, *Solar Phys.* **74**, 131
Howard, R.F., Stenflo, J.O.: 1972, *Solar Phys.* **22**, 402
Hoyng, P.: 1990, in *Solar Photosphere: Structure, Convection and Magnetic Fields*, J.O. Stenflo (Ed.), Kluwer, Dordrecht, *IAU Symp.* **138**, 359
Huber, M.C.E., Sandeman, R.J.: 1986, *Rep. Prog. Phys.* **49**, 397
Hudson, H., Hildner, E.: 1990, in *Astrophysics from the Moon*, M.J. Mumma, H. Smith (Eds.), Proc. IAP Conference 207, Institute of Physics Press, p. 584
Hughes, D.W., Proctor, M.R.E.: 1988, *Ann. Rev. Fluid Mech.* **20**, 187
Hurlburt, N.E., Toomre, J.: 1988, *Astrophys. J.* **327**, 920
Hurlburt, N.E., Toomre, J., Massaguer, J.M.: 1984, *Astrophys. J.* **282**, 557
Hurlburt, N.E., Weiss, N.O.: 1987, in *The Role of Fine-Scale Magnetic Fields on the Structure of the Solar Atmosphere*, E.-H. Schröter, M. Vázquez, A.A. Wyller (Eds.), p. 35
Illing, R.M.E., Landman, D.A., Mickey, D.L.: 1974a, *Astron. Astrophys.* **35**, 327
Illing, R.M.E., Landman, D.A., Mickey, D.L.: 1974b, *Astron. Astrophys.* **37**, 97
Illing, R.M.E., Landman, D.A., Mickey, D.L.: 1975, *Astron. Astrophys.* **41**, 183
Immerschitt, S., Schröter, E.H.: 1989, *Astron. Astrophys.* **208**, 307
Ingersoll, A.P., Chapman, G.A.: 1975, *Solar Phys.* **42**, 279
Ionson, J.A.: 1978, *Astrophys. J.* **226**, 650
Jefferies, J.T.: 1991, *Astrophys. J.* **377**, 337
Jefferies, J.T., Lites, B.W., Skumanich, A.: 1989, *Astrophys. J.* **243**, 920
Jefferies, J.T., Mickey, D.L.: 1991, *Astrophys. J.* **372**, 694
Jennings, D.E., Deming, D., McCabe, G.H., Noyes, R.W., Wiedemann, G.R., Espenak, F.: 1992, in *Infrared Solar Physics*, D. Rabin, J. Jefferies (Eds.), Kluwer, Dordrecht, *IAU Symp.* **154**, in press
Johannesson, A.: 1992, *Ph.D. Thesis*, University of Lund
Johannesson, A., Bida, T., Lites, B., Scharmer, G.B.: 1992, *Astron. Astrophys.* **258**, 572
Johansson, S., Learner, R.C.M.: 1990, *Astrophys. J.* **354**, 755
Jones, H.P.: 1985, in *Chromospheric Diagnostics and Modelling*, B.W. Lites (Ed.), National Solar Obs., Sunspot, NM, p. 175
Jones, H.P., Giovanelli, R.G.: 1983, *Solar Phys.* **87**, 37
Kaisig, M., Schröter, E.H.: 1983, *Astron. Astrophys.* **117**, 305
Kalkofen, W.: 1987, (Ed.) *Numerical Radiative Transfer*, Cambridge University Press, Cambridge
Kalkofen, W., Rosner, R., Ferrari, A., Massaglia, S.: 1986, *Astrophys. J.* **304**, 519
Kalkofen, W., Bodo, G., Massaglia, S., Rossi, P.: 1989, in *Solar and Stellar Granulation*, R.J. Rutten and G. Severino (Eds.), Reidel, Dordrecht, p. 571
Kálmán, B.: 1991, *Solar Phys.* **135**, 299
Katz, J.M.: 1971, *Solar Phys.* **20**, 362
Kawaguchi, I., Kitai, R.: 1976, *Solar Phys.* **46**, 125
Kawakami, H.: 1983, *Publ. Astron. Soc. Japan* **35**, 459
Kawakami, S., Makita, M., Kurohawa, H.: 1989, *Publ. Astron. Soc. Japan* **41**, 175
Keil, S.L.: 1984, (Ed.) *Small-Scale Dynamical Processes in Quiet Stellar Atmospheres*, National

Solar Obs., Sunspot, NM
Keil, S.L., Bonaccini, D., Tamblyn, P., November, L.: 1989, in *High Spatial Resolution Solar Observations*, O. von der Lühe (Ed.), National Solar Obs., Sunspot, NM, p. 272
Keil, S.L., Roudier, R., Cambell, E., Koo, B.C., Marmolino, C.: 1989, in *Solar and Stellar Granulation*, R.J. Rutten, G. Severino (Eds.), Kluwer, Dordrecht, p. 273
Keller, C.U.: 1988, *Diplomarbeit*, E.T.H. Zürich.
Keller, C.U.: 1989, in *High Spatial Resolution Solar Observations*, O. Von der Lühe (Ed.), National Solar Obs., Sunspot, NM, p. 208
Keller, C.U.: 1992a, *Nature* **359**, 307
Keller, C.U.: 1992b, *Ph.D. Thesis*, ETH, Zürich, pp. 165
Keller, C.U., Koutchmy, S.: 1991, *Astrophys. J.* **379**, 751
Keller, C.U., Solanki, S.K., Steiner, O., Stenflo, J.O.: 1990a, *Astron. Astrophys.* **233**, 583
Keller, C.U., Solanki, S.K., Tarbell, T.D., Title, A.M., Stenflo J.O.: 1990b, *Astron. Astrophys.* **236**, 250
Keller, C.U., Stenflo, J.O., Von der Lühe, O.: 1992, *Astron. Astrophys.* **254**, 355
Keller, C.U., Von der Lühe, O.: 1992, *Astron. Astrophys.* **261**, 321
Kemp, J.C., Henson, G.D., Steiner, C.T., Powell, E.R.: 1987, *Nature* **326**, 270
Kemp, J.C., Macek, J.H., Nehring, F.W.: 1984, *Astrophys. J.* **278**, 863
Kiepenheuer, K.O.: 1953, *Astrophys. J.* **117**, 447
Kim, I.S.: 1990, in *Dynamics of Quiescent Prominences*, V. Ruždjak, E. Tandberg-Hanssen (Eds.), Springer-Verlag, Berlin, *IAU Coll.* **117**, 49
Kitai, R., Muller, R.: 1984, *Solar Phys.* **90**, 303
Kjeldseth Moe, O.: 1967, in *Structure and Development of Active Regions*, K.O. Kiepenheuer (Ed.), Reidel, Dordrecht, *IAU Symp.* **35**, 202
Kjeldseth-Moe, O., Maltby, P.: 1974, *Solar Phys.* **36**, 106
Kneer, F.: 1986, in *Small Scale Magnetic Flux Concentrations in the Solar Photosphere*, W. Deinzer, M. Knölker, H.H. Voigt (Eds.), Vandenhoeck and Ruprecht, Göttingen, p. 147
Kneer, F., Trujillo-Bueno, J.: 1987, *Astron. Astrophys.* **183**, 91
Kneer, F., Von Uexküll, M.: 1985, *Astron. Astrophys.* **144**, 443
Kneer, F., Von Uexküll, M.: 1986, *Astron. Astrophys.* **155**, 178
Kneer, F., Von Uexküll, M.: 1991, *Astron. Astrophys.* **247**, 556
Knölker, M., Grossmann-Doerth, U., Schüssler, M., Weisshaar, E.: 1990, *Adv. Space Res.* **11**, 285
Knölker, M., Schüssler, M.: 1988, *Astron. Astrophys.* **202**, 275
Knölker, M., Schüssler, M., Weisshaar E.: 1988, *Astron. Astrophys.* **194**, 257
Kömle, N.: 1979, *Solar Phys.* **64**, 213
Koutchmy, S.: 1977, *Astron. Astrophys.* **61**, 397
Koutchmy, S.: 1991, in *Solar Polarimetry*, L. November (Ed.), National Solar Observatory, Sunspot, NM, p. 237
Koutchmy, S., Stellmacher, G.: 1978, *Astron. Astrophys.* **67**, 93
Koutchmy, S., Zirker, J.B., Darvann, T., Koutchmy, O., Stauffer, F., Mann, R., Coulter, R., Hegwer, S.: 1991, in *Solar Polarimetry*, L. November (Ed.), National Solar Observatory, Sunspot, NM, p. 263
Kovitya, P., Cram, L.: 1983, *Solar Phys.* **84**, 45
Krall, K.R., Smith, J.B., Hagyard, M.J., West, E.A., Cumings, N.P.: 1982, *Solar Phys.* **79**, 59
Krat, V.A.: 1973, *Solar Phys.* **32**, 307
Kučera, A.: 1992, in *Infrared Solar Physics*, D. Rabin, J. Jefferies (Eds.), Kluwer, Dordrecht, *IAU Symp.* **154**, in press
Kučera, A., Scherbakova, Z., Baranovsky, E.: 1991, in *Mechanisms of Chromospheric and Coronal Heating*, P. Ulmschneider, E. Priest, R. Rosner (Eds.), Springer-Verlag, Berlin, p. 109
Kuhn, J.R., Libbrecht, K.G., Dicke, R.H.: 1988, *Science* **242**, 908
Kurucz, R.L.: 1979, *Astrophys. J. Suppl. Ser.* **40**, 1
Kurucz, R.L.: 1991a, in *Stellar Atmospheres: Beyond Classical Models*, L. Crivellari, I. Hubeny, D.G. Hummer (Eds.), Kluwer, Dordrecht, p. 441
Kurucz, R.L.: 1991b, in *Precision Photometry: Astrophysics of the Galaxy*, A.G. Davis Philip, A.R. Upgren, Janes, K.A. (Eds.), L. Davis Press, Schenectady

Küveler, G., Wiehr, E.: 1985, *Astron. Astrophys.* **142**, 205
Kuzminykh, V.D.: 1963, *Sov. Astron.* **6**, 751
Kuzminykh, V.D.: 1965, *Sov. Astron.* **8**, 551
Landi Degl'Innocenti, E.: 1976, *Astron. Astrophys. Suppl. Ser.* **25**, 379
Landi Degl'Innocenti, E.: 1979, *Solar Phys.* **63**, 237
Landi Degl'Innocenti, E.: 1983, *Solar Phys.* **85**, 3
Landi Degl'Innocenti E.: 1985a, in *Theoretical Problems in High Resolution Solar Physics*, H.U. Schmidt (Ed.), Max Planck Inst. f. Astrophys., Munich, p. 162
Landi Degl'Innocenti, E.: 1985b, in *Measurements of Solar Vector Magnetic Fields*, M.J. Hagyard (Ed.), NASA Conf. Publ. 2374, p. 279
Landi Degl'Innocenti, E.: 1990, in *Dynamics of Quiescent Prominences*, V. Ruždak, E. Tandberg-Hanssen (Eds.), , Springer Verlag, Berlin, p. 206
Landi Degl'Innocenti, E.: 1992, in *Methods of Solar and Stellar Magnetic Field Determination*, M. Faurobert-Scholl, H. Frisch, N. Mein (Eds.), Obs. de Paris, Meudon, p. 7
Landi Degl'Innocenti, E., Landi Degl'Innocenti, M.: 1972, *Solar Phys.* **27**, 319
Landi Degl'Innocenti, E., Landi Degl'Innocenti, M.: 1973, *Solar Phys.* **31**, 299
Landi Degl'Innocenti, E., Landi Degl'Innocenti, M.: 1977, *Astron. Astrophys.* **56**, 111
Landi Degl'Innocenti, E., Landi Degl'Innocenti, M.: 1981, *Il Nuovo Cimento B* **62**, 1
Landi Degl'Innocenti, E., Landi Degl'Innocenti, M.: 1985, *Solar Phys.* **97**, 239
Landi Degl'Innocenti, E., Landolfi, M.: 1982, *Solar Phys.* **77**, 13
Landi Degl'Innocenti, E., Landolfi, M.: 1983, *Solar Phys.* **87**, 221
Landolfi, M.: 1987, *Solar Phys.* **109**, 287
Landolfi, M., Landi Degl'Innocenti, E.: 1982, *Solar Phys.* **78**, 355
Landolfi, M., Landi Degl'Innocenti, E., Arena, P.: 1984, *Solar Phys.* **93**, 269
Larsson, B., Solanki, S.K., Grossmann-Doerth, U.: 1991, in *Solar Polarimetry*, L. November (Ed.), National Solar Observatory, Sunspot, NM, p. 479
Lawrence, J.K., Chapman, G.A.: 1988, *Astrophys. J.* **335**, 996
Lawrence, J.K., Chapman, G.A., Herzog, A.D.: 1988, *Astrophys. J.* **324**, 1184
Lee, J.W.,:1992, *Solar Phys.* **139**, 267
Lee, M.A., Roberts, B.: 1986, *Astrophys. J.* **301**, 430
Leighton, R.B.: 1965, in *Stellar and Solar Magnetic Fields*, R. Lüst (Ed.), Reidel, Dordrecht, *IAU Symp.* **22**, 158
Lemaire, P.: 1987, in *The Sun, Proc. 10th European Regional Astron. Meeting of the IAU*, L. Hejna, M. Sobotka (Eds.), Astron. Inst. Czechoslovak Acad. Sci., Prag, p. 185
Lemke, M.: 1986, *Diplomarbeit*, University of Kiel
Lemke, M., Holweger, H.: 1987, *Astron. Astrophys.* **173**, 375
Lemoine, B., Demuynck, C., Destombes, J.L.: 1988, *Astron. Astrophys.* **191**, L4
Leroy, J.L.: 1962, *Ann. Astrophys.* **25**, 127
Leroy, J.L.: 1985, in *Measurements of Solar Vector Magnetic Fields*, M.J. Hagyard (Ed.), NASA Conf. Publ. 2374, p. 121
Leroy, J.L.: 1988, in *Dynamics and Structure of Solar Prominences*, E.R. Priest (Ed.), p. 33
Leroy, J.L.: 1989, *Astron. Astrophys.* **215**, 360
Leroy, J.L.: 1990, *Astron. Astrophys.* **237**, 237
Leroy, J.L.: 1991, in *Solar Polarimetry*, L. November (Ed.), National Solar Obs., Sunspot, NM, p. 330
Libbrecht, K.G, Kuhn, J.R.: 1984, *Astrophys. J.* **277**, 889
Libbrecht, K.G, Kuhn, J.R.: 1985, *Astrophys. J.* **299**, 1047
Lindsey, C.A., Heasley, J.N.: 1981, *Astrophys. J.* **247**, 348
Lindsey, C.A., Jefferies, J.T.: 1991, *Astrophys. J.* **383**, 443
Lindsey, C., Becklin, E.E., Orrall, F.Q., Werner, M.W., Jefferies, J.T., Gatley, I.: 1986, *Astrophys. J.* **308**, 448
Lindsey, C.A., Yee, S., Roellig, T.L., Hills, R., Brock, D., Duncan, W., Watt, G., Webster, A., Jefferies, J.T.: 1990, *Astrophys. J.* **353**, L53
Lites B.W., Chipman E.G., 1979, *Astrophys. J.* **231**, 570
Lites, B.W., Chipman, E.G., White, O.R.: 1982, *Astrophys. J.* **253**, 376
Lites, B.W., Elmore, D.F., Tomczyk, S., Seagraves, P., Skumanich, A., Streander, K.V.: 1992, in *The*

Magnetic and Velocity Fields of Solar Active Regions, H. Zirin (Ed.), Astron. Soc. Pacific Conf. Ser., *IAU Coll.* **141** in press
Lites, B.W., Scharmer, G.B, Skumanich, A.: 1990, *Astrophys. J.* **355**, 329
Lites, B.W., Bida, T.A., Johannesson, A., Scharmer, G.B.: 1991, *Astrophys. J.* **373**, 683
Lites, B.W., Skumanich, A.: 1985, in *Measurements of Vector Magnetic Fields*, M.J. Hagyard (Ed.), NASA Conference Publication 2374, p. 342
Lites, B.W., Skumanich, A.: 1990, *Astrophys. J.* **348**, 747
Lites, B.W., Skumanich, A., Rees, D.E., Murphy, G.A.: 1988, *Astrophys. J.* **330**, 493
Lites, B.W., Skumanich, A., Rees, D.A., Murphy, G.A., Carlsson, M.: 1987, *Astrophys. J.* **318**, 930
Litzén, U.: 1976, *Physica Scr.* **14**, 165
Liu, S.Y., Sheeley, N.R., Jr., 1971, *Solar Phys.* **20**, 282
Livi, S.H.B., Wang, J., Martin, S.F.: 1985, *Australian J. Phys.* **38**, 855
Livingston, W.C.: 1968, *Astrophys. J.* **153**, 929
Livingston, W.C.: 1982, *Nature* **297**, 208
Livingston, W.C.: 1983, in *Solar and Stellar Magnetic Fields: Origins and Coronal Effects*, J.O. Stenflo (Ed.), Reidel, Dordrecht, *IAU Symp.* **102**, 149
Livingston, W.: 1991, in *Solar Polarimetry*, L. November (Ed.), National Solar Obs., Sunspot, NM, p. 356
Livingston, W., Harvey, J.W.: 1969, *Solar Phys.* **10**, 294
Livingston, W., Harvey, J.W.: 1971, in *Solar Magnetic Fields*, R. Howard (Ed.), Reidel, Dordrecht, *IAU Symp.* **43**, 51
Livingston, W., Harvey, J.W.: 1975, *Bull. American Astr. Soc.*, **7**, 346.
Livingston, W., Milkey, R., Slaughter, C.: 1977, *Astrophys. J.* **211**, 281
Livingston, W., Wallace, L.: 1985, *Solar Phys.* **95**, 251
Livshits, M.A.: 1964, *Sov. Astron.* **7**, 28
Livshits, M.A.: 1968, *Soln. Akt.* **3**, 78
Lou, Y.-Q.: 1990, *Astrophys. J.* **230**, 905
Low, B.C.: 1975, *Astrophys. J.* **197**, 251
Low, B.C.: 1980, *Solar Phys.* **67**, 57
Lozitskaja, N.I., Lozitskij, V.G.: 1982, *Sov. Astron. Lett.* **8**, 270
Lozitskaja, N.I., Lozitskij, V.G.: 1988, in *Solar Maximum Analysis*, V.E. Stepanov, V.N. Obridko, G.Ya. Smolkov (Eds.), Nauka, Novosibirsk, p. 80
Lozitskij, V.G., Tsap, T.T.: 1990, in *Solar Photosphere: Structure, Convection and Magnetic Fields*, J.O. Stenflo (Ed.), Kluwer, Dordrecht, *IAU Symp.* **138**, 125
Lundstedt, H., Johannesson, A., Larsson, B.: 1991, in *Solar Polarimetry*, L.J. November (Ed.), National Solar Obs., Sunspot, NM, p. 272
MacKinnon, A.L., Brown, J.C.: 1989, *Astron. Astrophys.* **215**, 371
MacKinnon, A.L., Brown, J.C.: 1990, *Astron. Astrophys.* **232**, 544
Makita, M.: 1979, *Publ. Astron. Soc. Japan* **31**, 575
Makita, M.: 1981, in *Proc. Japan-France Seminar on Solar Physics*, F. Moriyama, J.C. Henoux (Eds.), p. 99
Makita, M.: 1986, *Solar Phys.* **106**, 269
Makita, M., Nishi, K.: 1970, *Ann. Tokyo Astron. Obs.* **12**, 121
Makita, M., Hamana, S., Nishi, K., Shimizu, M., Koyano, H., Sakurai, T., Komatsu, H.: 1985, *Publ. Astron. Soc. Japan* **37**, 561.
Malagoli, A., Cattaneo, F., Brumell, N.H.: 1990, *Astrophys. J.* **361**, L33
Maltby, P.: 1971, in *Solar Magnetic Fields*, R.F. Howard (Ed.), Reidel, Dordrecht, *IAU Symp.* **43**, 141
Maltby, P., Avrett, E.H., Carlsson, M., Kjeldseth-Moe, O., Kurucz, R.L., Loeser, R.: 1986, *Astrophys. J.* **306**, 284
Marcy, G.W.: 1983, in *Solar and Stellar Magnetic Fields: Origins and Coronal Effects*, J.O. Stenflo (Ed.), Reidel, Dordrecht, *IAU Symp.* **102**, 3
Marcy, G.W., Basri, G.: 1989, *Astrophys. J.* **345**, 480
Marcy, G.W., Bruning, D.H.: 1984, *Astrophys. J.* **281**, 286
Martin, S.F.: 1984, in *Small-Scale Dynamical Processes in Quiet Stellar Atmospheres*, S.L. Keil

(Ed.), National Solar Obs., Sunspot, NM, p. 30
Martin, S.F.: 1988, *Solar Phys.* **117**, 243
Martin, S.F.: 1990, in *Solar Photosphere: Structure, Convection and Magnetic Fields*, J.O. Stenflo (Ed.), Kluwer, Dordrecht, *IAU Symp.* **138**, p. 129
Martin, S.F., Livi, S.H.B., Wang, J.: 1985a, *Australian J. Phys.* **38**, 929
Martin, S.F., Livi, S.H.B., Wang, J., Shi, Z.: 1985b, in *Measurements of Solar Vector Magnetic Fields*, M.J. Hagyard (Ed.), NASA Conf. Publ. 2374, p. 403
Martínez Pillet, V., García López, R.J., Del Toro Iniesta, J.C., Rebolo, R., Vázquez, M., Beckman, J.E., Char, S.: 1990, *Astrophys. J.* **361**, L81
Martínez Pillet, V., Sánchez Almeida, J.: 1991, *Astron. Astrophys.* **252**, 861
Massaglia, S., Bodo, G., Rossi, P.: 1989, *Astron. Astrophys.* **209**, 399
Massaglia, S., Bodo, G., Kalkofen, W., Rosner, R.: 1988, *Astrophys. J.* **333**, 925
Mathys, G.: 1983, *Ph.D. Thesis*, University of Liège
Mathys, G.: 1989, *Fundam. Cosmic Phys.* **168**, 184
Mathys, G.: 1990, *Astron. Astrophys.* **232**, 151
Mathys, G., Stenflo, J.O.: 1987, *Astron. Astrophys.* **171**, 368
Mathys, G., Solanki, S.K.: 1989, *Astron. Astrophys.* **208**, 189
McMath, R.R., Mohler, O.C., Pierce, A.K., Goldberg, L.: 1956, *Astrophys. J.* **124**, 1
Mehltretter, J.P.: 1974, *Solar Phys.* **38**, 43
Mein, P.: 1971, *Solar Phys.* **20**, 3
Mein, N.: 1977, *Solar Phys.* **52**, 283
Mein, N., Mein, P.: 1976, *Solar Phys.* **49**, 231
Merkle, F., Engvold, O., Falamo, R.: 1987, (Eds.), LEST Technical Report No. 28, Proc. Workshop on Adaptive Optics in Solar Observatories.
Meyer, F.: 1976, in *The Energy Balance and Hydrodynamics of the Solar Chromosphere and Corona*, R.-M. Bonnet, Ph. Delache (Eds.), *IAU Coll.* **36**, 111.
Meyer, F., Schmidt, H.U.: 1968, *Z. Angew. Math. Mech.* **48**, 218
Meyer, F., Schmidt, H.U., Simon, G.W., Weiss, N.O.: 1979, *Astron. Astrophys.* **76**, 35.
Meyer, E., Schmidt, H.U., Weiss, N.O.: 1977, *Monthly Notices Royal Astron. Soc.* **179**, 741
Meyer, F., Schmidth, H.-U., Weiss, N., Wilson, P.R.: 1974, *Monthly Notices Royal Astron. Soc.* **169**, 35
Miles, A.I., Roberts, B.: 1989, *Solar Phys.* **119**, 257
Miles, A., Roberts, B.: 1992, *Solar Phys.* **141**, 205
Miles, A., Allen, H.R., Roberts, B.: 1992, *Solar Phys.* **141**, 235
Miller, P., Foukal, P., Keil, S.: 1984, *Solar Phys.* **92**, 33
Minasyants, T.M., Minasyants, G.S.: 1977, *Soln. Dannye* **3**, 86
Molotovshchikov, A.L., Ruderman, M.S.: 1987, *Solar Phys.* **109**, 247
Montesinos, B., Thomas, J.H.: 1989, *Astrophys. J.* **337**, 977.
Moran, T., Foukal, P., Rabin, D.: 1992, *Solar Phys.* **142**, 35
Moreno Insertis, F.: 1986, *Astron. Astrophys.* **166**, 291
Moreno Insertis, G.: 1992, in *Sunspots: Theory and Observations*, J.H. Thomas, N. Weiss (Eds.), Cambridge University Press, 385
Moreno Insertis, G., Schüssler, M., Ferriz Mas, A.: 1992, *Astron. Astrophys.* **264**, 686
Morrison, N.D., Linsky, J.L.: 1978, *Astrophys. J.* **222**, 723
Moruzzi, G.: 1991, in *The Hanle Effect and Level-Crossing Spectroscopy*, G. Moruzzi, F. Strumia (Eds.), Plenum Press, New York, p. 1
Muchmore, D., Kurucz, R.L., Ulmschneider, P.: 1988, *Astron. Astrophys.* **201**, 138
Muchmore, D., Ulmschneider, P.: 1985, *Astron. Astrophys.* **142**, 393
Muglach, K.: 1991, *Diplomarbeit*, University of Graz
Muglach, K., Solanki, S.K.: 1991, in *Solar Polarimetry*, L. November (Ed.), National Solar Observatory, Sunspot, NM, p. 489
Muglach, K., Solanki, S.K.: 1992, *Astron. Astrophys.* **263**, 301
Muller, R.: 1975, *Solar Phys.* **45**, 105
Muller, R.: 1977, *Solar Phys.* **52**, 249
Muller, R.: 1983, *Solar Phys.* **85**, 113

Muller, R.: 1987, in *The Sun, Proc. 10th European Regional Astron. Meeting of the IAU*, L. Hejna, M. Sobotka (Eds.), Astron. Inst. Czechoslovak Acad. Sci., Prag, p. 15
Muller, R.: 1990, in *Solar Photosphere: Structure, Convection and Magnetic Fields*, J.O. Stenflo (Ed.), *IAU Symp.* **138**, p. 85
Muller, R., Keil, S.L.: 1983, *Solar Phys.* **87**, 243
Muller, R., Mena, B.: 1987, *Solar Phys.* **112**, 295
Muller, R., Roudier, Th.: 1984, *Solar Phys.* **94**, 33.
Muller, R., Roudier, Th.: 1992, *Solar Phys.* **141**, 27
Muller, R., Roudier, Th., Hulot, J.C.: 1989, *Solar Phys.* **119**, 229.
Murcray, F.J., Goldman, A., Murcray, F.H., Bradford, C.M., Murcray, D.G, Coffey, M.T., Mankin, W.G.: 1981, *Astrophys. J.* **247**, L97
Murphy, G.A.: 1990, NCAR Cooperative Thesis No. 124
Murphy, G.A.: 1991, in *Solar Polarimetry*, L. November (Ed.), NSO, Sunspot, NM., p. 457
Mürset, U., Solanki, S.K., Stenflo, J.O.: 1988, *Astron. Astrophys.* **204**, 279
Musielak, Z.E.: 1991, in *Mechanisms of Chromospheric and Coronal Heating*, P. Ulmschneider, E. Priest, R. Rosner (Eds.), Springer-Verlag, Berlin, p. 369
Musielak, Z.E., Rosner, R.: 1987, *Astrophys. J.* **315**, 371
Musielak, Z.E., Rosner, R.: 1988, *Astrophys. J.* **329**, 376
Musielak, Z.E., Rosner, R., Ulmschneider, P.: 1987, in *Cool Stars, Stellar Systems and the Sun, V*, J.L. Linsky, R.E. Stencel (Eds.), Springer Verlag, New York, p. 66
Musielak, Z.E., Rosner, R., Ulmschneider, P.: 1989, *Astrophys. J.* **337**, 470
Musielak, Z.E., Rosner, R., Ulmschneider, P.: 1990, in *Cool Stars, Stellar Systems and the Sun, VI*, G. Wallerstein (Ed.), Astron. Soc. Pac. Conf. Series, **9**, p. 79
Nadeau, D.: 1988, *Astrophys. J.* **325**, 480
Nakagawa, Y., Raadu, M.A., Harvey, J.W.: 1973, *Solar Phys.* **30**, 421
Nesis, A., Fleig, K.-H., Mattig, W.: 1989, in *Solar and Stellar Granulation*, R.J. Rutten, G. Severino (Eds.), Kluwer, Dordrecht, p. 289
Nordlund, Å.: 1977, in *Highlights of Astronomy*, Vol. 4, No. II, E.A. Müller (Ed.), p. 272.
Nordlund, Å.: 1983, in *Solar and Stellar Magnetic Fields: Origins and Coronal Effects*, J.O. Stenflo (Ed.), Reidel, Dordrecht, *IAU Symp.* **102**, 79
Nordlund, Å.: 1984a, in *Small–Scale Dynamical Processes in Quiet Stellar Atmospheres*, S.L. Keil (Ed.), National Solar Obs., Sunspot, NM, p. 181
Nordlund, Å.: 1984b, in *The Hydromagnetics of the Sun*, T.D. Guyenne, J.J. Hunt (Eds.), ESA SP-220, p. 37.
Nordlund, Å.: 1985a, in *Theoretical Problems in High Resolution Solar Physics*, H.U. Schmidt (Ed.), Max Planck Inst. f. Astrophys., Munich, p. 1
Nordlund, Å.: 1985b, in *Theoretical Problems in High Resolution Solar Physics*, H.U. Schmidt (Ed.), Max Planck Inst. f. Astrophys., Munich, p. 101
Nordlund, Å.: 1986, in *Proc. Workshop on Small Magnetic Flux Concentrations in the Solar Photosphere*, W. Deinzer, M. Knölker, H.H. Voigt (Eds.), Vandenhoeck & Ruprecht, Göttingen, p. 83
Nordlund, Å, Stein, R.F.: 1989, in *Solar and Stellar Granulation*, R.J. Rutten, G. Severino (Eds.), Kluwer, Dordrecht, p. 453
Nordlund, Å, Stein, R.F.: 1990, in *Solar Photosphere: Structure, Convection and Magnetic Fields*, J.O. Stenflo (Ed.), *IAU Symp.* **138**, p. 191
November, L.J.: 1986, *Appl. Optics* **25**, 392
November, L.J.: 1991, (Ed.) *Solar Polarimetry*, National Solar Observatory, Sunspot, NM
November, L.J., Simon, G.W.: 1988, *Astrophys. J.* **333**, 427
Nozawa, S., Shibata, K., Matsumoto, R., Sterling, A.C., Tajima, T., Uchida, Y., Ferrari, A., Rosner, R.: 1992, *Astrophys. J. Suppl. Ser.* **78**, 267
Orrall, F.Q.: 1966, *Astrophys. J.* **143**, 917
Osherovich, V.A.: 1982, *Solar Phys.* **77**, 63
Osherovich, V.A., Flå, T., Chapman, G.A.: 1983, *Astrophys. J.* **286**, 412
Pantellini, F.G.E., Solanki, S.K., Stenflo, J.O.: 1988, *Astron. Astrophys.* **189**, 263
Parker, E.N.: 1955, *Astrophys. J.* **121**, 491

Parker, E.N.: 1963, *Astrophys. J.* **138**, 552
Parker, E.N.: 1974, *Solar Phys.* **37**, 127
Parker, E.N.: 1975a, *Astrophys. J.* **198**, 205
Parker, E.N.: 1975b, *Solar Phys.* **40**, 291
Parker, E.N.: 1976, *Astrophys. Space Sci.* **44**, 107
Parker, E.N.: 1978, *Astrophys. J.* **221**, 368
Parker, E.N.: 1979a, *Cosmical Magnetic Fields*, Clarendon Press, Oxford
Parker, E.N.: 1979b, *Astrophys. J.* **230**, 914
Parker, E.N.: 1982a, *Astrophys. J.* **256**, 736
Parker, E.N.: 1982b, *Astrophys. J.* **256**, 746
Parker, E.N.: 1984a, *Astrophys. J.* **281**, 839
Parker, E.N.: 1984b, *Astrophys. J.* **283**, 343
Parker, E.N.: 1985, in *Measurements of Vector Magnetic Fields*, M.J. Hagyard (Ed.), NASA Conference Publication 2374, p. 7
Parker, E.N.: 1986, in *Small Scale Magnetic Flux Concentrations in the Solar Photosphere*, W. Deinzer, M. Knölker, H.H. Voigt (Eds.), Vandenhoeck & Ruprecht, Göttingen, p. 13
Parker, E.N.: 1991, *Astrophys. J.* **376**, 355
Pizzo, V.J.: 1986, *Astrophys. J.* **302**, 785
Pizzo, V.J.: 1987, in *Theoretical Problems in High Resolution Solar Physics II*, G. Athay, D.S. Spicer (Eds.), NASA Conference Publication 2483, p. 1
Pizzo, V.J.: 1990, *Astrophys. J.* **365**, 764
Pizzo, V.J., McGregor, K.B., Kunasz, P.B.: 1993, *Astrophys. J.* **404**, 788
Pneuman, G.W., Solanki, S.K., Stenflo, J.O.: 1986, *Astron. Astrophys.* **154**, 231
Porter, J.G., Moore, R.L., Reichmann, E.J., Engvold, O., Harvey, J.L.: 1987, *Astrophys. J.* **323**, 380
Priest, E.R.: 1982, *Solar Magnetohydrodynamics*, Reidel, Dordrecht
Priest, E.R.: 1987, in *The Role of Fine-Scale Magnetic Fields on the Structure of the Solar Atmosphere*, E.-H. Schröter, M. Vázquez, A.A. Wyller (Eds.), Cambridge University Press, Cambridge, p. 297.
Priest, E.R.: 1990, in *Physics of Magnetic Flux Ropes*, C.T. Russell, E.R. Priest, L.C. Lee (Eds.), Geophysical Monograph 58, American Geophys. Union, Washington, DC, p. 1
Priest, E.R., Forbes, T.G.: 1986 *J. Geophys. Res.* **91**, 5579
Proctor, M.R.E., Weiss, N.O.: 1982, *Rep. Prog. Phys.* **45**, 1317
Qu, Z.-Q., Ding, Y.-J., Xuan, J.-Y., Ye, S.-H.: 1992, preprint
Querfeld, C.W., Smartt, R.N., Bommier, V., Landi Degl'Innocenti, E., House, L.L.: 1985, *Solar Phys.* **96**, 277
Rabin, D.: 1992a, *Astrophys. J.* **390**, L103
Rabin, D.: 1992b, *Astrophys. J.* **391**, 832
Rabin, D.: 1992c, in *Cool Stars, Stellar Systems and the Sun, VII*, M.S. Giampapa, J.A. Bookbinder (Eds.), Astron. Soc. Pacific Conf. Ser., p. 201
Rabin, D.: 1992d, in *Infrared Solar Physics*, D. Rabin, J. Jefferies (Eds.), Kluwer, Dordrecht, *IAU Symp.* **154**, in press
Rabin, D., Jashka, D., Plymate, C., Wagner, J., Iwata, K.: 1991, in *Solar Polarimetry*, L. November (Ed.), National Solar Observatory, Sunspot, NM, p. 361
Rabin, D., Moore, R., Hagyard, M.J.: 1984, *Astrophys. J.* **287**, 404
Rachkovsky, D.N.: 1962, *Izv. Krymsk. Astrofiz. Obs.* **28**, 259
Rachkovsky, D.N.: 1967, *Izv. Krymsk. Astrofiz. Obs.* **37**, 56
Rachkovsky, D.N., Tsap, T.T.: 1985, *Izv. Krymskoj Astrofiz. Obs.* **71**, 79
Rae, I.C., Roberts, B.: 1982, *Astrophys. J.* **256**, 761
Ramsey, H.E., Schoolman, S.A., Title, A.M: 1977, *Astrophys. J.* **215**, L41
Rees, D.E.: 1987, in *Numerical Radiative Transfer*, W. Kalkofen (Ed.), Cambridge University Press, Cambridge, p. 213
Rees, D.E., Murphy, G.A., Durrant, C.J.: 1989, *Astrophys. J.* **339**, 1093
Rees, D.E., Semel, M.D.: 1979, *Astron. Astrophys.* **74**, 1
Reichel, M.: 1953, *Z. Astrophys.* **33**, 79
Ribes, E., Rees, D.E., Fang, Ch.: 1985, *Astrophys. J.* **296**, 268

Rieger, E., Reppin, C., Kanbach, G., Forrest, D.J., Chupp, E.L. Share, G.H.: 1983, *18th Int. Cosmic Ray Conf. Papers* **10**, 338
Ringenbach, A.: 1987, *Diplomarbeit*, ETH, Zürich
Roberts, B.: 1976, *Astrophys. J.* **204**, 268
Roberts, B.: 1981a, *Solar Phys.* **69**, 27
Roberts, B.: 1981b, *Solar Phys.* **69**, 39
Roberts, B.: 1983, *Solar Phys.* **87**, 77
Roberts, B.: 1984, in *The Hydromagnetics of the Sun*, ESA SP-220, p. 137.
Roberts, B.: 1985, *Phys. Fluids* **28**, 3280
Roberts, B.: 1986, in *Small Scale Magnetic Flux Concentrations in the Solar Photosphere*, W. Deinzer, M. Knölker, H.H. Voigt (Eds.), Vandenhoeck & Ruprecht, Göttingen, p. 169
Roberts, B.: 1990, in *Physics of Magnetic Flux Ropes*, C.T. Russell, E.R. Priest, L.C. Lee (Eds.), Geophysical Monograph 58, American Geophys. Union, Washington, DC, p. 113
Roberts, B.: 1991, in *Mechanisms of Chromospheric and Coronal Heating*, P. Ulmschneider, E. Priest, R. Rosner (Eds.), Springer-Verlag, Berlin, p. 494
Roberts, B., Mangeney, A.: 1982, *Monthly Notices Royal Astron. Soc.* **198**, 7p
Roberts, B., Webb, A.R.: 1978, *Solar Phys.* **56**, 5
Roberts, B., Webb, A.R.: 1979, *Solar Phys.* **64**, 77
Robinson, R.D.: 1980, *Astrophys. J.* **239**, 961
Rogerson, J.B.: 1961, *Astrophys. J.* **134**, 331
Ronan, R.S., Mickey, D.L., Orrall, F.Q.: 1987, *Solar Phys.* **113**, 353
Rosenthal, C.S.: 1991, *Solar Phys.* **122**, 350
Rosenthal, C.S.: 1992, *Solar Phys.* **139**, 25
Rosner, R., Golub, L., Vaiana, G.S.: 1985, *Ann. Rev. Astron. Astrophys.* **33**, 413
Rüedi, I.: 1991, Diplomarbeit, ETH, Zürich
Rüedi, I., Solanki, S.K., Livingston, W., Stenflo, J.O.: 1992a, *Astron. Astrophys.* **263**, 323
Rüedi, I., Solanki, S.K., Rabin, D.: 1992b, *Astron. Astrophys.* **261**, L21
Ruiz Cobo, B., Del Toro Iniesta, J.C.: 1992, *Astrophys. J.* **398**, 375
Rust, D.M.: 1968, in *Structure and Development of Solar Active Regions*, K.O. Kiepenheuer (Ed.), Reidel, Dordrecht, *IAU Symp.* **35**, 77
Rust, D.M., Keil, S.L.: 1992, *Solar Phys.* **140**, 55
Rust, D.M., Nakagawa, Y., Neupert, W.M.: 1975, *Solar Phys.* **41**, 397
Rutten, R.J., Carlsson, M.: 1992, in *Infrared Solar Physics*, D. Rabin, J. Jefferies (Eds.), Kluwer, Dordrecht, *IAU Symp.* **154**, in press
Rutten, R.J., Kostik, R.I.: 1982, *Astron. Astrophys.* **115**, 104
Rutten, R.J., Severino, G.: 1989, (Eds.) *Solar and Stellar Granulation*, Kluwer, Dordrecht
Rutten, R.J., Uitenbroek, H.: 1991, *Solar Phys.* **134**, 15
Ruzmaikin, A.A.: 1990, in *Solar Photosphere: Structure, Convection and Magnetic Fields*, J.O. Stenflo (Ed.), Kluwer, Dordrecht, *IAU Symp.* **138**, 343
Ryutov, D.D., Ryutova, M.P.: 1976, *Sov. Phys. JETP* **43**, 491
Ryutova, M.P.: 1988, *JETP* **94**, 138
Ryutova, M.P.: 1990, in *Solar Photosphere: Structure, Convection and Magnetic Fields*, J.O. Stenflo (Ed.), Kluwer, Dordrecht, *IAU Symp.* **138**, 229
Saar, S.H.: 1987, in *Cool Stars, Stellar Systems and the Sun. V.* J.L. Linsky, R.E. Stencel (eds.), Springer, New York, p. 10
Saar, S.H.: 1988, *Astrophys. J.* **324**, 441
Saar, S.H.: 1990, in *Solar Photosphere: Structure, Convection and Magnetic Fields*, J.O. Stenflo (Ed.), Kluwer, Dordrecht, *IAU Symp.* **138**, 427
Saar, S.H.: 1991, in *Memorie della Società Astronomia Italiana*, R. Pallavicini (Ed.), **61**, 559
Saar, S.H., Linsky, J.L.: 1985, *Astrophys. J.* **299**, L47
Sánchez Almeida, J.: 1992, *Solar Phys.* **137**, 1
Sánchez Almeida, J., García López, R.J.: 1991, in *The Sun and Cool Stars: Activity, Magnetism, Dynamos*, I. Tuominen, D. Moss, R. Rüdiger (Eds.), Springer-Verlag, Berlin, *IAU Coll.* **130**, 414
Sánchez Almeida, J., Lites, B.W.: 1992, *Astrophys. J.* **398**, 359
Sánchez Almeida, J., Solanki, S.K., Collados, M., del Toro Iniesta, J.C.: 1988a, *Astron. Astrophys.*

196, 266
Sánchez Almeida, J., Collados, M., Del Toro Iniesta, J.C.: 1988b, *Astron. Astrophys.* **201**, L37
Sánchez Almeida, J., Collados, M., Del Toro Iniesta, J.C.: 1989, *Astron. Astrophys.* **222**, 311
Sánchez Almeida, J., Collados, M., Del Toro Iniesta, J.C.: 1990, *Astrophys. Space Sci.* **170**, 31
Sánchez Almeida, J., Martínez Pillet, V., Wittmann, A.D.: 1991, *Solar Phys.* **134**, 1
Scharmer, G.B.: 1989, in *Solar and Stellar Granulation*, R.J. Rutten, G. Severino (Eds.), Kluwer, Dordrecht, p. 161
Schlüter, A., Temesvary, S.: 1958, in *Electromagnetic Phenomena in Cosmical physics*, B. Lehnert (Ed.), *IAU Symp.* **6**, 263
Schmahl, G.: 1967, *Z. Astrophys.* **66**, 81
Schmidt, H.U., Simon, G.W., Weiss, N.O.: 1985, *Astron. Astrophys.* **148**, 191.
Schmidt, H.U., Wegmann, R.: 1983, in *Dynamical Problems in Mathematical Physics*, B. Brosowski, E. Martensen (Eds.), Verlag P. Lang, Frankfurt a.M., p. 137.
Schmieder B., 1976, *Solar Phys.* **47**, 435
Scholiers, W., Wiehr, E.: 1985, *Solar Phys.* **99**, 349
Schoolman, S.A.: 1971, *Solar Phys.* **21**, 57
Schoolman, S.A.: 1973, *Solar Phys.* **32**, 379
Schoolman, S.A., Ramsey, H.E.: 1976, *Solar Phys.* **50**, 25
Schrijver, C.J.: 1987, *Astron. Astrophys.* **172**, 111
Schrijver, C.J.: 1990, *Astron. Astrophys.* **234**, 315
Schrijver, C.J.: 1991, in *Mechanisms of Chromospheric and Coronal Heating*, P. Ulmschneider, E.R. Priest, R. Rosner (Eds.), p. 257
Schrijver, C.J., Coté, J., Zwaan, C., Saar, S.H.: 1989, *Astrophys. J.* **337**, 964
Schrijver, C.J., Zwaan, C., Balke, A.C., Tarbell, T.D., Lawrence, J.K.: 1992, *Astron. Astrophys.* **253**, L1
Schröter, E.-H.: 1957, *Z. Astrophys* **41**, 141
Schröter, E.-H.: 1965a, *Z. Astrophys* **62**, 228
Schröter, E.-H.: 1965b, *Z. Astrophys* **62**, 256
Schröter, E.-H., Wöhl, H.: 1975, *Solar Phys.* **42**, 3
Schüssler, M.: 1979, *Astron. Astrophys.* **71**, 79
Schüssler, M.: 1983, in *Solar and Stellar Magnetic Fields: Origins and Coronal Effects*, J.O. Stenflo (Ed.), Reidel, Dordrecht, *IAU Symp.* **102**, 213
Schüssler, M.: 1984, *Astron. Astrophys.* **140**, 453
Schüssler, M.: 1986, in *Small Scale Magnetic Flux Concentrations in the Solar Photosphere*, W. Deinzer, M. Knölker, H.H. Voigt (Eds.), Vandenhoeck & Ruprecht, Göttingen, p. 103
Schüssler, M.: 1987, in *The Role of Fine-Scale Magnetic Fields on the Structure of the Solar Atmosphere*, E.-H. Schröter, M. Vázquez, A.A. Wyller (Eds.), Cambridge University Press, p. 223
Schüssler, M.: 1990, in *Solar Photosphere: Structure, Convection and Magnetic Fields*, J.O. Stenflo (Ed.), Kluwer, Dordrecht, *IAU Symp.* **138**, 161
Schüssler, M.: 1991, Habilitationsschrift, Universität Göttingen
Schüssler, M.: 1992, in *The Sun — a Laboratory for Astrophysics*, J.T. Schmelz, J.C. Brown (Eds.), Kluwer, Dordrecht, p. 191
Schüssler, M., Solanki, S.K.: 1988, *Astron. Astrophys.* **192**, 338
Semel, M.D: 1962, *Compt. Rend. Acad. Sci. Paris* **254**, 3978
Semel, M.D.: 1967, *Ann. Astrophys.* **30**, 513
Semel, M.: 1971, in *Solar Magnetic Fields*, R.F. Howard (Ed.), Reidel, Dordrecht, *IAU Symp.* **43**, 37
Semel, M.D.: 1981, *Astron. Astrophys.* **97**, 75
Semel, M.D.: 1985, in *High Resolution in Solar Physics*, R. Muller (Ed.), Springer, Berlin, p. 178.
Semel, M.: 1986, in *Small Scale Magnetic Flux Concentrations in the Solar Photosphere*, W. Deinzer, M. Knölker, H.H. Voigt (Eds.), Vandenhoeck & Ruprecht, Göttingen, p. 39
Servajean, R.: 1961, *Ann. Astrophys.* **24**, 1
Severny, A.B.: 1967, *Soviet Astron.* **11**, 383
Severny, A.B.: 1968, in *Mass Motions in Solar Flares and Related Phenomena*, Öhmann (Ed.), *Nobel Symp.* **9**, 71

Shao, M., Feinleib, J., Bowker, K., Schmutz, L., Tubbs, S.: 1981, in *Solar Instrumentation; What's Next?*, R.B. Dunn (Ed.), National Solar Obs., Sunspot, NM, p. 471
Sheeley, N.R., Jr.: 1966, *Astrophys. J.* **144**, 723
Sheeley, N.R., Jr.: 1967, *Solar Phys.* **1**, 171
Sheeley, N.R., Jr.: 1969, *Solar Phys.* **9**, 347
Sheeley, N.R., Jr.: 1971a, in *Solar Magnetic Fields*, R. Howard (Ed.), *IAU Symp.* **43**, 310
Sheeley, N.R., Jr.: 1971b, *Solar Phys.* **20**, 19
Sheeley, N.R., Jr.: 1972, *Solar Phys.* **25**, 98
Sheeley, N.R., Jr., Bhatnagar, A.: 1971, *Solar Phys.* **19**, 338
Sheeley, N.R., Bohlin, J.D., Brueckner, G.E., Purcell, J.D., Scherrer, V., Tousey, R.: 1975, *Solar Phys.* **40**, 103.
Sheeley, N.R.,Jr., Engvold, O.: 1970, *Solar Phys.* **12**, 69
Shibata, K.: 1980, *Solar Phys.* **66**, 61
Shibata, K.: 1982, *Solar Phys.* **81**, 9
Shibata, K., Suematsu, Y.: 1982, *Solar Phys.* **78**, 333
Shibata, K., Nishikawa, T., Kitai, R., Suemtasu, Y.: 1982, *Solar Phys.* **77**, 121
Shibata, K., Nozawa, S., Matsumoto, R.: 1992, *Publ. Astron. Soc. Japan* **44**, 265
Shibata, K., Nozawa, S., Matsumoto, R., Sterling, A.C., Tajima, T.: 1990, *Astrophys. J.* **351**, L25
Shibata, K., Tajima, T., Matsumoto, R., Horiuchi, T., Hanawa, T., Rosner, R., Uchida, Y.: 1989a, *Astrophys. J.* **338**, 471
Shibata, K., Tajima, T., Steinolfson, R.S., Matsumoto, R.: 1989b, *Astrophys. J.* **345**, 584
Shine, R.A., Linsky, J.L.: 1974, *Solar Phys.* **37**, 145
Šidlichovský, M.: 1976, *Bull. Astron. Inst. Czech.* **27**, 71
Simon, G.W.: 1990, in *Astrophysics from the Moon*, M.J. Mumma, H. Smith (Eds.), Proc. IAP Conference 207, Institute of Physics Press, p. 111
Simon, G.W., Leighton, R.B.: 1964, *Astrophys. J.* **140**, 1120
Simon, G.W., Noyes, R.W.: 1971, in *Solar Magnetic Fields*, R. Howard (Ed.), Reidel, Dordrecht, *IAU Symp.* **43**, 663
Simon, G.W., Title, A.M., Topka, K.P., Tarbell, T.D., Shine, R.A., Ferguson, S.H., Zirin, H., and the SOUP Team: 1988, *Astrophys. J.* **327**, 964
Simon, G.W., Weiss, N.O.: 1970, *Solar Phys.* **13**, 85
Simon, G.W., Weiss, N.O.: 1989, in *High Spatial Resolution Solar Observations*, O. Von der Lühe (Ed.), National Solar Obs., Sunspot, NM, p. 529
Simon, G.W., Weiss, N.O., Nye, A.H.: 1983, *Solar Phys.* **87**, 65
Simon, G.W., Wilson, P.R.: 1985, *Astrophys. J.* **295**, 241
Simon, G.W., Zirker, J.B.: 1974, *Solar Phys.* **35**, 331
Sivaraman, K.R., Livingston, W.C.: 1982, *Solar Phys.* **80**, 227
Skumanich, A., Lites, B.W.: 1987, *Astrophys. J.* **322**, 473
Skumanich, A., Grossmann-Doerth, U., Lites, B.W.: 1992, in *Methods of Solar and Stellar Magnetic Field Determination*, M. Faurobert-Scholl, H. Frisch, N. Mein (Eds.), Obs. de Paris, Meudon, p. 57
Skumanich, A., Rees, D.E., Lites, B.W.: 1985, in *Measurements of Vector Magnetic Fields*, M.J. Hagyard (Ed.), NASA Conference Publication 2374, p. 306
Skumanich, A., Smythe, C., Frazier, E.N.: 1975, *Astrophys. J.* **200**, 747
Smithson, R.C.: 1973, *Solar Phys.* **29**, 365
Smithson, R., Tarbell, T.: 1981, in *Solar Instrumentation; What's Next?*, R.B. Dunn (Ed.), National Solar Obs., Sunspot, NM, p. 480
Sobel'man, I.I.: 1972, *Introduction to the Theory of Atomic Spectra*, Pergamon Press, London
Solanki, S.K.: 1982, *Diplomarbeit*, ETH, Zürich
Solanki, S.K.: 1986, *Astron. Astrophys.* **168**, 311
Solanki, S.K.: 1987a, in *The Role of Fine-Scale Magnetic Fields on the Structure of the Solar Atmosphere*, E.-H. Schröter, M. Vázquez, A.A. Wyller (Eds.), Cambridge University Press, p. 67
Solanki, S.K.: 1987b, in *Proc. Tenth European Regional Astronomy Meeting of the IAU. Vol. 1: The Sun*, L. Hejna, M. Sobotka (Eds.), Publ. Astron. Inst. Czechoslovak Acad. Sci., p. 95
Solanki, S.K.: 1987c, *Ph.D. Thesis*, No. 8309, ETH, Zürich

Solanki, S.K.: 1989, *Astron. Astrophys.* **224**, 225
Solanki, S.K.: 1990, in *Solar Photosphere: Structure, Convection and Magnetic Fields*, J.O Stenflo (Ed.), *IAU Symp.* **138**, 103
Solanki, S.K.: 1991, *Rev. Modern Astron.* **4**, 208
Solanki, S.K.: 1992a, in *Methods of Solar and Stellar Magnetic Field Determination*, M. Faurobert-Scholl, H. Frisch, N. Mein (Eds.), Obs. de Paris, Meudon, p. 39
Solanki, S.K.: 1992b, in *Infrared Solar Physics*, D. Rabin, J. Jefferies (Eds.), Kluwer, Dordrecht, *IAU Symp.* **154**, in press
Solanki, S.K.: 1992c, in *Solar Physics and Astrophysics at Interferometric Resolution*, L. Damé, T.-D. Guyenne (Eds.), ESA SP-344, p. 27
Solanki, S.K., Brigljević, V.: 1992, *Astron. Astrophys.* **262**, L29
Solanki, S.K., Biémont, E., Mürset, U.: 1990, *Astron. Astrophys. Suppl. Ser.* **83**, 307
Solanki, S.K., Keller, C., Stenflo, J.O.: 1987, *Astron. Astrophys.* **188**, 183
Solanki, S.K., Mathys, G.: 1987, in *Activity in Cool Star Envelopes*, O. Havnes et al. (Eds.), Reidel, Dordrecht, p. 39
Solanki, S.K., Montavon, C.A.P.: 1992, *Astron. Astrophys.* , in press
Solanki, S.K., Pahlke, K.D.: 1988, *Astron. Astrophys.* **201**, 143
Solanki, S.K., Roberts, B.: 1990, in *Solar Photosphere: Structure, Convection and Magnetic Fields*, J.O. Stenflo (Ed.), Kluwer, Dordrecht, *IAU Symp.* **138**, Kluwer, Dordrecht, p. 259
Solanki, S.K., Roberts, B.: 1992, *Monthly Notices Royal Astron. Soc.* **256**, 13
Solanki, S.K., Rüedi, I., Livingston, W.: 1992a, *Astron. Astrophys.* **263**, 312
Solanki, S.K., Rüedi, I., Livingston, W.: 1992b, *Astron. Astrophys.* **263**, 339
Solanki, S.K., Steenbock, W.: 1988, *Astron. Astrophys.* **189**, 243
Solanki, S.K., Steiner, O.: 1990, *Astron. Astrophys.* **234**, 519
Solanki, S.K., Steiner, O., Uitenbroek, H.: 1991, *Astron. Astrophys.* **250**, 220
Solanki, S.K., Stenflo, J.O.: 1984, *Astron. Astrophys.* **140**, 185
Solanki, S.K., Stenflo, J.O.: 1985, *Astron. Astrophys.* **148**, 123
Solanki, S.K., Stenflo, J.O.: 1986, *Astron. Astrophys.* **170**, 120
Solov'ev, A.A.: 1984, *Sov. Astron.* **28**, 54
Spiegel, E.A.: 1957, *Astrophys. J.* **126**, 202
Spruit, H.C.: 1976, *Solar Phys.* **50**, 269
Spruit, H.C.: 1977, *Solar Phys.* **55**, 3
Spruit, H.C.: 1979, *Solar Phys.* **61**, 363
Spruit, H.C.: 1981a, in *The Sun as a Star*, S. Jordan (Ed.) NASA SP-450, p. 385
Spruit, H.C.: 1981b, *Astron. Astrophys.* **98**, 155
Spruit, H.C.: 1982, *Solar Phys.* **75**, 3
Spruit, H.C.: 1983, in *Solar and Stellar Magnetic Fields: Origins and Coronal Effects*, J.O. Stenflo (Ed.), Reidel, Dordrecht, *IAU Symp.* **102**, 41
Spruit, H.C.: 1984, in *Small-Scale Dynamical Processes in Quiet Stellar Atmospheres*, S.L. Keil (Ed.), National Solar Obs., Sunspot, NM, p. 249
Spruit, H.C., Bogdan, T.J.: 1992, *Astrophys. J.* **391**, L109
Spruit, H.C., Roberts, B.: 1983, *Nature* **304**, 401
Spruit, H.C., Nordlund, Å, Title, A.M., 1990, *Ann. Rev. Astron. Astrophys.* **28**, 263
Spruit, H.C., Schüssler, M., Solanki, S.K.: 1992, in *Solar Interior and Atmosphere*, A.N. Cox, W. Livingston, M.S. Matthews (Eds.), Arizona University Press, Tucson, AZ, p. 890
Spruit, H.C., Van Ballegooijen, A.A.: 1982, *Astron. Astrophys.* **106**, 58
Spruit, H.C., Van Ballegooigen, A.A., Title, A.M.: 1987, *Solar Phys.* **110**, 115
Spruit, H.C., Zwaan, C.: 1981, *Solar Phys.* **70**, 207
Spruit. H.C., Zweibel, E.G.: 1979, *Solar Phys.* **62**, 15
St. John, C.E., 1913, *Astrophys. J.* **37**, 322
St. John, C.E.: 1922, *Phys. Rev.* **19**, 390
Staude, J.: 1969, *Solar Phys.* **8**, 264
Staude, J.: 1972, *Solar Phys.* **24**, 255
Steffen, M.: 1990, *Astron. Astrophys.* **239**, 443
Steffen, M.: 1991, in *Stellar Atmospheres: Beyond Classical Models*, L. Crivellari, I. Hubeny (Eds.),

Kluwer, Dordrecht, p. 247
Steffen, M., Freytag, B.: 1991, *Reviews of Modern Astron.* **4**, 43
Stein, R., Nordlund, Å.: 1989, *Astrophys. J.* **342**, L95
Stein, R., Nordlund, Å.: 1991, in *Mechanisms of Chromospheric and Coronal Heating*, P. Ulmschneider, E. Priest, R. Rosner (Eds.), Springer-Verlag, Berlin, p. 386
Steiner, O.: 1990, *Ph.D. Thesis*, No. 9292, ETH-Zürich
Steiner, O.: 1992, in *Infrared Solar Physics*, D. Rabin, J. Jefferies (Eds.), Kluwer, Dordrecht, *IAU Symp.* **154**, in press
Steiner, O., Pizzo, V.J.: 1989, *Astron. Astrophys.* **211**, 447
Steiner, O., Pneuman, G.W., Stenflo, J.O.: 1986, *Astron. Astrophys.* **170**, 126
Steiner, O., Stenflo, J.O.: 1990, in *Solar Photosphere: Structure, Convection and Magnetic Fields*, J.O. Stenflo (Ed.), Kluwer, Dordrecht, *IAU Symp.* **138**, 181
Stellmacher, G., Wiehr, E.: 1971, *Solar Phys.* **18**, 220
Stellmacher, G., Wiehr, E.: 1973, *Astron. Astrophys.* **29**, 13
Stellmacher, G., Wiehr, E.: 1979, *Astron. Astrophys.* **75**, 263
Stellmacher, G., Wiehr, E.: 1991, *Astron. Astrophys.* **251**, 675
Stenflo, J.O.: 1968, *Acta Univ. Lund* **II**, No. 2 =*Medd. Lunds Astron. Obs.* **II**, No. 153
Stenflo, J.O.: 1970, *Solar Phys.* **14**, 263
Stenflo, J.O.: 1971, in *Solar Magnetic fields*, R. Howard (Ed.), Reidel, Dordrecht, *IAU Symp.* **43**, 101
Stenflo, J.O.: 1973, *Solar Phys.* **32**, 41
Stenflo, J.O.: 1975, *Solar Phys.* **42**, 79
Stenflo, J.O.: 1976, in *Basic Mechanisms of Solar Activity*, V. Bumba, J. Kleczek (Eds.), Reidel, Dordrecht, *IAU Symp.* **71**, 69
Stenflo, J.O.: 1977, in *The Energy Balance and Hydrodynamics of the Solar Chromosphere and Corona*, R.-M. Bonnet, Ph. Delache (Eds.), G. de Bussac, Clermont-Ferrand, *IAU Coll.* **36**, p. 143
Stenflo, J.O.: 1978, *Rep. Prog. Phys.* **41**, 865
Stenflo, J.O.: 1980, *Astron. Astrophys.* **84**, 68
Stenflo, J.O.: 1982, *Solar Phys.* **80**, 209
Stenflo, J.O.: 1984a, *Adv. Space Res.* **4**, 5
Stenflo, J.O.: 1984b, *Applied Optics* **23**, 1267
Stenflo, J.O.: 1985a, *Solar Phys.* **100**, 189
Stenflo, J.O.: 1985b, in *Measurements of Solar Vector Magnetic Fields*, M.J. Hagyard (Ed.), NASA Conf. Publ. 2374, p. 263
Stenflo, J.O.: 1986, in *Small Scale Magnetic Flux Concentrations in the Solar Photosphere*, W. Deinzer, M. Knölker, H.H. Voigt (Eds.), Vandenhoek & Ruprecht, Göttingen, p. 59
Stenflo, J.O.: 1987, *Solar Phys.* **114**, 1
Stenflo, J.O.: 1989, *Astron. Astrophys. Review* **1**, 3
Stenflo, J.O.: 1991a, in *The Hanle Effect and Level-Crossing Spectroscopy*, G. Moruzzi, F. Strumia (Eds.), Plenum Press, New York, p. 237
Stenflo, J.O.: 1991b, in *Solar Polarimetry*, L.J. November (Ed.), National Solar Obs., Sunspot, MN, p. 416
Stenflo, J.O.: 1991c, in *JOSO Annual Report 1990*, A. von Alvensleben (Ed.), Kiepenheuer Inst. für Sonnenphysik, Freiburg/Br, p. 49
Stenflo, J.O.: 1992, in *Electromechanical coupling of the Solar Atmosphere*, D.S. Spicer, R. Rosner (Eds.), Proc. 3rd OSL Workshop, Capri, preprint
Stenflo, J.O., Harvey, J.W.: 1985, *Solar Phys.* **95**, 99
Stenflo, J.O., Harvey, J.W., Brault, J.W., Solanki, S.K.: 1984a, *Astron. Astrophys.* **131**, 333
Stenflo, J.O., Lindegren, L.: 1977, *Astron. Astrophys.* **59**, 367
Stenflo, J.O., Solanki, S.K., Harvey, J.W.: 1987a, *Astron. Astrophys.* **171**, 305
Stenflo, J.O., Solanki, S.K., Harvey, J.W.: 1987b, *Astron. Astrophys.* **173**, 167
Stenflo, J.O., Twerenbold, D., Harvey, J.W.: 1983, *Astron. Astrophys. Suppl. Ser.* **52**, 161
Stenflo, J.O., Twerenbold, D., Harvey, J.W., Brault, J.W.: 1984b, *Astron. Astrophys. Suppl. Ser.* **54**, 505
Stenholm, L.G., Stenflo, J.O.: 1977, *Astron. Astrophys.* **58**, 273

Stenholm, L.G., Stenflo, J.O.: 1978, *Astron. Astrophys.* **67**, 33
Sterling, A.C., Hollweg, J.V.: 1988, *Astrophys. J.* **327**, 950
Steshenko, N.V.: 1960, *Izv. Krymsk. Astrofiz. Obs.* **22**, 49
Stix, M.: 1990, *The Sun, an Introduction*, Springer, Berlin
Stoyanova, M.N.: 1970, *Solar Phys.* **15**, 349
Stürenburg, S., Holweger, H.: 1990, *Astron. Astrophys.* **237**, 125
Suematsu, Y., Shibata, K., Nishikawa, T., Kitai, R.: 1982, *Solar Phys.* **75**, 99
Sugar, J., Corliss, C.: 1985, *J. Phys. Chem. Ref. Data* **14**, Supplement No. 2
Sun, W.-H., Giampapa, M.S., Worden, S.P., 1987, *Astrophys. J.* **312**, 930
Tanenbaum, A.S., Wilcox, J.M., Frazier, E.N., Howard, R.: 1969, *Solar Phys.* **9**, 328
Tanenbaum, A.S., Wilcox, J.M., Howard, R.: 1971, in *Solar Magnetic Fields*, R. Howard (Ed.), Reidel, Dordrecht, *IAU Symp.* **43**, 348
Tarbell, T.D., Smithson, R.C.: 1981, in *Solar Instrumentation; What's Next?*, R.B. Dunn (Ed.), National Solar Obs., Sunspot, NM, p. 491
Tarbell, T.D., Title, A.M.: 1976, *Solar Phys.* **47**, 563
Tarbell, T.D., Title, A.M.: 1977, *Solar Phys.* **52**, 13
Tarbell, T.D., Title, A.M., Schoolman, S.A.: 1979, *Astrophys. J.* **229**, 387
Tarbell, T., Topka, K., Ferguson, S., Frank, Z., Title, A.: 1989, in *High Spatial Resolution Solar Observations*, O. von der Lühe (Ed.), National Solar Obs., Sunspot, NM, p. 506
Ten Bruggencate, P.: 1940, *Z. Astrophys* **19**, 59
Thévenin, F.: 1989, *Astron. Astrophys. Suppl. Ser.* **77**, 137
Thévenin, F.: 1990, *Astron. Astrophys. Suppl. Ser.* **82**, 179
Thiessen, G.: 1952, *Z. Astrophys.* **30**, 185
Thomas, J.H.: 1985, in *Theoretical Problems in High Resolution Solar Physics*, H.U. Schmidt (Ed.), Max Planck Inst. f. Astrophys., Munich, p. 126
Thomas, J.H.: 1988, *Astrophys. J.* **333**, 407
Thomas, J.H.: 1990, in *Physics of Magnetic Flux Ropes*, C.T. Russell, E.R. Priest, L.C. Lee (Eds.), Geophysical Monograph 58, American Geophys. Union, Washington, DC, p. 133
Thomas, J.H., Montesinos, B.: 1990, *Astrophys. J.* **359**, 550
Thomas, J.H., Montesinos, B.: 1991, *Astrophys. J.* **375**, 404
Title, A.M., Tarbell, T.D.: 1975, *Solar Phys.* **41**, 255
Title, A.M., Tarbell, T.D., Topka, K.P.: 1987a, *Astrophys. J.* **317**, 892
Title, A.M., Tarbell, T.D., Topka, K.P., Shine, R.A., Simon, G.W., Zirin, H. and the SOUP Team, 1987b, in *Solar and Stellar Physics*, E.-H. Schröter, M. Schüssler (Eds.), Lecture Notes in Physics No. 292, Springer, Berlin etc., p. 173
Title, A.M., Tarbell, T.D., Topka, K.P, Ferguson, S.H., Shine, R.A. and the SOUP Team: 1989, *Astrophys. J.* **336**, 475.
Title, A.M., Tarbell, T.D., Topka, K.P., Cauffman, D., Balke, C., Scharmer, G.: 1990a, in *Phys. of Magn. Flux Ropes*, C.T. Russell, E.R. Priest, L.C. Lee (Eds.), Geophysical Monograph 58, American Geophys. Union, Washington, DC, p. 171
Title, A.M., Shine, R.A., Tarbell, T.D., Topka, K.P., Scharmer, G.B.: 1990b, in *Solar Photosphere: Structure, Convection, Magnetic Fields*, J.O. Stenflo (Ed.), Kluwer, Dordrecht, *IAU Symp.* **138**, 49
Title A.M., Topka K.P., Tarbell T.D., Schmidt W., Balke C., Scharmer G.: 1992, *Astrophys. J.* **393**, 782
Topka, K., Tarbell, T.D.: 1984, in *Small-Scale Dynamical Processes in Quiet Stellar Atmospheres*, S.L. Keil (Ed.), National Solar Obs., Sunspot, NM, p. 278
Topka, K.P., Tarbell, T.D., Title, A.M.: 1986, *Astrophys. J.* **306**, 304
Topka, K.P., Tarbell, T.D., Title, A.M.: 1992, *Astrophys. J.* **396**, 351
Trujillo-Bueno, J., Kneer, F.: 1987a, *Astron. Astrophys.* **174**, 183
Trujillo-Bueno, J., Kneer, F.: 1987b, in *The Role of Fine-Scale Magnetic Fields on the Structure of the Solar Atmosphere*, E.-H. Schröter, M. Vázquez, A.A. Wyller (Eds.), Cambridge University Press, Cambridge, p. 281
Tsap, T.T.: 1965, *Izv. Krymsk. Astrofiz. Obs.* **33**, 92.
Tsinganos, K.C.: 1980, *Astrophys. J.* **239**, 746

Ulmschneider, P.:1991, in *Mechanisms of Chromospheric and Coronal Heating*, P. Ulmschneider, E. Priest, R. Rosner (Eds.), Springer-Verlag, Berlin, p. 328
Ulmschneider, P., Muchmore, D.: 1986, in *Small Scale Magnetic Flux Concentrations in the Solar Photosphere*, W. Deinzer, M. Knölker, H.H. Voigt (Eds.), Vandenhoeck & Ruprecht, Göttingen, p. 191
Ulmschneider, P., Muchmore, D., Kalkofen, W.: 1987, *Astron. Astrophys.* **177**, 292
Ulmschneider, P., Zähringer, K., Musielak, Z.E.: 1991, *Astron. Astrophys.* **241**, 625
Unno, W.: 1959, *Astrophys. J.* **129**, 375
Unno, W., Ando, H.: 1979, *Geophys. Astrophys. Fluid Dyn.* **12**, 107
Unno, W., Ribes, E.: 1979, *Astron. Astrophys.* **73**, 314
Unno, W., Spiegel, E.A.: 1966, *Publ. Astron. Soc. Japan* **18**, 85
Vaiana, G.S., Cassinelli, J.P., Fabbiano, G., Giacconi, R., Golub, L., Gorenstein, P., Haisch, B.M., Harnden, F.R.,Jr., Johnson, H.M., Linsky, J.L., Maxson, C.W., Mewe, R., Rosner, R., Seward, F., Topka, K., Zwaan, C: 1981, *Astrophys. J.* **245**, 163.
Vaiana, G.S., Krieger, A.S., Timothy, A.F.: 1973, *Solar Phys.* **37**, 81
Van Ballegooijen, A.A.: 1983, *Astron. Astrophys.* **118**, 275
Van Ballegooijen, A.A.: 1984a, in *Small-Scale Dynamical Processes in Quiet Stellar Atmospheres*, S.L. Keil (Ed.), National Solar Obs., Sunspot, NM, p. 260
Van Ballegooijen, A.A.: 1984b, *Solar Phys.* **91**, 195
Van Ballegooijen, A.A.: 1985a, in *Measurements of Solar Vector Magnetic Fields*, M.J. Hagyard (Ed.), NASA Conf. Publ. 2374, p. 322
Van Ballegooijen, A.A., 1985b, in *Theoretical Problems in High Resolution Solar Physics*, H.U. Schmidt (Ed.), Max Planck Inst. f. Astrophys., Munich, p. 177.
Van Ballegooijen, A.A.: 1985c, in *Theoretical Problems in High Resolution Solar Physics*, H.U. Schmidt (Ed.), Max Planck Inst. Astrophys., Garching, p. 167
Topka, K.P., Tarbell, T.D., Title, A.M.: 1992, *Astrophys. J.* **396**, 351
Van Ballegooijen, A.A., Choudhuri, A.R.: 1988, *Astrophys. J.* **333**, 965
Veeder, G.H., Zirin, H.: 1970, *Solar Phys.* **12**, 391.
Venkatakrishnan, P.: 1983, *J. Astrophys. Astron.* **4**, 135 Venkatakrishnan, P.: 1985, *J. Astrophys. Astron.* **6**, 21
Venkatakrishnan, P.: 1986a, *Nature* **322**, 156
Venkatakrishnan, P.: 1986b, *Solar Phys.* **104**, 347
Venkatakrishnan, P., Hagyard, M.J., Hathaway, D.H.: 1988, *Solar Phys.* **115**, 125
Vernazza, J.E., Avrett, E.H., Loeser, R.: 1976, *Astrophys. J. Suppl. Ser.* **30**, 1
Vernazza, J.E., Avrett, E.H., Loeser, R.: 1981, *Astrophys. J. Suppl. Ser.* **45**, 635
Vestrand, W.T., Forrest, D.J., Chupp, E.L., Rieger, E., Share, G.H.: 1987, *Astrophys. J.* **322**, 1010
Voigt, H.H.: 1950, *Z. Astrophys.* **27**, 385
Von der Lühe, O.: 1987, in *The Role of Fine-Scale Magnetic Fields on the Structure of the Solar Atmosphere*, E.-H. Schröter, M. Vázquez, A.A. Wyller (Eds.), Cambridge University Press, p. 156
Von der Lühe, O.: 1988, *Astron. Astrophys.* **205**, 354
Von der Lühe, O.: 1989, in *High Spatial Resolution Solar Observations*, O. von der Lühe (Ed.), Sunspot, NM, p. 147
Von der Lühe, O., Widener, A.L., Rimmele, Th., Spence, G., Dunn, R.B., Wiborg, P.: 1989, *Astron. Astrophys.* **224**, 351
Von Uexküll, M., Kneer, F., Malherbe, J.-M., Mein, P.: 1989, *Astron. Astrophys.* **208**, 290
Vrabec, D.: 1971, in *Solar Magnetic Fields*, R.F. Howard (Ed.), Reidel, Dordrecht, *IAU Symp.* **43**, 329
Vrabec, D.: 1974, in *Chromospheric Fine Structure*, R.G. Athay (Ed.), Reidel, Dordrecht, *IAU Symp.* **56**, 201
Waldmeier, M.: 1940, *Helv. Phys. Acta* **13**, 13
Waldmeier, M.: 1949, *Z. Astrophys.* **26**, 147
Wallenhorst, S.G., Howard, R.F.: 1982, *Solar Phys.* **76**, 203
Wallenhorst, S.G., Topka, K.P.: 1982, *Solar Phys.* **81**, 33
Walther, U.: 1992, Diplomarbeit, ETH Zürich
Walton, S.R.: 1987, *Astrophys. J.* **312**, 909

Wang, H., Zirin, H.: 1987, *Solar Phys.* **110**, 281
Wang, H., Zirin, H.: 1992, *Solar Phys.* **140**, 41
Wang, H., Varsik, J., Zirin, H., Canfield, R.C., Leka, K.D., Wang, J.: 1992, *Solar Phys.* **142**, 11
Wang, H., Zirin, H., Ai, G.: 1991, *Solar Phys.* **131**, 53
Wang, H., Zirin, H., Patterson, A., Ai, G., Zhang, H.: 1989, *Astrophys. J.* **343**, 489
Wang, J., Zirin, H., Shi, Z.: 1985, *Solar Phys.* **98**, 241
Wang, J., Shi, Z., Martin, S.F., Livi, S.H.B.: 1988, *Vistas in Astronomy* **31**, 79
Wang, Y.-M., Sheeley, N.R.,Jr.: 1989, *Solar Phys.* **124**, 81
Webb, A.R., Roberts, B.: 1978, *Solar Phys.* **59**, 249
Webb, A.R., Roberts, B.: 1980a, *Solar Phys.* **68**, 71
Webb, A.R., Roberts, B.: 1980b, *Solar Phys.* **68**, 87
Weiss, N.O.: 1966, *Proc. Roy. Soc. London, Ser.A* **293**, 310
Weiss, N.O.: 1977, in *Highlights of Astronomy, Vol. 4*, E.A. Müller (Ed.), p. 241
Weiss, N.O.: 1981a, *J. Fluid. Mech.* **108**, 247
Weiss, N.O.: 1981b, *J. Fluid. Mech.* **108**, 273
Weisshaar, E.: 1989, *Phys. Fluids* **A1**, 1406.
Wentzel, D.G.: 1979a, *Astrophys. J.* **227**, 319
Wentzel, D.G.: 1979b, *Astron. Astrophys.* **76**, 20
Wiehr, E.: 1977, in *Highlights of Astronomy, Vol. 4*, E.A. Müller (Ed.), p. 251
Wiehr, E.: 1978, *Astron. Astrophys.* **69**, 279
Wiehr, E.: 1979, *Astron. Astrophys.* **73**, L19
Wiehr, E.: 1985, *Astron. Astrophys.* **149**, 217
Wiehr, E.: 1987, in *Cool Stars, Stellar Systems, and the Sun, V.*, J.L. Linsky, R.E. Stencel (Eds.), Lecture Notes in Physics Vol. 291, Springer-Verlag, Berlin, p. 54
Wiehr, E., Lustig, G.: 1989, in *Solar and Stellar Flares: Poster Papers*, B.M. Haisch, M. Rodonò (Eds.), Catania Astrophys. Obs., *IAU Coll.* **104**, 349
Wiehr, E., Rossbach, M.: 1974, *Solar Phys.* **35**, 343
Willson, R.C.: 1981, *Solar Phys.* **74**, 217
Willson, R.C., Gulkis, S., Janssen, M., Hudson, H.S., Chapman, G.A.: 1981, *Science* **211**, 700
Willson, R.C., Hudson, H.S.: 1981, *Astrophys. J.* **254**, L185
Willson, R.C., Hudson, H.S.: 1988, *Nature* **332**, 810
Wilson, O.C., 1978, *Astrophys. J.* **226**, 379
Wilson, P.R.: 1977a, *Astrophys. J.* **214**, 611
Wilson, P.R.: 1977b, *Astrophys. J.* **214**, 917
Wilson, P.R.: 1978a, *Astrophys. J.* **221**, 672
Wilson, P.R.: 1978b, *Astrophys. J.* **225**, 1058
Wilson, P.R.: 1979, *Astron. Astrophys.* **71**, 9
Wilson, P.R.: 1980a, *Astrophys. J.* **237**, 1008
Wilson, P.R.: 1980b, *Astron. Astrophys.* **87**, 121
Wilson, P.R.: 1981a, *Astrophys. J.* **251**, 756
Wilson, P.R.: 1981b, *Solar Phys.* **69**, 9
Wilson, P.R., Simon, G.W.: 1983, *Astrophys. J.* **273**, 805
Wittmann, A.D.: 1974, *Solar Phys.* **35**, 11
Worden, S.P.: 1975, *Solar Phys.* **45**, 521
Xanthakis, J.: 1969, *Solar Phys.* **10**, 168
Yun, H.S.: 1970, *Astrophys. J.* **162**, 975
Yun, H.S.: 1971, *Solar Phys.* **16**, 398
Zachariadis, Th.G.: 1987, in *Proc. Tenth European Regional Astronomy Meeting. Vol. I: The Sun*, L. Hejna, M. Sobotka (Eds.), Publ. Astron. Inst. Czechoslovak Acad. Sci., p. 37
Zähringer, K., Ulmschneider, P.: 1987, in *The Role of Fine-Scale Magnetic Fields on the Structure of the Solar Atmosphere*, E.-H. Schröter, M. Vázquez, A.A. Wyller (Eds.), Cambridge University Press, p. 243
Zayer, I.: 1990 *Ph.D. Thesis*, No. 8995, ETH, Zürich
Zayer, I., Solanki, S.K., Stenflo, J.O.: 1989, *Astron. Astrophys.* **211**, 463
Zayer, I., Solanki, S.K., Stenflo, J.O., Keller, C.U.: 1990, *Astron. Astrophys.* **239**, 356

Zirin, H.: 1972, *Solar Phys.* **22**, 34
Zirin, H.: 1985, *Australian J. Phys.* **38**, 961
Zirin, H.: 1987, *Solar Phys.* **110**, 101
Zirin, H., Popp, B.: 1989, *Astrophys. J.* **340**, 571
Zirin, H., Wang, H.: 1992, *Astrophys. J.* **385**, L27
Zwaan, C.: 1967, *Solar Phys.* **1**, 478
Zwaan, C.: 1978, *Solar Phys.* **60**, 213
Zwaan, C.: 1985, *Solar Phys.* **100**, 397
Zwaan, C.: 1987, *Ann. Rev* **25**, 83
Zwaan, C.: 1989, in *High Spatial Resolution Solar Observations*, O. Von der Lühe (Ed.), National Solar Obs., Sunspot, NM, p. 420
Zwaan, C., Brants, J.J., Cram, L.E.: 1985, *Solar Phys.* **95**, 3

BOOK REVIEWS